Lipid production in microalgae

Anne José Klok

Thesis committee

Promotor
Prof. Dr R.H. Wijffels
Professor of Bioprocess Engineering
Wageningen University

Co-promotors
Dr D.E. Martens
Assistant professor, Bioprocess Engineering
Wageningen University

Dr P.P. Lamers
Assistant professor, Bioprocess Engineering
Wageningen University

Other members
Prof. Dr R.J. Bino, Wageningen University
Dr J.M. Brusson, Total S.A., Paris, France
Prof. Dr Q. Hu, Institute of Hydrobiology, Chinese Academy of Sciences, Hubei, China
Prof. Dr B. Teusink, VU University Amsterdam

This research was conducted under the auspices of the Graduate School VLAG
(Advanced studies in Food Technology, Agrobiotechnology, Nutrition and Health Sciences).

Lipid production in microalgae

Anne José Klok

Thesis

submitted in fulfilment of the requirement for the degree of doctor
at Wageningen University
by the authority of the Rector Magnificus
Prof. Dr M.J. Kropff,
in the presence of the
Thesis Committee appointed by the Academic Board
to be defended in public
on Friday 20 December 2013
at 4 p.m. in the Aula.

A.J. Klok
Lipid production in microalgae
224 pages

PhD thesis, Wageningen University, Wageningen, NL (2013)
With references, with summaries in Dutch and English

ISBN 978-94-6173-776-2

Voor Machteld

Contents

Chapter 1 9
Introduction and thesis outline

Chapter 2 15
Simultaneous growth and neutral lipid accumulation in microalgae

Chapter 3 41
A model for customising biomass composition in continuous microalgae production

Chapter 4 75
Metabolic modeling of *Chlamydomonas reinhardtii*: energy requirements for photoautotrophic growth and maintenance

Chapter 5 115
Maximisation of TAG production in microalgae: metabolic modeling of energy partitioning in nitrogen-limited *Neochloris oleoabundans*

Chapter 6 163
General discussion

References 183

Summary 203

Samenvatting 209

Dankwoord 215

Curriculum Vitae 219

List of publications 221

Overview of completed training activities 223

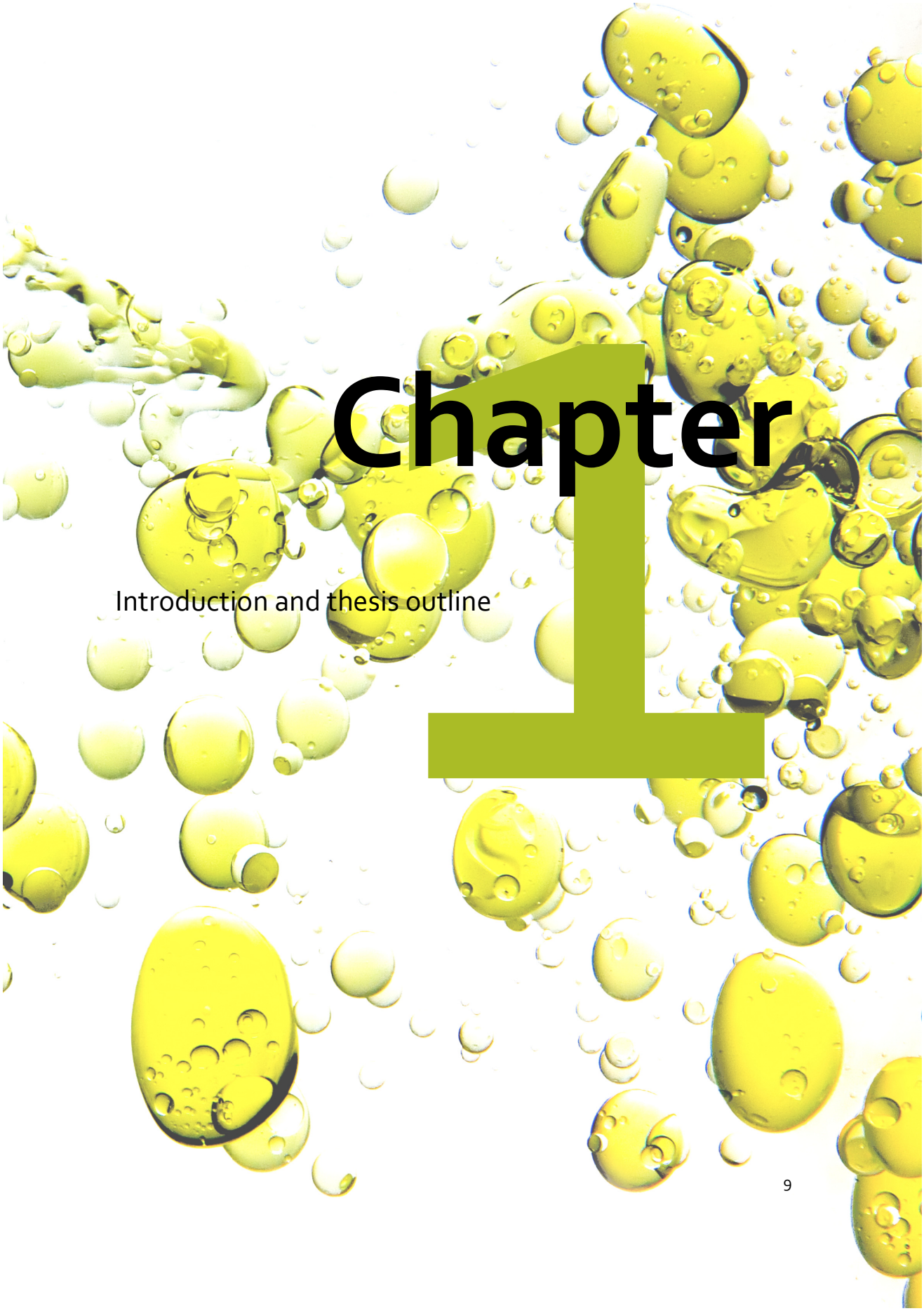

Chapter 1

Introduction and thesis outline

1.1 Microalgal lipids as a renewable feedstock for food and fuel production

Photosynthesis performed by microscopic plants was responsible for the formation of our fossil oil reserves, millions of years ago. As currently these reserves are declining, we are again looking at the potential of photosynthesis to (re)capture inorganic carbon and convert it into the organic molecules that are the feedstock of all carbon based food and fuel available today. Microalgae have great potential as a photosynthetic catalyst as they have some important advantages over traditional agricultural crops. For example, the predicted areal productivities of microalgae are much higher (Chisti, 2007) and can be obtained without the use of arable land. Furthermore, many algal species are salt tolerant (Ben-Amotz et al., 1982) and therefore sea water can be used for cultivation.

The range of products that can be produced with microalgae varies from fine chemicals, such as pigments and polyunsaturated fatty acids, to products that are suitable for bulk applications, such as starch, protein and lipids. Algal lipids are considered a promising source for the production of next generation biofuels (Hu et al., 2008). In particular triacylglycerides (TAG) are suitable to produce a stable and energy dense biofuel (Haik et al., 2011).

Although the application of microalgal lipids as biofuel is very promising, commercial production of algae derived products is currently only feasible for fine chemicals (Pulz and Gross, 2004). For bulk applications, such as biodiesel, to become viable, production costs should be decreased by a factor 10 (Wijffels and Barbosa, 2010). Increasing the microalgal TAG production rates could substantially contribute to lowering the production costs of lipid rich biomass.

1.2 Lipid accumulation in microalgae

Under adverse growth conditions such as nitrogen starvation, algae will stop dividing and accumulate TAG. The exact mechanism of TAG accumulation in microalgae is not well understood, which is an important bottleneck in accomplishing efficient TAG production.

An often used hypothesis for TAG synthesis is that it is triggered by an energy imbalance experienced by the cells upon nitrogen starvation. Due to the lack of nitrogen, protein synthesis is prevented, leading to an imbalance between energy generated in the photosystems and energy used in metabolism. This imbalance causes overreduction of the photosynthetic machinery with the risk of redundant electrons being transferred to oxygen and forming reactive oxygen species (ROS), which could damage vital cell components (Ledford and Niyogi, 2005). Highly reduced compounds such as TAG are thought to act as a sink for these dangerous excess electrons, allowing the cell to contin-

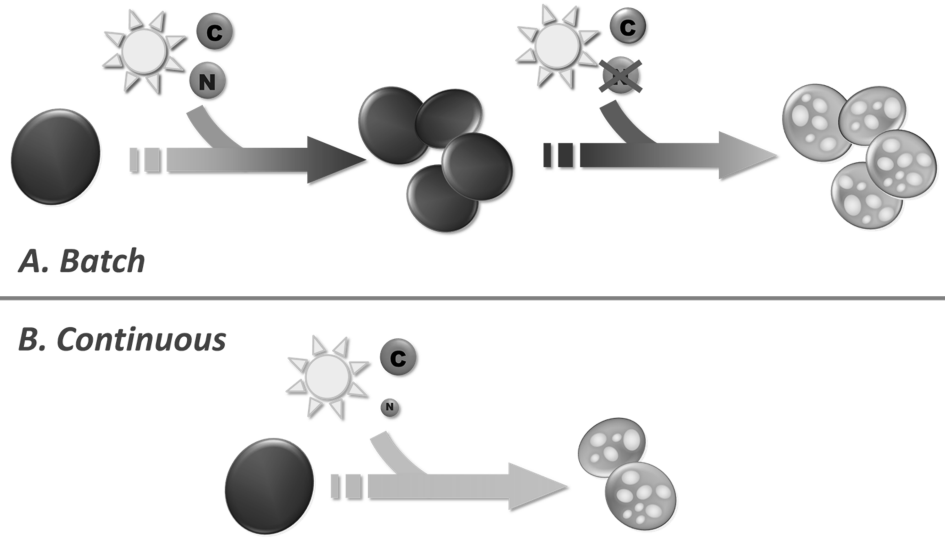

Figure 1.1 *TAG production in a batch (A) and a continuous (B) process.*

ue harvesting light energy while at the same time preventing the formation of ROS (Li et al., 2013).

As nitrogen starvation hampers cell proliferation, TAG is usually produced in a batch process, in which first biomass is produced in the presence of nitrogen, followed by a starvation phase where TAG is accumulated (Figure 1.1A). Alternatively, if TAG accumulation is indeed caused by an energy imbalance, it should be possible to stimulate TAG synthesis by merely reducing the nitrogen supply to a cell compared to its energy intake. This creates an energy imbalance sufficient to stimulate TAG synthesis, while the supply of nitrogen would allow cell proliferation to carry on, enabling a continuous process (Figure 1.1B).

In a continuous system, the effects of light and nitrogen supply on TAG accumulation can be studied simultaneously, yet independently, in contrast to in a batch system. Also, continuous production of both biomass and product is possibly beneficial for commercial production of TAG (Wijffels et al., 2010).

1.3 Modeling as a tool for process optimisation

Models are useful tools when aiming at optimising a biotechnological production system. They reduce a complex process to an elementary form, simplifying calculations and predictions. For example, kinetic models allow for the evaluation of cultivation condi-

tions with a minimal amount of experiments. Also, they allow prediction of the optimal cultivation conditions for biomass or product formation. Alternatively, metabolic models permit a look into the processes occurring on a cellular level, leading to understanding of the regulation of metabolic fluxes in response to environmental conditions and giving an indication of possible bottlenecks for product formation. In combination with controlled lab-scale experiments, models can thus be used to obtain valuable insight into the kinetics and mechanism of TAG accumulation, on which basis organisms and processes can be optimized.

1.4 Thesis outline

The aim of the work presented in this thesis is to obtain insight in the kinetics and metabolism of TAG accumulation in microalgae in order to optimise photosynthetic TAG production for bulk applications. In **Chapter 2** a novel continuous growth system is presented that allows for simultaneous growth and TAG accumulation. Using turbidostat control and a separate nitrogen supply, the effects of nitrogen and light supply on TAG synthesis can be studied simultaneously, yet independently, under steady state growth conditions. By cultivating the oleaginous microalga *Neochloris oleoabundans* in this system, it was found that TAG production rates rise when the imbalance between photosynthetic energy supply and metabolic energy demand was increased by progressive nitrogen starvation. Also, it was revealed that the bulk of the excess energy did not end up in TAG, but was dissipated, which likely occurred in the photosystems.

The kinetics of TAG accumulation as a result of nitrogen limitation were studied in **Chapter 3.** A kinetic model was developed based on the measured electron distributions in *N. oleoabundans* grown in a nitrogen limited turbidostat. Using the model, the performance of this continuous TAG production system was evaluated. It was shown that in this system algal biomass can be easily customised by manipulating nitrogen and light supply rates, as the synthesis of TAG, starch and protein require distinct cultivation conditions.

Metabolic models were used to study the changes in microalgal metabolism upon nitrogen limitation. In **Chapter 4,** a genome based model is presented that describes the primary metabolism of green microalga *C. reinhardtii*. At the time of developing this model, the genome of this model alga was the only one that was fully sequenced and partly annotated. Moreover, knowledge on its metabolism was readily available and therefore this alga, although not very oleaginous by nature, was chosen as the best candidate for our first model on algal metabolism. Using the data obtained in chemostat experiments at several growth rates as input for the metabolic model, the energy requirements for

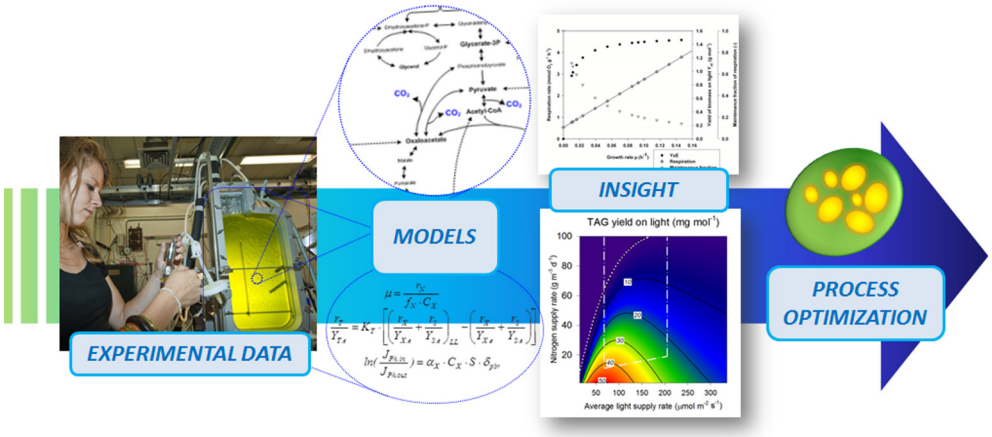

Figure 1.2 *Experimental data obtained under laboratory conditions can be used to develop models. These models allow for a better understanding of the kinetics and metabolism of TAG accumulation, which is beneficial for optimisation of a commercial TAG production system using microalgae.*

growth and maintenance in microalgae were determined.

Subsequently, the metabolic model was extended and validated for oleaginous algae using a *de novo* constructed transcriptome of *N. oleoabundans*. In **Chapter 5**, this model is used to study the interaction between nitrogen assimilation, photosynthesis and TAG accumulation. It was shown that under steady state nitrogen limitation, *N. oleoabundans* was able to balance its metabolic energy demands with the photosynthetic energy supply by redirecting carbon and energy towards TAG synthesis and reducing linear electron transport. The room for improvement of TAG yield on light was evaluated using the metabolic model in combination with different engineering scenarios.

In **Chapter 6**, an overview of the current understanding of TAG accumulation biology is given and the most important existing knowledge gaps are identified. Based on current developments in the field and the research presented in this thesis, three hypotheses on the cause and function of TAG accumulation are proposed. With these hypotheses in mind, several considerations for improving TAG productivity and optimising commercial outdoor production are presented, both via improving photobioreactor operational strategies, as well as strain improvement.

Chapter 2

Simultaneous growth and neutral lipid accumulation in microalgae

This chapter has been published as:

Anne J. Klok, Dirk E. Martens, René H. Wijffels, Packo P. Lamers (2013)

Simultaneous growth and neutral lipid accumulation in microalgae

Bioresource Technology 134, pp. 233-243

Abstract

In this paper the hypothesis was tested whether TAG accumulation serves as an energy sink when microalgae are exposed to an energy imbalance caused by nutrient limitation. In our continuous culture system, excess light absorption and growth-limiting nitrogen supply rates were combined, which resulted in accumulation of TAG (from 1.5 to 12.4% w/w) in visible lipid bodies in *Neochloris oleoabundans*, while cell replication was sustained. A fourfold increase in TAG productivity showed that TAG indeed served as an energy sink. However, the bulk of excess energy was dissipated leading to a substantially reduced biomass productivity and yield of biomass on light. This demonstrates that when aiming at industrial TAG production, sustaining efficient light energy use under nutrient stress is an important trait to look for in potential production organisms.

2.1 Introduction

2.1.1 Background

Microalgae are very promising for the production of sustainable biofuel. They can produce large amounts of triacylglycerides (TAGs) (Hu et al., 2008) that have a fatty acid composition comparable to vegetable oils and thus are easily converted into an effective and clean fuel for diesel engines (Haik et al., 2011). Furthermore, microalgae can potentially be grown year round on non-arable land using salt, brackish or waste stream water. Much higher areal yields can be achieved than with traditional agricultural crops (Wijffels and Barbosa, 2010), thus microalgae provide some major advantages over commonly grown oleaginous plants such as palm, soy or rapeseed.

2.1.2 Current research focus

Most microalgae only produce TAGs when cultivated under adverse growth conditions. Therefore, studies on TAG production in algae are usually done in a two-step, batch wise process. First, algae are grown under optimal conditions until sufficient biomass is obtained. Then TAG accumulation is triggered by arresting the growth using for example nutrient deprivation, of which nitrogen deprivation is the most commonly used method. Often, these studies are not so much focussed on the biological mechanism of TAG accumulation, but on the alga with the highest TAG content. Very high lipid contents (up to 60% total fatty acids (TFA) w/w) have been reported (Sheehan et al., 1998) and articles claiming to have found a new, better production organism based on its lipid content appear regularly.

Although a very high TAG content results in more efficient and cheap downstream processing, it is often overlooked that to obtain these contents, algae have to be exposed to unfavourable environmental conditions that limit growth for a relatively long time. The highest TAG formation rate is obtained in the first hours to days of nutrient depletion, after which the formation rate gradually decreases. Producing algae with contents of 50% TAG (w/w) or more takes considerably longer, in the order of 1 or 2 weeks of nutrient depletion, depending on the light conditions (Griffiths and Harrison, 2009; Rodolfi et al., 2009). Such prolonged stress periods typically lead to reduced overall biomass and TAG productivities and, correspondingly, to a reduced overall light use efficiency. Therefore producing biomass with a high TAG content demands more ground area and reactor material to be used for each litre of oil produced per year, compared to harvesting in the earlier stages of nutrient depletion (at a slightly lower TAG content).

To be able to make a fair comparison between different production systems and organisms, it is important to not only look at the TAG content but also at the yield of biomass

and TAG on light and the average production rate of TAG over the complete production period. This should also include the down-time required to start-up a new batch, and the growth phase to produce biomass. The ideal TAG production process will rely on an optimal balance between an efficient light conversion, a high TAG production rate and a TAG content that allows for economical downstream processing. Such optimization requires detailed understanding of the underlying mechanisms of TAG accumulation.

2.1.3 A hypothesis for the mechanism of TAG accumulation based on energy fluxes

Although some advances have been made in unravelling the genetic and biochemical processes of TAG accumulation in microalgae, a widely accepted explanation for this phenomenon is yet to be found (Liu and Benning, 2013; Merchant et al., 2012). Attempts have been made to increase TAG content by process optimisation, medium optimisation and also by genetic modification, revealing the ever recurring pattern that increasing TAG content seems to be countered by a loss in growth. This leads to a rather black and white approach in which TAG accumulation is seen as a part of secondary metabolism that can only be induced by extreme external factors that eventually completely halt growth, such as zero nitrogen.

An alternative hypothesis is that TAG accumulation is triggered by an energy imbalance experienced by the algal cell when exposed to an external stress factor, as was also suggested by (Hu et al., 2008). For example, a nutrient shortage will disturb the anabolic processes in the cell in need of these nutrients. Consequently, the energy demand for anabolism will fall behind with the energy supply through photosynthesis. This leads to overreduction of the photosynthetic machinery, which in turn can cause formation of damaging reactive oxygen species (Ledford and Niyogi, 2005). Under these conditions, microalgae are known to dissipate energy as heat and fluorescence (Kolber et al., 1988). Highly reduced compounds such as TAG, which do not contain the limiting nutrient, serve as an alternative energy sink and allow the cell to continue harvesting light energy and at the same time decrease the formation rate of reactive oxygen species.

This hypothesis applies to the production of TAG in lipid producing microalgae, but also to overproduction of various other compounds upon environmental stress, such as pigments or starch. (Lamers et al., 2008) already hypothesized that β-carotene accumulation in *Dunaliella salina* is similarly caused by an energy imbalance, in which the pigments serve as an electron sink. However, in this case the accumulated metabolites also function as a sunscreen, protecting the cells by absorbing part of the excess irradiation, giving it a dual protective function.

2.1.4 TAG accumulation in a continuous production system

If indeed this hypothesis is valid, TAG accumulation is not necessarily coupled to a complete halt of growth as is often suggested. It should be possible to create an energy imbalance by reducing the nutrient supply to the cells at constant light input, while simultaneously allowing cell division to continue. The energy imbalance should then induce a similar response of TAG accumulation as is observed in classical nutrient depletion experiments.

To test our hypothesis a system was designed in which turbidostat operation was combined with a separate continuous nitrogen supply, which can be regarded as a distinctive operating feature of this set-up. Turbidostat operation ensured that the amount of light absorbed by the culture was always the same and in this way a fixed energy intake could be imposed on the culture. Next, an energy imbalance was created by decreasing the nitrogen supply rate below the minimum value necessary to sustain nutrient replete, light limited growth.

The effect of two light energy uptake rates and several nitrogen supply rates on growth and TAG accumulation in *Neochloris oleoabundans* was tested in the dedicated turbidostat set-up. *N. oleoabundans* was used because it is known to accumulate up to 56% TFA (w/w) of its dry weight under nitrogen deprivation, in which up to 80% of total lipids consisted of TAG. Also, its growth rate under nitrogen replete conditions is substantial: up to 2.2 d^{-1}. It can be cultivated in fresh as well as in salt medium, and at elevated pH it shows substantial growth rates (Gouveia et al., 2009; Pruvost et al., 2009; Santos et al., 2012). This makes *N. oleoabundans* a very versatile and suitable model organism to study the trade-off between growth and TAG accumulation.

The present work describes how growth and TAG accumulation can occur simultaneously using the aforementioned experimental setup. It was shown that indeed a steady state energy imbalance can be created and that this energy imbalance can be the basis for TAG accumulation in microalgae. By controlling the fluxes of energy in the cell, TAG productivity could be increased, but also showed that increased TAG productivity was coupled to a loss in biomass yield on light due to substantial dissipation of energy.

2.2 Materials and methods

2.2.1 Preculture and media composition

Neochloris oleoabundans UTEX 1185 (The culture collection of Algae, University of Texas, Austin) was cultivated in 250 mL shake flasks to produce a starter culture. The shake flaks contained 100 mL filter sterilized (pore size 0.2 µm), defined medium (Table 2.1), at a pH of 7.5. This medium was designed in such a way, that 4 g L^{-1} nutrient-replete bio-

mass could be sustained, based on the elemental composition of *N. oleoabundans* measured by (Pruvost et al., 2009). Seven days prior to the start of the experiment, flasks were inoculated and placed in a shake incubator, with an irradiance of 80 µmol m^{-2} s^{-1} and a headspace enriched with 2% CO_2, operating at 25 °C and 120 rpm. To ensure a sufficiently high cell density, the irradiance was increased to 280 µmol m^{-2} s^{-1} two days prior to the start of the experiment.

Table 2.1 *Medium compositions of nitrogen containing medium (N+), dilution medium (N-) and shake flask (SF) growth medium. For the SF medium, N+ medium concentrations were doubled.*

Compound	*Concentration (mmol L^{-1})*	*Trace elements*	*Concentration (µmol L^{-1})*
KNO_3 [a]	14.84 (LL)	$Na_2EDTA \cdot 2\ H_2O$	179.70
	29.86 (HL)	$ZnSO_4 \cdot 7\ H_2O$	46.05
K_2SO_4	1.15	$MnCl_2 \cdot 4\ H_2O$	10.95
$KH_2PO_4 \cdot H_2O$	0.35	$Na_2MoO_4 \cdot 2\ H_2O$	7.35
$K_2HPO_4 \cdot H_2O$	0.68	$CoCl_2 \cdot 6\ H_2O$	2.55
$MgCl_2 \cdot 6\ H_2O$	0.15	$CuSO_4 \cdot 5\ H_2O$	9.45
$CaCl_2 \cdot 2\ H_2O$	0.09		
NaCl	0.22	*Buffer* [b]	*(mmol L^{-1})*
$NaHCO_3$	10.00	Hepes	50
NaFeEDTA	0.03		

[a] *KNO_3 was only added in the N+ medium in a concentration adapted to the desired nitrogen supply: high growth rates (at high light intensities: HL) required a higher nitrogen concentration in the N+ medium compared to lower growth rates (at low light intensities: LL).*

[b] *Buffer was added to shake flask growth medium only.*

2.2.2 Photobioreactor set-up

N. oleoabundans was continuously cultivated in a newly designed flat panel photobioreactor (Figure 2.1). The baffle and sparger-tube with holes on one side of the baffle ensure proper airlift operation. The curved design of the reactor improves the mixing pattern and minimises dead angles. The photobioreactor consists of three glass plates, which are held in place by three aluminium cover frames, all mounted onto the stainless

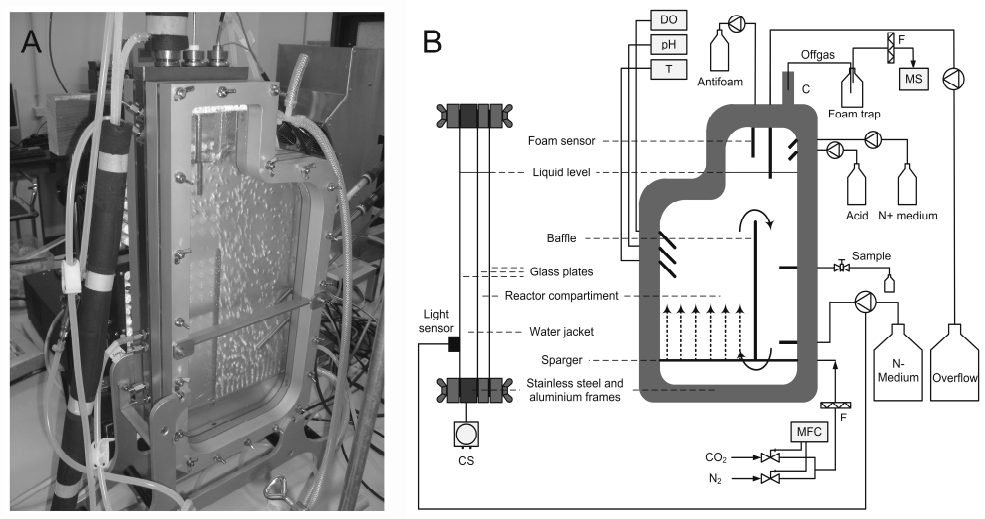

Figure 2.1 *(**A**) Newly designed flat panel photobioreactor and (**B**) Schematic overview of setup. C = condenser connected to separate cryostat (not shown), DO = dissolved oxygen sensor, F = air filter, MFC = mass flow controllers for both N_2 and CO_2, MS = mass spectrometer for off-gas analysis, pH = pH sensor connected via controller to acid pump, T = temperature sensor connected cryostat, CS = cryostat*

steel inner frame of the culture chamber. The culture chamber has a working volume of 1.7 L, a light path of 20 mm and an illuminated area of 0.085 m^2 (22.5 x 40 cm^2, minus the rounded corners).

Continuous illumination was provided by two red LED panels of 20x20 cm (LED Light Source SL 3500, average optimum 630-635 nm and a spectral half width of 20 nm, PSI, Czech Republic), stacked on top of each other. The exact photon flux density (PFD_{in}) at the surface of the algal culture was measured with a LI-COR 190-SA 2π sensor (PAR range 400-700 nm) at 44 fixed points before the start of the experiment at the inside of the front glass panel of the culture chamber. The measured irradiance was averaged to determine the exact amount of light entering the system.

A similar measurement at the rear of the reactor gave the amount of light falling through the system during cultivation ($PFD_{out.pbr}$). To obtain the proper value for light leaving the culture (PFD_{out}) the measured value was corrected for the light absorbed by the water jacket and the rear glass panels. This was done by measuring the light leaving the system when only medium and no cells were present (PFD_{blank}), and correcting $PFD_{out.pbr}$ for the amount of light loss in the system using the ratio between PFD_{blank} and

PFD_{in} (Equation 1):

$$PFD_{out} = \frac{PFD_{out.pbr}}{PFD_{blank}/PFD_{in}} \quad (1)$$

To be able to study light and nitrogen supply separately an experimental set-up was designed in which algae are grown in a continuous mode under turbidostat conditions. Turbidostat control was ensured by means of a light sensor (LI-COR 190-SA 2π sensor, PAR range 400-700 nm) attached to the rear glass panel of the reactor and connected to an ADAM-5000/485-AE data acquisition and control module (Advantech) and controlled via a LabView virtual instrument running on a PC (LabView 7.1, National Instruments Corporation, Austin). The amount of light falling through the reactor was monitored and compared to a set-point. When a value below the set-point was detected, the dilution pump was automatically switched on and the culture was diluted with filter sterilized (pore size 0.2 µm) dilution medium (N-) (Table 2.1). Continuous removal of the culture broth ensured a constant liquid level in the photobioreactor. The chosen set-point, together with the PFD_{in}, determined the average photon flux density in the system (PFD_{av}):

$$PFD_{av} = \frac{PFD_{in} - PFD_{out}}{\ln(PFD_{in}/PFD_{out})} \quad (2)$$

The corresponding light uptake rate in the system (quantum uptake rate r_γ in mol L^{-1} d^{-1}) could be calculated by dividing the light absorbed over the system by the light path of the reactor (δ_{pbr} in m):

$$r_\gamma = \frac{(PFD_{in} - PFD_{out}) \cdot 3600 \cdot 24 \cdot 10^{-9}}{\delta_{pbr}} \quad (3)$$

2.3 Experimental conditions

The culture was continuously supplied with a sterile and moisturized N_2 flow enriched in CO_2 (2% v/v) at a rate of 1200 mL min^{-1} using mass flow controllers (Brooks, Smart TMF SLA5850). The pH was maintained at 7.5 ± 0.1 by on demand addition of 1M hydrochlo-

ric acid and temperature was kept constant at 30°C by an external cryostat connected to the water jacket of the photobioreactor. Foam build-up was prevented by supplying a 1% (w/w) antifoam solution (Antifoam B® silicone emulsion, Mallinckrodt Baker B.V., Deventer, the Netherlands) when foam formation was detected by the foam sensor in the headspace of the photobioreactor. Dissolved oxygen was monitored online to ascertain that the culture was not subjected to inhibiting amounts of oxygen. The off gas composition was analysed using a prima dB mass spectrometer (ThermoFisher Scientific, USA). Both DO and gas composition were used to assess whether steady state conditions were maintained.

Two distinct light conditions were chosen in which $PFD\text{-}_{av}$ was kept at approximately 70 µmol m^{-2} s^{-1} (low light conditions; LL) and 200 µmol m^{-2} s^{-1} (high light conditions; HL). This corresponds with an r_γ of 0.76 and 1.68 mol L^{-1} d^{-1} respectively. To achieve this, PFD_{in} was set to approximately 200 µmol m^{-2} s^{-1} at LL and 500 µmol m^{-2} s^{-1} at HL. The threshold settings used for $PFD_{out.bpr}$ were 10 µmol m^{-2} s^{-1} and 50 µmol m^{-2} s^{-1} respectively.

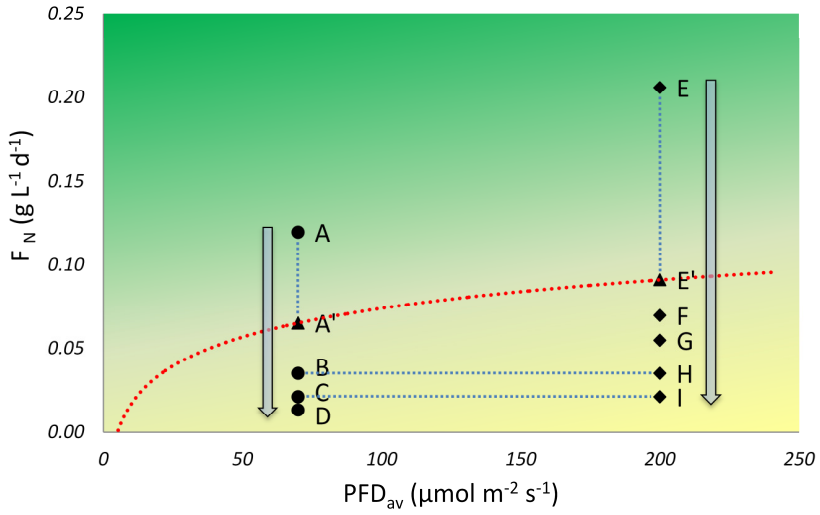

Figure 2.2 *Average photon flux densities ($PFD\text{-}_{av}$) of 70 (LL) and 200 µmol m^{-2} s^{-1} (HL) were combined with several nitrogen supply rates (F_N), resulting in nine different growth conditions ([A]-[I]). The red dotted line represents the settings where light supply rate and nitrogen supply rate are in balance. It is drawn through [A'] and [E'], which represent the calculated nitrogen consumption rates (r_N) of [A] and [E]. With F_N above this line (green area) the culture will be light limited, below the line it will be nitrogen limited (yellow area), where F_N is equal to r_N. The blue dotted lines connect experiments with the same r_N.*

The effect of nitrogen supply was studied independently from the effect of PFD_{av}, by using a continuous filter sterilized (pore size 0.2 μm) nitrogen feed (N+ medium, Table 2.1) which was added separately from the dilution medium (Figure 2.1). In total nine settings were tested, combining LL and HL with several nitrogen supply rates (F_N): [A] 0.120; [B] 0.035; [C] 0.021; and [D] 0.013 g L^{-1} d^{-1} for LL and [E] 0.206; [F] 0.070; [G] 0.055; [H] 0.035 and [I] 0.021 g L^{-1} d^{-1} for HL. These combinations of PFD_{av} and F_N put experimental conditions [A] and [E] in the light limited regime, while all the other conditions were nitrogen limited, as can be seen in Figure 2.2. Furthermore, experiment [C] and [I] and experiment [B] and [H] had similar nitrogen supply rates (and thus consumption rates, r_N) at two different light intensities.

2.2.4 Photobioreactor operation

After sterilization of the system (3 hours at 121°C), it was filled with filter sterilized N+ medium and was inoculated at an optical density at 750 nm (OD_{750}) of 0.05. The culture was grown in batch mode and when a biomass concentration of 0.5 g L^{-1} was reached, the continuous nitrogen supply and the turbidostat control were started, and the culture was allowed to reach steady state. In these experiments, steady state was defined as a constant biomass concentration, cell characteristics (e.g. pigmentation, cell size), off gas concentrations and dilution rate during a period of at least 3 residence times, or at least 6 days at the lowest growth rates ([C],[D] and [I]). The growth rate μ (d^{-1}), which is equal to the dilution rate D (d^{-1}) in steady state, was calculated by monitoring the amount of overflow produced in 24 hours.

$$\mu = D = \frac{V_{24h}}{V_{pbr}} \qquad (4)$$

2.5 Biomass Analysis

Every day at the same time biomass samples were taken from the photobioreactor to monitor the steady state. The samples were analysed for dry weight biomass concentration, optical density (OD_{750}, OD_{480} and OD_{680}), cell concentration and cell size, as described by (Kliphuis et al., 2012). The absorption cross section of the dry biomass (α_{DW} in m^2 g^{-1}) was monitored as a measure for cell pigmentation and could be determined by using a spectrophotometer with an integrating sphere, as described by (Vejrazka et al., 2011). The supernatant of each sample was analysed for residual nitrate, phosphate and sulphate, by means of ion chromatography (Metrohm Compact IC 761 equipped with a

conductivity detector, using the pre-column Metrohm Metrosep A Supp 4/5 Guard and the column Metrohm Metrosep A Supp 5, 150/4.0 mm).

When steady state was achieved, formation of lipid bodies in the algal cells was evaluated by staining TAG with a lipophilic fluorescent dye BODIPY 505/515 (4,4-difluoro-1,3,5,7-tetramethyl-4-bora-3a,4a-diazasindacene; Invitrogen Molecular Probes, Carlsbad, CA) and subsequent visualization using a confocal laser scanning microscope (LSM510; Carl Zeiss, Jena, Germany), as described by (Cooper et al., 2010) with several modifications. A 40 µM BODIPY stock solution was prepared by dissolving the dye in 0.2% (v/v) anhydrous dimethyl sulfoxide (DMSO). 4 µL of this solution was added directly to 200 µL undiluted cell suspension and incubated for 10 minutes. Stained lipid bodies (fluorescent at 515nm, visualised in yellow) and chlorophyll (auto fluorescent at 690 nm, visualised in red) were excited using a 488 nm Argon Laser and detected through a band pass (505-550 nm) and long pass filter (650 nm) respectively.

A larger biomass sample was taken when steady state was reached, by collecting the overflow of the reactor on ice for a period of exactly 24 hours. This biomass was centrifuged, washed and lyophilized as described by (Kliphuis et al., 2012). Freeze dried algae powder was used for further biomass composition analysis.

The total fatty acid (TFA) content and fatty acid composition of the algal cells was determined by gas chromatography after extraction with a 5:4 methanol:chloroform mixture and subsequent transesterification, as described by (Bligh and Dyer, 1959) with modifications as suggested by (Lamers et al., 2010) and (Santos et al., 2012). The TAG content of the cells was determined after separating the apolar lipids from the polar membrane lipids, by eluting 2 mg of the total lipid extract (obtained in similar fashion as for the fatty acids) over a silica SPE column (Sep-Pak Vac Silica cartridge 6cc/1000mg, 125Å, 55-105 µm, Waters) with 10 mL of chloroform. All polar lipids were retained by the column, while the TAG containing pool was eluted. This pool was collected and was analysed for its fatty acid content and composition in the same way as described for the total fatty acids.

The elemental composition of biomass (CHN, in mol/C-mol) was determined using a Flash EA 2000 elemental analyser (ThermoFisher Scientific, USA). CHN was corrected for the ash present in biomass, which was determined as described by (Kliphuis et al., 2012). The remainder of the biomass was assumed to be oxygen.

2.3 Results and discussion

2.3.1 Nitrogen limitation in a turbidostat operated photobioreactor

2.3.1.1 Growth

When an excess of nitrogen was supplied, the specific growth rate μ was limited by the light supplied to the system. For the average photon flux density (PFD_{av}) of 70 μmol m^{-2} s^{-1} a μ of 1.15 ± 0.10 d^{-1} was found, while a PFD_{av} of 200 μmol m^{-2} s^{-1} resulted in a μ of 1.74 ± 0.03 d^{-1}. The data points of these reference experiments are encircled in Figure 2.3A. Residual nitrogen was observed in these cultures (0.047± 0.002 and 0.066±0.002 g L^{-1} for [A] and [E] respectively), which confirms the nitrogen replete status. The nitrogen consumption rate (r_N in g L^{-1} d^{-1}) for these cultures was calculated on the basis of a nitrogen balance over the system. Figure 2.3A also shows the light limited specific growth rates as a function of their calculated nitrogen consumption rate and these are connected to the equivalent supply rate with dashed lines.

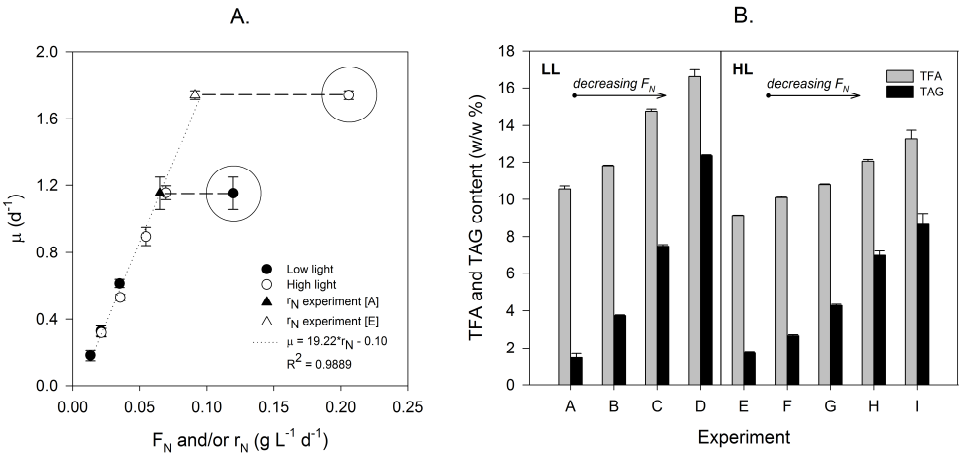

Figure 2.3.

A. *The effect of nitrogen supply rate F_N (g L^{-1} d^{-1}) on specific growth rate μ (d^{-1}). The encircled points are the reference experiments [A] and [E] under light limited growth conditions. The nitrogen consumption rates r_N (g L^{-1} d^{-1}) of these experiments are also shown (filled and open triangles) and connected to their corresponding F_N with dashed lines.*

B. *Total fatty acid (TFA) and triacylglyceride (TAG) content.*

F_N was reduced to several set-points below the nitrogen consumption rate of the reference experiment. This resulted in 3 additional steady states under low light (LL) and 4 steady states under high light (HL) conditions. Residual nitrate measurements of these steady states showed no detectable residual nitrate in the medium, indicating that these growth conditions were nitrogen limited.

Hence, the nitrogen supply rates plotted in Figure 2.3A equal the nitrogen consumption rates for these experiments. A linear positive correlation was found between r_N and μ throughout the tested experimental conditions (dotted line in Figure 2.3A). Linear regression on all measured specific growth rates and their corresponding consumption rates gave a slope of 19.22 ± 0.77 L g^{-1} and an intercept of -0.10 ± 0.04 d^{-1}, with an R^2 of 0.9889. The inverse of the slope can be regarded as the amount of nitrogen assimilated per reactor volume: 0.052 g L^{-1} of reactor. The linear relationship suggests that the amount of nitrogen that is assimilated per reactor volume is approximately constant for all experiments.

In Table 2.2, the amount of nitrogen bound in biomass is given for each steady state. This number is calculated by multiplying the measured biomass concentration in the system (C_X in g L^{-1}) with its measured nitrogen content (f_N in g g^{-1}). The values calculated for the amount of nitrogen bound in biomass per reactor volume approximate the value for assimilated nitrogen obtained through linear regression. At the lowest nitrogen supply rates the $C_X \cdot f_N$ values tend to be lower, which may be explained by an increase of cell lysis under severe nutrient limitation. Dissolved extracellular compounds will not end up in C_X and therefore the measured $C_X \cdot f_{N\text{-}}$ values for the most extreme stress conditions may be lower than the values obtained through regression on μ and r_N. Values for this latter parameter are calculated based on the nitrogen balance (i.e. the amount of nitrogen entering and leaving the system) and therefore regard N bound in dissolved organic material as part of the biomass.

Turbidostat regulation implies a fixed light absorbance over the system, since the amount of light coming out of the reactor is kept at a set point. The fixed absorbance for either the LL or HL experiments, together with a constant amount of nitrogen assimilated per reactor volume suggests that the total amount of light absorbing material (e.g. photosystems) at each light setting is closely correlated with the total amount of nitrogen assimilated. This correlation seems plausible when assuming photosynthetic proteins (and thus nitrogen) should be present in a certain ratio with respect to absorbing material to have a functional photosystem. The percentage of absorbed light ($[PFD_{in}-PFD_{out}]/PFD_{in}*100\%$) was slightly different for both light settings: 91% of incident light for LL and 85% for HL. This difference indicates that under high light conditions, less

absorbing material was present at the same amount of nitrogen assimilated, compared to the low light experiments. In other words, the algal cells contained more nitrogen per absorbing matter under HL than they did under LL conditions. This capability of algae to adapt the amount of pigments in their photosystems to the amount of light they are exposed to is commonly known as photoacclimation (Falkowski and LaRoche, 1991).

2.3.1.2 TAG accumulation

The CLSM pictures of Figure 2.4 (page 31) clearly show the presence of multiple TAG containing particles in *Neochloris oleoabundans* under nitrogen limited conditions [B], [C], [H] and [I]. These TAG containing particles are lipid bodies, in which TAG is known to be accumulated (Goodson et al., 2011). Under nitrogen replete conditions ([A], [E]) some individual cells already contained a minor amount of relatively small lipid bodies. When the nitrogen supply rate was progressively decreased (from left to right in Figure 2.4), the amount of lipid bodies increased and they became larger. More and larger lipid bodies also resulted from increasing the average photon flux density for the same nitrogen supply rate (from top to bottom in Figure 2.4). This increase in TAG containing material confirms our hypothesis that excess of absorbed energy is at least partly channelled into storage compounds when growth is reduced by nitrogen limitation.
Analysis of the total fatty acid (TFA) and triacylglyceride (TAG) content confirmed the CLSM observations. TAG content increased with declining F_N at equal PFD_{av} (Figure 2.3B), and TAG content also increased with increasing PFD_{av} at equal F_N (Figure 2.3B, compare [B] with [H] and [C] with [I]). These measurements prove that nitrogen limitation in combination with turbidostat operation can be used to continuously sustain a dividing cell population with a tuneable, elevated TAG content.

2.3.1.3 Physiological changes

While the TAG content increased substantially when decreasing F_N, the TFA content did not show such a strong rise (Figure 2.3B). Because of this, the percentage of TAG in TFA increased upon nitrogen limitation (Table 2.2). This indicates that acyl lipids other than TAG, such as the polar acyl lipids in the cell and organelle membranes, were less abundant in the 'stressed' cells.

Table 2.2 *Summary of experimental results.*

[a] *Rows indicated with '±' indicate the standard deviation of the measurement (n≥3).*

[b] *For the calculation of % r_X the measured volumetric productivity was compared to the reference experiment ([A] for LL and [E] for HL).*

Experiment	A	B	C	D	E	F	G	H	I
F_N (g L^{-1} d^{-1})	0.120	0.035	0.021	0.013	0.206	0.070	0.055	0.035	0.021
± [a]	0.000	0.000	0.000	0.000	0.000	0.000	0.000	0.000	0.000
r_N (g L^{-1} d^{-1})	0.065	0.035	0.021	0.013	0.091	0.070	0.055	0.035	0.021
±	0.009	0.000	0.000	0.000	0.005	0.000	0.000	0.000	0.000
PFD_{av} (µmol m^{-2} s^{-1})	73	71	71	73	206	207	207	209	207
r_Y (mol L^{-1} d^{-1})	0.76	0.77	0.77	0.76	1.69	1.68	1.68	1.68	1.68
μ (d^{-1})	1.15	0.61	0.33	0.18	1.74	1.15	0.89	0.53	0.32
±	0.10	0.02	0.03	0.03	0.03	0.04	0.05	0.02	0.03
C_X (g L^{-1})	0.65	0.94	1.07	1.43	0.74	0.89	0.99	1.24	1.41
±	0.04	0.05	0.06	0.07	0.04	0.03	0.03	0.04	0.04
r_X (g L^{-1} d^{-1})	0.75	0.57	0.35	0.26	1.29	1.03	0.88	0.66	0.45
% r_X (-) [b]	100	76	47	35	100	80	68	51	35
TFA content (w/w%)	10.5	11.8	14.8	16.6	9.1	10.1	10.8	12.0	13.3
±	0.2	0.0	0.1	0.4	0.0	0.1	0.0	0.1	0.5
TAG content (w/w%)	1.5	3.7	7.5	12.4	1.7	2.7	4.3	7.0	8.7
±	0.2	0.0	0.1	0.1	0.1	0.1	0.1	0.2	0.6
% TAG in TFA (w/w%)	14	32	51	74	19	26	40	58	65
r_{TFA} (mg L^{-1} d^{-1})	79	67	52	43	118	104	95	79	60
r_{TAG} (mg L^{-1} d^{-1})	11	21	26	32	22	27	38	46	39
f_N (g g^{-1})	0.076	0.058	0.049	0.032	0.067	0.058	0.052	0.038	0.031
±	0.000	0.000	0.000	0.000	0.000	0.001	0.000	0.000	0.000
C_X*f_N (g L^{-1})	0.050	0.055	0.053	0.045	0.049	0.052	0.051	0.047	0.044
α_{DW} (m^2 g^{-1})	0.161	0.114	0.102	0.062	0.14	0.103	0.090	0.064	0.054
±	0.004	0.01	0.004	0.005	0.007	0.003	0.003	0.005	0.003
PNR (mol y mol N^{-1})	163	307	509	805	259	339	432	663	1102
$Y_{X.E}$ (g mol^{-1})	0.99	0.75	0.46	0.34	0.76	0.61	0.52	0.39	0.27
$Y_{TAG.E}$ (g mol^{-1})	0.015	0.028	0.034	0.042	0.013	0.016	0.022	0.027	0.023

Besides the accumulation of TAG containing lipid bodies and a reduction in membrane lipids, other physiological changes were observed in nitrogen limited *N. oleoabundans* as well. For example, the absorption cross section of the dry biomass, α_{DW} (m^2 g^{-1}), decreased at lower F_N and the same effect was found when more light was supplied to the system (Table 2.2). Because α_{DW} can be regarded as a measure for cell pigmentation, its decline indicated that the amount of pigments per gram of dry weight decreased when more 'stress' was experienced by the cells. The CLSM pictures of Figure 2.4 also support this observation, since the autofluorescence of chlorophyll became substantially less under nitrogen limiting conditions. A decreasing chlorophyll content (chlorosis) and photosynthetic membrane degradation upon nitrogen limitation and/or increased light intensity are well described and may be considered as a general response of microalgae to nitrogen shortage (Falkowski and LaRoche, 1991; Rhiel et al., 1985; Turpin, 1991).

An additional effect of a lower α_{DW} was the higher biomass concentration C_X (g L^{-1}), as the turbidostat operation of the system dictates that a fixed amount of light should be absorbed. Hence more biomass was allowed in the system when cell pigmentation decreased due to nitrogen limitation. C_X ranged from 0.65 ± 0.04 g L^{-1} and 0.74 ± 0.04 g L^{-1} under replete conditions, to 1.07 ± 0.06 g L^{-1} and 1.41 ± 0.04 g L^{-1} under comparable nitrogen limited conditions, for LL and HL conditions respectively (Table 2.2).
Finally, the cellular nitrogen content (f_N) decreased from 0.076 and 0.067 g g^{-1} for LL and HL, to a minimum of 0.032 and 0.031 g g^{-1} respectively. This is a commonly observed effect of nitrogen starvation in microalgae and can be attributed mainly to a decrease in protein content (Rhiel et al., 1985).
The physiological changes and the appearance of lipid bodies in *Neochloris oleoabundans* observed in our nitrogen-limited turbidostat experiments are comparable to the effects of nitrogen starvation in other green microalgae in batch culture. This suggests that our experimental set-up, although different from the classic two phase stress approach, triggers a similar stress response in *N. oleoabundans*. In this case however, steady states were obtained for various levels of stress with cell division and TAG accumulation occurring simultaneously, which enables thorough analysis of the specific stress response.

2.3.1.4 Biomass and TAG productivities

Under nutrient replete conditions specific biomass productivity r_x (g L^{-1} d^{-1}) was much higher under HL (1.29 g L^{-1} d^{-1}) than under LL conditions (0.75 g L^{-1} d^{-1}), as can be seen in Figure 2.5A. Nitrogen limitation caused a substantial decrease in r_x for both average

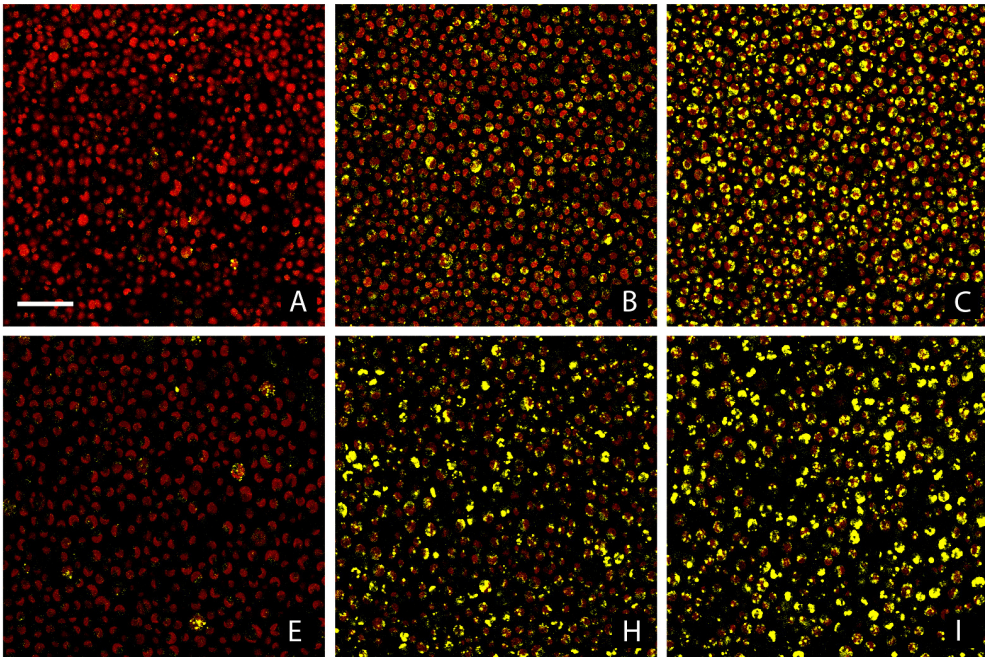

Figure 2.4 *CLSM pictures of Neochloris oleoabundans with TAG containing lipid bodies. Chlorophyll autofluorescence is pictured in red, Bodipy fluorescence (indicating TAG lipid bodies) in yellow. The white scale bar indicates 20 µm and the letters indicate the experiment during which the picture was taken. Nitrogen supply rate decreases from left to right, light supply rate increases from top to bottom.*

photon flux densities. Only 35% of the specific biomass productivity was found for the lowest F_N for each light intensity, compared to the nutrient replete conditions (Table 2.2).

While the rate of both biomass and total fatty acid production (r_{TFA} in mg L^{-1} d^{-1}) dwindled, the rate of TAG production (r_{TAG} in mg L^{-1} d^{-1}) increased (Figure 2.5B) due to the accumulation of TAG in the cells (Figure 2.3B). A maximum r_{TAG} of 46 mg L^{-1} d^{-1} was observed for HL conditions (square in Figure 2.5B). Decreasing F_N even further did not yield a higher r_{TAG} under HL conditions, as the rise in TAG content no longer compensated for the loss in biomass productivity. TAG productivity was lower at LL compared to HL, but the highest level observed in this study (32 mg L^{-1} d^{-1}) was almost 3 times higher than the reference productivity at replete conditions (11 mg L^{-1} d^{-1}).

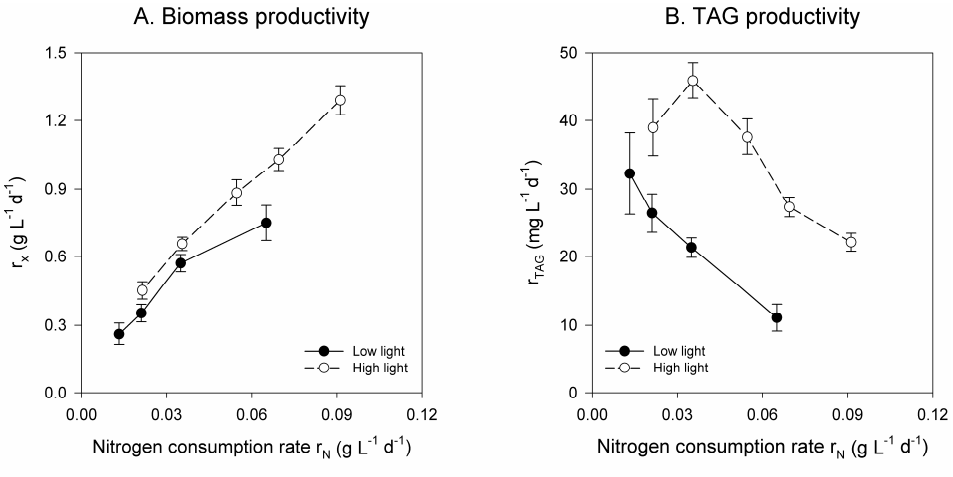

Figure 2.5 *Productivities of biomass (**A**) and TAG (**B**) at different nitrogen consumption rates.*

2.3.2 Energy use in N. oleoabundans under nitrogen limitation

The biomass productivity in our experiments declined with increasing nitrogen limitation (Figure 2.5A). Because turbidostat operation ensured a constant amount of light to be absorbed by the system, an identical specific rate of light uptake was maintained for every steady state at either LL or HL. Therefore nitrogen limitation caused a decrease in the yield of biomass on light ($Y_{X.E}$ in gram biomass produced per mol photons absorbed) as well.

$$Y_{X.E} = \frac{\text{biomass produced}}{\text{photons absorbed}} = \frac{r_x}{r_\gamma} \qquad (5)$$

The decreasing yields suggest that a large part of the energy absorbed by the system under nitrogen limitation is not ending up in biomass. To illustrate this, biomass yield on light was plotted against the photon-nitrogen uptake ratio (PNR) in Figure 2.6A. PNR is defined as mol photons absorbed per mol nitrogen assimilated (Equation 6), and a high PNR thus indicates a large imbalance between energy and nitrogen fluxes into the cell.

$$PNR = \frac{\text{photon absorption rate}}{\text{nitrogen consumption rate}} = \frac{r_\gamma \cdot MW_N}{r_N} \qquad (6)$$

A clear negative correlation between the biomass yield on light and PNR was observed, regardless of the average photon flux density applied. Accumulation of energy sinks such as TAG at increasing PNR could increase the electron demand for biomass production and therefore negatively affect the yield of biomass on light. To assess whether an increased electron demand for biomass formation could (partly) explain the observed decrease in $Y_{X.E}$, the degree of reduction (DR) of biomass for growth on nitrate was calculated, based on the measured elemental composition measured for each steady state (Table 2.3).

Table 2.3 *Elemental composition, ash content and degree of reduction.*

Experiment	A	B	C	D	E	F	G	H	I
C (mol/ C-mol)	1.00	1.00	1.00	1.00	1.00	1.00	1.00	1.00	1.00
H (mol/ C-mol)	1.70	1.60	1.70	1.71	1.73	1.68	1.69	1.73	1.74
N (mol/ C-mol)	0.14	0.10	0.09	0.06	0.12	0.11	0.09	0.07	0.06
O (mol/ C-mol)	0.58	0.59	0.59	0.62	0.64	0.65	0.65	0.66	0.68
Ash content (g g^{-1})	0.062	0.054	0.049	0.037	0.067	0.059	0.057	0.043	0.039
DR (mol e^- g^{-1})	0.21	0.20	0.20	0.19	0.20	0.19	0.19	0.19	0.18

The DR represents the amount of electrons required to produce one gram of biomass of a given composition from its substrates. As shown in Figure 2.6A, the DR only marginally differs between the experiments. Whilst TAG accumulation up to 12.4% increased the DR, the decrease in nitrogen content counteracted this, since the reduction of nitrate for assimilation into biomass is an important electron sink as well. The rather constant DR observed in these experiments implies that the electron demand per gram biomass was hardly affected by nitrogen limitation. Thus, the observed change in macromolecular biomass composition (e.g. TAG) cannot be the cause of the 3-fold reduction of $Y_{X.E}$ at high PNR.

Other causes for the observed decrease in $Y_{x.E}$ may be an increased energy demand for non-growth related maintenance (e.g. damage repair or proton gradient stabilization) and for transport and assembly of macromolecules (Kliphuis et al., 2012), or an increased dissipation of absorbed light energy as heat and fluorescence. The latter phenomenon occurs when excess light causes saturation of the photosystems (Krause and Weis, 1991) and is most likely the main cause of energy wastage observed in our nitrogen-limited turbidostat experiments. Similar behaviour has been observed for cells under nitrogen limitation and starvation by (Kolber et al., 1988) and (Pan et al., 2011) and

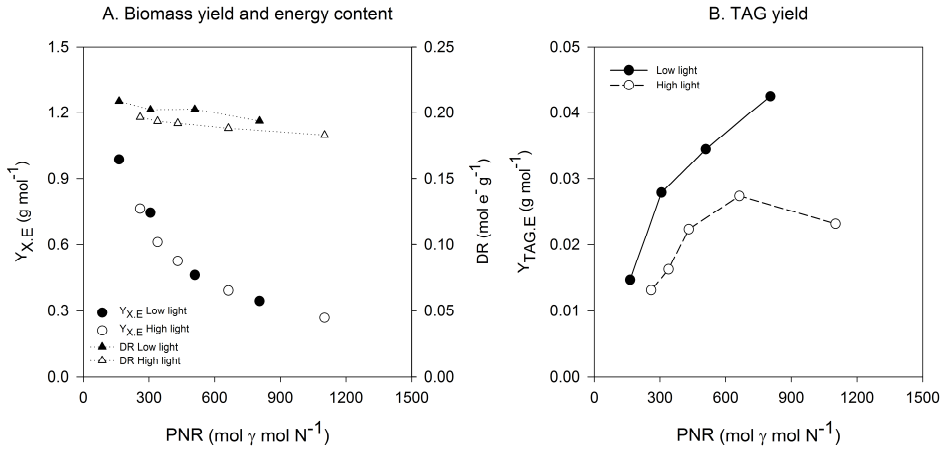

Figure 2.6

A. *Yield of biomass on light and biomass energy content (i.e. degree of reduction) as a function of PNR.*

B. *Yield of TAG on light as a function of PNR.*

in particular by (Jakob et al., 2007) who also found substantial reduction of $Y_{X.E}$ in *Phaeodactylum tricornutum* grown under continuous nitrogen limitation.

In contrast to biomass productivity, TAG productivity increased as r_N was reduced (Figure 2.5B). This was expected based on our hypothesis that reducing r_N results in an excess of energy in the photosystems and that TAG could act as an energy sink. Because the surplus of energy received under HL is larger than under LL conditions, a higher r_{TAG} was observed under HL for similar r_N. As TAG productivity increased upon nitrogen limitation, the yield of TAG on light ($Y_{TAG.E}$) increased accordingly:

$$Y_{TAG.E} = \frac{\text{TAG produced}}{\text{photons absorbed}} = \frac{r_{TAG}}{r_{\gamma}} \qquad (7)$$

In Figure 2.6B, $Y_{TAG.E}$ is presented as a function of PNR. In contrast to $Y_{X.E}$, the efficiency of TAG accumulation at elevated energy pressures increased. Also, a clear discrepancy between $Y_{TAG.E}$ under LL and HL conditions was observed. Apparently, the yield of TAG on light is not only influenced by the extent of the energy imbalance in the photosystems, but also by the total amount of energy that is absorbed by the cells.

2.3.3 Algae cope with energy imbalances by wasting energy, rather than storing it in energy sinks

The wasting of light energy at high 'nitrogen stress' that was observed may have been caused by several phenomena, of which the most likely is dissipation of light energy as heat and fluorescence. It was also shown that the TAG content of biomass increased upon increasing PNR, indicating that TAG is indeed used as an electron sink by *Neochloris oleoabundans*. However, the loss in $Y_{X.E}$ was at least an order of magnitude larger than the gain in $Y_{TAG.E}$ due to nitrogen limitation. Thus the contribution of TAG as an energy sink is minimal when considering the total amount of light energy wasted by dissipation before even entering the metabolism, suggesting that under nitrogen limited conditions energy is dissipated rather than stored into macromolecules like TAG.

At higher PNR, *N. oleoabundans* produced less absorptive surface per gram biomass. This trend is reflected in a lower f_N (indicating a lower protein content), less membrane lipids and less chlorophyll fluorescence. Taken together these trends suggest a smaller amount of photosynthetic machinery per gram biomass. Recently, (Davis et al., 2012) showed the presence of unbound chlorophyll in lipid bodies in nitrogen starved *N. oleoabundans*, which suggests that photosystems are degraded under nitrogen starvation. This puts a new perspective on the function of lipid body formation as a stress response. Lipid bodies do not merely serve as an electron sink and energy storage, but also as a place for (temporarily) storing building blocks of the photosystem. Recent discoveries of a chloroplast pathway for TAG synthesis by (Fan et al., 2011) and the association of lipid body formation with the chloroplast membrane by (Goodson et al., 2011) support this assumption.

Overall it seems that reducing the amount of energy entering metabolism, either through a reduction of the photosystems or through energy dissipation or a combination of both, is the prevailing mechanism of *N. oleoabundans,* and possibly more green algae, for coping with a high PNR.

2.3.4 $Y_{X.E}$ is a reflection of the capacity of a microalga to channel light energy into its metabolism

To have a higher TAG production rate and yield, the energy pressure on algal photosystems should be increased. However, this will lead to a loss in biomass productivity and yield, because energy is wasted rather than used for TAG production. The extent to which excess energy can be channelled into the metabolism and thus into macromolecules such as TAG under nitrogen limitation or starvation is likely to be species specific.

(Breuer et al., 2012) already showed that under nitrogen depleted conditions, in standardized experiments, 9 algal species reacted very differently towards the excess of light energy experienced by the cells. A striking example was *Scenedesmus obliquus,* which was able to keep on producing biomass under nitrogen deprived conditions up to almost 8 times the amount present at the onset of starvation, compared to a factor 3 for *N. oleoabundans*. In other words, *S. obliquus* was much more efficient under nitrogen depleted conditions in converting energy into nitrogen-free molecules than *N. oleoabundans*.
This example illustrates that the capacity to maintain high $Y_{X.E}$ under nitrogen depletion can vary tremendously between species. The capability to continue converting energy under nitrogen stress is a factor that should be taken into consideration when optimising a TAG production system, but also when screening for a suitable host for storage metabolite production in general. As $Y_{X.E}$ puts an upper limit on the amount of energy that can be channelled into storage macromolecules such as TAG, it also puts the upper limit on the possible gain in TAG accumulation that can be made through altering secondary metabolism.

2.3.5 Future research perspective

With this experimental set-up it was demonstrated that TAG productivity could be increased several times, while maintaining steady state growth, in green microalgae that scarcely produce TAG under optimal growth conditions. Earlier studies in which the effect of continuous nitrogen limitation on (neutral) lipid productivity was tested without controlling the light energy uptake rate (chemostat mode), reported contradicting results ranging from either no significant change in lipid content (Richardson et al., 1969), and a small increase in lipid content (Sukenik and Wahnon, 1991) and a decreasing neutral lipid productivity (Lacour et al., 2012b). (Hoffmann et al., 2010) grew *Nannochloropsis salina* under turbidostat operation with growth limiting nitrogen loads in the diluting medium, but did not observe increased TFA productivity (TAG was not assessed). It was shown that by controlling light energy intake by turbidostat operation and energy used for growth by a separate nitrogen supply, TAG production in *N. oleoabundans* can indeed be increased. The maximum productivity obtained in this study (46 mg L^{-1} d^{-1}) is still up to a factor 10 lower than the highest TAG production rates that can be obtained in classic batch or semi-continuous run out systems (Breuer et al., 2012; Griffiths et al., 2011; Mata et al., 2010; Rodolfi et al., 2009). It should be noted that the highest TAG productivities found in (fed) batch systems are reached for short periods of time at the start of the accumulation phase, while in our nitrogen limited turbidostats TAG is continuously being produced. Therefore optimisation of the nitrogen limited

turbidostat system may eventually lead to higher productivities and thus deserves further exploration.

The strength of this particular experimental set-up is not necessarily in commercial TAG production, but in its application in research. Because it enables cells to keep dividing, steady state conditions can be obtained in which the energy balance can be precisely controlled. These stable conditions provide an opportunity to thoroughly investigate the effect of the imposed stress on cell physiology, without the complicating effects of changing environmental conditions. The output generated by these experiments is very suitable for metabolic modelling and flux balance analysis, as well as transcriptomics and proteomics, all of which are techniques that are becoming more and more important for a better understanding of the regulation of TAG accumulation in green microalgae.

2.4 Conclusions

A flat panel photobioreactor with turbidostat control was used to create a defined energy imbalance in the metabolism of *Neochloris oleoabundans* under steady state, nitrogen-limited conditions. These settings allowed simultaneous cell replication as well as elevated TAG accumulation rates, supporting the hypothesis that TAG production is caused by an imbalance in energy demand and supply. However, excess energy was preferably dissipated rather than incorporated into energy storage molecules. The extent of energy dissipation is likely species specific and thus the capability to sustain efficient light use under stress conditions is an important consideration when searching for efficient TAG producing microalgae.

Acknowledgements

The authors would like to thank Jan Willem Borst and Boudewijn van Veen (Laboratory of Biochemistry, Wageningen University) for their help with obtaining the CLSM pictures presented in this article, Laura Garcia Alba (Laboratory of Sustainable Process Technology, University of Twente) for her help with the analysis of the elemental compositions and Ana Santos (Bioprocess Engineering, Wageningen University) for her courtesy of providing the CLSM pictures of *Neochloris* for the graphical abstract. As this work was performed within the TTIW-cooperation framework of Wetsus, Centre of Excellence for Sustainable Water Technology (www.wetsus.nl), the authors would like to thank the participants of the Wetsus research theme 'Algae' for the discussions and their financial support. Wetsus is funded by the Dutch Ministry of Economic Affairs.

Nomenclature

α_{DW}	Absorption cross section of the dry biomass ($m^2\ g^{-1}$)
CLSM	Confocal laser scanning microscopy
C_X	Biomass concentration ($g\ L^{-1}$)
D	Dilution rate (d^{-1})
DR	Degree of reduction (mol electrons per g biomass^{-1})
δ_{pbr}	Light path of the photobioreactor(m)
F_N	Nitrogen supply rate ($g\ L^{-1}\ d^{-1}$)
HL	High light intensity
LL	Low light intensity
μ	Specific growth rate (d^{-1})
MW_N	Molecular weight of nitrogen ($g\ mol^{-1}$)
PFD_{av}	Average photon flux density in the system ($\mu mol\ m^{-2}\ s^{-1}$)
PFD_{blank}	Photon flux density leaving the photobioreactor containing only growth medium ($\mu mol\ m^{-2}\ s^{-1}$)
PFD_{in}	Photon flux density entering the algal culture ($\mu mol\ m^{-2}\ s^{-1}$)
PFD_{out}	Photon flux density leaving the algal culture ($\mu mol\ m^{-2}\ s^{-1}$)
$PFD_{out.pbr}$	Photon flux density leaving the photobioreactor ($\mu mol\ m^{-2}\ s^{-1}$)
PNR	Photon Nitrogen uptake Ratio: photon absorption rate over the nitrogen uptake rate in the system (mol γ mol N^{-1})
f_N	Mass fraction of nitrogen in biomass ($g\ g^{-1}$)
r_γ	Light uptake rate ($mol\ L^{-1}\ d^{-1}$)
r_N	Nitrogen consumption rate ($g\ L^{-1}\ d^{-1}$)
r_{TAG}	Volumetric TAG productivity ($mg\ L^{-1}\ d^{-1}$)
r_X	Volumetric biomass productivity ($g\ L^{-1}\ d^{-1}$)
$\%r_X$	Relative volumetric biomass productivity (-)
TAG	Triacylglycerol
TFA	Total fatty acids
V_{24h}	Volume of overflow collected over 24 hours ($L\ h^{-1}$)
V_{pbr}	Working volume of the photobioreactor (L)
$Y_{x.E}$	Yield of biomass on light ($g\ mol^{-1}$)
$Y_{TAG.E}$	Yield TAG on light ($g\ mol^{-1}$)

Chapter 3

A model for customising biomass composition in continuous microalgae production

This chapter has been published as:

Anne J. Klok , Johannes A. Verbaanderd, Packo P. Lamers, Dirk E. Martens, Arjen Rinzema, René H. Wijffels (2013 *A model for customising biomass composition in continuous microalgae production* Bioresource Technology 146, pp. 89-100

Abstract

A kinetic model is presented that describes functional biomass, starch and storage lipid (TAG) synthesis in the microalga *Neochloris oleoabundans* as a function of nitrogen and light supply rates to a nitrogen-limited turbidostat cultivation system. The model is based on the measured electron distribution in *N. oleoabundans*, which showed that starch is the primary storage component, whereas TAG was only produced after an excess of electrons was generated, when growth was limited by nitrogen supply. A fixed 8.6% of the excess electrons ended up in TAG, suggesting close metabolic interactions between nitrogen assimilation and TAG accumulation, such as a shared electron pool. The proposed model shows that by manipulating the cultivation conditions in a light or nitrogen limited turbidostat, algal biomass composition can be customised and the volumetric productivities and yields of the major biomass constituents can be changed on demand.

3.1 Introduction

Microalgae are considered promising candidates for the sustainable production of numerous products. These products range from pigments, poly-unsaturated fatty acids and proteins for the food or pharmaceutical market, to storage compounds such as triacylglyceride (TAG) or starch as raw materials for biofuel and commodity materials (Mata et al., 2010). However, when aiming at competitive production of microalgal products for the commodity market, the full potential of algal biomass must be exploited to compensate for the current production cost (Harrison et al., 2013; Wijffels et al., 2010). This biorefinery concept implies that total biomass composition will largely determine the profit that can be made on an algal product.

As the composition of algal biomass is heavily dependent on the culture conditions, manipulating these conditions can be a strategy for obtaining a tailor-made biomass composition (Harrison et al., 1990). For example, nitrogen depletion is the preferred strategy to increase TAG and starch fractions in biomass, at the expense of protein synthesis which requires the presence of nitrogen in the growth medium (Ball et al., 1990; Hu et al., 2008). Nitrogen availability directly influences the balance between energy absorbed in the photosystems and reducing potential used in anabolism, as up to 55% of microalgal carbon assimilation is coupled to nitrogen assimilation (Huppe and Turpin, 1994). Based on this close interaction, it is often hypothesized that under nitrogen limitation, the excess of reducing potential and energy produced in the photosystems can be used in the synthesis of storage compounds (Li et al., 2013). This helps to maintain a safe level of reducing potential in the photosystems and thus to prevent damage to the photosystems (Ledford and Niyogi, 2005), while at the same time energy is stored (Hu et al., 2008; Li et al., 2010b).

Besides resulting in storage compound accumulation, nitrogen limitation has as an undesirable effect: more energy is dissipated in the photosystems in order to equilibrate the energy imbalance (Kolber et al., 1988) and this strongly reduces the carbon assimilation capacity of the alga (Turpin, 1991). Recently we have shown that energy dissipation is the predominant mechanism for dealing with an excess of reducing potential in the photosystems in *Neochloris oleoabundans* cultivated under nitrogen limitation (Klok et al., 2013a).This links storage compound accumulation to a lower yield of algal biomass on available light, which is detrimental for production economics, as yield on light is directly proportional to the aerial productivity (Richmond, 2004).

Understanding the interactions between nitrogen assimilation, storage compound accumulation and photosynthesis will help to determine the optimal culture conditions for obtaining biomass of a desired composition. Several models have been developed that

describe the effects of light and nutrient supply on photosynthesis, growth, TAG and/or carbohydrate accumulation in microalgae in batch (Packer et al., 2011; Quinn et al., 2011) and continuous processes (Mairet et al., 2011). However, to date no model is available that evaluates biomass composition, as well as the productivities and yields of separate biomass components as a function of cultivation conditions and as such explores the potential of algal biomass as a whole.

In this paper a kinetic model is presented that describes the combined effect of nitrogen and light supply on the electron distribution in microalgal cells, and on the biomass composition that is the result of this electron distribution. Based on the electron distribution, productivities and yields on light could be calculated for the major biomass components; functional biomass (rich in protein), starch and TAG. Previously obtained data of *Neochloris oleoabundans* grown under both nitrogen and light limitation in a flat panel photobioreactor, operated as a turbidostat, was used to derive the model equations and parameters (Klok et al., 2013a). Turbidostat control in a photobioreactor allows for steady state conditions in which the light absorption of the culture is fixed. Combining this type of control with a separate continuous nitrogen supply allows for controlling the ratio between nitrogen uptake rate and energy intake in steady state cultures. These stable conditions enable thorough investigation of the effect of the imposed stress on cell physiology, without the complicating effects of changing environmental conditions that are typically observed in batch experiments.

The model shows that reducing the electron flux towards functional biomass by limiting the nitrogen supply rate, gives control over the electron distribution in *N. oleoabundans*. As a result, the macromolecular composition of biomass can be steered into many directions.

3.2 Methods

3.2.1 Photobioreactor set-up and experimental conditions

Neochloris oleoabundans was grown in a turbidostat operated flat panel photobioreactor, with a nitrogen feed separate from the diluting medium (Klok et al., 2013a). This type of system allows for independent control of the light absorption and nitrogen supply rates of the culture. In this way, combinations of excess light absorption and growth-limiting nitrogen supply rates can be applied, which results in accumulation of storage compounds such as TAG, while at the same time maintaining a dividing algal population. Because growth and storage accumulation are taking place simultaneously under steady state conditions, the system is well suited to study the interactions between growth, nitrogen assimilation and storage metabolite accumulation. This as opposed to

the use of classic nitrogen starvation (i.e. batch) experiments for the evaluation of growth and nitrogen stress in microalgae, where growth and storage metabolite accumulation are taking place in different experimental phases.

In a nitrogen limited turbidostat, F_N (the nitrogen supply rate, in g m^{-3} d^{-1}), $J_{Ph.in}$ (photon flux density entering the system, in µmol m^{-2} s^{-1}) and $J_{Ph.out}$ (photon flux density leaving the system, in µmol m^{-2} s^{-1}) were the only control variables, and therefore these variables are used as the only input for the model presented in this paper. Algae were grown under two light regimes: average photon absorption rates (r_{Ph}) of 762 ± 4 (low light conditions) and 1684 ± 4 mol m^{-3} d^{-1} (high light conditions) resulted from a $J_{Ph.in}$ of 193 and 460 µmol m^{-2} s^{-1} and a $J_{Ph.out}$ of 17 ± 1 and 70 ± 1 µmol m^{-2} s^{-1}, for low and high light conditions respectively. These light regimes were combined with several nitrogen supply rates to the system and resulted in 9 steady states, for which growth rate, medium composition, biomass concentration and biomass composition (TAG, starch, nitrogen content, ash content and absorptive cross section) were measured. For more details on this experiment and the analyses see (Klok et al., 2013a). Three additional analyses were carried out and are discussed below. A summary of all relevant measurements can be found in Appendix 3.A.

3.2.2 Additional measurements

Biomass samples were collected on ice over a period of exactly 24 hours in each steady state. Starch was measured in the lyophilized biomass samples using a commercial kit (Total Starch (AA/AMG), Megazyme International, Bray, Ireland).

The supernatant of the 24h samples was evaluated for TOC (Total Organic Carbon), which was measured as the difference between total carbon (TC) and inorganic carbon (IC), using a TOC-V_{CPH}/TOC-V_{CPN} Total Organic Carbon Analyser (Shimadzu corp, Kyoto, Japan). With the determination of dissolved organic carbon, the measured biomass concentrations ($C_{measured}$ in g DW m^{-3}) were corrected for any biomass lost due to cell lysis (C_{TOC} in g DW m^{-3}), assuming that all organic material in solution had the same elemental composition as suspended biomass. The corrected biomass concentrations (C_{TOTAL} in g DW m^{-3}) were then used as input for the model.

The dark respiration rate was determined using a biological oxygen monitor (BOM) (Hansatech Instruments Limited, Norfolk, England), as described by (Sousa et al., 2012).

3.3 Theory

3.3.1 Electron distributions

Figure 3.1A presents a schematic overview of the distribution of photon-derived electrons over the algal cell. Light energy (r_{Ph}) is used to drive electrons from water into the electron transport chain. At the end of the chain, electrons are donated to temporary electron carriers, such as NADPH, and algae use the reducing power stored in these carriers to fix carbon and construct the molecules that make up the algal cell (total biomass). Electrons either end up in functional biomass (r_X), which is rich in proteins, or in the storage products starch (r_S) and TAG (r_T), which are accumulated in starch granules and lipid bodies, respectively. Not all light energy that is absorbed by an alga is used to liberate electrons that end up in new cell material.

Part of the light energy is dissipated in the photosystems and in addition part of the electrons ending up in NADPH is returned to oxygen, forming water and generating ATP for catabolism. In this paper the term 'catabolism' is used for the collection of all pro-

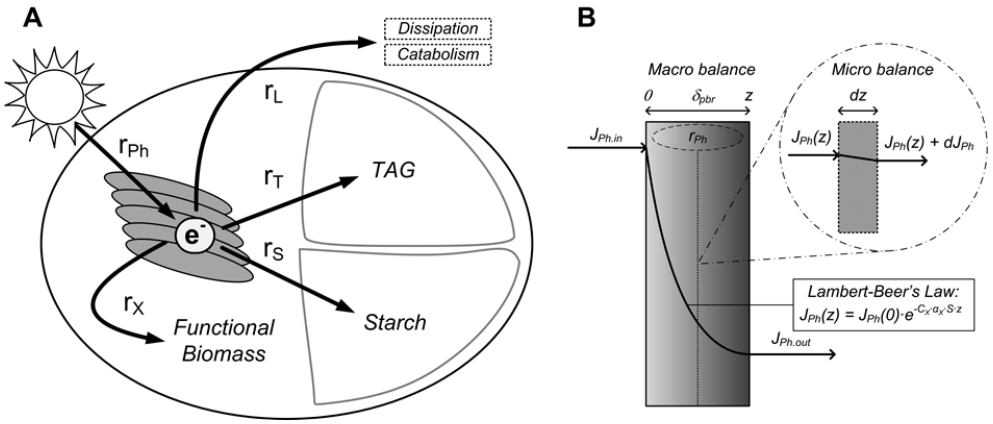

Figure 3.1

A. *Schematic representation of the electrons distribution over the microalgal cell. Photons (r_{Ph}) are absorbed and used to drive electrons from water. These end up in functional biomass (r_X), TAG (r_T) and starch (r_S). r_L represents the light energy that was dissipated in the thylakoids as well as the rate of photon-derived electrons that is used for the generation of ATP (catabolism), and as such does not end up in cell material.*

B. *Schematic representation of light distribution in the culture vessel. A macro balance was constructed to obtain the volumetric photon absorption rate (r_{Ph}) of the whole culture (Equation 1). A micro balance was constructed to describe the light profile inside the culture (Equation 2). Integration of this micro balance gives Lambert-Beer's law (Equation 3).*

cesses that use respiratory ATP for the synthesis and assembly of biomass constituents including the storage polymers, or energy that is necessary for cellular maintenance (Kliphuis et al., 2012). 'Dissipation' refers to the processes of chlorophyll fluorescence and heat production in the chloroplast (Kolber et al., 1988; Pan et al., 2011), which are used to adjust electron production rates to the actual demand for electrons in lower metabolism. Both catabolism and dissipation are considered as a loss of electrons in this model, because these processes do not result in the incorporation of electrons into the molecules that make up cell material. Both processes are therefore represented in the remaining, rate of electron loss (r_L).

3.3.2 Assumptions

The following assumptions were made for the model:

- No other electrons sinks are produced besides functional biomass, starch and TAG.
- The first priority of an alga is to use the available electrons for its maintenance requirements, the second priority is to produce functional biomass (Meeuwse et al., 2011).
- Functional biomass production is either limited by the supply of light or by the supply of nitrogen source. All other necessary nutrients are present in abundance.
- Nitrate uptake rates are independent of external nitrate concentrations (zero order kinetics).
- Starch is the primary storage component during growth and therefore its production rate is proportional to functional biomass production.
- TAG is only produced under nitrogen limitation.
- There is no maximum to the TAG or starch fraction in an algal cell, and no minimum to the fraction of functional biomass for sustaining cell division.
- The composition of TAG is constant, and equal to the average composition of TAG measured in the turbidostat experiments.
- TAG and starch do not absorb light. They can, however, cause scattering of the light.
- When moving through the light gradient in the reactor, algae adapt to the average light intensity that they experience, and the specific growth rate under light limiting conditions is the result of this average experi-

enced light intensity.

- A minimum quantum requirement ($Y_{Ph.e}$) of 2 photons per electron was assumed for the light-driven liberation of electrons from water, which is in agreement with the Z-scheme of photosynthesis.
- Absorption of photons always results in the generation of electrons. Energy dissipation processes and photosynthetic inefficiencies are therefore accounted for in the model as electron losses.

3.3.3 Balances

The model is based on balances for absorbed light and consumed nitrogen, the products that are formed (X, T and S) in the system, and for the electrons that are the intermediate between substrates and products. These balances are discussed in the following sections; a summary can be found in Table 3.1.

3.3.3.1 Light

A macro balance can be derived for the volumetric photon absorption rate over the system (Figure 3.1B):

$$0 = \left(J_{Ph.in} - J_{Ph.out}\right) \cdot 3600 \cdot 24 \cdot 10^{-6} - r_{Ph} \cdot \delta_{pbr} \qquad (1)$$

with r_{Ph} as the rate of photons absorbed by the algae in mol photons m^{-3} d^{-1}, δ_{pbr} as the culture depth (m) and $J_{Ph.in}$ and $J_{Ph.out}$ (µmol m^{-2} s^{-1}) as the photon fluxes entering and leaving the culture, respectively. Secondly, a micro balance can be derived for an arbitrary, infinitively small slice (*dz*) parallel to the illuminated side of the culture vessel (Figure 3.1B):

$$0 = -dJ_{Ph} - \alpha_X \cdot C_X \cdot J_{ph} \cdot S \cdot dz \qquad (2)$$

with dJ_{Ph} as the change in photon flux (mol m^{-2} s^{-1}) over *dz* (m), which is caused by the absorption of light by functional biomass (C_X in g m^{-3}) with a certain absorption cross section of dry functional biomass (α_X in m^2 g^{-1}). Integration of the micro balance gives Lambert-Beer's law, a function that describes transmission in a solution as a function of

Table 3.1 *Balances over the system with their target variables (i.e. the variables that are calculated from the balances) and other unknowns.*

#	Component	Balance	Target variable	Other unknowns
1	*Light macro*	$0 = \left(J_{Ph.in} - J_{Ph.out}\right) \cdot 3600 \cdot 24 \cdot 10^{-6} - r_{Ph} \cdot \delta_{pbr}$	$\mathbf{r_{Ph}}$	-
3	*Light micro*	$\ln\left(\frac{J_{Ph,in}}{J_{Ph,out}}\right) = \alpha_X \cdot C_X \cdot S \cdot \delta_{pbr}$	$\mathbf{C_X}$	α_X, S
4	*Nitrate*	$0 = F_N - r_N - D \cdot C_{N.out}$	$\mathbf{r_N}$	D, $C_{N.out}$
5	*Nitrogen*	$0 = r_N - \mu \cdot f_{N.X} \cdot C_X$	$\boldsymbol{\mu}$	r_N, $f_{N.X}$, C_X
6	*Biomass*	$0 = -D \cdot C_X + \mu \cdot C_X = -D \cdot C_X + r_X$	$\mathbf{r_X}$	D, C_X, μ
7	*Starch*	$0 = -D \cdot C_S + r_S$	$\mathbf{C_S}$	D, r_S
8	*TAG*	$0 = -D \cdot C_T + r_T$	$\mathbf{C_T}$	D, r_T
9	*Electrons*	$\frac{r_{Ph}}{Y_{Ph.e}} = \frac{r_X}{Y_{X.e}} + \frac{r_S}{Y_{S.e}} + \frac{r_T}{Y_{T.e}} + r_L$	$\mathbf{r_L}$	$(r_X/Y_{X.e})$, $(r_S/Y_{S.e})$, $(Y_{T.e}/Y_{T.e})$

concentration, absorption characteristics and length of the light path. Lambert-Beer's law only describes absorptive effects and does not account for light scattering in algal suspensions. Scattering largely depends on the concentration of biomass in the system (Yun and Park, 2001). It effectively causes a lengthening of the light path, increasing the probability of absorption within the microalgal culture. A scattering factor S was used to correct for the scattering effect of cells (section 3.4.1.7). Integration of dJ_{PH} over the entire culture depth (δ_{pbr}) results in:

$$\ln\left(\frac{J_{Ph,in}}{J_{Ph,out}}\right) = \alpha_X \cdot C_X \cdot S \cdot \delta_{pbr} \qquad (3)$$

3.3.3.2 Nitrogen

Two balances are needed for nitrogen: a component balance for the nitrate that is supplied to the system, and a balance for the nitrogen atoms that are used by the algae:

$$0 = F_N - r_N - D \cdot C_{N.out} \quad (4)$$

$$0 = r_N - \mu \cdot f_{N.X} \cdot C_X \quad (5)$$

in which F_N represents the volumetric nitrate supply rate to the system (g N m^{-3} d^{-1}), r_N the volumetric nitrogen consumption rate (g N m^{-3} d^{-1}), D the dilution rate(d^{-1}), $C_{N.out}$ (g N m^{-3}) the concentration of nitrate in the outgoing medium, μ the specific growth (d^{-1}), $f_{N.X}$ the fraction of nitrogen in functional biomass (g N (g DW)$^{-1}$) and C_X the concentration of functional biomass in the system (g m^{-3}). In the experiments, two limitations were set by separately controlling the rates of nitrate supply and light absorption in the turbidostat. Either the nitrate supply was sufficient to sustain light limited growth and therefore $C_{N.out} > 0$, or the nitrate supply rate was insufficient for light limited growth and it was assumed that $C_{N.out} = 0$. In the latter situation, F_N is equal to r_N.

3.3.3.3 Products

The balances for functional biomass (X), starch (S) and TAG(T) read, respectively:

$$0 = -D \cdot C_X + \mu \cdot C_X = -D \cdot C_X + r_X \quad (6)$$

$$0 = -D \cdot C_S + r_S \quad (7)$$

$$0 = -D \cdot C_T + r_T \quad (8)$$

Equation 6 shows that under steady state conditions the specific growth rate (μ) equals the dilution rate (D). Eqns. 6-8 can be used to find the concentrations of X, S and T in the

system (C_X, C_S and C_T, respectively, in g m^{-3}) from the volumetric production rates (r_X, r_S and r_T, respectively, in g m^{-3} d^{-1}). The latter rates are derived from the electron distributions in the cell (sections 3.4.1.1-3.4.1.3). When all concentrations are known, the biomass composition (i.e. the fractions of X, S and T) can be calculated.

3.3.3.4 Electrons

The electron balance is derived from the simplified distribution of electrons in the cell that is presented in Figure 3.1A:

$$\frac{r_{Ph}}{Y_{Ph.e}} = \frac{r_X}{Y_{X.e}} + \frac{r_S}{Y_{S.e}} + \frac{r_T}{Y_{T.e}} + r_L \qquad (9)$$

r_{Ph} represents the rate of light absorption in the system (mol photons m^{-3} d^{-1}) and r_X, r_S and r_T the production rates of X, S and T, respectively (g m^{-3} d^{-1}). $Y_{Ph.e}$ is the minimum theoretical quantum requirement for electron release from water, which is 2 mol photons per mol electrons generated. $Y_{X.e}$, $Y_{L.e}$ and $Y_{S.e-}$ represent the yields of biomass, TAG and starch on electrons that end up in the product (g (mol e^-)$^{-1}$). These yields can be calculated from the degree of reduction of each product (Appendix 3.B). r_L represents the rate of electrons that do not end up in cell constituents X, S or T (mol m^{-3} d^{-1}), either because electrons are used for ATP generation needed for maintenance and biomass formation (catabolism), or because part of r_{Ph} is dissipated before any electrons are liberated from water. For simplicity it was assumed that absorbed photons are always used to generate electrons and that these electrons are subsequently dissipated. Therefore $r_{Ph}/Y_{Ph.e}$ is referred to as the rate of electron generation throughout this paper. This implies that diversion from the minimum quantum requirement due to photosynthetic inefficiency is accounted for in r_L.

3.4 Results and discussion

3.4.1 Additional equations

All variables in the balances (Table 3.1) are a function of the rates of light absorption (r_{Ph}) and volumetric nitrogen supply rate (F_N), which can be controlled independently in the nitrogen limited turbidostat. Additional equations are needed to calculate the production rates and fractions of functional biomass, TAG and starch under nitrogen limitation. These were derived based on the measured electron distributions and some additional experimental results (growth rate, absorptive cross section and scattering), as a function

of nitrogen and light supply rates. A summary of the relevant experimental data can be found in Appendix 3.A, the calculations of the rates at which electrons are incorporated into the three biomass constituents in Appendix 3.B. It should be noted that it was assumed that the small TAG fraction (f_{TAG}) observed in the reference conditions (light limited growth; [A] and [E]), as reported in (Klok et al., 2013a), is a part of functional biomass, and therefore all values of f_{TAG} were corrected for the value measured in the reference condition.

3.4.1.1 Functional biomass

As the nitrogen supply rate was progressively reduced, the fraction of electrons incorporated in functional biomass decreased (Figure 3.2). All assimilated nitrogen ends up in functional biomass (X), the rate of electrons ending up in X ($r_X/Y_{X.e}$) was assumed to be proportional to the nitrogen assimilation rate r_N (Figure 3.3A). A linear correlation (R^2 = 0.99) with a slope (σ_N) of 2.38 ± 0.04 mol electrons per gram N assimilated was found when the intercept was forced to zero:

$$\frac{r_X}{Y_{X.e}} = \sigma_N \cdot r_N \qquad (10)$$

This shows that the electrons ending up in functional biomass that contains one gram of nitrogen (σ_N) was constant over the range of experiments, regardless of the light intensity used, regardless whether nitrogen supply was sufficient or limiting, and regardless of changes in the nitrogen content of functional biomass ($f_{N.X}$; see Appendix 3.A). Equation 10 allows calculation of $r_X/Y_{X.e}$ for any combination of light absorption and nitrogen uptake rates. It should be noted, however, that $Y_{X.e}$ (the yield X on electrons, in g (mol e^-)$^{-1}$) was not a constant, and that r_X did not decrease proportionally with r_N. Consequently, r_X could not be calculated using Equation 10. Therefore, additional equations were derived (sections 3.4.1.5-3.4.1.7), that allowed for calculation of μ and C_X as a function of light and nitrogen supply rates. Subsequently, the balance for functional biomass (Equation 6) was used to obtain r_X.

3.4.1.2 Starch

The rate of electrons ending up in starch decreased as nitrogen assimilation declined (Figure 3.2), indicating that starch does not have a secondary, nitrogen stress related storage function, but a storage function related to growth. This is in agreement with

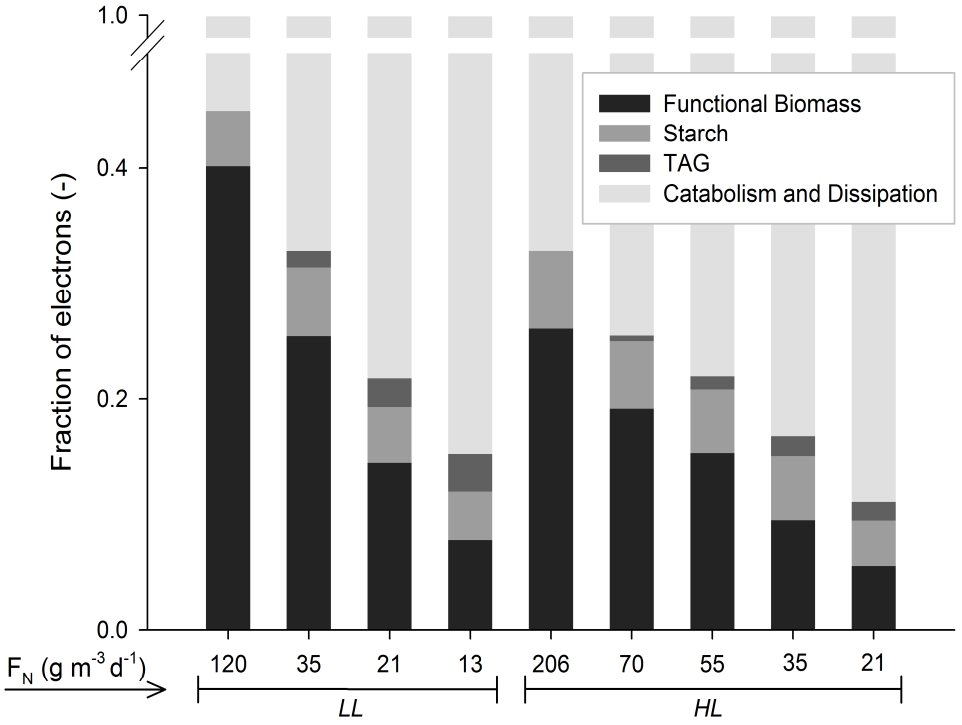

Figure 3.2 *Electron distributions for the nitrogen limitation experiment at several nitrogen supply rates and two different light regimes; low (LL) and high light conditions (HL).*

findings of (Li et al., 2011), who found a decreased starch content in *Pseudochlorococcum sp.* after prolonged nitrogen depletion, combined with a decrease in activity of ADP-glucose pyrophosphorylase (AGPase), the enzyme that catalyses the first committed step of starch synthesis. Moreover, (Rismani-Yazdi et al., 2012) observed a reduction of AGPase and starch synthase, which catalyses the subsequent step in starch synthesis, in *N. oleoabundans* grown under nitrogen depleted conditions. (Cohen and Parnas, 1976; Turpin, 1991) also suggested that starch synthesis has a growth related function: starch is used to store energy during the day, which can be employed to power several processes in the absence of light, such as cell division, the assimilation of nitrogen and maintenance.

The number of electrons ending up in starch was proportional to the number of electrons ending up in functional biomass (or to r_N, according to Equation 10), with an intercept dependent on the light supply rate (Figure 3.3B):

$$\frac{r_S}{Y_{S.e}} = \sigma_S \cdot \frac{r_X}{Y_{X.e}} + \sigma_M \cdot \frac{r_{Ph}}{Y_{Ph.e}} = \sigma_S \cdot \sigma_N \cdot r_N + \sigma_M \cdot \frac{r_{Ph}}{Y_{Ph.e}} \qquad (11)$$

This intercept indicates that a certain amount of starch is always produced, even when there is no functional biomass production. Such production might be related to storage of starch for maintenance purposes. Furthermore, the damaging effect of increased light supply rates might explain why algae store more starch at higher light intensities, as photosystem repair rates increase under elevated light supply rates (Melis, 1999).
The measured starch production rate at $r_x/Y_{X.E}$ = 152 mol m^{-3} d^{-1} and low light conditions ([A] in Figure 3.2) is an outlier to the observed trend in Figure 3.3B, and was therefore not used to fit Equation 11 to the data. The fit to the remaining 8 points gave σ_S = 0.112 mol mol^{-1} and σ_M = 0.038 mol mol^{-1} (R^2 = 0.96). An explanation for the apparent outlier is that insufficient electrons were left for starch synthesis under this low average light intensity, because processes with a higher priority level, i.e. functional biomass production and catabolism, used most of the electrons generated. As catabolism cannot be distinguished from other electron losses in the model, it is accounted for in Equation 11, and the model will therefore slightly overestimate the electrons used in starch synthesis at light limited growth conditions with low light supply rates.

3.4.1.3 TAG

As the amount of electrons ending up in TAG increased when less electrons were ending up in functional biomass and starch (Figure 3.2), it was hypothesized that the rate at which electrons are channelled into TAG ($r_T/Y_{T.e}$) is proportional to the electron excess that is the result of a decrease in functional biomass and starch production compared to the light limited reference conditions:

$$\frac{r_T}{Y_{T.e}} = \sigma_T \cdot \left[\left(\frac{r_X}{Y_{X.e}} + \frac{r_S}{Y_{S.e}} \right)_{ref} - \left(\frac{r_X}{Y_{X.e}} + \frac{r_S}{Y_{S.e}} \right) \right] \qquad (12)$$

The term between brackets represents the excess electrons not ending up in functional biomass and starch compared to the light limited reference situation and σ_T the fraction of these electrons (mol mol^{-1}) that is ending up in TAG. Equation 12 can be combined with Eqns. 10 and 11, resulting in a function that is only dependent on light and nitrogen

supply rates:

$$\frac{r_T}{Y_{T.e}} = \sigma_T \cdot \sigma_N \cdot (1+\sigma_S) \cdot (r_{N.ref} - r_N) \quad (13)$$

in which $r_{N.ref}$ is the nitrogen consumption rate under light limitation (see section 3.4.1.5). $r_T/Y_{T.e}$ was calculated for each steady state and linear regression to ($r_{N.ref} - r_N$) with intercept zero gave σ_{-T} = 0.086 ± 0.005 mol mol^{-1} (R^2=0.97, see Figure 3.3C, where $r_T/Y_{T.e}$ is plotted against r_N). This means, that in *N. oleoabundans*, 8.6% of the excess electrons resulting from nitrogen shortage, is used for TAG accumulation. A fixed percentage of 'excess' electron used for TAG synthesis suggests a close metabolic relationship between nitrogen assimilation and TAG accumulation. As nitrogen assimilation and the synthesis of fatty acids are mainly taking place in the plastid (Huppe and Turpin, 1994; Liu and Benning, 2013), both processes are drawing electrons from the same pool of reducing equivalents. This might explain why TAG synthesis can directly take up part of the excess electrons that are formed when nitrogen assimilation is limited, but it does not explain why this is such a small and constant part. Further studies of the sensing and regulating mechanisms involved in the energy distribution towards dissipation, maintenance, starch and TAG under nitrogen starvation are necessary to explain the fixed 8.6% that was found.

3.4.1.4 Energy loss

Electrons that do not end up in cell constituents are either used for generation of ATP for biomass synthesis or maintenance (catabolism), or lost in dissipation processes in the chloroplast. As it is difficult to distinguish these processes, they are lumped into one 'loss' term, which can be calculated by combining the electron balance (Equation 9), with Eqns. 10, 11 and 13:

$$r_L = \sigma_N \cdot (\sigma_T - 1) \cdot (\sigma_S + 1) \cdot r_N + (1-\sigma_M) \cdot \frac{r_{Ph}}{Y_{Ph.e}} - \sigma_T \cdot \sigma_N \cdot (\sigma_S + 1) \cdot r_{N.ref} \quad (14)$$

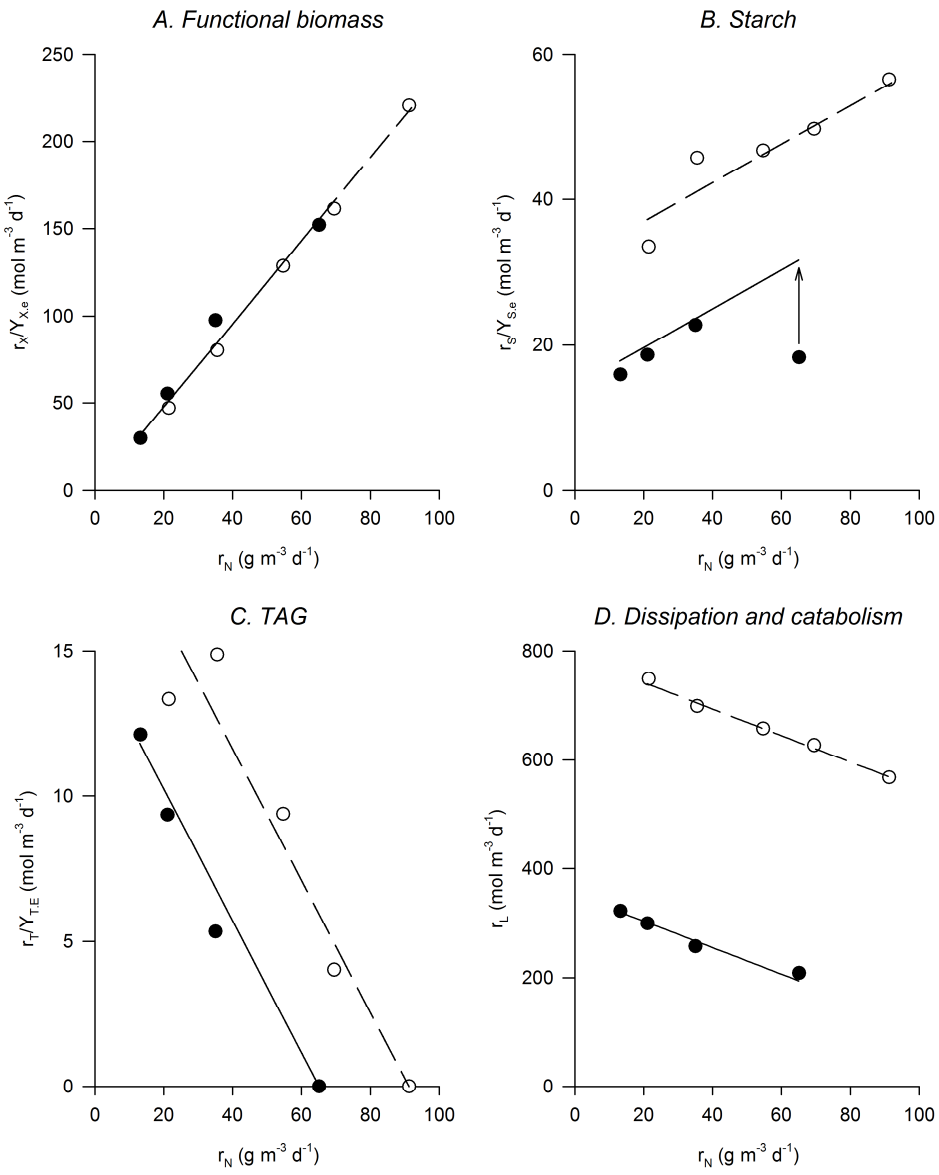

Figure 3.3 *The electrons ending up in functional biomass (**A**), electrons ending up in starch (**B**), electrons ending up in TAG (**C**) and electrons lost in dissipation and catabolic processes (**D**) as function of r_N. Closed circles represent experiments that were performed under low light conditions, open circles represent experiments performed under high light conditions. Lines represent the fit of the model equations to the data, within the experimental range.*

In Figure 3.3D it can be seen that the electron loss is indeed linearly dependent on the nitrogen consumption rate (r_N) (R^2 = 0.99). As, due to the decline in specific growth rate, ATP use for biomass synthesis is likely to decrease under nitrogen limitation, it is likely that dissipation processes are accounting for the bulk of the electron loss under nitrogen limitation, making dissipation a more important sink for excess reducing potential than TAG synthesis.

To calculate the production rates of X, S, and T from the electron distributions in the cell, the rate of electrons ending up in each component should be multiplied by the yield of that component on electrons. r_S and r_T could be calculated using Eqns. 11 and 12 as $Y_{S.e}$ and $Y_{T.e}$ are constants (for calculation, see Appendix 3.B.II). However, $Y_{X.e}$ is not constant (section 3.4.1.1) and therefore additional equations are derived in the following sections, that allow calculation of μ and C_X as a function of light and nitrogen supply rates. Subsequently, the balance for functional biomass (Equation 6) was used to obtain r_X. With μ (and thus D) known, the concentration of all biomass components and the biomass composition (i.e f_X, f_S and f_T) can be calculated using Eqns. 6-8.

3.4.1.5 Specific growth rate

Growth is limited by either light supply or by nitrogen supply, the two input variables. In the first situation, residual nitrate is present in the outflow of the system and $F_N > r_N$. In the second situation, residual nitrogen is assumed to be zero and the nitrate balance (Equation 4) simplifies to $F_N = r_N$.

Light limitation: $F_N > r_N$

The hyperbolic tangent model (Platt and Jassby, 1976) was used to calculate the specific growth rate under light limited conditions (μ_{ref}). It was assumed that the specific growth rate under light limited growth conditions is a result of the average light intensity experienced by the cells. Therefore, the specific growth rate under light limited conditions is:

$$\mu_{ref} = \mu_{\max} \cdot \tanh\left(\frac{\theta \cdot J_{Ph.av} \cdot 3600 \cdot 24 \cdot 10^{-6}}{\mu_{\max}}\right) - k_D \qquad (15)$$

with μ_{max} as the maximum specific growth rate (d^{-1}), and θ in m^2 mol^{-1}. k_D is the specific cell decay rate (d^{-1}), which is a measure for the minimal maintenance rate at $J_{Ph.av}$ = 0 μmol m^{-2} s^{-1}. $J_{Ph.av}$ (μmol m^{-2} d^{-1}) in Equation 15 can be calculated by dividing the integral

of the light profile over the culture (Figure 3.1B) by δ_{pbr}:

$$J_{Ph.av} = \frac{1}{\delta_{pbr}} \int_{0}^{\delta_{pbr}} J_{Ph}(z)dz = \frac{J_{Ph.in} - J_{Ph.out}}{\ln\left(J_{Ph.in} / J_{Ph.out}\right)} \quad (16)$$

k_D was determined using *N. oleoabundans* adapted to the lowest tested $J_{Ph.av}$ (73 µmol m^{-2} s^{-1}). Cells were harvested from the reactor during steady state and a dark respiration rate of 11.3x10^{-3} ± 0.7x10^{-3} mol O_2 g^{-1} d^{-1} was determined (n=3). From this dark respiration rate a k_D of 0.31 ± 0.02 d^{-1} was calculated (Appendix 3.BIII). Subsequently, μ_{max} and θ could be determined using the obtained value for k_D, μ_{ref} of the two light limited steady states, and the highest reported net specific growth rate for *N. oleobundans* with sufficient information on the average light supply rate (1.92 d^{-1} at an average light supply rate of 300 µmol m^{-2} s^{-1} (Santos et al., 2012)). This resulted in values of 2.17 d^{-1} for μ_{max} and 0.28 m^2 mol^{-1} for θ (Figure 3.4A, R^2=0.99), and sets the maximum possible net specific growth rate in the model to $\mu_{max} - k_D$ = 1.86 ± 0.02 d^{-1}.

Nitrogen limitation: $F_N = r_N$

To calculate µ under nitrogen limitation, the nitrate balance and the nitrogen atom balance were combined, giving:

$$\mu = \frac{r_N}{f_{N.x} \cdot C_X} \quad (17)$$

In previous work, it was shown that $f_{N.x} \cdot C_X$ (assimilated nitrogen in functional biomass, g m^{-3}) is constant in a turbidostat, due to the relation between the turbidity in a system and the total amount of nitrogen assimilated (Childers and Gosselink, 1990; Klok et al., 2013a). In Figure 3.4B, the measured µ is plotted against r_N. Linear regression with intercept zero gave $f_{N.x} \cdot C_X$ = 57 ± 1.6 g m^{-3} (R^2 = 0.98), which is comparable to the average measured value (58 ± 4.2 g m^{-3}; Appendix 3.A). As Equation 17 is valid under both nitrogen replete as well as nitrogen limited conditions, combination with Equation 15 gives the value of $r_{N.ref}$, the nitrogen consumption rate achieved under light limitation under a given light regime, which is used in Equation 13 and 14.

It should be noted that modelling cultures which are more dilute than those described here, requires experimental evaluation of $f_N \cdot C_X$, or an additional equation that describes

the relation between achieved turbidity and nitrogen assimilated in functional biomass. In absence of such data, the model is limited to describing cultures with approximately 90% light absorption.

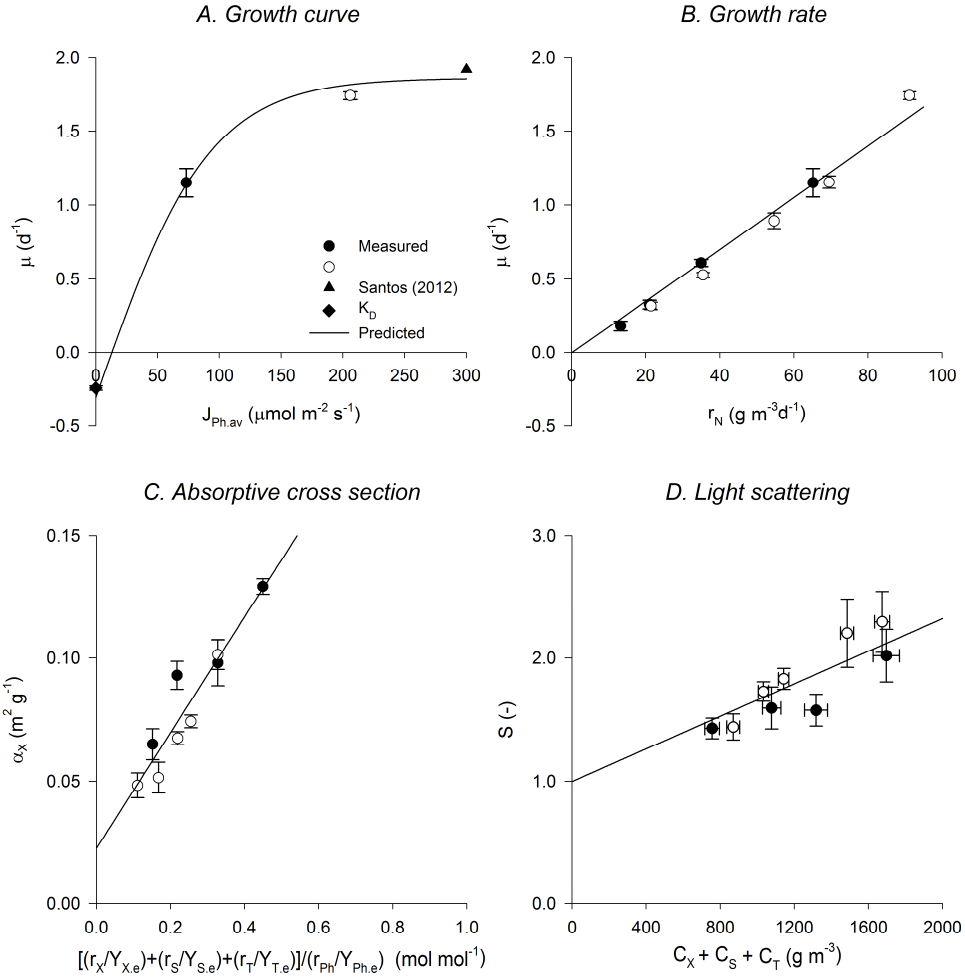

Figure 3.4 *Fitted growth curve of Neochloris oleoabundans (**A**); Specific growth rate (μ) and nitrogen consumption rate (r_N) are proportional (**B**); Absorptive cross section (α_X) is proportional to the ratio between electrons ending up in biomass constituents X, T and S and the electrons that could be generated from the absorbed light (**C**); Light scattering is proportional to $C_X + C_S + C_T$ (**D**): Closed circles represent experiments that were performed under low light conditions , open circles represent experiments performed under high light conditions. Lines represent the fit to the mentioned equations.*

3.4.1.6 Absorptive cross section

The change of the absorptive cross section (α_X) in response to changes in environmental conditions is known as photoacclimation. Geider et al. developed several models that describe photoacclimation as a function of light and nutrient availability, and correlated photoacclimation to the ratio of actually achieved and maximum potential photosynthesis rates (Geider et al., 1997). This ratio quantifies the balance between energy demand and supply in the chloroplast, and can be seen as a measure of the reduction state of the plastoquinone pool, which is the primary signal responsible for regulation of light harvesting complex proteins (Escoubas et al., 1995).A similar 'photosynthetic ratio' was calculated from the experimental data by dividing the number of electrons used to form biomass constituents X, T and S, by the number of electrons that could potentially be generated from the absorbed light ($r_{ph}/Y_{ph.e}$-). Evaluating α_X, expressed as m^2 per gram of functional biomass, as a function of this ratio revealed a linear relationship:

$$\alpha_X = \sigma_\alpha \cdot \left(\frac{r_X / Y_{X.e} + r_S / Y_{S.e} + r_T / Y_{T.e}}{r_{Ph} / Y_{Ph.e}} \right) + \alpha_{X.\min} \qquad (18)$$

Fitting this equation to the experimental data resulted in values of 0.235 ± 0.032 $m^2\ g^{-1}$ and 0.023 ± 0.009 $m^2\ g^{-1}$ for σ_a and $\alpha_{X.min}$, respectively (R^2 = 0.88, Figure 3.4C). $\alpha_{X.min}$ can be regarded as the hypothetical minimum absorptive cross section of functional biomass for capturing light energy under severe nitrogen shortage or extremely high light intensities at steady state growing conditions.

3.4.1.7 Scattering

Lambert-Beer's law, which was adopted in this model, does not account for scattering of light by cells and thus effectively overestimates the light falling through a suspension. Several more accurate models exist in literature that do take scattering into account (Yun and Park, 2001), but due to the complexity of these models, a more simple solution was adopted by multiplying the light path with a scattering coefficient S (-) (Equation 3). The relation between the measured scattering coefficient S (-) and the total biomass concentration ($C_{TOTAL} = C_X + C_S + C_T$) in the system was derived from the experimental data using Equation 3. By setting S≥1, a linear relation was found (Figure 3.4D):

$$S = \left(C_X + C_S + C_T\right) \cdot \sigma_{Scat} + 1 \qquad (19)$$

with σ_{Scat} = 6.6 x10^{-4} ± 1.9x10^{-4} (m^3 g^{-1}) and R^2 = 0.73.

A summary of all auxiliary equations and their parameters discussed in this section can be found in Table 3.2.

Table 3.2 *Auxiliary model equations (**A**) and summary of measured and calculated parameters (**B**). Standard deviations (indicated with +/-) are based on n=3 (for k_D), n=8 (for σ_S and σ_M) and n=9 (other parameters).*

A.

#	Equation
10	$\frac{r_X}{Y_{X.e}} = \sigma_N \cdot r_N$
11	$\frac{r_S}{Y_{S.e}} = \sigma_S \cdot \sigma_N \cdot r_N + \sigma_M \cdot \frac{r_{Ph}}{Y_{Ph.e}}$
13	$\frac{r_T}{Y_{T.e}} = \sigma_T \cdot \sigma_N \cdot (1+\sigma_S) \cdot (r_{N.ref} - r_N)$
15-17	$\mu = \min\left[\mu_{\max} \cdot \tanh\left(\frac{\theta \cdot J_{Ph.av} \cdot 3600 \cdot 24 \cdot 10^{-6}}{\mu_{\max}}\right) - k_D, \mu = \frac{r_N}{f_N \cdot C_X}\right]$
18	$\alpha_X = \sigma_\alpha \cdot \left(\frac{r_X/Y_{X.e} + r_S/Y_{S.e} + r_T/Y_{T.e}}{r_{Ph}/Y_{Ph.e}}\right) + \alpha_{X.\min}$
19	$S = (C_X + C_S + C_T) \cdot \sigma_{Scat} + 1$

B.

Parameter	Value	Units	Parameter	Value	Units
σ_N	2.38 ± 0.04	mol e$^-$ (g N)$^{-1}$	μ_{max}	2.17	d^{-1}
σ_S	0.112	mol m^{-3}	θ	0.28	m^2 mol^{-1}
σ_M	0.038	mol m^{-3}	k_D	0.31 ± 0.02	d^{-1}
σ_T	0.086 ± 0.005	mol mol^{-1}	$f_N \cdot C_X$	57 ± 1.6	g m^{-3}
$Y_{T.E}$	2.78	g mol^{-1}	σ_a	0.235 ± 0.032	m^2 g^{-1}
$Y_{S.E}$	6.76	g mol^{-1}	$\alpha_{X.min}$	0.023 ± 0.009	m^2 g^{-1}
$Y_{Ph.e}$	2	mol γ (mol e$^-$)$^{-1}$	σ_{Scat}	6.6 x10^{-4} ± 1.9x10^{-4}	m^3 g^{-1}
δ_{pbr}	0.02	m			

3.4.2 Model predictions

Figure 3.5 shows the model predictions and the measured data for the two tested light intensities at several nitrogen supply rates. Within the experimental range, the model describes the measured variables very well.

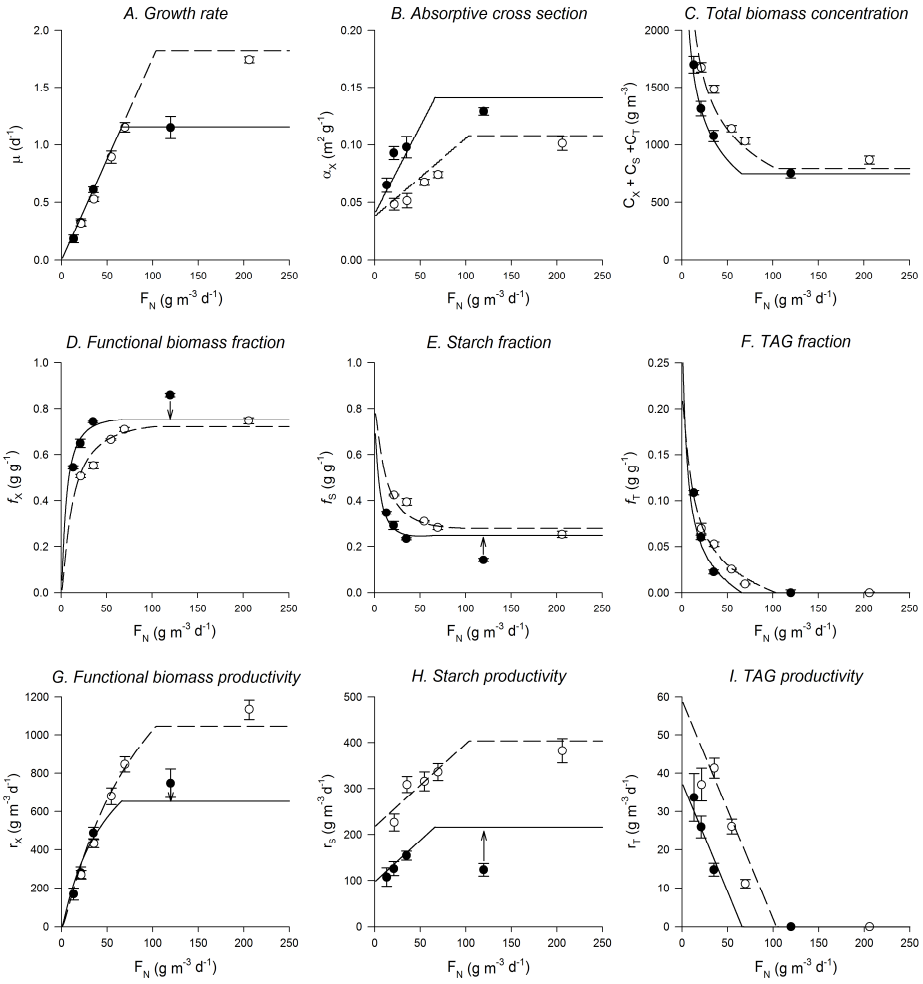

Figure 3.5 *Model simulations of specific growth rate (**A**); absorptive cross section (**B**); total biomass concentration (**C**); mass fractions of functional biomass (**D**), starch (**E**) and TAG (**F**); volumetric productivities of functional biomass (**G**), starch (**H**) and TAG (**I**). Closed circles represent experiments that were performed under low light conditions, open circles represent experiments performed under high light conditions. The arrows indicate the respective under- and overestimation of functional biomass and starch under light limited conditions (see section 3.4.1.2).*

The model can be used to predict biomass composition (i. e. the fractions of X, S and T), production rates and yields of the biomass components in a nitrogen limited turbidostat outside the experimental range, provided that 90% of the light is absorbed in the system (Figure 3.6). These predictions can be used to find the optimal cultivation conditions for functional biomass, starch and TAG.

To evaluate the optimal cultivation conditions for each biomass component, three parameters were considered. First of all, the mass fraction of the component of interest (Figure 3.6A), as this is an important parameter for product recovery. Secondly, the volumetric production rate (Figure 3.6B), as this reflects the photobioreactor performance. Finally the yield of the product on light (Figure 3.6C) was calculated, which is an indicator of how efficiently light energy is used for biosynthesis of that product. This yield is a parameter that facilitates direct comparison of algae strains and photobioreactor performance of different reactor types and operation strategies. Moreover, yield on light is directly proportional to the aerial productivity, an important parameter to consider when optimising commercial outdoor production of any microalgal product, since in outdoor production the amount of light available per surface area is limiting.

3.4.2.1 Functional biomass and protein

Functional biomass is rich in proteins, and the model predictions for functional biomass can therefore directly be translated into recommendations for protein production. Nitrogen limitation is not beneficial for both functional biomass and protein content, productivity and yield, since nitrogen is vital for protein synthesis. This is reflected by the model predictions, where functional biomass content, productivity and yield are lower under nitrogen limited conditions. As can be seen in the upper row of Figure 3.6, increasing average light intensities will increase the functional biomass volumetric production rate. It will reach its maximum value under nitrogen repletion and at the average light supply rate at which μ_{max} is reached in the system. However, increasing the average light intensity will be at the expense of content and yield. The yield is optimal under low average light supply rates, as light is used most efficiently under these conditions (Goldman, 1979). The content is highest under these conditions because starch production rates are low and TAG is not produced at all. Therefore, nitrogen replete conditions combined with a low average light supply rate is the preferred window of operation for functional biomass, and thus protein production.

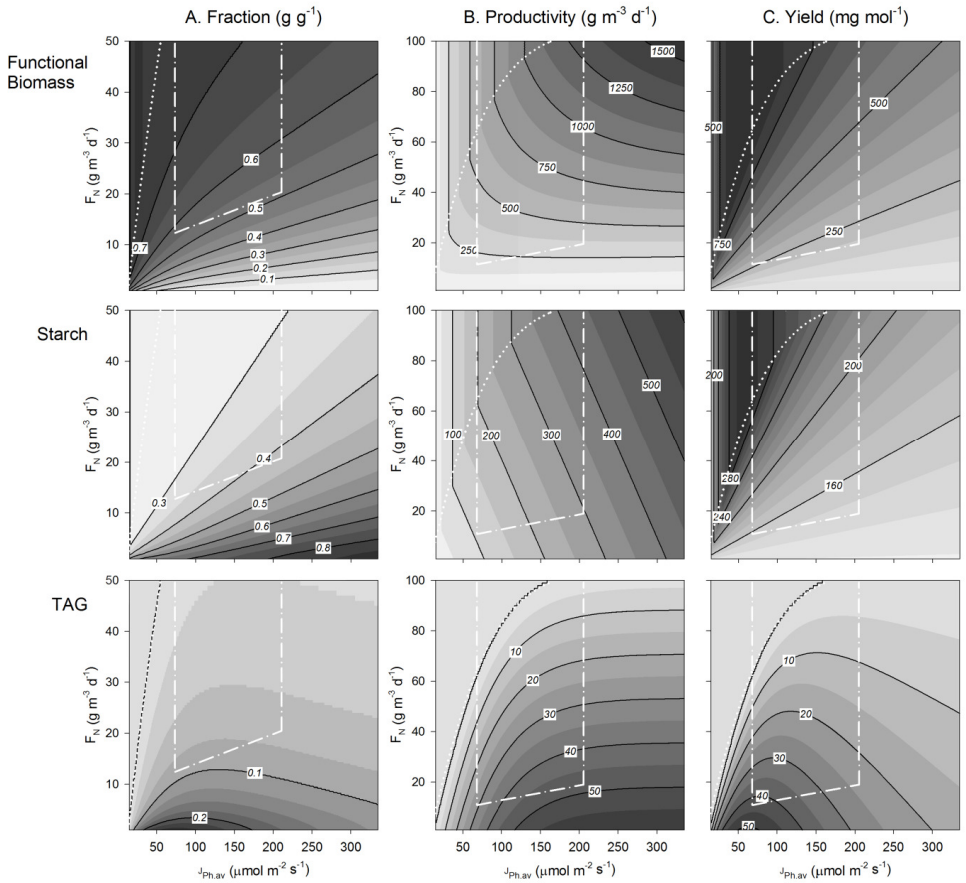

Figure 3.6 *Model predictions of functional biomass high in proteins (upper graphs), starch (middle graphs) and TAG (lower graphs) fractions (**A**), productivity (**B**) and yield on light (**C**) for combinations of nitrogen and average light supply rates, at 90% light absorption over the system. The experimental range is indicated by white dashed lines. The white dotted line represents the transition between light and nitrogen limitation. This line follows from the hyperbolic tangent model for the light-limited specific growth rate and this line coincides with the minimal F_N necessary for TAG accumulation.*

3.4.2.2 Starch

As starch synthesis is coupled to the production of functional biomass (see section 3.4.1.2), starch productivity will be lower when growth is hampered by nitrogen limitation. The highest starch production rates are thus found under light limited conditions, with high average light intensities. However, nitrogen limitation must be applied when aiming at starch contents above 30%, as this will lower the functional biomass produc-

tivity. It should be noted that under light limited conditions at low light supply rates, the model overestimates starch production rates (see section 3.4.1.2) and starch yields. However, it is not expected that this overestimation affects the trend predicted by the model, i.e: starch yield on light is optimal under low average light supply rates and nitrogen replete conditions. In short, the optimal conditions for starch content (high light, low N), volumetric productivity (high light, sufficient N) and yield (low light, sufficient N) are found under very different cultivation conditions.

3.4.2.3 TAG

Storage lipid productivity is highest at minimal nitrogen supply rate, and the optimum is found under high light supply rates because under these conditions the maximum electron excess is created. The model simulations show that high volumetric TAG production rates and high TAG contents are mutually exclusive, because the necessary increased light supply will result in more starch to be produced as well. The highest TAG contents are thus found under lower average light supply rates (roughly between a J_{av} of 50 and 150 µmol m^{-2} s^{-1}), where the starch production rate is less high. Interestingly, the optimum for TAG yield on light seems to coincide with the optimum for TAG content (between a J_{av} of 50 and 100 µmol m^{-2} s^{-1}), which makes lower light supply rates and severe nitrogen limitation favourable cultivation conditions for TAG production in a nitrogen limited turbidostat. The optima for TAG production predicted by the model are in agreement with findings in batch experiments with *Scenedesmus obliquus,* where nitrogen run-outs led to higher TAG yields under low light supply rates (Breuer et al., 2013).

3.4.3 Model limitations and implications

When extrapolating, it must be kept in mind that the model predictions are less certain if the system approaches complete nitrogen depletion (F_N = 0 g m d^{-1}). It is questionable whether it is even possible to run a system continuously in steady state with extremely low nitrogen supply rates, since the functional biomass production rate, and thus also the mass fraction of viable cell material, approaches zero. Also, it is possible that some of the calculated starch fractions (f_S > 0.8 g g^{-1}) cause a physical limitation for cell functioning and division under these conditions. In the model definition for r_L, energy use for cellular maintenance is not distinguished from energy losses in dissipation processes and also not from energy use for the synthesis and assembly of biomass constituents (growth associated maintenance). Therefore, the results predicted for very low light intensities will diverge, as under these conditions, cellular maintenance will become a larger energy sink than growth associated maintenance (Kliphuis et al., 2012). The in-

creasing importance of maintenance at very low average light intensities could, for example, become important when optimising functional biomass content and yield, and starch yield on light, as their optima are found under these conditions. Similarly, the model predictions can deviate for extremely high light intensities since damaging processes such as photoinhibition, which is not taken into account in the model, can cause an increase in maintenance requirement. Nevertheless, as this model has a physiological basis, it can be used to calculate the trends in biomass composition, and in production rates and yields of the separate components as a function of nitrogen and light supply, and the model outcomes can be used as an indication for the optimal cultivation conditions for tailor-made biomass in a nitrogen limited turbidostat.

As the work presented here describes a continuous process, the question rises whether it can be directly applied to discontinuous processes, such as the commonly used batch nitrogen starvation approach used for the production of TAG-rich biomass. It is expected that translation of the model equations is only partly possible as the process described here is in a steady state, which means that the algae are fully adapted to environmental conditions, while during nitrogen starvation, these conditions are constantly changing. This means that the 'rates of change' as a function of environmental conditions should be known, where applicable. For example, modelling starch synthesis will require some additional regulatory terms, that allow for describing the down regulation of starch synthesis after growth is halted. Furthermore, it should be further investigated whether the fixed percentage of excess electrons ending up in TAG is also observed under nitrogen starvation conditions, or in other algal species.

On the other hand, it is expected that the biological principles, such as TAG synthesis being a result of an electron excess, decreased light use efficiency under high light and/or limiting nitrogen supply rates, and electrons ending up functional biomass being proportional to the available nitrogen are not dependent on the process used. Moreover, as the locations of several predicted optima coincide with results obtained for batch cultivation, it is expected that the trends predicted by the presented model can indeed be generalised.

From the model predictions it can be concluded that each biomass component requires very distinct cultivation conditions, and that optimising for a certain compound is always a compromise between yield, content and/or volumetric productivity. Also, a profitable production process will rely on many more factors than those calculated by the model (i.e productivity, content and yield), such as development of inexpensive harvesting methods, low-cost photobioreactors and additional biorefinery, in order to maximize the potential profit that can be made on biomass components. However, the biological

model presented here is a good starting point for further development and modelling of continuous production chains for commercial microalgal products.

3.5 Conclusion

A kinetic model was presented based on the electron distribution in *Neochloris oleoabundans*, grown at several light and nitrogen supply rates. It was shown that starch acts as growth-related storage component, whereas TAG is only overproduced if an excess of electrons is generated due to nitrogen limitation. The proposed model describes the experimental data well and shows that by manipulating the cultivation conditions in a nitrogen limited turbidostat, algal biomass composition, and the volumetric productivities and yields on light of each of the major biomass constituents (protein, starch and TAG) can be controlled on demand.

Acknowledgements

This work was performed in the TTIW-cooperation framework of Wetsus, Centre of Excellence for Sustainable Water Technology (www.wetsus.nl). Wetsus is funded by the Dutch Ministry of Economic Affairs. The authors like to thank the members of the theme 'Algae' from Wetsus for the discussions and their financial support.

Nomenclature

α_X	Absorption cross section of dry functional biomass in red light ($m^2\ g^{-1}$)
$\alpha_{X.min}$	Hypothetical minimum absorption cross section of dry functional biomass in red light ($m^2\ g^{-1}$)
C_i	Concentration of compound *i* ($g\ m^{-3}$)
D	Dilution rate (d^{-1})
δ_{pbr}	Light path of the photobioreactor (m)
f_i	Mass fraction of compound *i* in dry biomass ($g\ (g\ DW)^{-1}$)
F_N	Volumetric nitrogen supply rate ($g\ N\ m^{-3}\ d^{-1}$)
$f_{N.X}$	Mass fraction of nitrogen in dry functional biomass($g\ (g\ DW)^{-1}$)
HL	High light conditions
$J_{Ph.av}$	Average photon flux density experienced by the algae ($\mu mol\ m^{-2}\ s^{-1}$)
$J_{Ph.in}$	Photon flux density entering the system ($\mu mol\ m^{-2}\ s^{-1}$)
$J_{Ph.out}$	Photon flux density leaving the system ($\mu mol\ m^{-2}\ s^{-1}$)
k_D	Specific cell decay rate (d^{-1})
LL	Low light conditions
μ	Specific growth rate (d^{-1})
μ_{ref}	Specific growth rate under light limited reference conditions (d^{-1})
r_i	Volumetric production rate of compound *i* ($g\ m^{-3}\ d^{-1}$)
r_L	Rate of electrons lost in catabolism or dissipation processes ($mol\ e^-\ m^{-3}\ d^{-1}$)
r_N	Volumetric nitrogen consumption rate ($g\ N\ m^{-3}\ d^{-1}$)
$r_{N.ref}$	Volumetric nitrogen consumption rate under light limited reference conditions($g\ N\ m^{-3}\ d^{-1}$)
r_{Ph}	Volumetric photon absorption rate ($mol\ \gamma\ m^{-3}\ d^{-1}$)
σ	Slope, as determined by linear regression
S	Starch
S	Scattering correction coefficient (-)
ϑ	Initial slope that relates irradiance to growth rate in the hyperbolic tangent model for algal growth ($m^2\ mol^{-1}$)
T	TAG (Triacylglyceride)
X	Functional biomass (i.e. non starch or TAG)
$Y_{i.e}$	Yield of compound *i* on electrons ($g\ (mol\ e^-)^{-1}$)
$Y_{Ph.e}$	Minimum theoretical quantum requirement for electron release from water ($mol\ \gamma\ (mol\ e^-)^{-1}$)

Appendix 3.A

Table 3.A.1 *Summary of experimental results*

Experiment	A	B	C	D	E	F	G	H	I
$J_{Ph.in}$ (µmol m^{-2} s^{-1})	193	193	193	193	460	460	460	460	460
$J_{Ph.out}$ (µmol m^{-2} s^{-1}	18	16	16	17	69	70	70	71	70
$J_{Ph.av}$ (µmol m^{-2} s^{-1})	73	71	71	73	206	207	207	209	207
r_{Ph} (mol m^3 d^{-1})	758	766	766	760	1690	1684	1684	1678	1684
F_N (g m^{-3} d^{-1})	120	35	21	13	206	70	55	35	21
r_N (g m^{-3} d^{-1})	65	35	21	13	91	70	55	35	21
µ (d^{-1})	1.15	0.61	0.33	0.18	1.74	1.15	0.89	0.53	0.32
±[a]	0.10	0.02	0.03	0.03	0.03	0.04	0.05	0.02	0.02
$C_{measured}$ (g DW m^{-3})[b]	650	935	1074	1430	741	892	987	1244	1414
±	40	50	62	72	35	28	28	35	41
C_{TOC} (g DW m^{-3})[b]	106	142	243	266	129	141	155	241	260
±	1	0	0	0	1	1	0	0	0
C_{TOTAL} (g DW m^{-3}) [b]	756	1077	1317	1697	870	1033	1142	1485	1674
±	40	50	62	72	35	28	28	35	41
f_x (g (g DW)$^{-1}$)	0.86	0.74	0.65	0.54	0.75	0.71	0.67	0.55	0.51
±	0.01	0.00	0.02	0.01	0.01	0.01	0.00	0.01	0.01
f_S (g (g DW)$^{-1}$)	0.14	0.23	0.29	0.35	0.25	0.28	0.31	0.39	0.42
±	0.01	0.00	0.02	0.01	0.01	0.01	0.00	0.01	0.00
f_T (g (g DW)$^{-1}$)	0.00	0.02	0.06	0.11	0.00	0.01	0.03	0.05	0.07
±	0.00	0.00	0.00	0.00	0.00	0.00	0.00	0.00	0.01
r_X (g m^{-3} d^{-1})	748	489	281	169	1131	846	680	432	270
±	74	30	30	31	53	39	44	22	22
r_S (g m^{-3} d^{-1})	123	154	126	107	382	336	316	309	226
±	14	10	15	20	26	18	21	17	18
r_T (g m^{-3} d^{-1})	0.0	14.8	26.0	33.7	0.0	11.2	26.1	41.3	37.0
±	-	1.7	2.8	6.2	-	1.1	1.9	2.6	4.3

DR (mol e^- (g ash free DW)$^{-1}$)		0.209	0.202	0.202	0.193	0.196	0.192	0.192	0.188	0.183
f_{ash} (g g DW^{-1})		0.062	0.054	0.049	0.037	0.067	0.059	0.057	0.043	0.039
$r_X/Y_{x.e}$ (mol e^- m^{-3} d^{-1})		152	97	55	30	221	161	129	80	47
$r_S/Y_{S.e}$ (mol e^- m^{-3} d^{-1})		18	23	19	16	57	50	47	46	34
$r_T/Y_{T.e}$ (mol e^- m^{-3} d^{-1})		0	5	9	12	0	4	9	15	13
r_L		209	257	300	322	568	627	657	698	748
$f_{N.x}$ (g g X^{-1})		0.089	0.078	0.076	0.058	0.089	0.082	0.078	0.068	0.061
	±	0.001	0.001	0.002	0.001	0.002	0.001	0.001	0.002	0.001
$f_{N.x}*C_X$		57.7	62.8	65.0	53.9	58.0	60.4	59.4	56.2	51.5
α_X (m^2 g^{-1}) [d]		0.129	0.098	0.093	0.065	0.101	0.074	0.068	0.052	0.048
	±	0.003	0.009	0.006	0.006	0.006	0.003	0.003	0.006	0.005
S (-)		1.43	1.59	1.58	2.02	1.44	1.73	1.83	2.20	2.29
	±	0.08	0.17	0.13	0.21	0.11	0.08	0.08	0.28	0.25

[a] *Rows indicated with '±' indicate the standard deviation of the measurement (n≥3).*

[b] *C_{TOTAL} is the sum of all suspended biomass ($C_{measured}$) and biomass in solution due to cell lysis (C_{TOC}), of which the latter value was determined using a TOC (Total Organic Carbon) measurement and the assumption that all organic material in solution had the same composition as suspended biomass.*

[c] *TAG content was corrected for the TAG content under light limiting conditions ([A] and [E]). See (Klok et al., 2013a) for uncorrected values.*

[d] *These values represent the absorptive cross section of algal cells in red light, and were corrected for 'dissolved' biomass, as well as TAG and starch content. Therefore they only reflect the absorption characteristics of functional biomass in red light (630-635 nm).*

Appendix 3.B: Calculations

I. Calculation of $Y_{S.e}$ and $Y_{T.e}$

$Y_{T.e}$ was calculated to be **2.78 g (mol electrons)$^{-1}$,** based on the average fatty acid composition in TAG (see Table 3.B.1) for all steady states (TAG = $C_{55.7}H_{100.5}O_2$):

$$Y_{T.e} = 1/DR_T \quad \text{(B.1)}$$

$Y_{S.e}$ was calculated to be **6.76 g (mol electrons)$^{-1}$,** based on an average composition of starch ($[C_6H_{10}O_{-5}]_n$):

$$Y_{S.e} = 1/DR_S \quad \text{(B.2)}$$

The degree of reduction (DR in mol electrons g^{-1}) of any compound $CH_bN_cO_d$ can be calculated as follows:

$$DR = \left(\gamma_C + b \cdot \gamma_H + c \cdot \gamma_N + d \cdot \gamma_O / MW \right) \quad \text{(B.3)}$$

in which γ_i is the reductive state of the element i in its substrate per cmol, and MW is the molecular weight of the total compound in (g ash free DW) $cmol^{-1}$. Reductive states of 4, 1, 5 and -2 were used for C in CO_2, H in H_2O, N in NO_3^- and O in O_2, respectively (Heijnen et al., 2009).

Table 3.B.1 *Average fatty acid composition of TAG in all 9 experiments.*

Fatty acid	*Fraction (% w/w)*	*Fatty acid*	*Fraction (% w/w)*
C16:0	17.3 ± 1.2	*C18:0*	1.7 ± 0.3
C16:1	1.7 ± 0.7	*C18:1*	47.2 ± 3.7
C16:2	3.5 ± 0.4	*C18:2*	28.6 ± 3.2
C16:3	-	*C18:3*	-

II. Calculation of $r_X/Y_{X.e}$

The amount of electrons used for functional biomass ($r_X/Y_{X.e-}$) was calculated for each steady state by subtracting the electrons ending up in starch and TAG from the sum of electrons ending up in total biomass:

$$\frac{r_X}{Y_{X.e}} = (r_X + r_S + r_T) \cdot (1 - f_{ash}) \cdot DR - \frac{r_S}{Y_{T.e}} - \frac{r_L}{Y_{S.e}} \qquad \text{(B.4)}$$

in which DR is the degree of reduction of total ash free biomass (mol electrons (g ash free DW)$^{-1}$) in every steady state. The DR is calculated according to Equation B.3 and the elemental composition for each steady state (Klok et al., 2013a). Since the ash fraction (f_{ash} in g g^{-1}) is not accounted for the calculation of the DR, the total biomass production rates ($r_X + r_S + r_T$) should be corrected for f_{ash}. With this correction it is automatically assumed that the 'ash' part of biomass (i.e. non CHNO), does not contribute to the total amount of electrons ending up in total biomass. All calculated values for ($r_X/Y_{X.e-}$) can be found in Appendix 3.A.

III. Calculation of k_D

The cell decay constant k_D (d^{-1})can be calculated from the measured dark respiration rate, assuming that starch is the only cell constituent that is respired in the dark:

$$k_D = \frac{r_O}{Y_{O.S}} \cdot MW_S \qquad \text{(B.5)}$$

with r_O as the measured oxygen consumption rate (mol O_2 g^{-1} d^{-1}), $Y_{O.S}$ as the yield of oxygen on starch (mol O_2 cmol^{-1}) and MW_S as the molar mass of starch (g cmol^{-1}). $Y_{O.S}$ can be deduced from the stoichiometric reaction equation for respiration of starch:

$$(C_6H_{10}O_5)_n\,(s) + 6n\,O_2\,(g)\,(aq) + 6n\,CO_2\,(g) + n\,H_2O\,(l) \qquad \text{(B.6)}$$

According to this relation, $Y_{O.S}$ = 1 mol O_2 cmol^{-1}. As MW_S = 27 g cmol^{-1} and r_O was measured to be 11.3x10^{-3} ± 0.7x10^{-3} mol g^{-1} d^{-1}, it can be calculated that k_D is equal to -0.31 ± 0.02 d^{-1}.

Chapter 4

Metabolic modeling of Chlamydomonas reinhardtii: energy requirements for photoautotrophic growth and maintenance

This chapter has been published as:

Anna M.J. Kliphuis*, Anne J. Klok*, Dirk E. Martens, Packo P. Lamers, Marcel Janssen, René H. Wijffels (2012)

* Both authors contributed equally

Metabolic modeling of Chlamydomonas reinhardtii: energy requirements for photoautotrophic growth and maintenance

Journal of Applied Phycology 24, pp. 253-266

Abstract

In this study a metabolic network describing the primary metabolism of *Chlamydomonas reinhardtii* was constructed. By performing chemostat experiments at different growth rates energy parameters for maintenance and biomass formation were determined. The chemostats were run at low light intensities resulting in a high biomass yield on light of 1.25 g mol^{-1}. The ATP requirement for biomass formation from biopolymers (K_x) was determined to be 109 mmol g^{-1} (18.9 mol mol^{-1}) and the maintenance requirement (m_{ATP}) was determined to be 2.85 mmol g^{-1} h^{-1}. With these energy requirements included in the metabolic network, the network accurately describes the primary metabolism of *C. reinhardtii* and can be used for modeling of *C. reinhardtii* growth and metabolism. Simulations confirmed that cultivating microalgae at low growth rates is unfavourable because of the high maintenance requirements which result in low biomass yields. At high light supply rates biomass yields will decrease due to light saturation effects. Thus, to optimize biomass yield on light energy in photobioreactors, an optimum between low and high light supply rates should be found. These simulations show that metabolic flux analysis can be used as a tool to gain insight into the metabolism of algae and ultimately can be used for the maximization of algal biomass and product yield.

4.1 Introduction

Microalgae are interesting organisms because of their ability to produce a wide range of compounds, such as carotenoids (Ben-Amotz et al., 1982; Kleinegris et al., 2010; Lamers et al., 2008), lipids (Chisti, 2007; Griffiths and Harrison, 2009; Hu et al., 2008), hydrogen (Ghirardi et al., 2000; Melis et al., 2000), protein (Becker, 2007; Boyd, 1968) and starch (Delrue et al., 1992). These algal compounds have numerous applications, varying from fine chemicals to biofuels to food additives. To make commercial bulk production of these compounds economically feasible, maximization of algal biomass production and optimization of biomass composition is necessary. Understanding of how compounds are produced in the algal metabolism will help to fully exploit the potential of microalgae and their products.

Metabolic Flux Analysis (MFA) is a powerful tool to study the fluxes through metabolic pathways of any organism of interest. It provides information on how nutrients and energy are utilized to form biomass and other components. Using information on metabolic fluxes and pathways a better understanding of metabolism is obtained and targets for process optimization or genetic modification can be identified. Several metabolic network models have been published for common production organisms, such as *E. coli* (Carlson and Srienc, 2004; Kayser et al., 2005), *Saccharomyces cerevisiae* (Forster et al., 2003) and *Corynebacterium glutamicum* (Kieldsen and Nielsen, 2009). Due to the increasing interest in microalgae as production organisms, metabolic networks for photoautotrophic organisms such as *Chlorella vulgaris* (Yang et al., 2000) and *Arthrospira platensis (Spirulina*) (Cogne et al., 2003) have been developed as well. MFA will improve understanding of algal metabolism and ultimately can be used for the maximization of algal biomass and product yield (Schmidt et al., 2010).

Chlamydomonas reinhardtii has been studied extensively in the past decades. It is regarded as a model organism for green microalgae because of its diverse metabolism and its ability to grow photoautotrophically as well as heterotrophically on acetate (Gfeller and Gibbs, 1984; Heifetz et al., 2000). In addition, *C. reinhardtii* is able to accumulate starch (Ball et al., 1990) and produce hydrogen when grown anaerobically (Melis et al., 2000). The *Chlamydomonas* genome has been sequenced (Merchant et al., 2007) and the availability of this genetic information provides a sound basis for the development of metabolic network models. Recently, (Boyle and Morgan, 2009) and (Manichaikul et al., 2009) developed two extensive genome-scale models describing the primary metabolism of *C. reinhardtii* divided over several cellular compartments and as such both models have a high degree of compartmentalization. They qualitatively and up to a limited extent quantitatively predict algal metabolism and are well suited to get a better insight

in algal metabolism. However, quantitative validation is very limited and there are some difficulties in developing such detailed models. For a number of reactions the localization is not known and has to be assumed. Also information on the exchange of metabolites between compartments is limited. Finally, to reduce the number of fluxes that cannot be calculated, many, often complex, measurements are needed. When developing a metabolic model the practical applicability should be considered. Extensive, fully compartmentalized models are excellent tools for the qualitative study of cellular reaction networks and their regulation, but are generally not suited for quantitative studies because of their underdetermined characteristics. A model for finding specific engineering bottlenecks and solutions would call for simple, easy to handle networks, which require less input parameters and optimization commands but still represent the important characteristics of metabolism (Burgard et al., 2001). Therefore, we developed a more condensed metabolic model describing the primary metabolism of *C. reinhardtii*, in which reactions are less extensively compartmentalized and which is thus less underdetermined.

Apart from the above mentioned uncertainties on compartmentalization and transport steps, the stoichiometry of the energy metabolism is not fixed in these models. The amount of energy in the form of adenosine triphosphate (ATP) required for biomass formation and maintenance is difficult to determine and varies between different micro-organisms and growth conditions (Pirt, 1965). These parameters are essential in metabolic modeling because they largely influence the growth dynamics and biomass or product yields calculated by the model. It is known from previous studies that theoretical estimates of the amount of ATP used for the production of biomass based solely on the required energy for the formation of biopolymers is much lower than the experimentally determined value (Baart et al., 2008; Kayser et al., 2005; Roels, 1983). Additional energy is required for the assembly of biopolymers into growing biomass. In order to obtain a correct metabolic network model these parameters have to be determined experimentally.

In this paper we describe the construction of a metabolic model for *Chlamydomonas reinhardtii* and the subsequent experimental determination of the energy requirements for maintenance and biomass formation. In this model photosynthesis and the Calvin cycle are the only processes that are compartmentalized in order to separate these processes from the pentose phosphate pathway in the cytosol and energy generation in the mitochondria. Furthermore, reactions in linear pathways are lumped. The energy parameters are estimated from a series of chemostats operated at different dilution rates, a commonly used method for heterotrophic micro-organisms (Kayser et al., 2005; Tay-

maz-Nikerel et al., 2010). To our best knowledge this has not been applied to photoautotrophically grown microalgae, most probably because light is a challenging energy source to measure accurately. This study shows how this method can be applied to determine energy parameters for photoautotrophic organisms. The final model including the determined energy parameters was used to calculate the respiration rate at different specific growth rates, which enabled prediction of optimal growth rates for efficient light use.

4.2 Materials & methods

4.2.1 Organism, medium and cultivation conditions

Chlamydomonas reinhardtii CC1690 (Chlamydomonas Genetics Centre, Duke University) was cultivated in 250 mL shake flasks containing 100 mL defined medium (Table 4.1) at pH 7.0. The medium was based on the Sueoka high salts (HS) medium, enriched for magnesium and calcium (Sueoka et al., 1967). Additional EDTA was added to prevent precipitation of salts. Nitrate was used as a nitrogen source and enough nitrogen was added to support 4.5 g L^{-1} biomass. Finally, 1 mL of trace element solution was added to the medium. This trace element solution was based on Hutner's trace element solution (Hutner et al., 1950). The medium was sterilized by filtering through a Whatman liquid filter (pore size 0.2 µm) into a pre-sterilized medium vessel. The medium for the photobioreactor experiments was enriched with 5.00 mmol L^{-1} $NaHCO_3$ to ensure sufficient

Table 4.1 *Composition of Chlamydomonas reinhardtii medium, designed to reach 4.5 g L^{-1} biomass dry weight. 1 mL of trace element stock was added per liter medium. $NaHCO_3$ was added to the medium for experiments in the photobioreactor.*

Medium		**Trace element stock**	
Compound	*Concentration (mmol L^{-1})*	*Compound*	*Concentration (mmol L^{-1})*
KNO_3	24.73	$FeSO_4 \cdot 7\,H_2O$	17.96
KH_2PO_4	5.29	$Na_2EDTA \cdot H_2O$	148.69
K_2HPO_4	8.28	$ZnSO_4 \cdot 7\,H_2O$	76.51
$MgSO_4 \cdot 7\,H_2O$	1.14	H_3BO_3	184.38
$CaCl_2 \cdot 2\,H_2O$	0.39	$MnCl_2 \cdot 4\,H_2O$	25.57
$Na_2EDTA \cdot 2\,H_2O$	0.18	$CoCl_2 \cdot 6\,H_2O$	6.77
$NaHCO_3$	5.00	$CuSO_4 \cdot 5\,H_2O$	6.29
		$(NH_4)_6Mo_7O_{24} \cdot 4\,H_2O$	0.89

dissolved CO_2 supply to the algae.
C. reinhardtii cultures were maintained in a culture chamber at a temperature of 25°C, a light intensity of 20-40 µmol m^{-2} s^{-1} and a 16/8h day/night cycle. To reach inoculation cell density the cultures were placed in a shake-incubator for three days at a continuous light intensity of 280 µmol m^{-2} s^{-1} and a headspace enriched with 5% carbon dioxide.

4.2.2 Reactor set-up and experiments
C. reinhardtii was cultivated in chemostat mode in a pre-sterilized flat panel photobioreactor. Dilution rates in a range of 0.018 h^{-1} to 0.064 h^{-1} were used. Figure 4.1 shows a schematic overview of the experimental setup. The photobioreactor consisted of two transparent polycarbonate sheets held together by a stainless steel frame. The reactor had a working volume (V_{pbr}) of 0.4 L, a light path of 25 mm and an illuminated area (A_{pbr}) of 195 cm^2 (10x19.5 cm).
Using mass flow controllers (Brooks, Smart TMF SLA5850) the system was aerated with pressurized air at an airflow of 0.2 L min^{-1}. The pH was controlled at 7.0 ± 0.2 by the automatic addition of CO_2 to the airflow. When the pH increased above the set point CO_2 was added to the airflow until the pH decreased and reached the set point again. This ensured that a sufficiently high concentration of CO_2 was present in the medium during the cultivation and the microalgae were only growing under light limited conditions. The temperature was maintained at 25°C by an external water bath.
Continuous illumination was provided by a red LED panel of 20x20 cm (LED Light Source SL 3500, average optimum 630-365 nm and spectral half width of 20 nm, Photon System Instruments, Czech Republic) placed on one side of the photobioreactor. An average light intensity of < 100 µmol m^{-2} s^{-1} was used. The photon flux density (PFD, µmol m^{-2} s^{-1}) was measured with a LI-COR 190-SA 2πsensor (PAR range: 400–700 nm) at 15 fixed points behind the reactor. The measured light intensities at all 15 points were averaged into a PFD for that particular experiment. During the experiments the light falling through the culture was measured in the same way. The average photon flux density absorbed by the algal culture (PFD_{abs}, µmol m^{-2} s^{-1}) could be calculated by subtracting the light falling through the culture at steady state from the amount of light falling through the reactor filled with medium only. The resulting value was corrected for the loss of light due to backscattering of light on the algal cells, for which a fixed loss of 2% was assumed (Pottier et al., 2005).

After inoculation at an optical density at 530 nm (OD_{530}) of 0.05, the culture was grown in batch mode until a sufficient optical density was reached. Then the medium supply

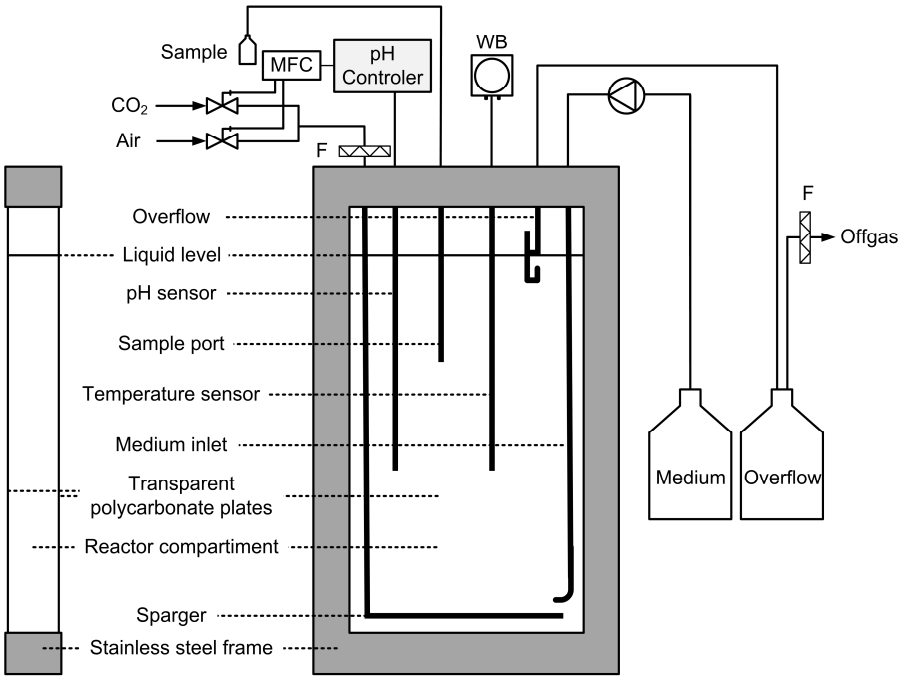

Figure 4.1 *Schematic front and side view of the photobioreactor set-up (not on scale) for the chemostat experiments. MFC = mass flow controller for both air and CO_2, WB = water bath, F = air filter*

was started at a constant dilution rate until steady state was reached. In these experiments steady state was defined as a constant optical density, biovolume and cell density (C_x, g L^{-1}) in the photobioreactor for at least 5 residence times. Biomass samples were taken from the middle of the reactor or from the overflow, which was collected on ice. Both sample methods gave the same results. Due to the small reactor volume it was necessary to take the larger samples for dry weight determination and biomass composition from the overflow in order to prevent disturbances of the steady state equilibrium.

4.2.3 Biomass determinations

Cell number and cell size

Cell number and cell size were determined in duplicate with a Beckman Coulter Multisizer 3 (Beckman Coulter Inc., Fullerton USA, 50 µm orifice). The samples were diluted with filtered (0.2 µm) Coulter® Isoton® II dilution buffer to a cell concentration between $1*10^5$ and $3*10^5$ cells mL^{-1}. The cell number and cell size were used to calculate the total biovolume.

Dry Weight Determination

Whatman glass microfiber filters (Ø 55 mm, pore size 0.7 µm) were dried at 95°C overnight and placed in a desiccator to cool to room temperature. The empty filters were weighed and pre-wet with de-mineralized water. Two grams of sample were diluted with de-mineralized water and filtrated under mild vacuum. The filter was rinsed twice with de-mineralized water to remove adhering inorganic salts. The wet filters containing the samples were dried at 95°C overnight, allowed to cool to room temperature in a desiccator and weighed. The microalgal dry weight of the samples was then calculated from the difference in weight between the dry filters with and without biomass.

Biomass composition

Liquid samples were centrifuged for 10 min at 1750 RCF and the resulting pellets were washed three times with de-mineralized water by re-suspending and centrifuging and stored at -20°C. Algae pellets stored at -20°C were freeze dried and ground to a fine powder. The freeze dried algae powder was used for all further biomass composition analyses. Ash content was determined by burning the freeze-dried algae samples in an oven at 550°C, so that all organic material was oxidized and the ash residue remained.

Lipids and pigments

Lipid content was determined gravimetrically after extraction of the freeze dried algal powder with a 5:4 methanol:chloroform mixture. This extraction was described by (Lamers et al., 2010). The resulting total lipid extract contained all lipid-like compounds present in the algal cells, including pigments. Therefore the weight of the total lipid extract had to be corrected for the amount of pigments present. Pigments were determined spectrophotometrically after dissolving the lipid residue in methanol. The total pigment content was calculated using absorption equations for chlorophyll in methanol (Porra, 2002). The relative fatty acid composition was determined by GC-analysis according to the method described by (Bosma et al., 2008).

Carbohydrates

Carbohydrates were measured by treating the freeze dried algae powder with a phenol solution and concentrated sulphuric acid, according to (Dubois et al., 1956) and (Herbert et al., 1971). The absorbance of the resulting solution was measured at 483nm. Pure glucose was used as a standard.

Protein content and amino acid composition

The nitrogen content of the biomass was determined on a Flash EA 1112 Protein Analyzer (Thermo Scientific, Waltham USA). To calculate the amount of protein from the nitrogen content a N:protein conversion factor of 4.58 ± 0.11 was used (Lourenço et al., 1998). This factor was determined specifically for several microalgal species at different growth phases.

The relative amino acid composition was determined by Ansynth Service BV (Berkel en Roodenrijs, The Netherlands), using classical ion-exchange liquid chromatography with post-column ninhydrin derivatisation and photometric detection. Proteins were hydrolyzed by acid hydrolysis prior to column injection. Cysteine, methionine and tryptophan were determined separately. Cysteine and methionine were measured by oxidation followed by acid hydrolysis, and tryptophan by alkaline hydrolysis followed by reverse phase HPLC.

Nucleic Acids

The nucleic acids DNA and RNA were not measured directly, but were calculated from cell number data. From the amount of different nucleotides in *Chlamydomonas reinhardtii* (Merchant et al., 2007) it could be calculated that each cell contains $1.3*10^{-13}$ g DNA per cell. RNA was assumed to be present in a 28 fold higher concentration than DNA. (Valle et al., 1981) determined this ratio RNA:DNA for *Chlamydomonas reinhardtii* by measuring DNA and RNA contents at various cell concentrations, by means of a fluorometric determination.

4.2.4 Flux balancing

The metabolism of an organism can be described by a set of reaction equations defining the stoichiometric conversion of substrates into products (Stephanopoulos et al., 1998). The stoichiometry matrix S contains the stoichiometric coefficients of the substrates and products for the different reactions in the metabolic network, which also includes the transport reactions over the membranes. To be able to calculate fluxes, mass balances are written for all the intracellular metabolites present in the network. Assuming steady state and neglecting the accumulation of intermediates this results in the next set of linear equations:

$$A \cdot x = 0 \qquad (1)$$

in which A is the transpose of the stoichiometry matrix S and x is the vector which contains the reaction rates.
The solution space of equation 1 was studied to find possible dead ends in the model, which were subsequently removed. Because part of the rates in x is usually measured, equation 1 can be converted to:

$$A_c \cdot x_c = -A_m \cdot x_m \qquad (2)$$

where x_c contains the unknown and x_m contains the measured rates. A_c and A_m are the corresponding parts of the matrix A. By studying the null space of A_c it was revealed that our system was underdetermined and therefore no unique solution of equation 2 exists. Underdeterminancies were solved by setting constraints to some of the fluxes in the underdetermined part of the metabolism and using optimization of an objective function. Thus, linear programming/optimization was used according to equation 3:

$$\begin{aligned} &\text{Objective function:} \quad \max(c \cdot x) \\ &\text{Constraints:} \qquad A \cdot x = 0 \\ &\qquad\qquad\quad LB \le x \le UB \end{aligned} \qquad (3)$$

in which c contains the objective function and LB and UB are the lower and upper boundary of reaction rate x.
In this study we used the objective functions 'maximize biomass yield' and 'maximize ATP yield'. Constraints were set on transport fluxes depending on whether a compound was consumed or produced. In case a rate was measured, the transport rate was constrained to the measured value. Reactions that are irreversible were constrained to one direction. To solve the underdetermined parts constraints were set in such a way that flux distributions that are thermodynamically impossible were excluded.

Mathcad 14.0 (M020, Parametric Technology Corporation, USA) was used for network analysis and Matlab (version 6.0.0.88, release 12, The MathWorks Inc., USA) was used for in silico simulations.

4.3 Theoretical Aspects - Energy parameters

The ATP balance for complete metabolic network models can be written as equation 4:

$$q_{ATP,ox} + q_{ATP,light} + \sum q_i^{ATP} - K_x \cdot \mu - m_{ATP} = 0 \qquad (4)$$

In this balance the first term, $q_{ATP,ox}$ (mmol g^{-1} h^{-1}), is the specific ATP production rate in oxidative phosphorylation in the mitochondria. The second term, $q_{ATP,light}$ (mmol g^{-1} h^{-1}), represents sum of the specific ATP production rate in the light reaction in the chloroplast. The third term, $\sum q_i^{ATP}$ (mmol g^{-1} h^{-1}), is the specific ATP production and consumption in the part of the metabolism that has a known ATP stoichiometry. Notably, the synthesis reactions of the biopolymers that make up biomass have a known ATP stoichiometry and are therefore included in this term. The energy requirements for the formation of protein, DNA, RNA and chlorophyll were assumed to be 4.306, 1.372, 0.4 and 2.0 mol ATP per mol of the respective macromolecule ((Berg et al., 2003; Kanehisa and Goto, 2000); http://www.kegg.com). The specific ATP consumption rate required to assemble these biopolymers into functional growing biomass does not have a fixed stoichiometry and is represented by the fourth term in the ATP balance equation. In this term μ (h^{-1}) is the specific growth rate and K_x (mmol g^{-1}) is a constant, which represents the additional amount of ATP needed to make biomass from biopolymers, by others defined as the 'growth associated maintenance' (Kayser et al., 2005; Taymaz-Nikerel et al., 2010). This parameter K_x also represents the energy needed for other processes which can be present in the cell and cannot be quantified separately, such as the CCM (Carbon Concentrating Mechanism) and ATP use for nutrient transport. Finally, the fifth term represents the maintenance ATP requirement, m_{ATP} (mmol $g^{-1}h^{-1}$), which vary with the type of organism and the culture conditions.

The specific ATP production rate in the mitochondria depends on the P/O ratio, which represents the amount of ATP formed per oxygen atom that is reduced. Here we assume a constant P/O ratio of 2.5 for NADH and 1.5 for $FADH_2$. The stoichiometry of the light reaction also depends on environmental conditions. Here we assume a fixed stoichiometry of 2 NADPH and 3 ATP generated per 8 photons entering the photosynthetic machinery. With these two assumptions all reactions contained in the first three terms have a fixed stoichiometry. The ATP balance (equation 4) thus shows that the sum of these three terms (hereafter 'q_{ATP}') must be equal to the amount of ATP required for maintenance and for biomass formation from biopolymers.

The parameters K_x and m_{ATP} can be determined from experiments by determining q_{ATP} at different growth rates. For this purpose a series of chemostat cultures operated at

different dilution rates were performed. By definition, the growth rate during steady state is equal to the dilution rate and thus by setting different dilution rates different growth rates can be studied. At steady state the biomass density (C_x, g L^{-1}) and the photon flux density absorbed by the algae (PFD_{abs}, µmol m^{-2} s^{-1}) were measured. With these values a light supply rate per amount of biomass (r_{Ex}, mmol g^{-1} h^{-1}) can be calculated for each growth rate µ (h^{-1}) according to equation 5.

$$r_{Ex} = \frac{PFD_{abs} \cdot A_{pbr}}{C_x \cdot V_{pbr}} \qquad (5)$$

in which PFD_{abs-} is the absorbed photon flux density (in mmol m^{-2} h^{-1} in this equation), A_{pbr} is the illuminated surface of the photobioreactor (m^2) and V_{pbr} the working volume of the photobioreactor (L).

At high light intensities light saturation occurs and light energy is dissipated as heat and fluorescence, causing a decrease in the efficiency of the photosystems (Krause and Weis, 1991; van der Tol et al., 2009). Consequently, the actual rate with which photons are used in algal metabolism is not known. Moreover, elevated light intensities also induce damage to the algal cells (Kok, 1955), possibly increasing the energy consumption for maintenace purposes. *Chlamydomonas reinhardtii* becomes light saturated at light intensities of 300 µmol m^{-2} s^{-1} (Janssen et al., 2000). At light intensities below 100 µmol m^{-2} s^{-1} light energy is limiting and is used at maximal efficiency as can be deduced from the fact that the growth curve increases linearly with light intensities below this level (Janssen et al., 2000). The model only considers photons that are taken up for photosynthesis because dissipation and other effects were not modeled. Hence the chemostat experiments to estimate the energy parameters for the metabolic model were performed at low light intensities (<100 µmol m^{-2} s^{-1}), to ensure that the photosystems were working at maximum efficiency and to prevent any light damage to the algal cells. However, even at low light intensities not all light is taken up by the photosystem and therefore the calculated light supply rate r_{Ex} should be corrected for the maximum efficiency (Φ_{Pmax}) of the photosystems. Φ_{Pmax} was assumed to be 0.8, which corresponds to a quantum requirement of oxygen evolution of 10 (instead of 8 according to the Z-scheme). This is in accordance with measurements of the quantum requirement under ideal low-light conditions for a variety of organisms using a variety of experimental techniques (Bjorkman and Demmig, 1987; Dubinsky et al., 1986; Emerson and Lewis, 1943; Evans, 1987; Ley and Mauzerall, 1982; Malkin and Fork, 1996; Tanada, 1951). The spe-

cific light utilization rate ($r_{Ex,u}$ in mmol g^{-1} h^{-1}), which is the rate with which light is used to generate ATP and NADPH, can now be calculated according to equation 6:

$$r_{Ex,u} = \Phi_{Pmax} \cdot r_{Ex} \quad (6)$$

with the specific light utilization rate r_{Ex} and the specific growth rate μ as input for the metabolic model, q_{ATP} can be calculated for each different growth rate. Since the composition of the biomass can have a significant effect on the flux distribution in the model (Pramanik and Keasling, 1998) and thus on q_{ATP}, the biomass composition was measured for each steady state and also used as input for the model. The q_{ATP} was calculated by setting K_x to zero in the overall biomass formation reaction (reaction 147). From equation 4 it can be seen that q_{ATP} is now equal to the maintenance term. In the metabolic model maintenance is represented as the hydrolysis of ATP in reaction 57 of the model. Thus by maximizing the flux through this reaction, using the specific light utilization rate, the specific growth rate and the biomass composition as input, the amount of ATP that is produced in the part of the network which has a known stoichiometry, q_{ATP}, can be calculated for each steady state. Subsequently, we can determine K_x and m_{ATP} by plotting q_{ATP} as a function of the specific growth rate μ. The slope of this line, obtained by linear regression, represents K_x and the intercept represents m_{ATP}, according to equation 4. Note that setting K_x to zero and maximizing the flux through the ATP hydrolysis reaction is just a method to calculate the ATP production rate. To complete the metabolic model with the correct energy requirements for biomass formation and maintenance, the value for K_x has to be incorporated in the biomass synthesis reaction (reaction 147) after conversion to the appropriate units (mol mol^{-1}). The maintenance ATP requirement is incorporated by constraining the ATP hydrolysis reaction to the value of m_{ATP}.

4.4 Results and discussion

4.4.1 Metabolic network construction

A metabolic network describing the primary metabolism of *Chlamydomonas reinhardtii* was constructed based on literature (Berg et al., 2003; Boyle and Morgan, 2009; Cogne et al., 2003; Harris, 2009; Yang et al., 2000) and the KEGG database ((Kanehisa and Goto, 2000); http://www.kegg.com). We cross checked the model with the genome of *Chlamydomonas reinhardtii* (Merchant et al., 2007) to ensure the presence of the en-

zymes catalyzing the modeled reactions. In this model we described two cell compartments, the chloroplast and the cytosol, to be able to uncouple the Calvin cycle, the PPP and the production and consumption of NADPH. For the light reaction only linear electron transport was modeled.

A large network with over 300 enzymatic reactions was obtained. This extensive model was reduced to a smaller, more practical network. This was done by lumping linear pathways into one reaction equation. The resulting network contains 160 reactions and 164 compounds and is listed in Appendix 4.A. A simplified overview of this metabolic network is shown in Figure 4.2.

We found that several enzymatic steps which were necessary in the network were not annotated in the KEGG database. Therefore we performed protein BLAST (Basic local alignment search tool (Altschul et al., 1990) searches against the *Chlamydomonas reinhardtii* genome, using amino acid sequences from green (micro)organisms for the 'missing' enzymes. Appendix 4.C shows the enzymes, the E.C. numbers and the corresponding geneIDs that were found in this way. The reactions in the network (partly) catalyzed by these enzymes are also given. In total 41 enzymes were found not to be annotated in the KEGG database, of which 39 were retrieved by BLAST searches. Of these 39 enzymes, several have a geneID and are annotated but are not taken up in the KEGG database yet. Other enzymes have a draft geneID and still need to be annotated.

Only two enzymes could not be found in this way. The first one is ATP phosphoribosyltransferase (E.C. 2.4.2.17). This enzyme is essential in histidine formation and is described in the Chlamydomonas sourcebook (Harris, 2009). The second enzyme is homoserine acetyltransferase (E.C. 2.3.1.31), which is necessary in cysteine formation. This enzyme is present in other green microalgae (*Ostreococcus lucimarinus*), cyanobacteria (*Synechococcus elongates*, *Anabaena variabilis*) and diatoms (*Phaeodactylum tricornutum*, *Thalassiosira pseudonana*). BLAST searches with the amino acid sequences from these organisms did not give a result. Therefore we assume this reaction is performed by another but similar enzyme because this step is essential in the formation of cysteine. Because both histidine and cysteine were measured in the amino acid composition and not added to the medium, they had to be formed within the metabolism. Thus both reactions were taken up in the model.

By studying the null space of matrix A_c (equation 2), twelve underdetermined parts were revealed in the model. This means that there is no unique solution for equation 2. By measuring and setting constraints to some of the fluxes in the underdetermined parts of the metabolism and using optimization of objective functions, unique solutions could be obtained. Reactions that are irreversible were constrained to one direction and thermo-

dynamically impossible combinations of reactions were also constrained in the correct direction. In the appendix the arrows indicate whether a reaction is reversible or irreversible and if so, in which direction it is set. By choosing the objective functions 'maximize biomass yield' and 'maximize ATP yield' unique values could be calculated for the fluxes in all but two underdetermined parts. The first remaining underdeterminancy involved the anaplerotic routes between phosphoenolpyruvate (PEP), pyruvate (PYR) and oxaloacetate (OXA). This was solved by setting the upper and lower boundaries of the flux through reaction 35 to zero. The second underdetermined part involved the cou-

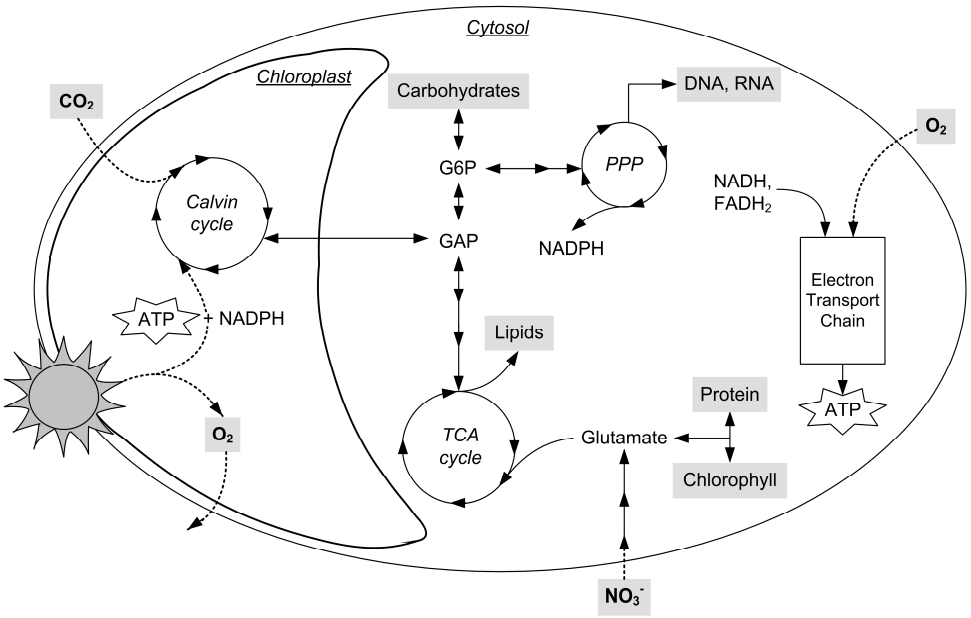

Figure 4.2 *Overview of an algal cell in the light, showing the main metabolic processes. Only the chloroplast and the cytosol were modeled as cell compartments, therefore mitochondrial processes such as respiration through the electron transport chain were placed in the cytosol. Light is fixed in the chloroplast, yielding O_2, ATP and NADPH. These are needed for the fixation of carbon dioxide in the Calvin cycle into glyceraldehyde 3-phosphate (GAP). GAP can be transported to the cytosol to be converted into building blocks for biomass. Lipids are formed through glycolysis and the tricarboxylic acid (TCA) cycle. Nitrate is taken up by the cell and converted into glutamate which in turn can be converted to protein and chlorophyll. GAP can be converted to glucose 6-phosphate (G6P) from which carbohydrates are formed. G6P can also enter the pentose phosphate pathway (PPP) which yields NADPH, DNA and RNA. Electrons are carried by NADH and $FADH_2$ to the mitochondrial electron transport chain, yielding ATP by taking up O_2.*

pling of the pentose phosphate pathway (PPP), the glycolysis and the tricarboxylic acid cycle (TCA). The aerobic degradation of sugars can occur through both the PPP as well as the TCA if NADPH and NADH are freely exchangeable through reaction 54, a transhydrogenase reaction. We restricted this by setting this reaction forward so NADPH can only be converted to NADH. In this way the fluxes through the PPP will only be dictated by the demand of NADPH and PPP intermediates.

4.4.2 Chemostat experiments

To estimate the energy parameters for maintenance and the formation of biomass, we performed seven chemostat experiments at low light intensities and low dilution rates ranging from 0.018 h^{-1} to 0.064 h^{-1}. The experiments were performed at low light intensities; to make sure the photosystems were working at maximum efficiency (Baker et al., 2007) and to prevent light damage to the algal cells. When steady state was reached the biomass density C_x (g L^{-1}) and the photon flux density absorbed by the algae (PFD_{abs}, µmol m^{-2} s^{-1}) were measured for each dilution rate. In Table 4.2 the biomass density and

Table 4.2 *Biomass density (C_x, g L^{-1}), absorbed photon flux density (PFD_{abs}, µmol m^{-2} s^{-1}) and growth rates (µ, h^{-1}) determined for each chemostat experiment. The residence time is calculated as 1/µ for each steady state. The specific light utilization rate ($r_{Ex,u}$, mmol g^{-1} h^{-1}) is calculated from these data using equations 5 and 6. Behind the ± sign standard deviations are given .*

Growth rate	***Biomass density***	***Photon flux density absorbed***	***Specific light utilization rate***
µ (h^{-1})	*C_x (g L^{-1})*	*PFD_{abs} (µmol m^{-2} s^{-1})*	*$r_{Ex,u}$ (mmol g^{-1} h^{-1})*
0.018 ± 0.000	0.78 ± 0.04	88	15.8 ± 1.5
0.019 ± 0.000	0.84 ± 0.08	87	16.7 ± 0.8
0.031 ± 0.001	0.41 ± 0.02	80	25.7 ± 1.4
0.034 ± 0.001	0.39 ± 0.02	73	26.8 ± 1.6
0.052 ± 0.001	0.21 ± 0.01	51	36.1 ± 1.7
0.061 ± 0.003	0.11 ± 0.01	36	45.5 ± 3.7
0.064 ± 0.001	0.10 ± 0.01	31	44.8 ± 3.7

[a] *N = 13, 4, 6, 7, 13, 6 , 8 respectively.*

[b] *N = 8, 3, 6, 5, 5, 4, 4 respectively.*

the photon flux density absorbed at the different growth rates are given as well as the residence time for each steady state. With the biomass density and the photon flux density values a light supply rate per amount of biomass (r_{Ex}, mmol g^{-1} h^{-1}) could be calculated for each growth rate μ (h^{-1}) according to equation 5. The relationship between the specific light supply rate r_{Ex} (mmol g^{-1} h^{-1}) and the growth rate μ (h^{-1}) can be described using the model of (Pirt, 1965) as used by (Zijffers et al., 2010) according to equation 7.

$$r_{Ex} = \frac{\mu}{Y_{xE}} + m_E \qquad (7)$$

in which m_E is the maintenance requirement (mmol photons g^{-1} h^{-1}) and Y_{xE} the yield of biomass on light (g biomass mmol $photons^{-1}$). The amount of light used by the algae increases proportionally to the growth rate while a fixed amount of maintenance light energy is necessary to keep the algae in a healthy state.

Table 4.3 *Comparison of biomass yields on light energy and the used light intensities for different microalgae from literature*

Organism	***Y_{xE} or Y_{xE}^{obs}***	***Light intensity***	***Reference***
	(g mol^{-1})	*(μmol m^{-2} s^{-1})*	
Chlamydomonas reinhardtii	1.25±0.06 [a, d]	80	This paper
Dunaliella tertiolecta	0.78 [a]	930	Zijffers et al. (2010)
Chlorella sorokiniana	0.75 [a]	930	Zijffers et al. (2010)
Chlorella sorokiniana	0.80 [b]	1500	Kliphuis et al. (2010)
Chlorella sorokiniana	1.0 [b]	2100	Cuaresma et al. (2009)
Chlamydomonas reinhardtii	1.11 [b, c]	110	Takache et al. (2010)
Chlamydomonas reinhardtii	0.73 [b, c]	500	Takache et al. (2010)
Chlamydomonas reinhardtii	0.51 [b, c]	1000	Takache et al. (2010)

[a] *$Y_{xE} = \mu / (r_{Ex} + m_E)$, according to equation 7.*

[b] *$Y_{xE}^{obs} = \mu / r_{Ex}$ (the observed yield was not corrected for maintenance requirements)*

[c] *recalculated from data obtained in flat Torus photobioreactor by Takache et al. (2010)*

[d] *Calculated by linear regression (P<0.05)*

Regression on the specific growth rates μ and specific light supply rates r_{Ex} for all chemostat experiments yields a straight line with a R^2 of 0.989. According to equation 7, the offset of this line gives a m_E of 5.98±1.63 mmol g h^{-1} and the inverse of the slope gives an Y_{xE} of 1.25±0.06 g mol^{-1}. This Y_{xE} is high compared to biomass yields found for other green microalgae as can be seen from Table 4.3. (Cuaresma et al., 2009; Kliphuis et al., 2010) and (Zijffers et al., 2010) found yields ranging from 0.5 g mol^{-1} to 1.0 g mol^{-1} for several green microalgae. These yields were all obtained at high light intensities of 1000 μmol m^{-2} s^{-1} or more. At low light intensities we expect a higher yield than at high light intensities because at high light intensities the antenna complexes in the algal photosystems become saturated. The remainder of the absorbed light will be dissipated as heat or fluorescence (Krause and Weis, 1991; van der Tol et al., 2009). In addition, elevated light intensities also induce damage to the algal cells (Kok, 1955), possibly increasing the energy consumption for maintenance purposes. Therefore, high light intensities will lead to low photosynthetic efficiencies as can also be seen from the yields for *Chlamydomonas reinhardtii* obtained by (Takache et al., 2010).
The difference between the yields at high and low light intensities in these experiments reflects the fact that a large part of the light is 'wasted' at higher light intensities. The high biomass yield found in our experiments supports the hypothesis that the efficiency of the algal photosystems was indeed high at a light intensity of 80 μmol m^{-2} s^{-1}. Moreover, it seems that we were working at maximal efficiency because the relation between specific light utilization and specific growth rate is linear (R^2 = 0.988). This shows that the biomass yield is constant and not influenced by the change in light regime (Table 4.2), indicating we reached the maximal value of this yield parameter. Furthermore, it also shows that photorespiration, which results in waste of ATP, is negligible.

It needs to be stressed that even at these low light intensities not all absorbed light can be converted in the photosystems. Therefore the light supply rate r_{Ex} was corrected for the maximum efficiency (Φ_{Pmax}= 0.8) of the photosystems to obtain the specific light utilization rate $r_{Ex,u}$ (equation 6), which is also shown in Table 4.2. This specific light utilization rate $r_{Ex,u}$ should be used for energy parameter estimation, since this rate represents the actual amount of photons that enter the algal metabolism. As expected, regression on the specific growth rates μ and specific light utilization rates $r_{Ex,u}$ also yields a straight line according to equation 7. The offset of this line gives a m_E of 4.79±1.31 mmol g^{-1} h^{-1} and the inverse of the slope gives an Y_{xE} of 1.57±0.07 g mol^{-1}. These values represent the yield and maintenance requirements corrected for the inefficiency of light use, Φ_{Pmax}.

Table 4.4 *Measured biomass composition (% w/w) normalized to 100% and average biomass composition of C. reinhardtii at different specific growth rates μ (h^{-1}) including the standard deviations. The sum of the individual biomass components including ash was comparable to the measured dry weights within 10%.*

	μ (h^{-1})						Average [c]
	0.018	**0.031**	**0.034**	**0.052**	**0.061**	**0.064**	
Protein [a]	42.48 ± 0.55	39.34 ± 0.77	40.17 ± 1.10	41.63 ± 0.67	40.16 ± 0.40	37.61 ± 0.88	40.23 ± 1.71
Carbohydrate [a]	24.09 ± 2.00	21.70 ± 0.73	24.62 ± 2.15	27.29 ± 4.08	26.26 ± 1.59	28.87 ± 1.11	25.47 ± 2.54
Lipids [a]	14.13 ± 0.28	22.16 ± 2.24	17.72 ± 0.88	14.25 ± 0.47	16.78 ± 3.85	18.65 ± 1.84	17.28 ± 3.01
DNA [b]	0.21 ± 0.008	0.20 ± 0.004	0.23 ± 0.006	0.22 ± 0.002	0.23 ± 0.002	0.19 ± 0.002	0.21 ± 0.02
RNA [b]	5.99 ± 0.23	5.57 ± 0.12	6.48 ± 0.16	6.04 ± 0.06	6.57 ± 0.06	5.27 ± 0.05	5.99 ± 0.50
Chlorophyll [a]	7.06 ± 0.07	5.59 ± 0.03	5.13 ± 0.05	4.73 ± 0.07	4.34 ± 0.20	4.01 ± 0.06	5.14 ± 1.09
Ash [a]	6.05 ± 0.03	5.44 ± 0.40	5.66 ± 0.24	5.84 ± 0.11	5.66 ± 0.24	5.41 ± 0.42	5.68 ± 0.24

[a] *N = 3 for each steady state.*

[b] *Based on literature values (Merchant et al. 2007; Valle et al. 1981) and the measured dry weight and cell numbers. N = 3, 6, 5, 5, 4, 8 respectively.*

[c] *Average biomass composition for all growth rates with the standard deviation for all six growth rates.*

4.4.3 Biomass composition

The composition of the biomass can have a significant effect on the flux distribution in the model and thus on the estimation of energy parameters (Pramanik and Keasling, 1998). Therefore, the macromolecular biomass composition (%w/w) was determined for six of the steady states as shown in Table 4.4. In addition, the average biomass composition for all growth rates is given here. These compositions, along with the corresponding growth rates μ and light utilization rates $r_{Ex,u}$, were used for the model simulation of each steady state. The macromolecular biomass composition was not measured for μ = 0.019 h^{-1} and therefore the composition of μ = 0.018 h^{-1} was used to perform model simulations for this growth rate.

The biomass composition did not show much variation as a function of growth rate, although the carbohydrate content seemed to increase at increasing growth rates. The pigment content, on the other hand, decreased at increasing growth rate, which can be explained by the fact that the amount of light per cell increased at increasing growth rate, because the culture became more diluted. Such a response of microalgae to decrease the amount of photosynthetic pigments upon an increase in irradiance is known as photoacclimation (Dubinsky and Stambler, 2009). Protein, nucleic acids and ash content did not vary substantially. Since the composition of the biomass did not change very much in this range of growth rates, the average biomass composition was used in the final model.

In Appendix 4.D the elemental composition of all macromolecules and of the *Chlamydomonas reinhardtii* biomass itself is given. The amino acid composition and the average fatty acid composition can be found in Appendix 4.E and 4.F.

4.4.4 Energy requirements for growth and maintenance

Using the specific growth rate μ, the specific light utilization rate $r_{Ex,u}$ (Table 4.2) and the biomass composition as determined for each steady state (Table 4.4) as input for the model, q_{ATP} can be calculated as described in the Theoretical aspects section. Figure 4.3 shows the plot of q_{ATP} against the specific growth rate, μ. Linear regression through these points yields a straight line ($P<0.05$).

According to equation 4, the offset of this line gives the ATP required for maintenance (m_{ATP}), being 2.85±0.82 mmol g^{-1} h^{-1}. The slope represents K_x, the amount of ATP needed to make biomass from biopolymers and has a value of 109±19 mmol g^{-1}. From this number it could be calculated that 18.9 mol ATP is required to transport and assemble one mol biomass. This amount was added to the biomass synthesis reaction (mol ATP per mol biomass, reaction 147) of the final model. The ATP hydrolysis flux (reaction 57)

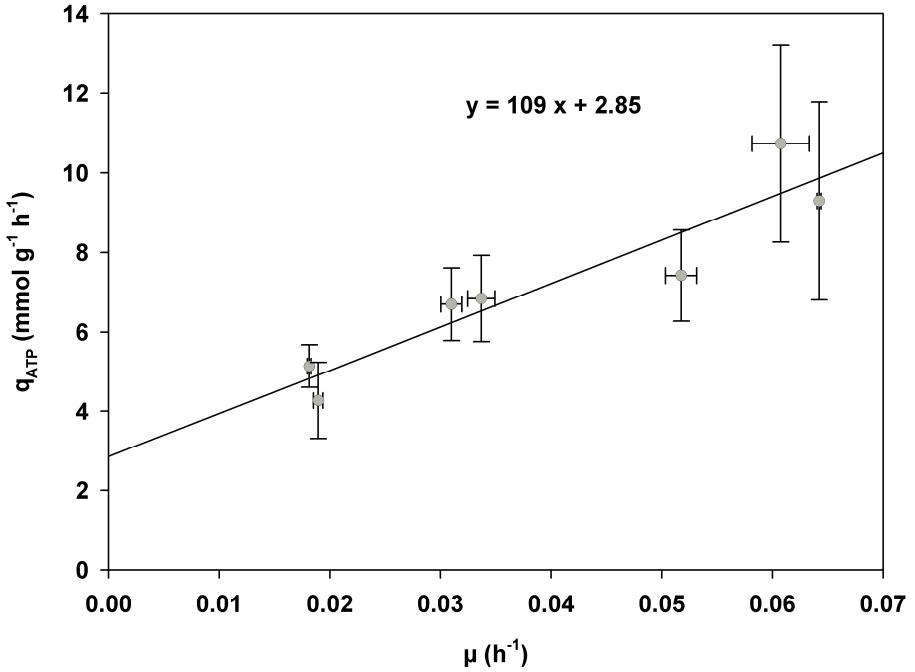

Figure 4.3 *Plot of the specific calculated overall ATP production rate q_{ATP} (mmol g^{-1} h^{-1}) against the experimentally determined growth rate (μ, h^{-1}). q_{ATP} was calculated with the model for each growth rate. Regression through these points yields a straight line of which the offset gives the ATP required for maintenance m_{ATP}, 2.85 mmol g^{-1} h^{-1}. The slope gives the constant which represents the additional amount of ATP needed to make biomass from the biopolymers (K_x), 109 mmol g^{-1}, according to equation 4. The error bars represent the minimum and maximum values for q_{ATP} and the growth rate μ, which follow from the relative errors of biomass measurements.*

was set to the value for m_{ATP} to fix the maintenance requirements of the final metabolic model.

An overview of values for K_x and m_{ATP} for several microorganisms is presented in Table 4.5. The value for K_x depends on the characteristics of the model, for example the degree of compartmentalization and the ATP stoichiometry for biopolymer formation and thus the value for K_x differs per model. To make a good comparison of the total ATP use in several species $1/Y_{xATP}$ (mol ATP g^{-1}) is also given, which is the total amount of ATP required to make 1 gram of biomass. As can be seen from Table 4.5 there is considerable variation in the values for $1/Y_{xATP}$, K_x and m_{ATP} for different microorganisms. This can be due to the type of microorganism, the culture conditions and the assumptions made in the models.

Table 4.5

Comparison of yields and maintenance coefficients of different microorganisms from literature.

Organism	***$1/Y_{xATP}$*** *($mol\ g^{-1}$)*	***K_x*** *($mol\ g^{-1}$)*	***m_{ATP}*** *($mmol\ g^{-1}\ h^{-1}$)*	***Reference***
Chlamydomonas reinhardtii [a]	0.43	0.11±0.018[c]	2.85±0.82[c]	This paper
Petunia hybrida (cell culture) [b]	0.44	0.15	1.41	(de Gucht and van der Plas, 1995)
Saccharomyces cerevisiae [b]	0.35	0.07	1.00	Forster et al. (2003)
Escherichia coli [b]	0.31	0.09	2.81	Kayser et al. (2005)
Escherichia coli [b]	0.40	0.10	4.70	Carlson and Srienc (2004)
Streptomyces coelicolor [b]	-	0.08	3.69	(Borodina et al., 2005)
Neisseria meningitides [b]	0.40	0.05	1.61	Baart et al. (2008)
Corynebacterium glutamicum [b]	0.29	0.03	-	Kieldsen and Nielsen (2009)

[a] *photoautotrophic growth on light and CO_2*

[b] *heterotrophic growth on glucose. Glucose yields 32 ATP (Berg et al. 2003)*

[c] *Values are given ± their standard error as calculated by linear regression (P<0.05)*

Firstly, these parameters depend on the assumed P/O ratio, the relationship between ATP synthesis and oxygen consumption. We assumed that NADH yields 2.5 ATP and $FADH_2$ yields 1.5 ATP upon respiration. However, lower values for these ratios would result in lower values for K_x and m_{ATP}.

Secondly, we assumed a ratio between NADPH and ATP production during linear electron transport in chloroplast of 3:2 (ATP:NADPH) which exactly fits the requirements of the Calvin cycle. Studies on Spinach chloroplasts, however, show that linear electron transport only can deliver 2.57 ATP per every 2 NADPH and that cyclic photosynthetic

electron transport (i.e. cyclic photophosphorylation) is needed to generate additional ATP (Allen, 2003). This cyclic pathway was not included in our model because the additional ATP requirement is small and it would make our model underdetermined. Its necessity, however, could partly explain the fact that the experimentally determined minimal quantum requirement of oxygen evolution is 10 instead of 8 as discussed before (equivalent to Φ_{Pmax} = 0.8) and as such it is implicitly present in our model. Besides the balance of ATP and NADPH in the chloroplast, the microalgal cells as a whole require substantial ATP as is extensively discussed in this study. According to our model ATP must be generated by the complete conversion of sugars (GAP) produced in the chloroplast by the combined action of glycolysis, TCA cycle and oxidative phosphorylation in the cytosol and mitochondria (Figure 4.2). It is interesting to note that this pathway ultimately yields 1 mol of ATP per 1.5 mol photons (see 'Simulation of oxygen uptake through respiration' for calculation). Cyclic photophosphorylation on the other hand, would only yield 1 molecule of ATP per 2 photons (Allen, 2003). This shows that energy generation through linear photosynthetic electron transport is energetically more favorable than through cyclic electron transport and supports our description of *C. reinhardtii* metabolism.

Thirdly, the parameter K_x accounts for the requirement of ATP for biomass formation which is not accounted for in the part of the network with a known energy stoichiometry. For more complex models involving more compartmentalization, a larger part of the ATP may be accounted for and consequently the value of this parameter would become lower. However, for the two more extensive models described for *Chlamydomonas* the energy parameters were not properly estimated. (Manichaikul et al., 2009) used parameters taken from yeast cultivation and not from *C. reinhardtii* itself. (Boyle and Morgan, 2009) estimated the energy parameters for autotrophic, heterotrophic and mixotrophic growth by fitting their model to one experimentally determined biomass yield, based on experiments performed in shake flasks. The maintenance parameter was taken from literature and not measured. Boyle and Morgan estimated a K_x of 29.89 mmol g^{-1}, which is indeed lower than our value, as would be expected for a more detailed model. However, they used shake flask experiments to estimate this parameter. Shake flasks usually have undefined light regimes, which makes it difficult to properly measure the absorbed light by the culture (PFD_{abs}) and thus the light supply rate (r_{Ex}). Also the efficiency of photosynthesis is unknown under these cultivation conditions. Furthermore, only a single growth rate was used, making the estimation highly dependent on the assumed value of the maintenance parameter.

4.4.5 Simulation of oxygen uptake through respiration

With the average biomass composition (Table 4.4) for all chemostats and the energy requirements for both maintenance and growth associated processes, a working model was obtained as shown in the appendix. With this model we simulated the mitochondrial respiration rate (mmol O_2 g^{-1} h^{-1}) at different growth rates (μ, h^{-1}). Appendix 4.G (separate figure sheet) shows the flux distribution through the network at a specific growth rate μ of 0 h^{-1} and 0.062 h^{-1}. The size of the fluxes in mmol g^{-1} h^{-1} are shown in boxes, red boxes for μ = 0 h^{-1} and black boxes for μ = 0.062 h^{-1}. Light is taken up in the light reaction of photosynthesis and with the energy that is formed CO_2 is fixed in the Calvin cycle. The carbon is moved to the cytosol in the form of GAP, where it enters the glycolysis and TCA cycle. Part of the GAP is used to synthesize biopolymers and part is used here to generate energy in the form of ATP, NADH and $FADH_2$. NADH and $FADH_2$ are in turn respired in the mitochondria to generate additional ATP to fulfill the energy requirements for growth and maintenance. The flux distribution at μ = 0 h^{-1} shows the maintenance metabolism without biomass formation. It also shows that the minimal light uptake rate is 4.28 mmol photons g^{-1} h^{-1}, which is used to provide energy for maintenance (2.85 mmol g^{-1} h^{-1}). Using these fluxes it can be calculated that in this model 1.5 mol photons should be consumed to produce 1 mol ATP.

Figure 4.4 shows the simulated biomass yield on light (Y_{xE} in g mol^{-1}, closed dots) for several growth rates μ. These simulations give an ideal situation since no light saturation is modeled and consequently the biomass yield Y_{xE} increases asymptotically to the maximal value of 1.57 g mol^{-1} at very high specific growth rates. In reality light saturation will occur due to the high light intensities necessary to reach maximal growth rates. The photons are absorbed, but the energy is only partly used for growth, causing a decrease in the biomass yield on light energy ($\Phi_P < \Phi_{Pmax}$, equation 6). If light saturation (Baker et al., 2007; Krause and Weis, 1991; van der Tol et al., 2009) would be taken into account the yield in Figure 4.4 would reach an optimum and decrease as soon as light saturation occurs.

The simulated respiration rate (open diamonds), calculated by the sum of the oxygen consumption rates in oxidative phosphorylation (reactions 52 and 53) and the fraction of oxygen used for maintenance (open triangles) are also plotted in Figure 4.4. Respiration is a linear function of the growth rate. This is expected, since most ATP required for growth is generated by oxidation of GAP in the mitochondria. Regression through these points yields a straight line with an intercept of 0.53 mmol O_2 g^{-1} h^{-1} at μ = 0 h^{-1}. This value is the oxygen uptake rate through respiration which is necessary for maintenance purposes. In earlier experimental work (Kliphuis et al., 2011) we measured that the respi-

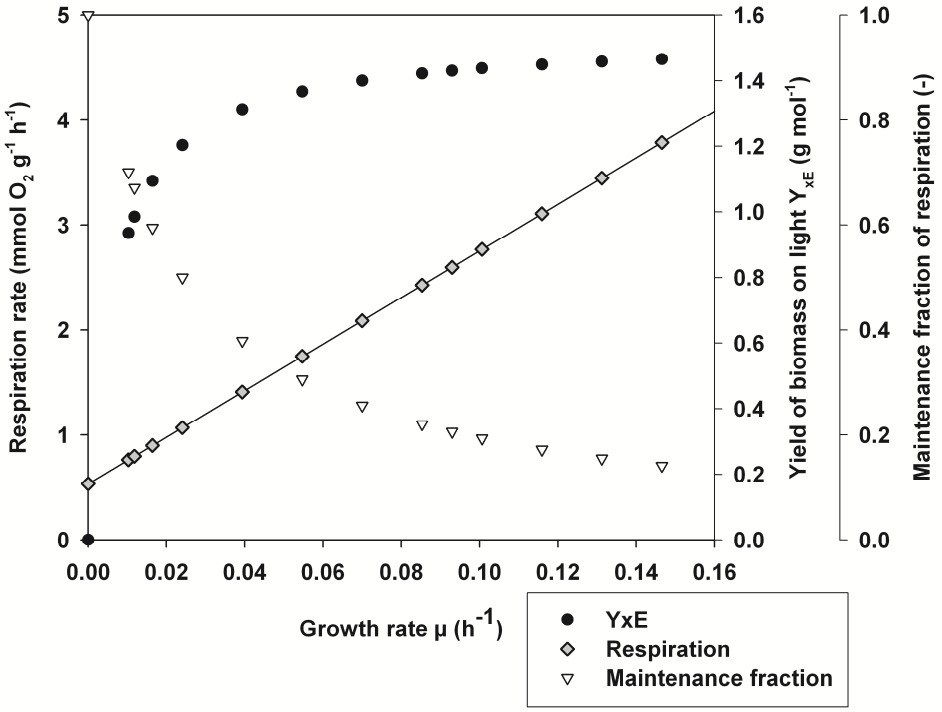

Figure 4.4 *Simulated respiration rates (mmol O_2 g^{-1} h^{-1}) at several growth rates (μ, h^{-1}). Regression through these points yields a straight line with an intercept at μ = 0 of 0.53 mmol O_2 g^{-1} h^{-1}. This value is the oxygen uptake rate through respiration which is necessary for maintenance purposes. The maintenance fraction of the respiration rate is also plotted and shows which part of respiration is used for maintenance purposes. This graph also shows the simulated biomass yields on light energy (Y_{xE}, g mol^{-1}) for these growth rates. The simulations give an ideal situation since light saturation is not modeled. If light saturation would be taken into account the yield would reach an optimum and decrease as soon as light saturation occurs.*

ration rate required for maintenance for *Chlorella sorokiniana* was 0.3 mmol O_2 g^{-1} h^{-1}. This is in the same order as the value we now calculated for *Chlamydomonas reinhardtii* but almost twofold lower. As mentioned before, this is likely to be species specific. It can be seen that at low growth rates a relatively large part of respiration is needed for maintenance purposes. At high growth rates the largest part of respiration is needed for energy generation for growth purposes. Consequently, cultivating microalgae at low specific growth rates results in a low biomass yield Y_{xE}, since a large part of the energy is used for maintenance processes rather than growth. This effect was experimentally confirmed for *Chlorella sorokiniana* and *Dunaliella tertiolecta* by (Zijffers et al., 2010).

4.5 Conclusions

A metabolic network describing the primary metabolism of *C. reinhardtii* was constructed. By performing chemostat experiments energy parameters for maintenance and biomass formation were obtained. The chemostats were run at low light intensities resulting in a high biomass yield on light of 1.25 g mol^{-1}. The ATP requirement for biomass formation from biopolymers (K_x) was determined to be 109 mmol g^{-1} (18.9 mol mol^{-1}) and the maintenance requirement (m_{ATP}) was determined to be 2.85 mmol g^{-1} h^{-1}. These values are in the same range as literature values. With these energy requirements included in the metabolic network, the network accurately describes the primary metabolism of *C. reinhardtii* and can be used for modeling of *C. reinhardtii* growth and metabolism. Simulations with this metabolic model confirmed that mitochondrial respiration both provides energy for maintenance and additional energy to support growth. The high maintenance requirements at low growth rates result in low biomass yields and thus cultivating algae at low growth rates is unfavourable. Cultivating algae at high light supply rates is less favourable as well, because the biomass yield will decrease due to light saturation effects. Thus, to optimize biomass yield on light energy in photobioreactors, an optimum between these two situations should be found. The simulations presented in this paper show that the metabolic model can be used as a tool to gain insight into the metabolism of *Chlamydomonas reinhardtii* and ultimately can be used for the maximization of biomass and product yield.

Acknowledgements

This research project is financially supported by Technology Foundation STW-VICI (WLM.6622) and was performed in the TTIW-cooperation framework of Wetsus, centre of excellence for sustainable water technology (www.wetsus.nl). Wetsus is funded by the Dutch Ministry of Economic Affairs. The authors like to thank the participants of the research theme 'algae' for their fruitful discussions and their financial support. The authors declare that they have no conflict of interest.

Nomenclature

μ	Specific growth rate (h^{-1})
Σq_i^{ATP}	Specific ATP production rate in the metabolism with known ATP stoichiometry (mmol g^{-1} h^{-1})
Φ_P	Photochemical quantum yield (-)
Φ_{Pmax}	Maximum photochemical quantum yield (-)
A	Transpose of the stoichiometric matrix of the network (-)
A_{pbr}	Illuminated surface of the photobioreactor (m^2)
C_x	Biomass concentration in the photobioreactor (g L^{-1})
K_x	ATP requirement for the formation of biomass from biopolymers (mmol g^{-1} or mol mol^{-1})
m_{ATP}	Maintenance ATP requirements (mmol ATP g^{-1} h^{-1})
m_E	Maintenance light energy requirements (mmol photons g^{-1} h^{-1})
N	Number of measurements (-)
OD_{530}	Optical density measured at 530nm on a spectrophotometer (-)
PFD	Photon flux density (µmol m^{-2} s^{-1})
PFD_{abs}	Average photon flux density absorbed by the microalgal culture (µmol m^{-2} s^{-1})
q_{ATP}	Total specific ATP production rate in the metabolism (mmol g^{-1} h^{-1})
$q_{ATP,light}$	Specific ATP production rate in the chloroplast (mmol g^{-1} h^{-1})
$q_{ATP,ox}$	Specific ATP production rate in oxidative phosphorylation (mmol g^{-1} h^{-1})
r_{Ex}	Specific light supply rate (mol g^{-1} h^{-1})
$r_{Ex,u}$	Specific light utilization rate (mmol g^{-1} h^{-1})
V_{pbr}	Working photobioreactor volume (L)
Y_{xATP}	Yield of biomass on ATP (g mol^{-1})
Y_{xE}	Biomass yield on light energy (g mol^{-1})
Y_{xE}^{obs}	Observed experimental biomass yield on light energy, not corrected for maintenance requirements (g mol^{-1})

Appendix

4.A Metabolic model of Chlamydomonas reinhardtii

Arrows indicate the direction and reversibility of the reactions. The compounds in the chloroplast are notated with a c before the abbreviation. All fluxes are in mmol g^{-1} h^{-1}. The factor in the biomass export reaction (159) converts the biomass flux through reaction 147 (in mmol g^{-1} h^{-1}) to mg g^{-1} h^{-1}, the biomass production rate.

Light reaction

0 8 Light + 3 ADP + 3 Pi + H[+] + 2 cNADP → O2 + H2O + 2 cNADPH + 3 ATP

Calvin cycle

1 CO2 + H2O + cRu15DP → 2 cG3P
2 ATP + cG3P → ADP + H[+] + c13DPG
3 H[+] + cNADPH + c13DPG ↔ cNADP + Pi + cGAP
4 cGAP ↔ cDHAP
5 cDHAP + cGAP ↔ cF16P
6 H2O + cF16P ↔ Pi + cF6P
7 cF6P + cGAP ↔ cE4P + cX5P
8 H2O + cE4P + cGAP ↔ Pi + cS7P
9 cGAP + cS7P ↔ cR5P + cX5P
10 cX5P ↔ cRu5P
11 cR5P ↔ cRu5P
12 ATP + cRu5P → ADP + H[+] + cRu15DP

Transport chloroplast to cytosol

13 cDHAP ↔ DHAP

Glycolysis

14 G6P ↔ G1P
15 F6P ↔ G6P
16 ATP + F6P → ADP + F16P + H[+]
17 F16P + H2O → F6P + Pi
18 DHAP + GAP ↔ F16P
19 DHAP ↔ GAP
20 GAP + NAD+Pi ↔ 13DPG + H[+] + NADH

21 13DPG + ADP ↔ 3PG + ATP

22 3PG ↔ 2PG

23 2PG ↔ H_2O + PEP

24 ADP + H[+] + PEP→ ATP + PYR

Citric acid cycle

25 CoA + NAD + PYR → AcCoA + CO_2 + NADH

26 AcCoA + H_2O + OXA ↔ CIT + CoA + H[+]

27 CIT + NAD ↔ AKG + CO_2 + NADH

28 AKG + CoA + NAD → CO_2 + NADH + SUCCoA

29 ADP + Pi + SUCCoA ↔ ATP + CoA + SUC

30 FAD + SUC ↔ $FADH_2$ + FUM

31 FUM + H_2O ↔ MAL

32 FAD + MAL ↔ $FADH_2$ + OXA

33 ATP + CO_2 + H_2O + PYR → ADP + OXA + Pi + 2 H[+]

34 ATP + OXA→ ADP + CO_2 + PEP

35 CO_2 + H_2O + PEP ↔ H[+] + OXA + Pi

Pentose phosphate pathway

36 G6P + H_2O + NADP ↔ 6PG + NADPH + 2 H[+]

37 6PG + NADP ↔ CO_2 + NADPH + RU5P

38 RU5P ↔ R5P

39 RU5P ↔ X5P

40 R5P + X5P ↔ GAP + S7P

41 GAP + S7P ↔ E4P + F6P

42 F6P + GAP ↔ E4P + X5P

Glycerol

43 DHAP + H_2O ↔ DHA + Pi

44 DHA + H[+] + NADPH ↔ GLYC + NADP

45 ATP + GLYC → ADP + $GLYC_3P$ + H[+]

46 $GLYC_3P$ + NAD ↔ DHAP + H[+] + NADH

N and S fixation

47 H[+] + NADH + NO_3 ↔ H_2O + NAD + NO_2

48 5 H[+] + 3 NADPH + NO_2 ↔ NH_4[+] + 2 H_2O + 3 NADP

49 $ATP + SO_4 \rightarrow APS + PPi$

50 $APS + NADH \rightarrow AMP + NAD + SO_3$

51 $5\ H[+] + 3\ NADPH + SO_3 \leftrightarrow H_2S + 3\ H_2O + 3\ NADP$

Oxidative phosphorylation

52 $1.5\ ADP + 1.5\ H[+] + 1.5\ Pi + FADH_2 + 0.5\ O_2 \rightarrow FAD + 1.5\ ATP + 2.5\ H_2O$

53 $3.5\ H[+] + 2.5\ ADP + 2.5\ Pi + NADH + 0.5\ O_2 \rightarrow NAD + 2.5\ ATP + 3.5\ H_2O$

54 $NAD + NADPH \rightarrow NADH + NADP$

55 $H_2O + PPi \rightarrow H[+] + 2\ Pi$

56 $AMP + ATP \rightarrow 2\ ADP$

57 $ATP + H_2O \rightarrow ADP + H[+] + Pi$

Amino acids and protein

58 $AKG + H[+] + NADPH + NH4[+] \rightarrow GLU + H2O + NADP$

59 $ATP + GLU + NH4[+] \rightarrow ADP + GLN + H[+] + Pi$

60 $AKG + GLN + H[+] + NADPH \leftrightarrow NADP + 2\ GLU$

61 $3PG + GLU + H2O + NAD \leftrightarrow AKG + H[+] + NADH + Pi + SER$

62 $SER \rightarrow NH4[+] + PYR$

63 $AcCoA + H2S + SER \leftrightarrow Ace + CYS + CoA + H[+]$

64 $ATP + Ace + CoA \rightarrow ADP + AcCoA + Pi$

65 $GLU + PYR \rightarrow AKG + ALA$

66 $H[+] + THR \leftrightarrow 2\text{-oxobutan} + NH_4[+]$

67 $2\text{-oxobutan} + GLU + H[+] + NADPH + PYR \leftrightarrow AKG + CO_2 + H_2O + ILE + NADP$

68 $2\ H[+] + ALA + NADPH + PYR \leftrightarrow CO_2 + H_2O + NADP + VAL$

69 $2\ PYR + AcCoA + GLU + H[+] + NAD + NADPH \Leftrightarrow AKG + CoA + LEU + NADH + NADP + 2\ CO_2$

70 $2\ PEP + ATP + E_4P + NADPH \rightarrow ADP + CHO + NAD\ P + 4\ Pi$

71 $CHO \leftrightarrow PRE$

72 $GLU + H[+] + PRE \leftrightarrow AKG + CO_2 + H_2O + PHE$

73 $GLU + NAD + PRE \leftrightarrow AKG + CO_2 + NADH + TYR$

74 $CHO + GLN \leftrightarrow ANTH + GLU + H[+] + PYR$

75 $ANTH + H[+] + PRPP + SER \leftrightarrow CO_2 + GAP + PPi + TRYP + 2\ H_2O$

76 $3\ H_2O + 2\ NAD + ATP + GLN + PRPP \rightarrow AICAR + AKG + HIS + Pi + 2\ NADH + 2\ PPi + 5\ H[+]$

77 $GLU + OXA \leftrightarrow AKG + ASP$

78 $ASP + ATP + GLN + H_2O \rightarrow ADP + ASN + GLU + H[+] + Pi$

79 2 ATP + 2 H_2O + CO_2 + GLN → CaP + GLU + Pi + 2 ADP + 3 H[+]

80 2 GLU + ASP + ATP + CaP + NADH → AKG + AMP + ARG + FUM + H_2O + NAD + PPi + Pi

81 3 H[+] + 2 NADH + GLU ↔ PRO + 2 H_2O + 2 NAD

82 AKG + O_2 + PRO ↔ CO_2 + HydPro + SUC

83 ASP + ATP + H[+] + NADPH → ADP + ASA + NADP + Pi

84 2 H[+] + ASA + GLU + NADH + PYR ↔ AKG + DAP + H_2O + NAD

85 DAP ↔ CO_2 + H[+] + LYS

86 ASA + H[+] + NADPH ↔ HSER + NADP

87 ATP + H_2O + HSER → ADP + H[+] + Pi + THR

88 AcCoA + CYS + H_2O + HSER ↔ Ace + CoA + HCYS + H[+] + NH_4[+] + PYR

89 HCYS + MTHF ↔ H[+] + MET + THF

90 4.306 ATP + 3.306 H_2O + 0.111 ALA + 0.094 GLY + 0.093 LEU + 0.059 PRO + 0.059 VAL + 0.058 LYS + 0.057 THR + 0.055 SER + 0.05 GLN + 0.05 GLU + 0.047 ARG + 0.047 ASN + 0.047 ASP + 0.045 PHE + 0.036 ILE + 0.031 TYR + 0.022 MET + 0.017 HIS + 0.013 HydPro + 0.012 CYS + 0.001 TRYP → PROTEIN + 4.306 ADP + 4.306 Pi + 4.314 H[+]

Photorespiration

91 H_2O + NAD + O_2 + cRu15DP → H[+] + NADH + Pi + cG3P + glyoxylate

92 GLY + H[+] + PYR ↔ ALA + glyoxylate

93 SER + glyoxylate ↔ GLY + HydPyr

94 GLY + H_2O + METHF ↔ SER + THF

95 GLY + NAD + THF ↔ CO_2 + METHF + NADH + NH_4[+]

96 H[+] + HydPyr + NADH ↔ Glycerate + NAD

97 ATP + Glycerate → ADP + 2 H[+] + 3PG

THF metabolism

98 ATP + R5P → AMP + H[+] + PRPP

99 5FTHF + H[+] ↔ H_2O + MYLTHF

100 H_2O + MYLTHF ↔ H[+] + N10FTHF

101 ATP + FORM + THF → ADP + N10FTHF + Pi

102 MYLTHF + NADPH ↔ METHF + NADP

103 H[+] + METHF + NADPH ↔ MTHF + NADP

104 5FTHF + ATP + H_2O → ADP + H[+] + N10FTHF + Pi

105 FORM + H[+] + THF ↔ H_2O + N10FTHF

106 DHF + H[+] + NADPH ↔ NADP + THF

Lipids (phosphatidic acid)

107 ACP + AcCoA + H[+] ↔ AcACP + CoA

108 ATP + AcCoA + CO_2 + H_2O → ADP + H[+] + MalCoA + Pi

109 ACP + MalCoA ↔ CoA + MalACP

110 10 H[+] + 10 NADPH + 5 MalACP + AcACP ↔ C12:0ACP + 5 ACP + 5 CO_2 + 5 H_2O + 10 NADP

111 12 H[+] + 12 NADPH + 6 MalACP + AcACP ↔ C14:0ACP + 6 ACP + 6 CO_2 + 6 H_2O + 12 NADP

112 14 H[+] + 14 NADPH + 7 MalACP + AcACP ↔ C16:0ACP + 7 ACP + 7 CO_2 + 7 H_2O + 14 NADP

113 C160ACP + H[+] + NADH + O_2 ↔ C16:1ACP + NAD + 2 H_2O

114 C161ACP + H[+] + NADH + O_2 ↔ C16:2ACP + NAD + 2 H_2O

115 C162ACP + H[+] + NADH + O_2 ↔ C16:3ACP + NAD + 2 H_2O

116 16 H[+] + 16 NADPH + 8 MalACP + AcACP ↔ C18:0ACP + 8 ACP + 8 CO_2 + 8 H_2O + 16 NADP

117 C180ACP + H[+] + NADH + O_2 ↔ C18:1ACP + NAD + 2 H_2O

118 C181ACP + H[+] + NADH + O_2 ↔ C18:2ACP + NAD + 2 H_2O

119 C182ACP + H[+] + NADH + O_2 ↔ C18:3ACP + NAD + 2 H_2O

120 GLYC3P + 0.474 C16:0ACP + 0.446 C18:3ACP + 0.276 C18:2ACP + 0.253 C16:3ACP + 0.16 C18:1ACP + 0.148 C16:2ACP + 0.104 C12:0ACP + 0.051 C14:0ACP + 0.048 C18:0ACP + 0.04 C16:1ACP ↔ PA + 2 ACP + 2 H[+]

Nucleic acids

121 4 ATP + 2 GLN + 2 H_2O + ASP + CO_2 + GLY + N10FTHF + PRPP → AICAR + FUM + PPi + THF + 2 GLU + 4 ADP + 4 Pi + 7 H[+]

122 ASP + CaP + H[+] + O_2 + PRPP ↔ CO_2 + H_2O + H_2O_2 + PPi + Pi + UMP

123 2 H_2O_2 ↔ O_2 + 2 H_2O

124 ATP + UMP → ADP + UDP

125 ATP + UDP ↔ ADP + UTP

126 ATP + GLN + H_2O + UTP → ADP + CTP + GLU + Pi + 2 H[+]

127 ATP + CDP ↔ ADP + CTP

128 AICAR + N10FTHF ↔ H_2O + IMP + THF

129 ATP + H_2O + IMP + NAD + NH_4[+] → AMP + GMP + NADH + PPi + 3 H[+]

130 ATP + GMP → ADP + GDP

131 ATP + GDP ↔ ADP + GTP

132 ASP + GTP + IMP ↔ AMP + FUM + GDP + Pi + 2 H[+]

133 ATP + H[+] + METHF + NADPH + UDP → ADP + DHF + H_2O + NADP + dTTP

134 ATP + CDP + H[+] + NADPH → ADP + H_2O + NADP + dCTP

135 ATP + GDP + H[+] + NADPH → ADP + H_2O + NADP + dGTP

136 ATP + H[+] + NADPH ↔ H_2O + NADP + dATP

137 2.372 H_2O + 1.372 ATP + 0.18 dATP + 0.18 dTTP + 0.32 dCTP + 0.32 dGTP → DNA + PPi + 1.372 ADP + 1.372 Pi + 2.372 H[+]

138 1.4 H_2O + 0.56 ATP + 0.34 GTP + 0.16 UTP + 0.34 CTP →0.4 ADP + 0.4 H[+] + 0.4 Pi + PPi + RNA

Chlorophyll

139 12 H[+] + 8 ATP + 8 GLU + 8 NADPH + 2.5 O_2 → PPorphyrin + 4 NH_4[+] + 6 CO_2 + 8 AMP + 8 NADP + 8 PPi + 13 H_2O

140 18 H[+] + 15 NADPH + 8 ATP + 4 GAP + 4 PYR → Phytyl-PP + 4 ADP + 4 AMP + 4 CO_2 + 7 PPi + 8 H_2O + 15 NADP

141 ATP + H_2O + MET → AdMET + H[+] + PPi + Pi

142 AdHCYS + H_2O ↔ Ad + HCYS

143 ATP + Ad → ADP + AMP + H[+]

144 4 NADPH + 2.5 O_2 + 2 ATP + AdMET + Mg_2[+] + PPorphyrin + Phytyl-PP → AdHCYS + Chlorophyll + PPi + 2 ADP + 2 H_2O + 2 Pi + 3 H[+] + 4 NADP

Starch and carbohydrates

145 G1P ↔ Pi + STARCH

146 G1P ↔ CARB + Pi

Biomass formation

147 32.687 ATP + 32.687 H_2O + 0.6417 PROTEIN + 0.2713 CARB + 0.0453 PA + 0.0305 RNA + 0.0102 Chlorophyll + 0.0011 DNA → Biomass + 32.687 H[+] + 32.687 ADP + 32.687 Pi

Transport

148 CO_2 ← CO_2_ex

149 O_2 → O_2_ex

150 H_2O ↔ H_2O_ex

151 Pi ↔ Pi_ex

152 $SO_4 \leftrightarrow SO_4_ex$
153 $NO_3 \leftrightarrow NO_3_ex$
154 $Mg_2[+] \leftrightarrow Mg_2[+]_ex$
155 Light ← Light_ex
156 $H[+] \leftrightarrow H[+]_ex$
157 GLYC → GLYC_ex
158 STARCH → STARCH_ex
159 Biomass → 172.848 Biomass_ex

4.B Compound abbreviations

13DPG	1,3-diPhosphoglycerate	ASP	Aspartate
2-oxobutan	2-Oxobutanoate	ATP	Adenosine triphosphate
2PG	2-Phosphoglycerate	Biomass	Biomass
3PG	3-Phosphoglycerate	Biomass_ex	Biomass (g)
5FTHF	5-Formyl-THF	C12:0ACP	Dodecanoyl-ACP
6PG	6-Phosphogluconate		(Lauric acid)
AcACP	Acetyl-ACP	C14:0ACP	Tetradecanoyl-ACP
AcCOA	Acetyl-CoA		(Myristic acid)
Ace	Acetate	C16:0ACP	Hexadecanoyl-ACP
ACP	Acetyl-carrier protein		(Palmitic acid)
Ad	Adenosine	C16:1ACP	Trans-Hexadec-2-enoyl-ACP
AdHCYS	S-Adenosyl-L-homocysteine		(Palmitoleic acid)
AdMET	S-Adenosyl-L-methionine	C16:2ACP	Hexadecadienoic acid
ADP	Adenosine diphosphate	C16:3ACP	Hexadecatrienoic acid
AICAR	5-Aminoimidazole-4-carboxamide ribonucleine	C18:0ACP	Octadecanoyl-ACP (Stearic acid)
AKG	2-Oxoglutarate (alpha-ketoglutarate)	C18:1ACP	Cis-11-ocadecanoate-ACP (Oleic acid)
ALA	Alanine	C18:2ACP	Linoleic acid
AMP	Adenosine monophosphate	C18:3ACP	Alpha-linoleic acid
ANTH	Anthranilate	CaP	Carbamoyl phosphate
APS	Adenylyl sulfate	CARB	Carbohydrate
ARG	Arginine	CDP	Cytidine diphosphate
ASA	L-Aspartic semialdehyde	Chlorophyll	Chlorophyll
ASN	Asparagine	CHO	Chorismate

CIT	Citrate	GMP	Guanosine monophosphate
CO_2	Carbon dioxide	GTP	Guanosine triphosphate
CoA	Coenzyme A	H[+]	Proton
CTP	Cytidine triphosphate	H_2O	Water
CYS	Cysteine	H_2O_2	Hydrogen peroxide
DAP	Diaminopimelate	H_2S	Hydrogen sulfide
dATP	Deoxy ATP	HCYS	Homocysteine
dCTP	Deoxy CTP	HIS	Histidine
dGTP	Deoxy GTP	HSER	Homoserine
DHA	Dihydroxyacetone (Glycerone)	HydPro	Hydroxyproline
		HydPyr	3-Hydroxypyruvate
DHAP	Dihydroxyacetone-P	ILE	Isoleucine
DHF	Dihydrofolate	IMP	Inosine monophosphate
DNA	Deoxyribonucleic acid	LEU	Leucine
dTTP	Deoxy TTP	Light	Photons
E_4P	Erythrose 4-phosphate	LYS	Lysine
F16P	Fructose 1,6-bisphosphate	MAL	Malate
F6P	Fructose 6-phosphate	MalCoA	Malonyl-CoA
FAD	Flavin adenine dinucleotide oxidized	MET	Methionine
		METHF	5,10-Methylene-THF
$FADH_2$	Flavin adenine dinucleotide reduced	Mg_2[+]	Magnesium
		MTHF	Methyl-THF
FORM	Formic acid	MYLTHF	5,10-Methenyl-THF
FUM	Fumarate	N10FTHF	10-Formyl-THF
G1P	Glucose 1-phosphate	NAD	Nicotinamide oxidized
G_3P	Glycerate 3-phosphate	NADH	Nicotinamide reduced
G6P	Glucose 6-phosphate	NADP	Nicotinamidephosphate oxidized
GAP	Glyceraldehyde 3-phosphate		
GDP	Guanosine diphosphate	NADPH	Nicotinamidephosphate reduced
GLN	Glutamine		
GLU	Glutamate	NH_4[+]	Ammonium
GLY	Glycine	NO_2	Nitrite
GLYC	Glycerol	NO_3	Nitrate
$GLYC_3P$	Glycerol 3-phosphate	O_2	Oxygen
Glycerate	Glycerate	OXA	Oxaloacetate
glyoxylate	Glyoxylate	PA	Phosphatidic acid

PEP	Phosphoenolpyruvate	S7P	Sedoheptulose 7-phosphate
PHE	Phenylalanine	SER	Serine
Phytyl-PP	Phytyl-diphosphate	SO_3	Sulphite
Pi	Orthophosphate	SO_4	Sulphate
PPi	Pyrophosphate	STARCH	Starch
PPorphyrin	Protoporphyrine	SUC	Succinate
PRE	Prephanate	SUCCoA	Succinyl Coenzyme A
PRO	Proline	THF	Tetrahydrofolate
PROTEIN	Protein	THR	Threonine
PRPP	Phosphorybosylpyrophos-phate	TRYP	Tryptophan
		TYR	Tyrosine
PYR	Pyruvate	UDP	Uridine diphosphate
R5P	Ribose 5-phosphate	UMP	Uridine monophosphate
RNA	Ribonucleic acid	UTP	Uridine triphosphate
Ru15DP	Ribulose 1,5-bisphosphate	VAL	Valine
RU5P	Ribulose 5-phosphate	X5P	Xylulose 5-phosphate

4.C 'Missing' reactions

'Missing' reactions in the *Chlamydomonas reinhardtii* KEGG database which were found by blasting the sequences from other green (micro)organisms against the genome.

#	EC	Name	GeneID
43	3.1.3.1	Alkaline phosphatase	5723324 PHOD
44	1.1.156	Dihydroxyacetone reductase	5720300 LCI28
47	1.7.1.1	Nitrate reductase	5722285 NIT1
50	1.8.99.2	Adynylyl sulfate reductase	5722644 MET16
54	1.6.1.2	NAD(P) transhydrogenase	5725773 CHLREDRAFT 139758
70	1.1.1.25	Shikimate dehydrogenase	5719875 SHKD1
	2.7.1.71	Shikimate kinase	5716011 SHKF1
71	5.4.99.5	Chorismate mutase	5723071 CHM1
72	4.2.1.51	Prephenate dehydratase	5722023 PRD1
73	1.3.1.43	Prephanate dehydrogenase	5720883 AGD1
76	2.4.2.17	ATP phosphoribosyltransferase	*not found, HIS1 (Harris, 2009)*
	2.4.2.-	Glutamine amidotransferase	5722944 HIS7

	3.1.3.15	Histidinolphosphatase	5720418 HIS2
81	1.5.1.2	Pyrroline-5-carboxylate reductase	5723082 PCR1
82	1.14.11.2	Prolyl 4-hydroxylase	5721719 PHX1
84	1.3.1.26	Dihydrodipicolinate reductase	5723456 DPR1
	2.6.1.83	LL-diaminopimelate aminotransferase	5718617 DPA1
88	2.3.1.31	Homoserine acetyltransferase	*not found*
91	3.1.3.18	Phosphoglycolate phosphatase	5728979 PGP1, 5716118 PGP2, 5721833 PGP3
	1.1.99.4	Glycolate dehydrogenase	5721055 GYD1
96	1.1.1.81	Hydroxypyruvate reductase	5717070 HPR1
97	2.7.1.31	Glycerate kinase	5719520 GLYK
100	3.5.4.9	Methenyl-THF cyclohydrolase	5728457 CHLREDRAFT 194856
101	3.5.4.9	Methenyl-THF cyclohydrolase	5728457 CHLREDRAFT 194856
102	1.5.1.5	Methylene-THF dehydrogenase	5728457 CHLREDRAFT 194856
103	1.5.1.20	Methylene-THF reductase	5728030 CHLREDRAFT 111330
104	6.3.3.2	5-formyl-THF cycloligase	5723199 FLC1
105	3.5.1.10	Formyl-THF deformylase	5728093 CHLREDRAFT 111421
106	1.5.1.3	Dihydrofolate reductase	5725986 CHLREDRAFT 139742
113	1.14.19.2	Stearyl-ACP desaturase	5717289 FAB2
115	1.14.19.-	Oxidoreductase (fatty acid desaturase)	5715517 FAD7
117	1.14.19.2	Stearyl-ACP desaturase	5717289 FAB2
119	1.14.19.-	Oxidoreductase (fatty acid desaturase)	5715517 FAD7
121	2.1.2.2	Phosphoribosylglycinamide formyltransferase	5719655 CHLREDRAFT 117678
	4.3.2.2	Adenylosuccinate lyase	5719041 CHLREDRAFT 99287
132	4.3.2.2	Adenylosuccinate lyase	5719041 CHLREDRAFT 99287
133	2.1.1.45	Thymidylate synthase	5725986 CHLREDRAFT 139742
140	2.5.1.29	Geranylgeranyl-diphosphate synthase	5728730 GGPS
144	2.1.1.11	Magnesium protoporphyrin IX methyltransferase	5727888 CHLM
	1.14.13.81	Mg-protoporphyrin IX monomethyl ester (oxidative) cyclase	5716556 CTH1
	1.3.1.75	Divinyl chlorophyllide a 8-vinyl-reductase	5715602 DVR1

4.D Elemental composition of macromolecules

	C	H	O	N	P	S	Charge
Protein	4.8	7.6	1.5	1.3	0	0.03	-
Carbohydrates	6	10	5	0	0	0	-
Lipids (PA)	36.3	63.4	8	0	1	0	-2
DNA	9.7	12.2	7	3.8	1	0	-2
RNA	9.5	12.8	8	3.8	1	0	-1
Chlorophyll	55	72	5	4	0	0	-
Biomass	7.2	11.7	3.0	1.0	0.08	0.02	-

The average elemental biomass composition thus becomes $CH_{1.62}O_{0.41}N_{0.14}P_{0.01}S_{0.003}$. The biomass contains an ash fraction of 0.057. This yields a molecular weight of 23.97 g C-mol^{-1}.

4.E Protein composition in % mol AA/mol protein

Amino Acid	%	Amino Acid	%
Alanine (Ala)	11.07	Leucine (Leu)	9.25
Arginine (Arg)	4.67	Lysine (Lys)	5.78
Asparagine (Asn)	4.68	Methionine (Met)	2.22
Aspartate (Asp)	4.68	Phenylalanine (Phe)	4.45
Cysteine (Cys)	1.17	Proline (Pro)	5.92
Glutamate (Glu)	4.96	Serine (Ser)	5.51
Glutamine (Gln)	4.96	Threonine (Thr)	5.71
Glycine (Gly)	9.36	Tryptophan (Trp)	0.1
Histidine (His)	1.69	Tyrosine (Tyr)	3.08
Hydroxyproline (HydPro)	1.3	Valine (Val)	5.86
Isoleucine (Ile)	3.59		

In the network, proteins were modeled as a coupling of one average amino acid, consuming 4.306 mol ATP. One average amino acid constitutes of the sum of the molar fractions of the various amino acids present in *C. reinhardtii*.

4.F Lipid composition in % mol FA/mol PA

Fatty acid	**%**	**Fatty acid**	**%**
12:0	10.42 ± 0.56	16:3	25.30 ± 0.57
14:0	5.14 ± 0.30	18:0	4.78 ± 0.34
16:0	47.35 ± 1.36	18:1	16.01 ± 0.11
16:1	3.96 ± 0.09	18:2	27.63 ± 0.31
16:2	14.78 ± 0.17	18:3	44.62 ± 1.29

[a] *The standard deviations represent the average molar fractions over 6 steady states.*

In the network, lipids (PA, phosphatidic acid) were modeled as a glycerol-3-phosphate molecule with two acetyl-ACP tails. The average acetyl-ACP chains constitute of the sum of two times the molar fractions of the various fatty acids present in *C. reinhardtii*.

4.G Flux distribution

See separate figure sheet.

Chapter 5

Maximisation of TAG production in microalgae: metabolic modeling of energy partitioning in nitrogen-limited Neochloris oleoabundans

To be submitted as:

Anne J. Klok, Benoit. M. Carreres, Peter J. Schaap, Packo P. Lamers, Dirk E. Martens, René H. Wijffels

Maximisation of TAG production in microalgae: metabolic modeling of energy partitioning in nitrogen-limited Neochloris oleoabundans

Abstract

A transcriptome based metabolic model is presented that describes the primary metabolism of the oleaginous microalgae *Neochloris oleoabundans*. Using this model, the carbon and energy partitioning of nitrogen limited *N. oleoabundans* was studied and the capacity of algal metabolism to produce TAG was evaluated. It was found that under nitrogen replete conditions over one third of the plastidic NADPH is used in nitrogen fixation and protein synthesis, indicating that nitrogen shortage will result in a considerable surplus of NADPH. Under steady state nitrogen limitation, however, *N. oleoabundans* was able to balance its metabolic energy demands with the photosynthetic energy supply by redirecting carbon and energy towards TAG synthesis and by reducing linear electron transport. Furthermore, optimisation scenarios revealed that increasing photosynthetic capacity by uncoupling TAG synthesis from adverse growth conditions provides a larger potential for improving TAG yields on light than redirecting carbon away from competing metabolites, such as starch. Finally, the model was used to evaluate the maximum capacity of *N. oleoabundans* to produce TAG. The maximum theoretical yield of TAG on light is 0.81-1.07 g (mol photons)$^{-1}$, depending on the maximum capacity of the GAP/3PG shuttle. This is more than 3 times higher than what is currently obtained under optimal conditions, and the optimal yield presented here can serve as a point of reference for future optimisation of TAG yield on light.

5.1 Introduction

Adverse growth conditions are often applied to induce microalgae to produce interesting compounds for human use. Well known examples are accumulation of the orange pigment β-carotene in *Dunalliela salina* (Lamers et al., 2012), or the storage lipid triacylglyceride (TAG) by many oleaginous algae (Hu et al., 2008), both of which can be triggered by a shortage of nitrogen in the growth medium. When nitrogen supply is taken away, nitrogen fixation is prevented and protein synthesis is severely hampered. This confronts the alga with an immediate excess of energy that would otherwise be used in the processing of inorganic nitrogen.

An often used explanation for the accumulation of carbon rich compounds in algae faced with nitrogen shortage is that these compounds provide a sink for the surplus of reducing potential generated in the photosystems (Li et al., 2013). Excess reducing potential in the photosystems is something that should be avoided at all times as it can result in the formation of damaging reactive oxygen species (Ledford and Niyogi, 2005). Because the biosynthesis of TAG and β-carotene requires reducing equivalents generated in the chloroplast, accumulating these compounds could be a strategy in safely channelling away redundant electrons, while maintaining considerable carbon fixation rates. Moreover, β-carotene provides a dual protective function, as the molecules can absorb part of the excess radiation.

Unfortunately, applying nitrogen starvation to increase the fraction of desirable compounds usually results in a considerable decline in photosynthetic energy conversion efficiency and growth rate (Frada et al., 2013). Not only are redundant electrons channelled towards highly reduced TAG, at the same time electron generation is reduced by channelling away excess energy in dissipative processes in the photosystems, such as heat formation and chlorophyll fluorescence (Müller et al., 2001). Energy dissipation provides algae with the flexibility to balance photosynthetic energy supply with the energy demands of lower metabolism (Kolber et al., 1988).

As a result of dissipative processes under nitrogen limitation only a small fraction of the electrons that potentially could be generated with the absorbed light actually end up in accumulated TAG molecules. Also, competing metabolites, such as starch, take up electrons that could have been used on TAG synthesis. (Klok et al., 2013b) This poses a problem, in particular in the outdoor production of compounds intended for bulk applications, such as TAG for the production of biodiesel or to replace traditional vegetable oils. Outdoor the inefficient use of the available light due to dissipation and competing products results in a low areal productivity, as the amount of solar light available per surface area is fixed. Efficient light use therefore is an important target in obtaining economical-

ly feasible large scale production of bulk products from microalgae. Studying the interplay between photosynthesis, nitrogen assimilation, carbon partitioning and energy dissipation will provide useful insights in how microalgae control energy and carbon fluxes. These insights can be used to direct carbon fluxes and energy towards TAG, leading to higher areal productivities of this desired compound.
To obtain more insight into carbon and energy partitioning towards TAG under nitrogen shortage , a transcriptome-verified metabolic model is presented that describes the primary metabolism of the oleaginous alga *N. oleoabundans*. This model was used to study the intracellular nitrogen, carbon and energy fluxes during nitrogen replete and nitrogen limited conditions, using the data of 9 previously published experiments (Klok et al., 2013a), along with additional measurements on biomass composition. Also, using the model the room for improvement of TAG productivity could be evaluated by optimising photosynthetic capacity and carbon distributions.

5.2 Materials and methods

5.2.1 Reactor set-up and experiments

To test the effect of nitrogen limitation on the energy and carbon fluxes in the oleaginous alga, *Neochloris oleoabundans* (UTEX 1185, The culture collection of Algae, university of Texas, Austin) was grown in a turbidostat operated flat panel photobioreactor with a nitrogen feed separate from the diluting medium. This type of system allows for independent control of light absorption and nitrogen supply rates to the culture (Klok et al., 2013a). Setting the nitrogen supply rate below the nitrogen demand of the culture, which is dictated by the fixed light absorption rate, will result in nitrogen limited steady state growth conditions.
Light absorption in the turbidostat was controlled by setting a fixed photon flux density entering the system (PFD_{in} in µmol m^{-2} s^{-1}). The photon flux density leaving the system (PFD_{out} in µmol m^{-2} s^{-1}) was measured by a light sensor connected to the rear glass panel of the reactor and compared to a set point. When a value below this set point was detected, a diluting flow of nitrogen free medium was supplied to the system. This control loop ensured a constant PFD_{out} and combined with the fixed PFD_{in}, a constant light absorption (r in mmol L^{-1} h^{-1}) over the entire culture depth (δ_{pbr} in m):

$$r_{\gamma} = \frac{\left(PFD_{in} - PFD_{out}\right) \cdot 3600 \cdot 10^{-6}}{\delta_{pbr}} \qquad (1)$$

A nitrate containing feed was constantly supplied independently of the nitrogen free diluting medium. By setting the flow rate of this feed, the nitrate supply to the system ($F_{NO_3^-.in}$ in mmol L^{-1} h^{-1}) was controlled and could be set above (N replete) or below (N limited) the required nitrogen consumption rate of the culture. The nitrogen consumption rate $r_{NO_3^-}$ (mmol L^{-1} h^{-1}) was calculated as follows:

$$r_{NO_3^-} = F_{NO_3^-.in} - D \cdot C_{NO_3^-.out} \qquad (2)$$

with D (h^{-1}) as the dilution rate that is the result of the culture growth, and $C_{NO_3^-.out}$ (mmol L^{-1}) as the residual nitrate concentration in the reactor. Under N-replete conditions, residual nitrate is present in the system, while under N-limited conditions, all nitrate is consumed and $r_{NO_3^-}$ equals $F_{NO_3^-.in.}$

Two light absorption rates (Low light; LL and High light; HL) were combined with several nitrate supply rates, which resulted in nine steady states ([A]-[I], see Table 5.1). Steady state was defined as a constant biomass concentration, cell characteristics, off gas concentrations and dilution rate during at least 6 consecutive days.

More information about photobioreactor specifications and operation, as well as a detailed description of culture media and conditions can be found in (Klok et al., 2013a).

Table 5.1 *Combinations of several nitrate supply rates with two light absorption rates resulted in 9 steady states. The nitrogen replete reference conditions [A] and [E], for low light and high light respectively, are indicated in grey.*

	Low light conditions				*High light conditions*				
Experiment	**A**	**B**	**C**	**D**	**E**	**F**	**G**	**H**	**I**
PFD_{in} ($\mu mol\ m^{-2}\ s^{-1}$)	193	193	193	193	460	460	460	460	460
PFD_{out} ($\mu mol\ m^{-2}\ s^{-1}$)	18	16	16	17	69	70	70	71	70
r_γ ($mmol\ L^{-1}\ h^{-1}$)	32	32	32	32	70	70	70	70	70
$F_{NO_3^-.in}$ ($mmol\ L^{-1}\ h^{-1}$)	0.36	0.10	0.06	0.04	0.61	0.21	0.16	0.11	0.06
$r_{NO_3^-}$ ($mmol\ L^{-1}\ h^{-1}$)	0.19	0.10	0.06	0.04	0.27	0.21	0.16	0.11	0.06

5.2.2 Biomass analysis and additional measurements

To monitor the culture, samples were taken every day at the same hour. These samples were analysed for dry weight biomass concentration, optical density, cell concentration, cell size and residual nitrate in the supernatant, as described by (Kliphuis et al., 2012).

The growth rate of the culture was equal to the steady state dilution rate, and was calculated by dividing the amount of overflow produced in 24h (V_{24} in L h^{-1}) by the reactor volume (V_{pbr} in L):

$$\mu = D = \frac{V_{24}}{V_{pbr}} \tag{3}$$

The composition of the gas mixture leaving the system was analysed using a prima dB mass spectrometer (ThermoFisher, USA). Additionally, a reference measurement was done by analysing the composition of the ingoing gas mixture. With these measurements, the volumetric oxygen production rate (r_{O_2}, mmol L^{-1} h^{-1}) and carbon dioxide consumption rate (r_{CO_2}, mmol L^{-1} h^{-1}) rates could be calculated:

$$r_{O_2} = F_{gas.out} \cdot x_{O_2.out} - F_{gas.in} \cdot x_{O_2.in} \tag{4}$$

$$r_{CO_2} = F_{gas.out} \cdot x_{CO_2.out} - F_{gas.in} \cdot x_{CO_2.in} \tag{5}$$

with $x_{O2.out}$, $x_{O2.in}$, $x_{CO2.out}$ and $x_{CO2.in}$ as the molar fractions of O_2 and CO_2 (-), and $F_{gas.in}$ and $F_{gas.out}$ as the total molar gas flow rates entering and leaving the system (mmol L^{-1} h^{-1}), respectively. To account for any difference between $F_{gas.in}$ and $F_{gas.out}$ due to CO_2 consumption and O_2 production inside the photobioreactor, the nitrogen gas feed flow ($F_{gas.in} \cdot x_{N2.in}$) was used as a reference to determine $F_{gas.out}$:

$$F_{gas.out} = \frac{x_{N_2.in}}{x_{N_2.out}} \cdot F_{gas.in} \tag{6}$$

When steady state was reached, biomass samples were collected on ice over a period of exactly 24h. The obtained biomass was centrifuged, washed and lyophilized as described by (Kliphuis et al., 2012). The supernatant of the 24h samples was evaluated for TOC (Total Organic Carbon), which was measured as the difference between total carbon (TC) and inorganic carbon (IC), using a TOC-V_{CPH}/TOC-V_{CPN} Total Organic Carbon Analyser (Shimadzu corp, Kyoto, Japan). This determination of dissolved organic carbon, allowed for the correction of the measured biomass concentrations for any biomass lost due to cell lysis, assuming that all organic material in solution had the same elemental composition as suspended biomass.

The freeze dried algae powder collected in each steady state was used for all biomass characterisations. The dry weigh content of 20 amino acids was determined by Ansynth Service BV (Berkel en Roodenrijs, The Netherlands), as described by (Kliphuis et al., 2012). The total amount of protein in biomass was assumed to be the sum of the water corrected mass of these 20 amino acids. The total fatty acid content and TAG content of dry biomass, and the fatty acid composition of each lipid pool was determined as described by (Klok et al., 2013a). Carbohydrates were measured by treating the freeze dried algae powder with a phenol solution and concentrated sulphuric acid, according to (Dubois et al., 1956) and (Herbert et al., 1971). The absorbance of the resulting solution was measured at 483nm. Glucose was used as a standard. Starch was measured in the lyophilized biomass samples using a commercial kit (Total Starch (AA/AMG), Megazyme International, Bray, Ireland).The carotenoid and porphyrin (i.e. chlorophyll) fractions were quantified using RP-UHPLC as previously described by (Weesepoel et al., 2013), with some minor adaptations (Appendix 5.B).

The ash content of biomass was determined as described by (Kliphuis et al., 2012).

The nucleic acids DNA and RNA were not measured directly, but determined from cell number data. *N. oleoabundans* has an estimated genome size of 68.2 Mb, with a CG content of 60% (internal communication). Assuming that each cell contains a single copy of DNA, it could be calculated that each cell contains $8.1x10^{-14}$ g DNA per cell. Transcriptome analysis revealed that RNA had an average GC content of 59%, and the RNA content was based on the observation that the cellular RNA:DNA ratio increase with increasing specific growth rate (μ, here in d^{-1}) of (Dortch et al., 1983). Their equation derived for 3 nitrogen limited marine phytoplankton cultures was used in our calculations:

$$\mu = 0.255 \cdot \frac{RNA}{DNA} - 0.287 \quad (7)$$

5.2.3 RNA sampling and Transcriptome assembly

To validate the metabolic model, a *de novo* assembled transcriptome of *N. oleoabundans* was used, which was constructed using RNA collected in experiments [A], [C], [E], [F] and [I].

Biomass for RNA extraction was obtained from 50 mL of culture volume, that was centrifuged at 3900 RCF, for 5 minutes at 4 ˚C. The resulting biomass pellets were quickly frozen and stored at -80 ˚C. Frozen pellets were ground under liquid nitrogen using a pestle and mortar. Subsequently, the total nucleic acid fraction of 0.5 g of ground and frozen pellet was extracted, using a preheated (65 ˚C) mixture of 1 mL liquefied phenol and 1 mL extraction buffer containing 1% SDS (v/v), 10 mM EDTA, 0.2 M NaAc (pH 5) and 2% β-mercaptoethanol (v/v). When samples were cooled to room temperature, they were mixed for 15 seconds using a vortex. Subsequently, 1 mL of chloroform was added and samples were mixed again. The aqueous phase was collected after 15 minutes of centrifugation (13.000 RCF), and reextracted with 1 mL chloroform. The last obtained aqueous phase was diluted 4 times with a 8 M LiCl solution containing 1% β-mercaptoethanol (v/v). Subsequently, RNA was allowed to precipitate overnight at 4 ˚C and collected by centrifugation (15 min at 13.000 RCF). The obtained RNA pellet was washed once with 2M LiCl and twice with 70% (v/v) ethanol, and finally dissolved in MilliQ water.

Sequencing libraries for the Illumina platform were generated from the isolated RNA, and subsequently sequenced, assembled and annotated, all at BaseClear BV (Leiden, The Netherlands). Total RNA was first assessed for quality on a Bioanalyzer 2100 (Agilent Technologies Inc, Santa Clara, USA) and used as input for library preparation using the Illumina TruSeq RNA library preparation kit (Illumina Inc, San Diego, USA). Briefly, the mRNA fraction was purified from total RNA by polyA capture, fragmented and subjected to first-strand cDNA synthesis with random hexamers. After second-strand synthesis, barcoded DNA adapters were ligated to both ends of the double-stranded cDNA, the ligated product was size-selected and subjected to PCR amplification for 15 cycles. The resultant sequencing library was checked on a Bioanalyzer (Agilent Technologies Inc, Santa Clara, USA) and quantified. The libraries were multiplexed, clustered, and sequenced on an Illumina HiSeq 2000 with paired-end protocol for 50 cycles. The sequencing run was analyzed with the Illumina CASAVA pipeline

(v1.8.2), with demultiplexing based on sample-specific barcodes. The raw sequencing data produced was processed removing the sequence reads which were of too low quality (only "passing filter" reads were selected) and discarding reads containing adaptor sequences or PhiX control.
The obtained FASTQ sequence reads were assembled using Trinity (Grabherr et al., 2011), which is specifically designed for transcriptome assembly without a reference genome. The resulting set of contigs were annotated with Rapsearch2 (Zhao et al., 2011), using the Swissprot/Uniprot database, followed by reannotation of the unknown entries using the NCBI non-redundant database, with a cut off E-value ≤ 10^{-3}. Associated enzyme commission (EC) numbers were retrieved where possible.

5.2.4 Flux balance analysis

The metabolism of any organism can be described by a set of reaction equations that define the stoichiometry of the conversion of substrates into products (Stephanopoulos et al., 1998). In this paper, a metabolic network is presented that describes the primary metabolism of the oleaginous green alga *Neochloris oleoabundans*. To calculate the fluxes through this network, flux balance analysis was applied, using the measured production and consumption rates of the nitrogen replete and nitrogen limited steady states.
The stoichiometry matrix S of the metabolic model contains the stoichiometric coefficients of the substrates and products for the different reactions in the metabolic network, including the transport reactions over the membranes. Mass balances are written for all the intracellular metabolites present in the network. Assuming steady state and neglecting the net production of intermediates, this results in the next set of linear equations, which are used to calculate the fluxes in the network:

$$A \cdot x = 0 \tag{8}$$

in which A is the transpose of the stoichiometry matrix S, and x is the vector which contains the reaction rates. The solution space of equation 8 was studied to find possible dead ends in the presented model, which were subsequently removed.
Three redundancy relations were extracted from the model stoichiometry being a nitrogen balance, a carbon balance and a redox balance. The measured production and consumption rates of functional biomass (i.e. biomass that does not contain starch, TAG and ash), starch, TAG, nitrate, carbon dioxide and oxygen were checked for consistency using these redundancy relations and a Chi-Squared test. Subsequently, consistent rates were balanced according to (van der Heijden et al., 1994).

Flux distributions were subsequently calculated using optimization of an objective function:

$$\begin{aligned} &\text{Objective function:} && \max(c \cdot x) \\ &\text{Constraints:} && A \cdot x = 0 \\ & && LB \le x \le UB \end{aligned} \qquad (9)$$

in which c contains the objective function and LB and UB are the lower and upper boundary of reaction rate x. In this study the objective functions 'maximise dissipation' or 'maximise product yield' were used. Reactions that are irreversible were constrained to one direction. Constraints were set on transport fluxes depending on whether a compound was consumed or produced. In case a rate was measured, the transport rate was constrained to the balanced value.
Due to underdetermined reaction sets the obtained solutions are not unique. In order to find the underdetermined reaction sets equation 8 is converted to:

$$A_c \cdot x_c = -A_m \cdot x_m \qquad (10)$$

where x_c contains the unknown and x_m contains the measured rates. A_c and A_m are the corresponding parts of A. Underdetermined reaction sets were next found by studying the null space of A_c using singular value decomposition. Using additional constraints as discussed in paragraph 3.1.5, unique solutions were obtained.
Mathcad 14.0 (M020, Parametric Technology Corporation, USA) was used for network analysis and Matlab (version 6.0.0.88, release 12, The MathWorks Inc., USA) was used for *in silico* simulations.

5.3 Results and Discussion

5.3.1 Metabolic Network reconstruction

A metabolic network was constructed describing the primary metabolism of the green alga *Neochloris oleoabundans*, based on a previously published genome based network of *Chlamydomonas reinhardtii* (Kliphuis et al., 2012). In the presented model compartmentalisation with respect to the chloroplast and lipid metabolism were included (sections 5.3.1.1-5.3.1.2), to better describe TAG accumulation and its effect on the car-

bon and energy distributions of *N. oleoabundans*. It comprises of 373 reactions divided over two cellular compartments: the chloroplast and the cytosol. This extensive network of 373 reactions was reduced to a more manageable size of 216 reactions and 219 metabolites by lumping linear pathways (Appendix 5.A and Figure 5.1A).

The 373 model reactions are carried out by 226 enzymes with known EC numbers, as several enzymes catalyse multiple reactions. In addition, complex processes such as the photosynthesis and respiration reactions were lumped into single reactions and assumed to be functional and as such not linked to specific EC numbers. Finally, the modelled transporting steps do not have a specific EC number and are often the result of gap filing to obtain a functional model as they have not been identified yet. The known EC numbers were cross-checked with the *de novo* assembled and annotated transcriptome of *N. oleoabundans*, to verify the presence of the enzymes catalysing the modelled reactions. Of the 226 unique EC numbers present in the model, 225 were retrieved from the transcriptome. The missing enzymatic step involves 1.17.1.2 (4-hydroxy-3-methylbut-2-enyl diphosphate reductase), which catalyses two steps in the biosynthesis of porphyrins and carotenes. As the *N. oleoabundans* transcriptome does contain the neighbouring enzymatic steps and is able to synthesize both chlorophyll as well as carotene, we assume that these reactions are performed by another protein, that could not be identified as such.

5.3.1.1 Compartmentalisation

The subcellular compartmentalisation of the presented model is more detailed than the previously published *C. reinhardtii* network, to get better insights into the production and use of energy carriers ATP, NADPH, NADH and $FADH_2$ in these compartments, and the separate contributions of photosynthesis and respiration on energy supply for cellular processes. The decision to place a certain reaction in either the chloroplast (metabolites denoted with a 'c') or the cytosol was based upon the well-defined, genome-scale *C. reinhardtii* model of (Chang et al., 2011) (Appendix 5.A). An exception were reactions 95 and 96 (biosynthesis of lysine), which were placed in the plastid on the basis of the NCBI database, which predicted a plastid targeting for all enzymes involved in these reactions based on homology with other similar enzymes.

5.3.1.2 Lipid biosynthesis

The model for *C. reinhardtii* was expanded with a more detailed lipid biosynthesis pathway. The compartmentalisation of fatty acyl lipid assembly and in particular the assembly of TAG, in green microalgae is rather complex. It was generally accepted that these

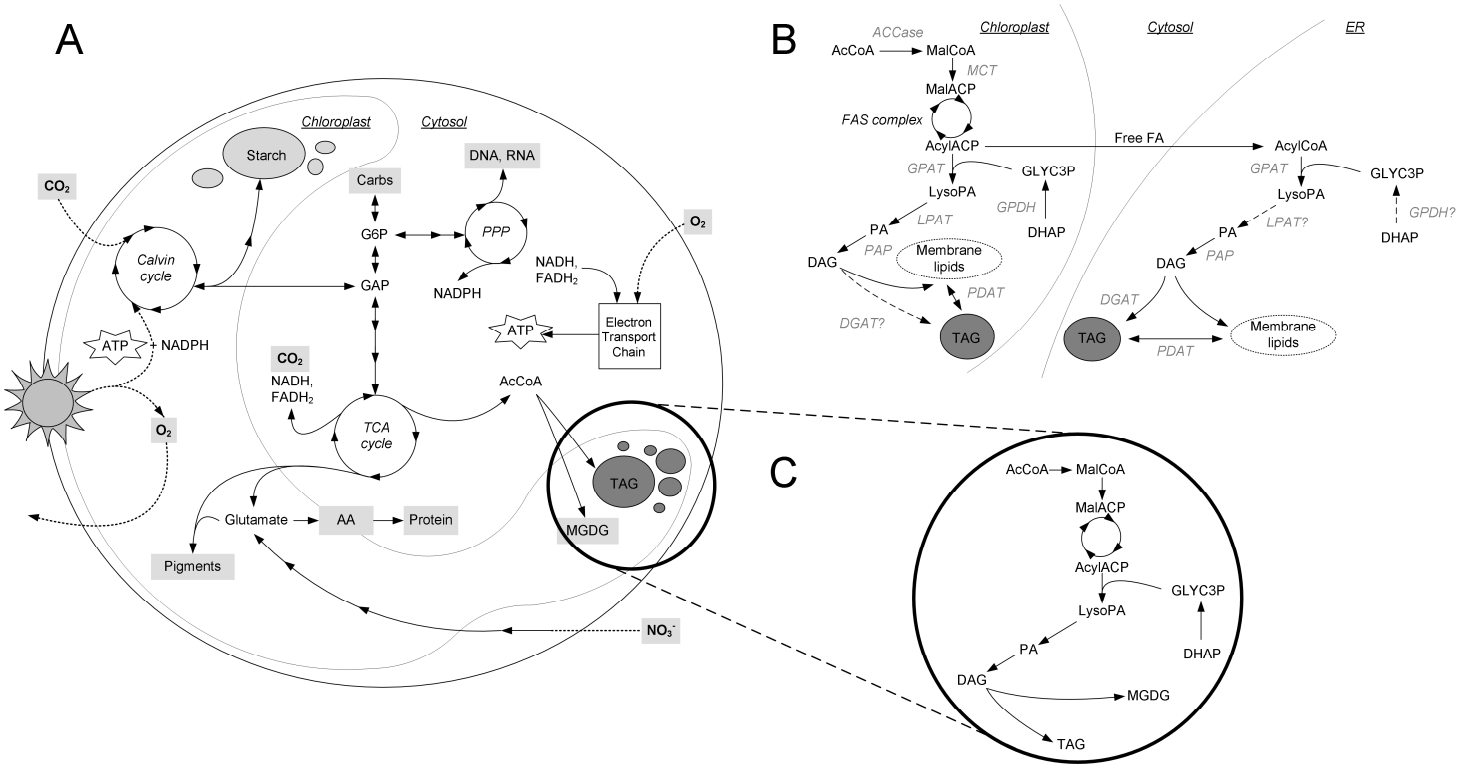

Figure 5.1 *A. Simplified overview of the metabolic network. B. Schematic overview of glycerolipid biosynthesis in microalgae. '?' denotes uncertainty about the existence of these enzymes. C. In the presented network, glycerolipid synthesis is simplified, occurs exclusively 'de novo' and is located in the chloroplast.*

pathways were similar as in plants with fatty acid biosynthesis strictly targeted to the plastid, membrane lipid assembly taking place in both the plastid and the ER and TAG assembly occurring only in the ER (Ohlrogge and Browse, 1995). However, the discovery of a chloroplast pathway for *de novo* TAG synthesis (Fan et al., 2011) in *C. reinhardtii* and the absence of extraplastidic LPAT (Lysophosphatidic acid acyltransferase) in all but one microalgae (Li et al., 2013), argues for a plastid targeted TAG pathway in algae (Figure 5.1B). The low activity of glycerol-3-phosphate dehydrogenase (GPDH) outside the plastid of *C. reinhardtii* (Johnson and Alric, 2013; Klöck and Kreuzberg, 1989), the enzyme catalysing the formation of the glycerol backbone in all lipids, seems to confirm that the bulk of lipid assembly takes place inside the chloroplast. On the other hand, the lack of plastid targeting sequences for DGAT (diacylglycerol acyltransferase) in *C. reinhardtii* (Liu and Benning, 2013) argues otherwise. Based on (and despite one of) these observations, both membrane, as well as TAG assembly were placed in the plastid in this metabolic model (Figure 5.1C).

Another complication in modeling the TAG biosynthesis pathway arose from the fact that TAG can be formed via two different routes (Figure 5.1B). After synthesis of the common precursor for both membrane and storage lipid, DAG (diacylglycerol), the formation of TAG is catalysed by either DGAT or PDAT (phospholipid:diacylglycerol acyltransferase). The first enzyme utilises a free acyl group and the second uses a membrane lipid as acyl donor, as such providing a turnover route between the TAG and membrane lipid pool. As we did not measure the turnover rate of membrane lipids to TAG, incorporating both TAG synthesis reactions in a metabolic network would result in an underdeterminancy. The latter reaction was therefore omitted and the model was restricted to only *de novo* lipid synthesis (Figure 5.1C).

The average membrane composition in algae and plants reflects that of the most dominantly present membrane type, the plastid and thylakoid membranes. These mainly consists of MGDG (monogalactosyl-diacylglycerol, 40-55%) and DGDG (digalactosyl-diacylglycerol, 15-35%) and sulfolipid SQDG (10-20%, sulfoquinovosyl-diacylglycerol) (Harwood, 2004). In absence of lipid class identification, galactolipid MGDG was therefore chosen as representative for the membrane lipids. Furthermore, the ATP, NAD(P)H and carbon requirements do not differ much for these lipids, suggesting a negligible effect of this simplification on our analysis.

5.3.1.3 Photosynthesis

Several fates can be distinguished for the excitation energy resulting from photon absorption. First of all, photons can be absorbed and their excitation energy is used for the

production of energy carriers ATP and NADPH (i.e. photochemistry). Secondly, the photosystems can be de-excited through emission of photons of a lower wavelength (i.e. fluorescence). Finally, part of the excitation energy can be thermally dissipated in processes that are known as non-photochemical quenching (NPQ). (Müller et al., 2001)
In the presented model, photochemistry was simplified and consisted out of the two most important photochemical processes that result in the production of ATP and/or NADPH: linear electron transport (LET) and cyclic electron transport (CET). Other processes that involved energy transfer in the photosystems or the plastoquinone pool, such as pseudo cyclic electron transport (Endo and Asada, 2006) and chlororespiration (Bennoun, 2004), were neglected. In the absence of measurements on fluorescence and NPQ, these dissipative processes were lumped into one dissipation reaction, which entails the absorption of a photon and the subsequent release of a fluorescent photon (reaction 3). This lumping does not influence the calculated flux distributions, and the calculated rate of fluorescent photon release can be regarded as a measure for all energy dissipation, without considering the relative contributions of NPQ and fluorescence.
According to the Z-scheme of photosynthesis, LET delivers 3 ATP and 2 NADPH per 8 photons when it is working at maximum quantum efficiency, which exactly matches the stoichiometry required for CO_2 fixation via the Calvin cycle. CET yields no NADPH, and 1 ATP per 2 photons absorbed. Measurements of the total quantum requirement under ideal low-light conditions for a variety of organisms using a variety of experimental techniques (Bjorkman and Demmig, 1987; Dubinsky et al., 1986; Emerson and Lewis, 1943; Evans, 1987; Ley and Mauzerall, 1982; Malkin and Fork, 1996; Tanada, 1951), showed that the minimum quantum requirement of oxygen evolution was equal to 10, instead of the theoretical minimum of 8, which is indicative of LET and CET occurring simultaneously. This is likely, as the actual ratio of ATP/NADPH delivered by LET is lower than 1.5, and some extent of CET is necessary to generate additional ATP (Allen, 2003). In the presented model, LET was therefore assumed to deliver 3 ATP and 2 NADPH for each 10 photons absorbed (reaction 0, see Appendix 5.A), implicitly assuming some level of CET in this equation. Also, it was assumed that the NADPH and/or ATP yields of both CET and LET remained unchanged under nitrogen limitation.
In addition, CET (reaction 1) was also modelled separately, to generate additional ATP when the stoichiometric demand for ATP:NADPH in the plastid exceeds 1.5. Alternatively, additional ATP can also be supplied by respiration. Finally, synthesis of highly reduced compounds could cause the stoichiometric demand of ATP:NADPH use in the plastid to decrease below 1.5, and as such create excess ATP. Because excess plastidic ATP cannot be transported from the chloroplast (section 5.3.1.4) to be dissipated in the

cytosol (reaction 10), a reaction for plastidic ATP hydrolysis was added to the model (reaction 2), which represents maintenance reactions in the chloroplast.

5.3.1.4 Transport of NADPH and ATP across the plastid membrane

As TAG synthesis under nitrogen limitation is thought to be caused by an imbalance in reducing equivalents (Li et al., 2013), it is relevant to evaluate the supplies and demands of ATP and NADPH in the plastid. Besides direct production and use of these compounds by reactions in the chloroplast, they can also be transported over the chloroplast membrane into or out of the cytosol. Several options for ATP and NADPH transport exist, either through direct transport, or by metabolic shuttles which indirectly move NADPH and/or ATP from one cell compartment to the other (Figure 5.2). These transporters and shuttles are discussed below.

ATP/ADP transporters are well described to be present in the plastid membrane, and exclusively transport ATP into the plastid (Heldt, 1969). This transport would allow respiratory ATP to complement the ATP demands in the plastid during excessive growth or in the dark (Hoefnagel et al., 1998). Therefore, ATP transport (reaction 201) was limited to transport from the cytosol into the plastid. The intact chloroplast membrane is impermeable to NAD(P)H (Heber, 1974), and no transporters have been described for these compounds. Therefore, direct transport of reducing equivalents was not incorporated in the model.

Alternatively, indirect transport of ATP and or NADPH can occur through specialized shuttles (Figure 5.2), such as the glyceraldehyde 3-phosphate (GAP)/3-phosphoglycerate (3PG) shuttle (Johnson and Alric, 2013), which involves reactions 12, 13, 172, 30, 31 and 173. This reaction is known to convert plastidic NADPH and ATP into cytosolic NADH and ATP, or vice-versa. A similar NADPH shuttle is formed by the reactions concerning glutamine and glutamate transport and synthesis (reactions 76-78, 177, 196 and 197) (Linka and Weber, 2005; Yu and Woo, 1988; Weber and Flügge, 2002). This glutamine/glutamate shuttle does not only link plastidic and cytosolic nitrogen metabolism, but also converts NADPH from the plastid into NADPH in the cytosol, at the expense of one cytosolic ATP.

In this study, the carbon and energy partitioning under nitrogen limitation is evaluated. Both shuttles can be used to change the pool sizes of ATP and NADPH in the plastid, and thus influence the imbalance of reducing equivalents that is thought to be the cause of TAG accumulation under nitrogen limitation. As these fluxes are underdetermined, both shuttles were restricted by disabling the transport of 3PG and glutamine across the plastid membrane (reaction 173 and 197). This situation was regarded as the base case

scenario, and the effect of both shuttles on the NADPH balances and the maximum yield of TAG on light was evaluated in section 5.3.4.

As a result of disabling the glutamine/glutamate shuttle, *de novo* glutamine is produced in the cytosol, and glutamine in the plastid serves as an intermediate for glutamate production. As glutamine synthesis from glutamate follows the same stoichiometry in both the plastid and the cytosol, the disabling of glutamine transport will not affect our energy analysis in this respect.

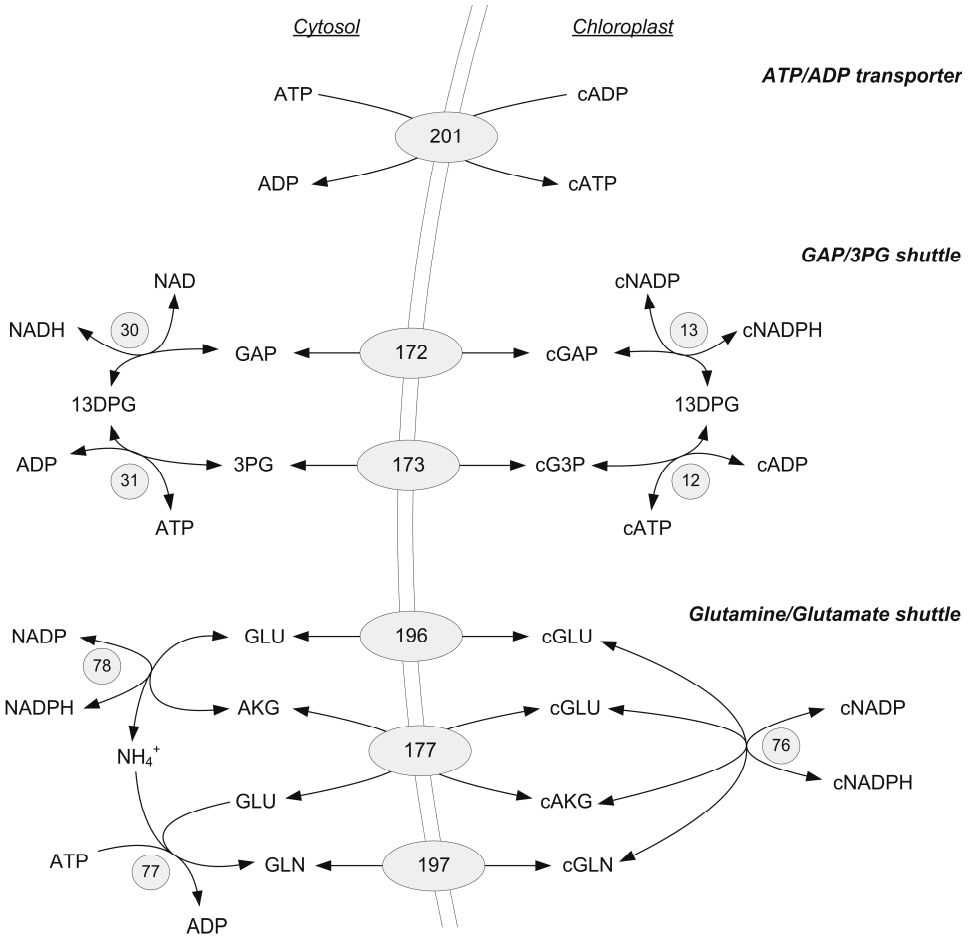

Figure 5.2 *Various transporters and shuttles are available to shuttle ATP and reducing equivalents across the plastid membrane. The ATP/ADP transporter exchanges plastidic ADP for cytosolic ATP. The GAP/3PG shuttle converts plastidic NADPH and ATP in cytosolic NADH and ATP, or vice-versa. Finally, the glutamine/glutamate shuttle converts NADPH from the plastid into NADPH in the cytosol, at the expense of 1 cytosolic ATP.*

5.3.1.5 Underdetermined parts

By studying the null-space of matrix A_c (Equation 10), it was revealed that the model contained 13 underdetermined parts. By constraining irreversible reactions and thermodynamically impossible combinations of reactions to the correct directions (Appendix 5.A), and by choosing the objective functions 'maximise dissipation' and 'maximise product yield', unique values could be calculated for all but one underdetermined part. This underdeterminancy involved the anaplerotic routes between phosphoenolpyruvate, pyruvate, and oxaloacetate, and was solved by disabling reaction 55, as described by (Kliphuis et al., 2012).

5.3.1.6 Energy parameter estimation

As described by (Kliphuis et al., 2012), one of the most important underdetermined parts in any metabolic network, concerns the generation and use of ATP. The ATP balance for the complete network can be written as:

$$q_{cATP.light} + q_{ATP.ox} + \sum q_i^{cATP} + \sum q_i^{ATP} - (K_{x.cATP} + K_{x.ATP}) \cdot r_x - m_{cATP} - m_{ATP} = 0 \quad (11)$$

The first four terms of this equation relate to the part of the network that has a known stoichiometry in the model, which include the specific cATP ('c' for chloroplast) production rate of the light reactions, $q_{cATP.light}$ (mmol (g protein)$^{-1}$ h^{-1}), and of oxidative phosphorylation in the cytosol, $q_{ATP.ox}$ (mmol (g protein)$^{-1}$ h^{-1}). The latter ATP production rate depends on the P/O ratio, which represents the amount of ATP generated per oxygen atom that is reduced. Here, a constant P/O ratio of 2.5 and 1.5 was assumed for respiration of NADH or $FADH_2$ respectively. Finally, the terms Σq_i^{cATP} and Σq_j^{ATP} (mmol (g protein)$^{-1}$ h^{-1}) represent the remaining specific cATP and ATP production and consumption rates of reactions in the network with a known stoichiometry.

Several ATP demanding processes in the cell that are necessary for growth have an unknown stoichiometry, such as the carbon concentrating mechanism, intracellular transport, and assembly of macromolecules into functional biomass. These "growth associated" ATP demands are linearly dependent on the specific production rate of functional biomass, r_x (mmol (g protein)$^{-1}$ h^{-1}), and are summarized in the term ($K_{x.cATP}$ + $K_{x.ATP}$) in mmol (mmol functional biomass)$^{-1}$, which represents the growth associated ATP demand in the chloroplast and cytosol. This will be called 'growth-associated

maintenance' to discriminate it from the maintenance treated further on. Since the term ($K_{x.cATP}$ + $K_{x.ATP}$) refers to functional biomass only, it is implicitly assumed that, besides the ATP requirement defined in the stoichiometric network, no further ATP is required for the production of starch and TAG for the packing of these macromolecules in starch granules and lipid bodies. Finally, ATP will be used for maintenance in both cell compartments, where m_{cATP} stands for maintenance demands in the plastid and m_{ATP} for maintenance demands in the cytosol, both in mmol (g protein)$^{-1}$ h^{-1}.

In order to estimate the unknown ATP consumption associated with maintenance and growth-associated maintenance, a number of nutrient replete steady states at different growth rates and low light intensities are required, as described by (Kliphuis et al., 2012). Under these conditions it can be assumed that light energy dissipation is kept to a minimum. Consequently, all absorbed photons are used for the generation of ATP ($q_{cATP.light}$-) according to the modelled LET stoichiometry, which is in accordance with the empirical minimum quantum requirement of 10, as described in section 5.3.1.3.

In the absence of multiple nutrient replete steady states at lower average light supply rates, we used the only steady state that met these requirements, steady state [A], and the assumption that the ATP maintenance requirement is the same as was measured in *C. reinhardtii*: 2.85 mmol g^{-1} h^{-1}, which is equal to 7.08 mmol (g protein)$^{-1}$ h^{-1} at an average protein content of 40.23% protein (w/AFDW) (Kliphuis et al., 2012). To determine the growth-associated maintenance, ($K_{x.cATP}$ + $K_{x.ATP}$) was set to zero in the functional biomass formation equation (reaction 170) and the consumption rates of CO_2, NO_3^-, and the production rates of TAG, starch, functional biomass and oxygen (reactions 202, 207, 212, 214, 215 and 204, respectively), were restricted to the balanced values obtained for experiment [A] (Table 5.3B).

Using the objective function 'maximise ATP + cATP yield', it was calculated that in total, 28.93 mmol ATP (g protein)$^{-1}$ h^{-1} was unaccounted for in the model. When evaluating the flux distribution it appeared that approximately 14% of this ATP was generated in the plastid. Assuming that the total ATP generation in [A] reflects the actual ATP demand *in*

Table 5.2 *Compartmentalised maintenance (m_{ATP}) and growth-associated maintenance ($K_{x.ATP}$).*

		Chloroplast	*Cytosol*
m_{ATP}	*in mmol (g protein)$^{-1}$ h^{-1}*	1.13	5.95
$K_{x.ATP}$	*in mmol (mmol functional biomass)$^{-1}$*	4.94	25.98

vivo, and that this ratio of plastidic and cytosolic ATP use is conserved for both maintenance and growth-associated maintenance throughout all tested conditions, it could be calculated that m_{cATP} and m_{ATP} are equal to 1.13 and 5.95 mmol (g protein)$^{-1}$ h^{-1}. The remaining cATP and ATP consumption rates are allocated to the functional biomass formation equation (reaction 170), which was working at a rate of 0.7067 mmol (g protein)$^{-1}$ h^{-1}. This means, that $K_{x.cATP}$ and $K_{x.ATP}$ are equal to 4.94 and 25.98 mmol (mmol functional biomass)$^{-1}$ respectively.

With this information, all ATP use in the model could be accounted for (Table 5.2). The values for $K_{x.cATP}$ and $K_{x.ATP}$ were incorporated in the functional biomass formation equation and were assumed to be constant under all experimental conditions. For further calculations, m_{cATP} and m_{ATP} were set as minimal values for ATP hydrolysis in the chloroplast (reaction 2) and in the cytosol (reaction 10), respectively. Also the maintenance demands were assumed to be unaffected by the experimental conditions, although it is possible that these demands increase under higher light supply rates or nitrogen limitation.

5.3.2 Turbidostat experiments

Combining two light absorption rates with several nitrate supply rates resulted in the 9 steady states that were described in (Klok et al., 2013a). The composition of the biomass collected in each steady state ([A]-[I]) can be found in Table 5.3A. Using the relative composition of functional biomass, the stoichiometry of the functional biomass synthesis reaction could be calculated for each steady state (Appendix 5.A). As the amino acid composition of protein and fatty acid composition of TAG and membrane lipids did not exhibit large variations throughout the tested experimental conditions, the average composition of these molecules was used for determining the stoichiometry of their respective formation equations (Appendix 5.A).

Based on their respective fractions and the measured growth rates and biomass concentrations, the production rates of starch, TAG and functional biomass were calculated. The combined balances for nitrogen, carbon and redox closed with a 95% confidence interval according to the Chi-Squared test, for all experiments with the exception of [E], which was just outside the 95% confidence interval (Appendix 5.A). In [E], the nitrogen consumption rate was slightly too low compared to what could be expected based on the measured functional biomass production rate, which could be explained from an unreliable nitrate measurement. Therefore, the rates in all other experiments were balanced using the nitrogen, carbon and redox balance according to (van der Heijden et al., 1994), while for [E] only the carbon and redox balance were used for balancing.

The nitrogen balance was used to calculate the nitrate consumption rate from the production rate of functional biomass. The balanced rates obtained for each steady state, expressed in mmol (g protein)$^{-1}$ h^{-1}, can be found in Table 5.3B.

Table 5.3 *Normalized compositions of total biomass and functional biomass (A) and balanced rates (B) obtained for each experimental condition.*

A[a]	*Normalised biomass composition (%w/w)*								
Experiment	A	B	C	D	E	F	G	H	I
Ash	6.2	5.4	4.9	3.7	6.7	5.9	5.7	4.3	3.9
TAG	1.5	3.7	7.5	12.4	1.7	2.7	4.3	7.0	8.7
Starch	14.2	23.4	29.1	34.7	25.2	28.2	30.9	39.5	42.4
Functional Biomass	78.1	67.5	58.6	49.2	66.3	63.3	59.1	49.3	45.0
	Functional biomass composition (%w/w)								
Protein	49.8	49.6	49.8	46.8	53.5	48.5	47.5	46.6	45.0
Carbohydrate	21.5	24.2	25.7	34.3	17.6	22.0	26.2	31.6	34.6
Membrane lipid	13.4	15.1	15.9	13.8	13.3	13.7	13.1	13.6	15.1
Chlorophyll	2.5	1.8	1.7	1.5	2.2	1.4	1.2	1.1	1.0
Carotenoid	0.4	0.4	0.3	0.3	0.4	0.4	0.3	0.3	0.3
RNA	10.5	7.0	4.6	2.2	11.5	11.9	9.6	5.2	2.8
DNA	1.9	2.0	1.9	1.2	1.4	2.1	2.1	1.6	1.2
B	*Balanced rates in mmol (g protein)$^{-1}$ h^{-1}*								
Experiment	A	B	C	D	E	F	G	H	I
$r_{NO_3^-}$	-0.83	-0.36	-0.21	-0.16	-1.34	-0.76	-0.60	-0.41	-0.28
r_X	0.71	0.33	0.20	0.17	1.08	0.64	0.54	0.41	0.30
r_{TAG} [b]	2.45	4.15	5.25	7.76	4.82	5.62	7.76	10.3	9.55
r_{STARCH}	0.13	0.14	0.11	0.12	0.38	0.32	0.30	0.31	0.25
r_{CO_2}	-5.48	-3.22	-2.24	-2.24	-9.48	-6.41	-5.69	-5.06	-3.97
r_{O_2}	7.47	4.19	2.88	2.81	12.64	8.27	7.24	6.28	4.88
r_γ	-124	-112	-107	-129	-271	-259	-259	-272	-304

[a] *N≥ 3 for each measurement, with the exception of ash, which consisted of a single measurement.*

[b] *These rates are given in µmol (g protein)$^{-1}$ h^{-1}.*

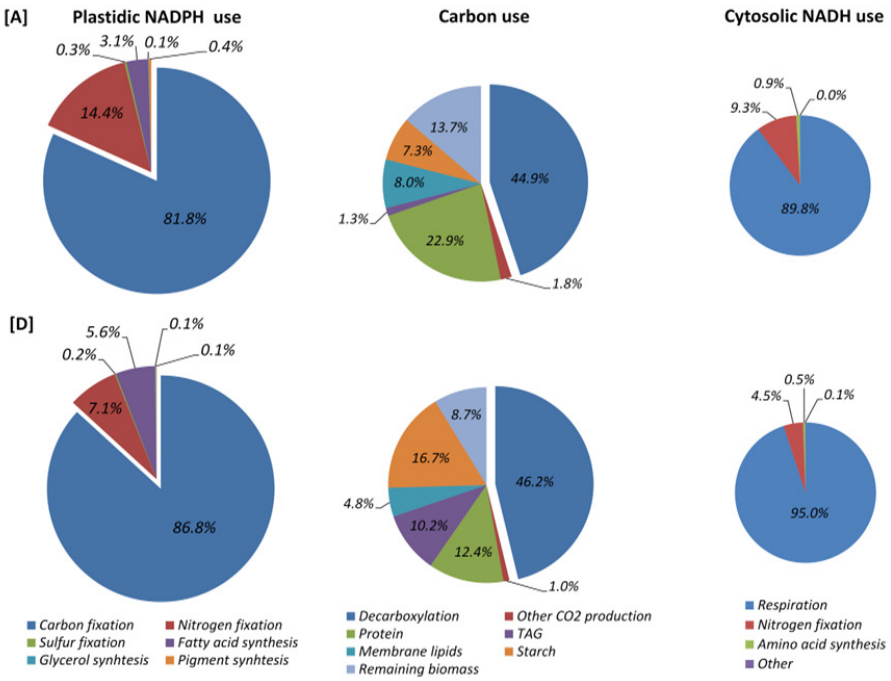

Figure 5.3 *The fate of plastidic NADPH, fixated carbon and cytosolic NADH, for representative examples of nitrogen replete [A], and nitrogen limited [D] conditions. The term decarboxylation refers to all CO_2 production in glycolysis and the TCA cycle.*

5.3.3 Flux balance analysis

To quantify the carbon and energy distributions under both nitrogen replete as well as limited conditions, the balanced rates of Table 5.3B were used to calculate the metabolic flux distributions of experimental condition [A]-[I] (Appendix 5.C). For these calculations it was assumed that all redundant energy from additional absorbed photons would be dissipated in reaction 3.

5.3.3.1 Carbon and energy partitioning

The bulk of plastidic NADPH was used for carbon fixation under both nitrogen replete as well as limited conditions with an average value of 85 ± 2.0% over all steady states (Figure 5.3). Under N-replete growth conditions, the second most important NADPH sink in the plastid was nitrogen fixation with on average 14 ± 0.1% for [A] and [E]. Adding to that the NADPH used to fixate carbon for protein synthesis, and the amount of NADPH used to produce cytosolic NADH used in nitrogen fixation and protein produc-

tion, it was calculated that at least 37 ± 0.3% of the NADPH formed in the chloroplast was used for protein synthesis under nitrogen replete conditions.

The high NADPH demand for nitrogen fixation and protein synthesis clearly illustrates the potential 'energy crisis' that a growing alga will be facing when it is exposed to a sudden nitrogen depletion. When nitrogen fixation comes to an immediate halt, 14% of the generated NADPH has no function. Moreover, if no alternative is found for NADPH normally used in carbon fixation for protein synthesis, over one third of plastidic NADPH will become redundant. As a result of this, the photosynthetic electron transport chains will become over-reduced and it is often thought that this triggers the redistribution of carbon towards highly reduced compounds such as TAG. Also under progressive nitrogen limited conditions this is observed, as relatively more carbon was used in the synthesis of storage components TAG and starch, while the relative carbon use in protein and membrane lipids (MGDG) decreased (Figure 5.3).

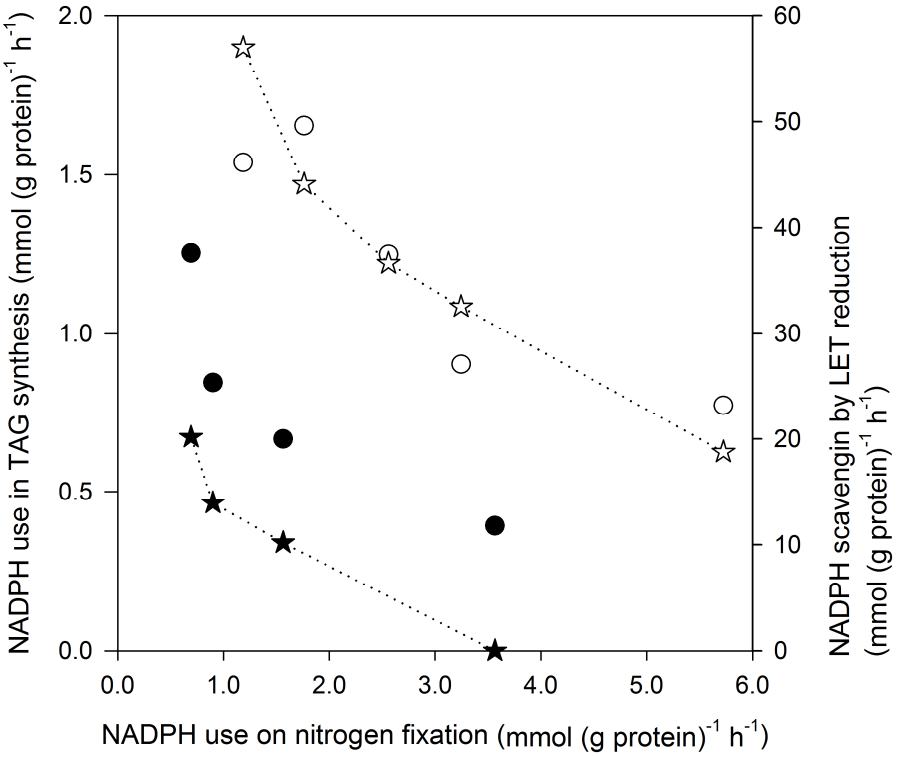

Figure 5.4 *Rate of NADPH used in TAG (circles) and NADPH scavenged by LET reduction (stars) as a function of NADPH use on nitrogen fixation. Closed and open symbols refer to the rates and fractions calculated for low (LL) and high light (HL) conditions respectively.*

The evaluation of carbon and energy distributions in a relative way only partially illustrates the effect of nitrogen limitation. Evaluation of the absolute fluxes revealed that both NADPH and carbon use on all mentioned metabolites decreased under nitrogen limitation, with the exception of TAG. This indicates, that only TAG functioned as a substantial sink in alleviating the NADPH imbalance in the plastid, as suggested by (Li et al., 2013). At the same time, NADPH generation by LET was considerably reduced under nitrogen limitation, and as a result of this, more energy was dissipated. Analysis of the 'NADPH scavenging effect' of reducing LET on the one hand, and increased TAG synthesis on the other, indicated that LET reduction led to 22 times more NADPH scavenging on average (Figure 5.4). This confirms our previous finding that under nitrogen limitation, *N. oleoabundans* copes with the imposed energy imbalance by wasting energy, rather than to store it in energy sinks (Klok et al., 2013a).

5.3.3.2 ATP/NADPH turnover ratios in the chloroplast

From the flux calculations obtained for experimental conditions [A]-[I], the ratio of plastidic ATP/NADPH turnover could be calculated for each experiment (Table 5.4A). As the ATP demands are calibrated for [A] (section 5.3.1.6), the plastidic ATP/NADPH consumption for [A] matches the supply of the modelled LET: 1.50. Interestingly, as nitro-

Table 5.4 *Model calculations of (**A**) the plastidic ATP/NADPH demand, the fraction of plastidic ATP used on plastidic maintenance, as well as the net flux of respiratory ATP towards the plastid for all experimental conditions and (**B**) the ratios of plastidic ATP/NADPH demand for functional biomass (including growth-associated maintenance), maintenance, TAG, protein and starch synthesis.*

A	A	B	C	D	E	F	G	H	I
ATP/NADPH	1.50	1.54	1.57	1.58	1.48	1.50	1.52	1.53	1.55
Maintenance fraction (%)	3.05	5.15	7.05	7.33	1.94	2.93	3.31	3.85	4.81
Net ATP flux towards plastid (mmol (g protein)$^{-1}$ h^{-1})	0.00	0.61	0.73	0.77	0.00	0.10	0.36	0.59	0.73

B	LET	Functional biomass [A]-[I]	Maintenance	TAG	Protein	Starch
ATP /NADPH	1.50	1.46± 0.02	1.95	1.25	1.13	1.58

gen limitation becomes more severe, the plastidic ATP/NADPH demand ratio remains rather close to 1.50. Apparently, under steady state growth conditions, metabolic demands are equilibrated to meet the supply of LET, regardless of the nitrogen shortage experienced. This is in agreement with (Falkowski et al., 1989), who found that the ratio of PSI to PSII reaction centres remained constant regardless of the nitrogen supply in steady state conditions, which suggests a constant ratio between CET and LET and thus a relatively stable ATP/NADPH turnover.

In contrast, under sudden nitrogen starvation this ratio is known to shift dramatically, judging from the observed state transition which increases CET relative to LET (Simionato et al., 2013).The state transition towards CET observed under nitrogen starvation can be explained by the metabolic shift of protein synthesis towards maintenance and synthesis of TAG and/or starch, all of which have a higher ATP/NADPH demand compared to protein synthesis (Table 5.4B).

Under progressive nitrogen limitation however, the ATP/NADPH demand ratio for functional biomass remains constant, despite of the decrease in protein synthesis rates. This is in concurrence with the fact that the composition of functional biomass is rather stable (Table 5.3A). The fact that the total plastidic ATP/NADPH demands hardly changed despite the measured increases in TAG and decreases in starch synthesis under progressive nitrogen starvation can be explained from the fact that the ATP/NADPH demands for functional biomass largely dictate the total plastidic demands under nitrogen limited conditions. Furthermore, the ATP excess that occurs due to TAG synthesis (low ATP/NADPH ratio) is compensated by the fact that at lower growth rates maintenance becomes more important (Table 5.4A) (Kliphuis et al., 2012). In the calculated flux distributions, this slightly elevated plastidic ATP demand is not satisfied through an increase in CET, but rather by an increase in respiratory rates compared to LET, resulting in a net flux of ATP from the cytosol into the chloroplast (Table 5.4A). Whether cells actually achieve ATP complementation through CET or through increased respiration remains a matter of debate (Noctor and Foyer, 1998). In the presented model, additional ATP production through respiration is more energetically favourable, since LET followed by respiration yields 0.57 ATP per absorbed photon, whereas CET would yield only 0.50.

It was assumed that the maintenance and growth-associated maintenance are constant throughout all tested experimental conditions. If these were to change due to nitrogen limitation, the true plastidic ATP/NADPH turnover would be different than what was calculated here.

5.3.4 Metabolic evaluations: maximising TAG yield on light

Under progressive nitrogen limitation, TAG yield on absorbed light gradually increased. However, the maximum yields obtained were much lower than what could be calculated to be the maximum possible yield according to the stoichiometry of algal metabolism, which is 0.81 g (mol photons)$^{-1}$.

This value is obtained from the metabolic model, by using all light energy for TAG synthesis, with a minimal quantum requirement of 10 photons per 2 NADPH generated (section 5.3.1.3) and a negligible maintenance demands for ATP. The relative importance of the maintenance demands depend on the total ATP turnover rates, which in turn is dependent on the amount of light received by the cell. Therefore, the ATP demands for maintenance will only reduce the predicted TAG yields on light under very low light intensities, where the ATP demands for maintenance can become larger than what is left after TAG synthesis.

A higher theoretical maximum TAG yield of 1.07 g (mol photons)$^{-1}$ is calculated when the GAP/3PG shuttle is active as discussed in section 5.3.1.4. NADPH and ATP are saved out by directly exporting 3PG instead of GAP over the plastid membrane, and the NADH and ATP that are resulting of the conversion of 3PG into Acetyl-CoA (reactions 32-34 and 45), the raw material for TAG synthesis, can be shuttled over the plastid membrane by reverting the GAP/3PG shuttle. TAG synthesis rates are limited by plastidic NADPH synthesis rates, and produce a surplus of ATP (Table 5.4B). Therefore, recycling NADH to the plastid as NADPH is beneficial for TAG synthesis and at the same time, it has a positive effect on the plastidic ATP:NADPH demand ratio, which increased from 1.25 to 1.33. The Glutamine/Glutamate shuttle has no effect on the TAG yield as it is only capable of shuttling NADPH across the plastid membrane and NADH cannot be converted in NADPH.

Several investigators have demonstrated the active transport of GAP and 3PG across the plastid membrane (see section 5.3.1.4). Although the capacity of the GAP/3PG shuttle does not limit photosynthesis under nutrient replete conditions (Bräutigam and Weber, 2011), it is unknown to what extent this shuttle remains active under nitrogen limited conditions. Applying this shuttle for additional NADPH transport into the plastid seems unlikely, as the transport would occur against the redox gradient that is the result of nitrogen shortage. Depending on the capacity of the GAP/3PG shuttle *in vivo*, the maximum theoretical yield of TAG on light will lie somewhere in between 0.81 and 1.07 g (mol photons)$^{-1}$. Further evaluation on its capacity is necessary before it can be concluded that this shuttle provides a possible engineering target for optimising TAG yield on light.

Two possible reasons exist for the low TAG yields obtained under nitrogen limited conditions, which are at most 6% of the theoretical maximum. First of all, light energy is dissipated as LET is progressively decreased as a response to the reduction in plastidic NADPH turnover. Secondly, energy is spent on other macromolecules, such as functional biomass and starch. This illustrates the possible room for improvement by redirecting the carbon and energy distribution under nitrogen limitation. For example, when no functional biomass is produced, the highest reported time averaged yield of fatty acids on light is 0.26 g (mol photons)$^{-1}$ (Breuer et al., 2013). This is approximately 32% of the theoretic maximum TAG yield of 0.81 g (mol photons)$^{-1}$.

To assess to what extent competing processes affect TAG yield on light under progressive nitrogen limitation, three scenarios were evaluated: a starch mutant of *N. oleoabundans*, a 'mutant' that does not lose photosynthetic capacity under nitrogen limited conditions, and a combination of both. It was assumed that the gained energy resulting from the mutation, was channelled towards TAG formation. Although every scenario results in an increase in TAG yield (Figure 5.5), the possible gain is much larger by improving photosynthetic capacity than by knocking out competing pathways.

These scenarios are purely theoretical and merely serve as an illustration as to what the microalgal stoichiometric network is capable of. Some of our assumptions might influence the effect of the putative mutations on TAG yield. First of all, it is not likely that in a starch mutant, all energy not used in starch will be used on TAG synthesis. For example, (Li et al., 2010b) already showed that a starch mutant of *C. reinhardtii* shows increased levels of energy dissipation. Similarly, an increase in photosynthetic capacity does not necessarily result in all additional energy to be used in TAG synthesis.

Increasing photosynthetic capacity under nitrogen limitation will not be as straight forward as producing a starch mutant, as photosynthesis is an intricate process with many reactions working in concert. Any alterations in this highly evolved and optimised process are likely to be detrimental for energy conversion and algal growth. Alternatively, uncoupling TAG synthesis from adverse growth conditions and the accompanying decrease in photosynthetic rate would be a more promising strategy. Although it seems likely that the redox/energy imbalance is important for triggering both TAG accumulation as well as a decrease in photosynthetic capacity, the exact mechanisms and signalling pathways involved remain unknown. Further investigation into which signalling pathway is responsible for TAG accumulation might help to invent other ways to mimic this signal without applying nitrogen stress. This will allow for TAG formation under nitrogen replete conditions at high photosynthetic efficiencies.

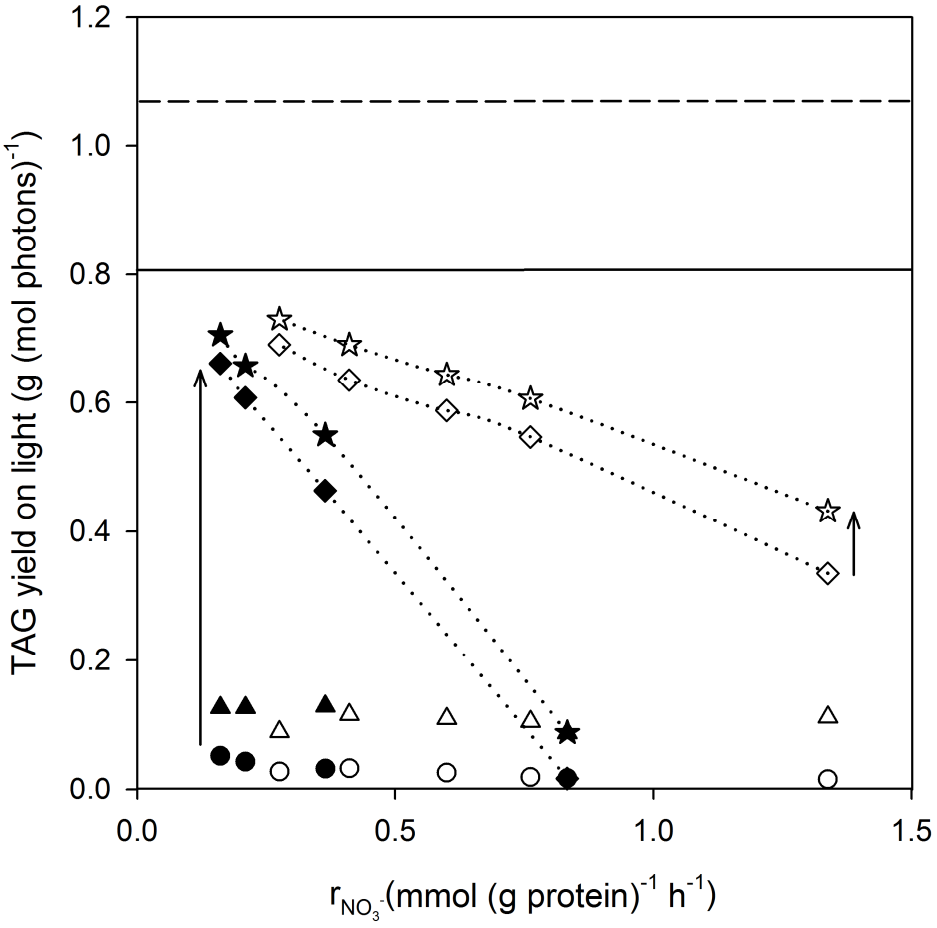

Figure 5.5 *Model calculations for TAG yield on light, as a function of the nitrogen consumption rate. Closed (LL) and open (HL) symbols represent a wild type (circles), a starch mutant (triangles), a photosynthetic optimal (diamonds) and a photosynthetic optimal starch mutant (stars) of N. oleoabundans. The solid line indicates the theoretical optimum of TAG yield on light, the broken line represents the theoretical optimal rate with an active GAP/3PG shuttle.*

5.4 Conclusion

A transcriptome based metabolic model was developed that describes the primary metabolism of the oleaginous microalga *Neochloris oleoabundans*. This model was used to evaluate carbon and energy partitioning under steady state, nitrogen limited conditions. It was found that the fixation of nitrogen and protein synthesis took up more than one third of the reducing potential generated in the plastid under nitrogen repletion. Under nitrogen limitation, reducing potential was redistributed towards TAG. At the same time, linear electron transport was severely reduced and this had an almost 22 times larger effect on preventing excess NADPH formation than NADPH scavenging by increased TAG synthesis. The ratio of ATP and NADPH turnover in the plastid was close to 1.5 over all experimental conditions, as the ATP/NADH demands of total biomass formation were not affected by nitrogen limitation.

Using the stoichiometric model a maximum theoretical yield of TAG on light of 0.81 g mol^{-1} was calculated. An active GAP/3PG shuttle could further increase this theoretical yield to 1.07 g mol^{-1}. Evaluation of several growth scenarios showed that redistribution of carbon from competing metabolites such as starch, will improve TAG yields, but increasing photosynthetic capacity by uncoupling TAG synthesis from adverse growth conditions has a much larger potential. These scenarios show the potential of microalgal metabolism and the calculated theoretical maximum gives a point of reference when aiming at increasing TAG yield on light.

Acknowledgements

The authors would like to thank Walter Pirovano (BaseClear, Leiden, the Netherlands), for his help on the sequencing and annotation of the transcriptome of *N. oleoabundans* and Yannick Weesepoel (Laboratory of Food Chemistry, Wageningen University) for analysing the pigment compositions of the samples presented in this paper. As this work was performed within the TTIW-cooperation framework of Wetsus, the authors would like to thank the members of the theme 'Algae' from Wetsus for the discussions and their financial support. Wetsus is funded by the Dutch Ministry of Economic Affairs.

Appendix

5.A Metabolic model of Neochloris oleoabundans

1. Reaction equations

Arrows indicate the direction and reversibility of the reactions. Metabolite extension '_ex' prefix 'c' denote an extracellular or chloroplast location, respectively.

Photosynthesis

0 10 photon+3 Pi+3cADP+2 cNADP + H[+] ⟶ H_2O+O_2+2 cNADPH+3 cATP

1 2 photon + H [+] +Pi + cADP ⟶ H_2O+cATP

2 H_2O + cATP ⟶ H[+] + Pi + cADP

3 photon ⟶ fluores

Oxidative Phosphorylation

4 1.5 ADP + 1.5 H[+] + 1.5 Pi + $FADH_2$ + 0.5 O_2 ⟶ FAD + 1.5 ATP + 2.5 H_2O

5 3.5 H[+] + 2.5 ADP + 2.5 Pi + NADH + 0.5 O_2 ⟶ NAD + 2.5 ATP + 3.5 H_2O

6 NAD + NADPH ⟶ NADH + NADP

7 H_2O + PPi ⟶ H[+] + 2 Pi

8 AMP + ATP ⟶ 2 ADP

9 cAMP + cATP ⟶ 2 cADP

10 ATP + H_2O ⟶ ADP + H[+] + Pi

Calvin Cycle

11 CO_2 + H_2O + cRu15DP ⟶ 2 cG3P

12 cATP + cG3P ⟶ H[+] + c13DPG + cADP

13 H[+] + c13DPG + cNADPH ↔ Pi + cGAP + cNADP

14 cGAP ↔ cDHAP

15 cDHAP + cGAP ↔ cF16P

16 H_2O + cF16P ⟶ Pi + cF6P

17 cF6P + cGAP ↔ cE_4P + cX5P

18 H_2O + cE_4P + cGAP ↔ Pi + cS7P

19 cGAP + cS7P ↔ cR_5P + cX5P

20 cX5P ↔ cRu5P

21 cR_5P ↔ cRu5P

22 cATP + cRu5P ⟶ H[+] + cADP + cRu15DP

Glycolysis / Gluconeogenesis

23 cATP + cF6P ⟶ H[+] + cADP + cF16P

24 cF6P ↔ cG6P

25 cG6P ↔ cG1P

26 G6P ↔ G1P

27 F6P ↔ G6P

28 F16P + H_2O ⟶ F6P + Pi

29 DHAP + GAP ↔ F16P

30 GAP + NAD + Pi ↔ 13DPG + H[+] + NADH

31 13DPG + ADP ↔ 3PG + ATP

32 3PG ↔ 2PG

33 2PG ↔ H_2O + PEP

34 ADP + H[+] + PEP ⟶ ATP + PYR

Glyoxylate metabolism /Photorespiration

35 H_2O + NAD + O_2 + cRu15DP ⟶ H[+] + NADH + Pi + cG3P + glyoxylate

36 GLY + H[+] + PYR ↔ ALA + glyoxylate

37 SER + glyoxylate ↔ GLY + HydPyr

38 GLY + H_2O + METHF ↔ SER + THF

39 GLY + NAD + THF ↔ CO_2 + METHF + NADH + NH_4[+]

40 H[+] + HydPyr + NADH ↔ Glycerate + NAD

41 ATP + Glycerate ⟶ 3PG + ADP + 2H[+]

42 Glycerate + H[+] + NADH ↔ GA + H_2O + NAD

43 GA + H[+] + NADPH ↔ GLYC + NADP

44 ATP + GLYC ⟶ ADP + $GLYC_3P$ + H[+]

Tricarboxylic Acid (TCA) cycle

45 CoA + NAD + PYR ⟶ AcCoA + CO_2 + NADH

46 AcCoA + H_2O + OXA ↔ CIT + CoA + H[+]

47 CIT + NAD ↔ AKG + CO_2 + NADH

48 AKG + CoA + NAD ⟶ CO_2 + NADH + SUCCoA

49 ADP + Pi + SUCCoA ↔ ATP + CoA + SUC

50 FAD + SUC ↔ $FADH_2$ + FUM

51 FUM + H_2O ↔ MAL

52 MAL + NAD ↔ H[+] + NADH + OXA

53 ATP + CO_2 + H_2O + PYR ⟶ ADP + OXA + Pi + 2H[+]

54 $ATP + OXA \rightarrow ADP + CO_2 + PEP$

55 $CO_2 + H_2O + PEP \rightarrow H[+] + OXA + Pi$

Pentose phosphate pathway (PPP)

56 $G6P + H_2O + NADP \leftrightarrow 6PG + NADPH + 2H[+]$

57 $6PG + NADP \rightarrow CO_2 + NADPH + Ru5P$

58 $Ru5P \leftrightarrow R5P$

59 $Ru5P \leftrightarrow X5P$

60 $R5P + X5P \leftrightarrow GAP + S7P$

61 $GAP + S7P \leftrightarrow E4P + F6P$

62 $F6P + GAP \leftrightarrow E4P + X5P$

63 $ATP + R5P \rightarrow AMP + H[+] + PRPP$

64 $cATP + cR5P \rightarrow H[+] + cAMP + cPRPP$

Starch synthesis and metabolism

65 $H[+] + cATP + cG1P \rightarrow PPi + cADPG$

66 $cADPG \rightarrow H[+] + STARCH + cADP$

67 $STARCH + cATP \rightarrow H[+] + STARCH\text{-}P + cADP$

68 $H_2O + STARCH + STARCH\text{-}P \rightarrow cMalt\text{-}P$

69 $Malt\text{-}P + Pi \leftrightarrow 2\ G1P$

Sulphur fixation

70 $cATP + cSO_4 \rightarrow PPi + cAPS$

71 $cAPS + cNADPH \rightarrow cAMP + cNADP + cSO_3$

72 $5H[+] + 3\ cNADPH + cSO_3 \leftrightarrow cH_2S + 3\ H_2O + 3\ cNADP$

Nitrogen fixation

73 $H[+] + NADH + NO_3 \leftrightarrow H_2O + NAD + NO_2$

74 $5\ H[+] + 3\ cNADPH + cNO_2 \leftrightarrow cNH_4[+] + 2\ H_2O + 3\ cNADP$

75 $cATP + cGLU + cNH_4[+] \rightarrow H[+] + Pi + cADP + cGLN$

76 $H[+] + cAKG + cGLN + cNADPH \leftrightarrow cNADP + 2\ cGLU$

Aminoacid biosynhtesis

77 $ATP + GLU + NH_4[+] \rightarrow ADP + GLN + H[+] + Pi$

78 $AKG + H[+] + NADPH + NH_4[+] \leftarrow GLU + H_2O + NADP$

79 $2\ cPEP + cATP + cE4P + cNADPH \rightarrow cADP + cCHO + cNADP + 4Pi$

80 cCHO ↔ cPRE

81 GLU + H[+] + PRE ↔ AKG + CO_2 + H_2O + PHE

82 GLU + NAD + PRE ↔ AKG + CO_2 + NADH + TYR

83 cCHO + cGLN ↔ H[+] + cANTH + cGLU + cPYR

84 H[+] + cANTH + cPRPP + cSER → CO_2 + PPi + cGAP + cTRYP + 2 H_2O

85 3 H_2O + 2 NAD + ATP + GLN + PRPP → AICAR + AKG + HIS + Pi + 2 NADH + 2 PPi + 5 H[+]

86 H_2O + cG_3P + cGLU + cNADP → H[+] + Pi + cAKG + cNADPH + cSER

87 cSER → cNH_4[+] + cPYR

88 cAcCoA + cH_2S + cSER ↔ H[+] + cAce + cCYS + cCoA

89 cATP + cAce + cCoA → PPi + cAMP + cAcCoA

90 AdHCYS + H_2O ↔ Ad + HCYS

91 GLU + PYR → AKG + ALA

92 GLU + OXA ↔ AKG + ASP

93 ASP + ATP + GLN + H_2O → AMP + ASN + GLU + H[+] + PPi

94 H[+] + cASP + cATP + cNADPH → Pi + cADP + cASA + cNADP

95 2 H[+] + cASA + cGLU + cNADPH + cPYR ↔ H_2O + cAKG + cDAP + cNADP

96 cDAP ↔ CO_2 + cLYS

97 H[+] + cASA + cNADPH ↔ cHSER + cNADP

98 H_2O + cATP + cCYS + cHSER ↔ H[+] + Pi + cADP + cHCYS + cNH_4[+] + cPYR

99 HCYS + MTHF ↔ H[+] + MET + THF

100 ATP + H_2O + MET → AdMET + H[+] + PPi + Pi

101 H_2O + cATP + cHSER → H[+] + Pi + cADP + cTHR

102 H[+] + cTHR → c2-oxobut + cNH_4[+]

103 H[+] + c2-oxobut + cGLU + cNADPH + cPYR ↔ CO_2 + H_2O + cAKG + cILE + cNADP

104 2 cPYR + H[+] + cAcCoA + cGLU ↔ cAKG + cCoA + cLEU + 2 CO_2

105 2 H[+] + 2 cPYR + cGLU + cNADPH ↔ CO_2 + H_2O + cAKG + cNADP + cVAL

106 2 ATP + 2 H_2O + CO_2 + GLN → CaP + GLU + Pi + 2 ADP + 3 H[+]

107 2 ATP + 2 GLU + ASP + CaP + H_2O + NADH → ADP + AKG + AMP + ARG + FUM + H_2O + H[+] + NAD + PPi + 2 Pi

108 3 H[+] + 2 NADH + GLU ↔ PRO + 2H_2O + 2 NAD

Fatty acid biosynhtesis

109 CO_2 + H_2O + cATP + cAcCoA → H[+] + Pi + cADP + cMalCoA

110 H[+] + cACP + cAcCoA ↔ cAcACP + cCoA

111 cACP + cMalCoA ↔ cCoA + cMalACP

112 12 H[+] + 12 cNADPH + 6 cMalACP + cAcACP ↔ cC140ACP + 6 CO_2 + 6 H_2O + 6 cACP + 12 cNADP

113 14 H[+] + 14 cNADPH + 7c MalACP + cAcACP ↔ cC160ACP + 7 CO_2 + 7 H_2O + 7 cACP + 14 cNADP

114 16 H[+] + 16 cNADPH + 8 cMalACP + cAcACP ↔ cC180ACP + 8 CO_2 + 8 H_2O + 8 cACP + 16 cNADP

115 H[+] + O_2 + cC160ACP + cNADPH ↔ cC161ACP + cNADP + 2 H_2O

116 H[+] + O_2 + cC180ACP + cNADPH ↔ cC181ACP + cNADP + 2 H_2O

117 H[+] + O_2 + cC161ACP + cNADPH ↔ cC162ACP + cNADP + 2 H_2O

118 C161CoA + H[+] + NADH + O_2 ↔ C162CoA + NAD + 2 H_2O

119 H[+] + O_2 + cC181ACP + cNADPH ↔ cC182ACP + cNADP + 2 H_2O

120 C181CoA + H[+] + NADH + O_2 ↔ C182CoA + NAD + 2 H_2O

121 H[+] + O_2 + cC162ACP + cNADPH ↔ cC163ACP + cNADP + 2 H_2O

122 H[+] + O_2 + cC182ACP + cNADPH ↔ cC183ACP + cNADP + 2 H_2O

123 H_2O + cC160ACP ↔ H[+] + cACP + cC160

124 H_2O + cC161ACP ↔ H[+] + cACP + cC161

125 H_2O + cC180ACP ↔ H[+] + cACP + cC180

126 H_2O + cC181ACP ↔ H[+] + cACP + cC181

127 ATP + C160 + CoA → AMP + C160CoA + PPi

128 ATP + C161 + CoA → AMP + C161CoA + PPi

129 ATP + C180 + CoA → AMP + C180CoA + PPi

130 ATP + C181 + CoA → AMP + C181CoA + PPi

Glycerol biosynthesis

131 cGLYC3P + cNADP → H[+] + cDHAP + cNADPH

Folate biosynthesis and metabolism

132 5FTHF + H[+] ↔ H_2O + MYLTHF

133 H_2O + MYLTHF ↔ H[+] + N10FTHF

134 ATP + FORM + THF → ADP + N10FTHF + Pi

135 MYLTHF + NADPH ↔ METHF + NADP

136 H[+] + METHF + NADPH ↔ MTHF + NADP

137 5FTHF + ATP + H_2O → ADP + H[+] + N10FTHF + Pi

138 FORM + H[+] + THF ↔ H_2O + N10FTHF

139 DHF + H[+] + NADPH ↔ NADP + THF

140 4 ATP + 2 GLN + 2 H_2O + ASP + CO_2 + GLY + N10FTHF + PRPP ⟶ AICAR + FUM + PPi + THF + 2 GLU + 4 ADP + 4 Pi + 7 H[+]

Purine and Pyrimidine metabolism

141 ASP + CaP + H[+] + O_2 + PRPP ↔ CO_2 + H_2O + H_2O_2 + PPi + Pi + UMP

142 2 H_2O_2 ↔ O_2 + 2 H_2O

143 ATP + UMP ⟶ ADP + UDP

144 G1P + UTP ⟶ PPi + UDPGal

145 ATP + UDP ↔ ADP + UTP

146 ATP + GLN + H_2O + UTP ⟶ ADP + CTP + GLU + Pi + 2 H[+]

147 ATP + CDP ↔ ADP + CTP

148 AICAR + N10FTHF ↔ H_2O + IMP + THF

149 2 H_2O + ATP + GLN + IMP + NAD ⟶ AMP + GLU + GMP + NADH + PPi + 3 H[+]

150 ATP + GMP ⟶ ADP + GDP

151 ATP + GDP ↔ ADP + GTP

152 ASP + GTP + IMP ↔ AMP + FUM + GDP + Pi + 2 H[+]

153 ATP + H[+] + METHF + NADPH + UDP ⟶ ADP + DHF + H_2O + NADP + dTTP

154 ATP + CDP + H[+] + NADPH ⟶ ADP + H_2O + NADP + dCTP

155 ATP + GDP + H[+] + NADPH ⟶ ADP + H_2O + NADP + dGTP

156 ATP + H[+] + NADPH ↔ H_2O + NADP + dATP

157 AMP + H_2O ⟶ Ad + Pi

158 ATP + Ad ⟶ ADP + AMP + H[+]

Pigment biosynhtesis

159 12 H[+] + 8 cATP + 8 cGLU + 8 cNADPH + 2.5 O_2 ⟶ cPPorphyr + 4 cNH_4[+] + 6 CO_2 + 8 PPi + 8 cAMP + 8 cNADP + 13 H_2O

160 18 H[+] + 15 cNADPH + 8 cATP + 4 cGAP + 4 cPYR ⟶ cPhytyl-PP + 4 CO_2 + 4 cADP + 4 cAMP + 7 PPi + 8 H_2O + 15 cNADP

161 4 cNADPH + 2.5 O_2 + 2 cATP + Mg_2[+] + cAdMET + cPPorphyr + cPhytyl-PP ⟶ Chlorophyl + PPi + cAdHCYS + 2 H_2O + 2 Pi + 2 cADP + 3H[+] + 4 cNADP

162 6 cNADP + 2 O_2 + 2 cPhytyl-PP ⟶ Carotene + 2 PPi + 4 H_2O + 6 cNADPH + 12 H[+]

Macromolecules and functional biomass formation

163 2.372 H_2O + 1.372 ATP + 0.3 dCTP + 0.3 dGTP + 0.2 dATP + 0.2 dTTP ⟶ DNA + PPi + 1.372 ADP + 1.372 Pi + 2.372 H[+]

164 1.4 H_2O + 0.6 ATP + 0.3 CTP + 0.3 GTP + 0.2 UTP → 0.4 ADP + 0.4 H[+] + 0.4 Pi + PPi + RNA

165 H_2O + cGLYC3P + cUDPGal + 0.63 cC182ACP + 0.53 cC160ACP + 0.34 cC183ACP + 0.23 cC181ACP + 0.10 cC163ACP + 0.08 cC162ACP + 0.05 cC140ACP + 0.03 cC161ACP + 0.01 cC180ACP → MGDG + Pi + cUDP + 2 H[+] + 2 cACP

166 1.38 cC181ACP + H_2O + cGLYC3P + 0.84 cC182ACP + 0.56 cC160ACP + 0.11 cC162ACP + 0.06 cC161ACP + 0.05 cC180ACP → Pi + cTAG + 3 H[+] + 3 cACP

167 1.38 C181CoA + GLYC3P + H_2O + 0.84 C182CoA + 0.56 C160CoA + 0.11 C162CoA + 0.06 C161CoA + 0.05 C180CoA → Pi + TAG + 3 CoA + 3 H[+]

168 4.306 ATP + 3.306 H_2O + 0.142 ALA + 0.099 GLY + 0.085 LEU + 0.063 VAL + 0.054 GLN + 0.054 GLU + 0.054 LYS + 0.052 PRO + 0.052 SER + 0.050 ARG + 0.049 THR + 0.042 ASN + 0.042 ASP + 0.037 ILE + 0.037 PHE + 0.024 TYR + 0.021 MET + 0.016 HIS + 0.015 CYS + 0.010 TRYP → PROTEIN + 4.306 ADP + 4.306 H[+] + 4.306 Pi

169 G1P → CARB + Pi

170 30.92 H_2O + 25.98 ATP + 4.94 cATP + α PROTEIN + β CARB + γ MGDG + δ Chlorophyl + ε Carotene + ζ RNA + η DNA → Biomass 'x' + 4.94 cADP + 25.98 ADP + 30.92 H[+] + 30.92 Pi

Transport

171 cDHAP ↔ DHAP

172 cGAP ↔ GAP

173 cG3P ↔ 3PG + H[+]

174 cMalt-P → Malt-P

175 NO_2 ↔ cNO_2

176 cSO_4 ↔ SO_4

177 AKG + cGLU ↔ GLU + cAKG

178 AcCoA + cCoA ↔ CoA + cAcCoA

179 cCoA ↔ CoA

180 cC160 ↔ C160

181 cC161 ↔ C161

182 cC180 ↔ C180

183 cC181 ↔ C181

184 UDPGal + cUDP ↔ UDP + cUDPGal

185 cPEP ↔ PEP

186 cPRE ↔ PRE

187 cTRYP ↔ TRYP
188 cCYS ↔ CYS
189 cHCYS ↔ HCYS
190 cAdHCYS ↔ AdHCYS
191 cSER ↔ SER
192 cILE ↔ ILE
193 cLEU ↔ LEU
194 cVAL ↔ VAL
195 cASP ↔ ASP
196 cGLU ↔ GLU
197 cGLN ↔ GLN
198 cLYS ↔ LYS
199 cTHR ↔ THR
200 cAdMET ↔ AdMET
201 ATP + cADP → ADP + cATP
202 CO_2 ↔ CO_2_ex
203 O_2 ↔ O_2_ex
204 H_2O ↔ H_2O_ex
205 2 Pi + ADP + H[+] ← ATP + H_2O + Pi_ex
206 ADP + H[+] + Pi + SO_4 ← ATP + H_2O + SO_4_ex
207 ADP + H[+] + NO_3 + Pi ← ATP + H_2O + NO_3_ex
208 Mg2[+] ↔ Mg2[+] _ex
209 photon ← photon_ex
210 fluores → fluores_ex
211 H[+] ↔ H[+] _ex
212 TAG → TAG_ex
213 cTAG → cTAG_ex
214 STARCH → STARCH_ex
215 Biomass 'x' → Biomass'x'_ex

2. Compound abbreviations

13DPG	1,3-diPhosphoglycerate	5FTHF	5-Formyl-THF
2-oxobut	2-Oxobutanoate	6PG	6-Phosphogluconate
2PG	2-Phosphoglycerate	AcACP	Acetyl-ACP
3PG	3-Phosphoglycerate	AcCoA	Acetyl CoA

Ace	Acetate	C181	Oleic acid
ACP	Acetyl Carrier Protein	C181ACP	Oleic acid ACP
Ad	Adenosine	C181CoA	Oleic acid Coenzyme A
AdHCYS	S-Adenosyl-L-homocysteine	C182ACP	Linoleic acid ACP
AdMET	S-Adenosyl-L-methionine	C182CoA	Linoleic acid Coenzyme A
ADP	Adenosine diphosphate	C183ACP	Linolenic acid ACP
ADPG	Glucose Adenosine diphosphate	CaP	Carbomyl phosphate
		CARB	Carbohydrate
AICAR	5-Aminoimidazole-4-carboxamide ribonucleine	Carotene	β Carotene
		cC180ACP	Stearic acid ACP
AKG	2-Oxoglutarate (alpha-ketoglutarate)	CDP	Cytidine diphosphate
		Chlorophyl	Chlorophyll *a*
ALA	Alanine	CHO	Chorismate
AMP	Adenosine monophosphate	CIT	Citrate
ANTH	Anthranilate	CO_2	Carbondioxide
APS	Adenylyl sulphate	CoA	Coenzyme A
ARG	Arginine	CTP	Cytosine triphosphate
ASA	L-Aspartic semialdehyde	CYS	Cysteine
ASN	Asparagine	DAP	Diaminopimelate
ASP	Aspartate	dATP	Deoxy ATP
ATP	Adenosine triphosphate	dCTP	Deoxy CTP
Biomass 'x'	Functional biomass measured under steady state 'x'	dGTP	Deoxy GTP
		DHAP	Dihydroxyacetone phosphate
C140ACP	Myristic acid ACP	DHF	Dihydrofolate
C160	Palmitic acid	DNA	Deoxyribonucleic acid
C160ACP	Palmitic acid ACP	dTTP	Deoxy TTP
C160CoA	Palmitic acid Coenzyme A	E4P	Erythrose 4-phosphate
C161	Palmitoleic acid	F16P	Fructose 1,6-biphosphate
C161ACP	Palmitoleic acid ACP	F6P	Fructose 6-phosphate
C161CoA	Palmitoleic acid Coenzyme A	FAD	Flavine adenosine dinucleotide
C162ACP	Hexadecadienoic ACP		
C162CoA	Hexadecadienoic acid Coenzyme A	$FADH_2$	Flavine adenosine dinucleotide dihydride
C163ACP	Hexadecatrienoic ACP	fluores	Fluorescent photon
C180	Stearic acid	FORM	Formic acid
C180CoA	Stearic acid Coenzyme A	FUM	Fumarate

G1P	Glucose 1-phospate	MTHF	Methyl-THF
G3P	Glycerate 3-phosphate	MYLTHF	5,10-methenyl-THF
G6P	Glucose 6-phosphate	N10FTHF	10-Formyl-THF
GA	Glyceraldehyde	NAD	Nicotinamide oxidised
GAP	Glyceraldehyde 3-phosphate	NADH	Nicotinamide reduced
GDP	Guanosine diphosphate	NADP	Nictoninamidephosphate
GLN	Glutamine		oxidised
GLU	Glutamate	NADPH	Nicotinamidephoshate
GLY	Glycine		reduced
GLYC	Glycerol	$NH_4[+]$	Ammonium
GLYC3P	Glycerol 3 phosphate	NO_2	Nitrite
Glycerate	Glycerate	NO_3	Nitrate
glyoxylate	Glyoxylate	O_2	Oxygen
GMP	Guanosime monophosphate	OXA	Oxaloacetate
GTP	Guanosine triphosphate	PEP	Phosphoenol pyruvate
H[+]	Proton	PHE	Phenylalanine
H_2O	Water	photon	Photon
H_2O_2	Hydrogen peroxide	Phytyl-PP	Phytyl-diphosphate
H_2S	Sulphite	Pi	Orthophosphate
HCYS	Homocysteine	PPi	Pyrophosphate
HIS	Histidine	PPorphyr	Protoporphyrine IX
HSER	Homoserine	PRE	Prephenate
HydPyr	3-Hydroxypyruvate	PRO	Proline
ILE	Isoleucine	PROTEIN	Protein
IMP	Inosine monophosphate	PRPP	Phosphorybosyl
LEU	Leucine		pyrophosphate
LYS	Lysine	PYR	Pyruvate
MAL	Malate	R5P	Ribose 5-phosphate
MalACP	Malonyl-ACP	RNA	Ribonucleic acid
MalCoA	Malonyl-CoA	Ru15DP	Ribulose 1,5-biphosphate
Malt-P	Maltose phosphate	Ru5P	Ribulose 5-phosphate
MET	Methionine	S7P	Sedoheptulose 7-phosphate
METHF	5,10-Methylene-THF	SER	Serine
$Mg2[+]$	Magnesium	SO_3	Sulphite
MGDG	Monogalactosyl	SO_4	Sulphate
	diacylglycerol	STARCH	Starch

STARCH-P	Starch phosphate	TYR	Tyrosine
SUC	Succinaat	UDP	Uridine diphosphate
SUCCoA	Succinyl CoenzymeA	UDPGal	UDP-Galactose
TAG	Triacylglyceride	UMP	Uradine monophosphate
THF	Tetrahydrofolate	UTP	Uracil triphosphate
THR	Threonine	VAL	Valine
TRYP	Tryptophane	X5P	Xylulose 5-phosphate

3. Elemental composition of macromolecules

	C	H	O	N	P	S	Charge
Protein	4.69	7.43	1.41	1.34		0.04	0.01
Starch	6.00	10.00	5.00				
Carb	6.00	10.00	5.00				
TAG	55.54	100.40	6.00				
MGDG	43.32	76.64	10.00				
Chlorophyll	55.00	72.00	5.00	4.00			
Carotene	40.00	56.00					
RNA	9.50	12.80	8.00	3.80	1.00		-1.00
DNA	9.70	12.20	7.00	3.80	2.00		-2.00

4. Functional biomass composition

Molar ratios correspond to letters α-η in functional biomass synthesis reaction 170.

	Functional biomass composition (mol mol^{-1})								
Experiment	**A**	**B**	**C**	**D**	**E**	**F**	**G**	**H**	**I**
α Protein	0.712	0.702	0.700	0.646	0.751	0.698	0.675	0.652	0.632
β Carbohydrates	0.201	0.225	0.236	0.310	0.161	0.208	0.244	0.289	0.318
γ MGDG	0.027	0.030	0.031	0.027	0.026	0.028	0.026	0.027	0.030
δ Chlorophyll	0.004	0.003	0.003	0.002	0.004	0.002	0.002	0.002	0.002
ε Carotenoids	0.001	0.001	0.001	0.001	0.001	0.001	0.001	0.001	0.001
ζ RNA	0.047	0.031	0.020	0.009	0.051	0.054	0.043	0.023	0.012
η DNA	0.008	0.008	0.008	0.005	0.006	0.009	0.009	0.007	0.005

5. Protein composition in % mol AA/mol protein

Amino Acid	**%**	**Amino Acid**	**%**
Alanine (Ala)	14.24 ± 0.71[a]	Leucine (Leu)	8.49 ± 0.2
Arginine (Arg)	5.02 ± 0.63	Lysine (Lys)	5.36 ± 0.09
Asparagine (Asn)	4.23 ± 0.1	Methionine (Met)	2.05 ± 0.06
Aspartate (Asp)	4.23 ± 0.1	Phenylalanine (Phe)	3.75 ± 0.14
Cysteine (Cys)	1.51 ± 0.13	Proline (Pro)	5.2 ± 0.12
Glutamate (Glu)	5.37 ± 0.25	Serine (Ser)	5.24 ± 0.23
Glutamine (Gln)	5.37 ± 0.25	Threonine (Thr)	4.94 ± 0.17
Glycine (Gly)	9.95 ± 0.18	Tryptophan (Trp)	1.02 ± 0.09
Histidine (His)	1.58 ± 0.05	Tyrosine (Tyr)	2.39 ± 0.13
Isoleucine (Ile)	3.72 ± 0.07	Valine (Val)	6.35 ± 0.19

[a] *The standard deviations represent the average molar fractions over the 9 steady states [A]-[I].*

Protein synthesis was modelled as the coupling of one single average amino acid, consuming 4.306 mol ATP. One average amino acid constitutes out of the sum of the molar fractions of the 20 amino acids present in *N. oleoabundans*.

6. Average fatty acid composition of MGDG and TAG

	TAG [a]	**Membrane lipids** [a]
Fatty acid	*% (mol FA/mol)*	*% (mol FA/mol)*
C14:0		2.72 ± 1.04
C16:0	18.56 ± 1.61	26.48 ± 4.70
C16:1	1.88 ± 0.73	1.39 ± 0.26
C16:2	3.77 ± 0.44	3.84 ± 1.05
C16:3		4.99 ± 1.21
C18:0	1.64 ± 0.34	0.60 ± 0.29
C18:1	46.04 ± 4.26	11.43 ± 3.68
C18:2	28.11 ± 3.40	31.60 ± 6.67
C18:3		16.95 ± 4.03

[a] *The standard deviations represent the average molar fractions over the 9 steady states [A]-[I].*

Lipid synthesis was modelled as the coupling of three or two average fatty acids to glycerol-3-phosphate, for TAG and MGDG respectively. One average fatty acid constitutes out of the sum of the molar fractions of the various fatty acids present in the TAG and the membrane lipids of *N. oleoabundans*.

7. Chi-Squared test values

The combined balances for nitrogen, carbon and redox closed with a 95% confidence interval according to the Chi-Squared test (Test value ≤ 7.81) for all experiments, with the exception of [E].

Experiment	**Chi-squared test value**
A	3.27
B	6.48
C	1.6
D	1.65
E	**8.74**
F	4.5
G	1.41
H	0.21
I	1.09

5.B Pigment analysis

Materials

Lutein (96%) was purchased from Carotenature (Lupsingen, Switzerland). Chlorophyll *a* (90.0%) was purchased from Wako Pure Chemical Industries (Osaka, Japan).

Methods

RP-UHPLC identification and quantification of carotenoids and porphyrins was performed as previously described by (Weesepoel et al., 2013) with minor adaptations. The elution program was started from 25% (v/v) A / 75% (v/v) B and then as follows: to 15 min – linear gradient to 100% (v/v) B; to 22.5 min – isocratic at 100% (v/v) B; to 29.5 min – linear gradient to 87.5% (v/v) B/ 12.5% (v/v) C; to 31.5 min – linear gradient to 70% (v/v) B / 30% (v/v) C; to 41.5 min – linear gradient to 100% (v/v) C; to 42.5 min - isocratic at 100% (v/v) C. After 42.5 min, the eluent composition returned to its initial composition in 7.5 min, followed by an equilibration phase of 2.5 min. Detection wavelengths for UV-Vis were set at 450 nm (carotenoids c) and 660 nm (porphyrins).

For quantification lutein and chlorophyll *a* were used. Approximately 1 mg of lutein was first dissolved in dichloromethane, and subsequently diluted with 4 volumes of ethanol. Chlorophyll *a* was first dissolved in ethyl acetate, and subsequently diluted with 3 volumes of 90% (v/v) aqueous acetone. Standard concentrations were measured prior to RP-UHPLC analysis, using their respective absorption coefficients (A1%1cm): 2550 g L^{-1} cm^{-1} (445 nm, 100% ethanol) for lutein and 887 g L^{-1} cm^{-1} (664 nm, 90% (v/v) aqueous acetone) for chlorophyll *a* (Roy et al., 2011) PDA calibration was performed using five different concentrations of the standards injected in duplicate. For this calibration, the response of the *all-trans* and *cis* form of the carotenoid standards was considered equal for quantification. The detector was found to be linear for lutein between 0.08 and 8.04 µg mL-1 with a R^2 of 0.996. For chlorophyll *a* the dectector was linear between 0.06 and 6.01 µg mL^{-1} with a R^2 of 0.968.

Carotenoids were expressed as lutein equivalents using the lutein calibration curve. The responses were corrected using the following carotenoids A1%1cm: 2330 g L^{-1} cm^{-1} (437 nm, 100% ethanol) for 9'-*cis* neoxanthin, 2550 g L^{-1} cm^{-1} (433 nm, 100% ethanol) for violaxanthin, and 2500 g L^{-1} cm^{-1} for antheraxanthin and unknown carotenoids were used. A similar procedure was used for porphyrins using the calibration curve of chlorophyll a: 1270 g L^{-1} cm^{-1} (664 nm, 90% (v/v) acetone) for chlorophyllide *a*, 742 g L^{-1} cm^{-1} (667 nm, 90% (v/v) acetone) for pheophorbide a, 514 g L^{-1} cm^{-1} (647 nm, 90% (v/v) acetone) for chlorophyll *b* and 512 g L^{-1} cm^{-1} (667 nm, 90% (v/v) acetone) for pheophytin *a* (Roy et al., 2011), (Britton, 1995).

5.C Flux distributions of experiments [A]-[I] in mmol (g protein)$^{-1}$ h^{-1}.

	A	B	C	D	E	F	G	H	I
0	12.37	7.12	5.10	4.88	19.63	12.85	11.25	9.60	7.60
1	0.00	0.00	0.00	0.00	0.00	0.00	0.00	0.00	0.00
2	1.13	1.13	1.13	1.13	1.86	1.13	1.13	1.13	1.13
3	**0.00**	**40.73**	**55.71**	**80.67**	**75.03**	**130.15**	**146.37**	**176.44**	**227.94**
4	1.40	0.84	0.63	0.57	1.97	1.28	1.12	0.90	0.73
5	8.07	4.85	3.70	3.47	11.48	7.54	6.64	5.52	4.54
6	0.19	0.08	0.04	0.03	0.31	0.19	0.14	0.08	0.05
7	0.40	0.25	0.17	0.16	0.81	0.56	0.48	0.42	0.32
8	0.12	0.05	0.03	0.02	0.20	0.12	0.09	0.05	0.03
9	0.08	0.03	0.02	0.01	0.13	0.06	0.05	0.03	0.02
10	5.95	5.95	5.95	5.95	5.95	5.95	5.95	5.95	5.95
11	10.30	6.11	4.44	4.28	16.33	10.88	9.62	8.32	6.64
12	20.29	12.07	8.79	8.50	32.16	21.48	19.02	16.48	13.18
13	20.29	12.07	8.79	8.50	32.16	21.48	19.02	16.48	13.18
14	3.80	2.30	1.67	1.62	6.15	4.18	3.72	3.26	2.60
15	3.58	2.19	1.60	1.55	5.86	3.97	3.53	3.10	2.47
16	3.58	2.19	1.60	1.55	5.86	3.97	3.53	3.10	2.47
17	3.46	2.05	1.49	1.43	5.48	3.65	3.22	2.79	2.22
18	3.42	2.03	1.48	1.42	5.43	3.62	3.20	2.77	2.21
19	3.42	2.03	1.48	1.42	5.43	3.62	3.20	2.77	2.21
20	6.88	4.08	2.96	2.86	10.91	7.27	6.42	5.55	4.43
21	3.42	2.03	1.47	1.42	5.42	3.61	3.20	2.76	2.21
22	10.30	6.11	4.44	4.28	16.33	10.88	9.62	8.32	6.64
23	0.00	0.00	0.00	0.00	0.00	0.00	0.00	0.00	0.00
24	0.13	0.14	0.11	0.12	0.38	0.32	0.30	0.31	0.25
25	0.13	0.14	0.11	0.12	0.38	0.32	0.30	0.31	0.25
26	0.16	0.08	0.05	0.06	0.20	0.15	0.15	0.13	0.10
27	0.16	0.08	0.05	0.06	0.20	0.15	0.15	0.13	0.10
28	0.19	0.10	0.06	0.06	0.25	0.18	0.17	0.14	0.11
29	0.19	0.10	0.06	0.06	0.25	0.18	0.17	0.14	0.11
30	2.38	1.38	1.03	0.98	3.51	2.25	1.97	1.65	1.34
31	2.38	1.38	1.03	0.98	3.51	2.25	1.97	1.65	1.34
32	2.38	1.38	1.03	0.98	3.51	2.25	1.97	1.65	1.34
33	2.38	1.38	1.03	0.98	3.51	2.25	1.97	1.65	1.34
34	2.31	1.35	1.01	0.96	3.40	2.18	1.92	1.62	1.32
35	0.00	0.00	0.00	0.00	0.00	0.00	0.00	0.00	0.00
36	0.00	0.00	0.00	0.00	0.00	0.00	0.00	0.00	0.00
37	0.00	0.00	0.00	0.00	0.00	0.00	0.00	0.00	0.00
38	-0.07	-0.03	-0.01	-0.01	-0.10	-0.06	-0.05	-0.03	-0.02
39	0.00	0.00	0.00	0.00	-0.01	0.00	0.00	0.00	0.00
40	0.00	0.00	0.00	0.00	0.00	0.00	0.00	0.00	0.00
41	0.00	0.00	0.00	0.00	0.00	0.00	0.00	0.00	0.00

42	0.00	0.00	0.00	0.00	0.00	0.00	0.00	0.00	0.00
43	0.00	0.00	0.00	0.00	0.00	0.00	0.00	0.00	0.00
44	0.00	0.00	0.00	0.00	0.00	0.00	0.00	0.00	0.00
45	1.97	1.19	0.92	0.89	2.85	1.88	1.68	1.44	1.20
46	1.53	0.89	0.66	0.60	2.17	1.39	1.20	0.96	0.78
47	1.53	0.89	0.66	0.60	2.17	1.39	1.20	0.96	0.78
48	1.40	0.84	0.63	0.57	1.97	1.28	1.12	0.90	0.73
49	1.40	0.84	0.63	0.57	1.97	1.28	1.12	0.90	0.73
50	1.40	0.84	0.63	0.57	1.97	1.28	1.12	0.90	0.73
51	1.46	0.86	0.64	0.58	2.06	1.34	1.16	0.92	0.75
52	1.46	0.86	0.64	0.58	2.06	1.34	1.16	0.92	0.75
53	0.27	0.12	0.07	0.06	0.43	0.24	0.19	0.14	0.09
54	0.00	0.00	0.00	0.00	0.00	0.00	0.00	0.00	0.00
55	0.00	0.00	0.00	0.00	0.00	0.00	0.00	0.00	0.00
56	0.00	0.00	0.00	0.00	0.00	0.00	0.00	0.00	0.00
57	0.00	0.00	0.00	0.00	0.00	0.00	0.00	0.00	0.00
58	0.03	0.01	0.01	0.00	0.05	0.03	0.02	0.01	0.01
59	-0.03	-0.01	-0.01	0.00	-0.05	-0.03	-0.02	-0.01	-0.01
60	-0.02	-0.01	0.00	0.00	-0.02	-0.02	-0.01	-0.01	0.00
61	-0.02	-0.01	0.00	0.00	-0.02	-0.02	-0.01	-0.01	0.00
62	0.02	0.01	0.00	0.00	0.02	0.02	0.01	0.01	0.00
63	0.05	0.02	0.01	0.00	0.07	0.05	0.03	0.02	0.01
64	0.01	0.00	0.00	0.00	0.01	0.00	0.00	0.00	0.00
65	0.13	0.14	0.11	0.12	0.38	0.32	0.30	0.31	0.25
66	0.13	0.14	0.11	0.12	0.38	0.32	0.30	0.31	0.25
67	0.00	0.00	0.00	0.00	0.00	0.00	0.00	0.00	0.00
68	0.00	0.00	0.00	0.00	0.00	0.00	0.00	0.00	0.00
69	0.00	0.00	0.00	0.00	0.00	0.00	0.00	0.00	0.00
70	0.02	0.01	0.00	0.00	0.03	0.02	0.01	0.01	0.01
71	0.02	0.01	0.00	0.00	0.03	0.02	0.01	0.01	0.01
72	0.02	0.01	0.00	0.00	0.03	0.02	0.01	0.01	0.01
73	0.83	0.36	0.21	0.16	1.34	0.76	0.60	0.41	0.28
74	0.83	0.36	0.21	0.16	1.34	0.76	0.60	0.41	0.28
75	1.07	0.47	0.27	0.21	1.72	0.96	0.76	0.53	0.36
76	1.07	0.47	0.27	0.21	1.71	0.96	0.76	0.53	0.36
77	0.16	0.06	0.03	0.02	0.26	0.16	0.12	0.07	0.04
78	-0.17	-0.07	-0.04	-0.03	-0.27	-0.16	-0.12	-0.07	-0.05
79	0.04	0.02	0.01	0.01	0.06	0.03	0.03	0.02	0.01
80	0.03	0.01	0.01	0.01	0.05	0.03	0.02	0.02	0.01
81	0.02	0.01	0.01	0.00	0.03	0.02	0.01	0.01	0.01
82	0.01	0.01	0.00	0.00	0.02	0.01	0.01	0.01	0.00
83	0.01	0.00	0.00	0.00	0.01	0.00	0.00	0.00	0.00
84	0.01	0.00	0.00	0.00	0.01	0.00	0.00	0.00	0.00
85	0.01	0.00	0.00	0.00	0.01	0.01	0.01	0.00	0.00
86	0.31	0.14	0.08	0.06	0.50	0.28	0.22	0.16	0.11

87	0.20	0.09	0.05	0.04	0.32	0.17	0.14	0.10	0.07
88	0.02	0.01	0.00	0.00	0.03	0.02	0.01	0.01	0.01
89	0.02	0.01	0.00	0.00	0.03	0.02	0.01	0.01	0.01
90	0.00	0.00	0.00	0.00	0.00	0.00	0.00	0.00	0.00
91	0.07	0.03	0.02	0.02	0.12	0.06	0.05	0.04	0.03
92	0.20	0.09	0.05	0.04	0.33	0.19	0.15	0.10	0.07
93	0.02	0.01	0.01	0.00	0.03	0.02	0.02	0.01	0.01
94	0.08	0.04	0.02	0.02	0.13	0.07	0.06	0.04	0.03
95	0.03	0.01	0.01	0.01	0.04	0.02	0.02	0.01	0.01
96	0.03	0.01	0.01	0.01	0.04	0.02	0.02	0.01	0.01
97	0.05	0.02	0.01	0.01	0.09	0.05	0.04	0.03	0.02
98	0.01	0.00	0.00	0.00	0.02	0.01	0.01	0.01	0.00
99	0.01	0.01	0.00	0.00	0.02	0.01	0.01	0.01	0.00
100	0.00	0.00	0.00	0.00	0.00	0.00	0.00	0.00	0.00
101	0.04	0.02	0.01	0.01	0.07	0.04	0.03	0.02	0.02
102	0.02	0.01	0.01	0.00	0.03	0.02	0.01	0.01	0.01
103	0.02	0.01	0.01	0.00	0.03	0.02	0.01	0.01	0.01
104	0.04	0.02	0.01	0.01	0.07	0.04	0.03	0.02	0.02
105	0.03	0.01	0.01	0.01	0.05	0.03	0.02	0.02	0.01
106	0.04	0.02	0.01	0.01	0.07	0.04	0.03	0.02	0.01
107	0.03	0.01	0.01	0.01	0.04	0.02	0.02	0.01	0.01
108	0.03	0.01	0.01	0.01	0.04	0.02	0.02	0.01	0.01
109	0.35	0.25	0.22	0.25	0.54	0.40	0.39	0.41	0.36
110	0.05	0.03	0.03	0.03	0.07	0.05	0.05	0.05	0.05
111	0.35	0.25	0.22	0.25	0.54	0.40	0.39	0.41	0.36
112	0.00	0.00	0.00	0.00	0.00	0.00	0.00	0.00	0.00
113	0.02	0.01	0.01	0.01	0.02	0.02	0.02	0.02	0.01
114	0.03	0.02	0.02	0.02	0.04	0.03	0.03	0.04	0.03
115	0.00	0.00	0.00	0.00	0.01	0.00	0.00	0.00	0.00
116	0.03	0.02	0.02	0.02	0.04	0.03	0.03	0.04	0.03
117	0.00	0.00	0.00	0.00	0.01	0.00	0.00	0.00	0.00
118	0.00	0.00	0.00	0.00	0.00	0.00	0.00	0.00	0.00
119	0.02	0.01	0.01	0.01	0.03	0.02	0.02	0.02	0.02
120	0.00	0.00	0.00	0.00	0.00	0.00	0.00	0.00	0.00
121	0.00	0.00	0.00	0.00	0.00	0.00	0.00	0.00	0.00
122	0.01	0.00	0.00	0.00	0.01	0.01	0.00	0.00	0.00
123	0.00	0.00	0.00	0.00	0.00	0.00	0.00	0.00	0.00
124	0.00	0.00	0.00	0.00	0.00	0.00	0.00	0.00	0.00
125	0.00	0.00	0.00	0.00	0.00	0.00	0.00	0.00	0.00
126	0.00	0.00	0.00	0.00	0.00	0.00	0.00	0.00	0.00
127	0.00	0.00	0.00	0.00	0.00	0.00	0.00	0.00	0.00
128	0.00	0.00	0.00	0.00	0.00	0.00	0.00	0.00	0.00
129	0.00	0.00	0.00	0.00	0.00	0.00	0.00	0.00	0.00
130	0.00	0.00	0.00	0.00	0.00	0.00	0.00	0.00	0.00
131	-0.02	-0.01	-0.01	-0.01	-0.03	-0.02	-0.02	-0.02	-0.02

132	0.00	0.00	0.00	0.00	0.00	0.00	0.00	0.00	0.00
133	0.05	0.02	0.01	0.00	0.07	0.05	0.03	0.02	0.01
134	0.00	0.00	0.00	0.00	0.00	0.00	0.00	0.00	0.00
135	-0.05	-0.02	-0.01	0.00	-0.07	-0.05	-0.03	-0.02	-0.01
136	0.01	0.01	0.00	0.00	0.02	0.01	0.01	0.01	0.00
137	0.00	0.00	0.00	0.00	0.00	0.00	0.00	0.00	0.00
138	0.00	0.00	0.00	0.00	0.00	0.00	0.00	0.00	0.00
139	0.00	0.00	0.00	0.00	0.00	0.00	0.00	0.00	0.00
140	0.02	0.01	0.00	0.00	0.03	0.02	0.01	0.01	0.00
141	0.02	0.01	0.00	0.00	0.03	0.02	0.01	0.01	0.00
142	0.01	0.00	0.00	0.00	0.02	0.01	0.01	0.00	0.00
143	0.02	0.01	0.00	0.00	0.03	0.02	0.01	0.01	0.00
144	0.02	0.01	0.01	0.00	0.03	0.02	0.01	0.01	0.01
145	0.04	0.02	0.01	0.01	0.06	0.04	0.03	0.02	0.01
146	0.01	0.00	0.00	0.00	0.02	0.01	0.01	0.00	0.00
147	0.00	0.00	0.00	0.00	0.00	0.00	0.00	0.00	0.00
148	0.03	0.01	0.00	0.00	0.04	0.03	0.02	0.01	0.01
149	0.01	0.00	0.00	0.00	0.02	0.01	0.01	0.00	0.00
150	0.01	0.00	0.00	0.00	0.02	0.01	0.01	0.00	0.00
151	0.03	0.01	0.00	0.00	0.04	0.03	0.02	0.01	0.01
152	0.02	0.01	0.00	0.00	0.03	0.02	0.01	0.01	0.00
153	0.00	0.00	0.00	0.00	0.00	0.00	0.00	0.00	0.00
154	0.00	0.00	0.00	0.00	0.00	0.00	0.00	0.00	0.00
155	0.00	0.00	0.00	0.00	0.00	0.00	0.00	0.00	0.00
156	0.00	0.00	0.00	0.00	0.00	0.00	0.00	0.00	0.00
157	0.00	0.00	0.00	0.00	0.00	0.00	0.00	0.00	0.00
158	0.00	0.00	0.00	0.00	0.00	0.00	0.00	0.00	0.00
159	0.00	0.00	0.00	0.00	0.00	0.00	0.00	0.00	0.00
160	0.00	0.00	0.00	0.00	0.01	0.00	0.00	0.00	0.00
161	0.00	0.00	0.00	0.00	0.00	0.00	0.00	0.00	0.00
162	0.00	0.00	0.00	0.00	0.00	0.00	0.00	0.00	0.00
163	0.01	0.00	0.00	0.00	0.01	0.01	0.00	0.00	0.00
164	0.03	0.01	0.00	0.00	0.06	0.03	0.02	0.01	0.00
165	0.02	0.01	0.01	0.00	0.03	0.02	0.01	0.01	0.01
166	0.00245	0.00415	0.00525	0.00776	0.00482	0.00562	0.00776	0.01028	0.00955
167	0.00	0.00	0.00	0.00	0.00	0.00	0.00	0.00	0.00
168	0.50	0.23	0.14	0.11	0.81	0.45	0.36	0.27	0.19
169	0.14	0.07	0.05	0.05	0.17	0.13	0.13	0.12	0.10
170	0.71	0.33	0.20	0.17	1.08	0.64	0.54	0.41	0.30
171	0.19	0.10	0.06	0.06	0.25	0.18	0.17	0.14	0.11
172	2.59	1.48	1.09	1.04	3.79	2.45	2.15	1.80	1.46
173	0.00	0.00	0.00	0.00	0.00	0.00	0.00	0.00	0.00
174	0.00	0.00	0.00	0.00	0.00	0.00	0.00	0.00	0.00
175	0.83	0.36	0.21	0.16	1.34	0.76	0.60	0.41	0.28
176	-0.02	-0.01	0.00	0.00	-0.03	-0.02	-0.01	-0.01	-0.01

177	0.63	0.28	0.16	0.12	1.02	0.57	0.45	0.31	0.21
178	0.43	0.30	0.26	0.29	0.68	0.50	0.48	0.48	0.42
179	0.00	0.00	0.00	0.00	0.00	0.00	0.00	0.00	0.00
180	0.00	0.00	0.00	0.00	0.00	0.00	0.00	0.00	0.00
181	0.00	0.00	0.00	0.00	0.00	0.00	0.00	0.00	0.00
182	0.00	0.00	0.00	0.00	0.00	0.00	0.00	0.00	0.00
183	0.00	0.00	0.00	0.00	0.00	0.00	0.00	0.00	0.00
184	0.02	0.01	0.01	0.00	0.03	0.02	0.01	0.01	0.01
185	-0.07	-0.03	-0.02	-0.02	-0.12	-0.06	-0.05	-0.04	-0.03
186	0.03	0.01	0.01	0.01	0.05	0.03	0.02	0.02	0.01
187	0.01	0.00	0.00	0.00	0.01	0.00	0.00	0.00	0.00
188	0.01	0.00	0.00	0.00	0.01	0.01	0.01	0.00	0.00
189	0.01	0.00	0.00	0.00	0.02	0.01	0.01	0.01	0.00
190	0.00	0.00	0.00	0.00	0.00	0.00	0.00	0.00	0.00
191	0.09	0.04	0.02	0.02	0.15	0.09	0.07	0.04	0.03
192	0.02	0.01	0.01	0.00	0.03	0.02	0.01	0.01	0.01
193	0.04	0.02	0.01	0.01	0.07	0.04	0.03	0.02	0.02
194	0.03	0.01	0.01	0.01	0.05	0.03	0.02	0.02	0.01
195	-0.08	-0.04	-0.02	-0.02	-0.13	-0.07	-0.06	-0.04	-0.03
196	-0.02	-0.01	0.00	0.00	-0.03	-0.01	-0.01	-0.01	0.00
197	0.00	0.00	0.00	0.00	0.00	0.00	0.00	0.00	0.00
198	0.03	0.01	0.01	0.01	0.04	0.02	0.02	0.01	0.01
199	0.02	0.01	0.01	0.01	0.04	0.02	0.02	0.01	0.01
200	0.00	0.00	0.00	0.00	0.00	0.00	0.00	0.00	0.00
201	0.00	0.61	0.73	0.77	0.00	0.10	0.36	0.59	0.73
202	-5.48	-3.22	-2.24	-2.24	-9.48	-6.41	-5.69	-5.06	-3.97
203	7.54	4.22	2.89	2.82	12.76	8.34	7.29	6.32	4.90
204	-3.94	-2.43	-1.74	-1.79	-6.88	-4.78	-4.32	-3.96	-3.15
205	-0.04	-0.01	-0.01	0.00	-0.06	-0.04	-0.03	-0.01	-0.01
206	-0.02	-0.01	0.00	0.00	-0.03	-0.02	-0.01	-0.01	-0.01
207	-0.83	-0.36	-0.21	-0.16	-1.34	-0.76	-0.60	-0.41	-0.28
208	0.00	0.00	0.00	0.00	0.00	0.00	0.00	0.00	0.00
209	-123.70	-111.90	-106.70	-129.50	-271.30	-258.60	-258.90	-272.40	-303.90
210	0.00	40.73	55.71	80.67	75.03	130.15	146.37	176.44	227.94
211	-1.21	-0.53	-0.30	-0.23	-1.95	-1.11	-0.87	-0.60	-0.40
212	0.00	0.00	0.00	0.00	0.00	0.00	0.00	0.00	0.00
213	0.00	0.00	0.01	0.01	0.00	0.01	0.01	0.01	0.01
214	0.13	0.14	0.11	0.12	0.38	0.32	0.30	0.31	0.25
215	0.71	0.33	0.20	0.17	1.08	0.64	0.54	0.41	0.30

Chapter 6

General Discussion

Part of this chapter is submitted for publication as:
Klok, A.J., Lamers, P.P., Martens, D.E., Draaisma, R.B., Wijffels, R.H.
Edible oils from microalgae: insights in TAG accumulation

6.1 Microalgal lipids: a sustainable and widely applicable feedstock.

Microalgae have attracted a lot of attention due to their potential to sustainably produce a wide range of compounds, including pigments, protein, lipids, carbohydrates (particularly starch) and alkanes (Wijffels et al., 2013; Spolaore et al., 2006). Currently, they attract most scientific attention for using their lipids in the production of next generation biofuels (Hu et al., 2008), such as diesel, kerosene or gasoline. An important reason for their popularity is that the prospected areal yields of algal oil are much higher than those achieved with traditional oleaginous crops used for biofuel production (e.g. palm, corn, soy) (Wijffels and Barbosa, 2010; Chisti, 2007). The potential of microalgal lipids is, however, much wider than fuel. The fatty acid composition of microalgal oil is comparable to that of oils derived from oleaginous plants and many algae produce the for humans essential fatty acids linoleic (18:2), linolenic (18:3), eicosapentaenoic (EPA; 20:5) and docosahexaenoic (DHA; 22:6) acid (Guschina and Harwood, 2009). Therefore, algal lipids have the potential to replace bulk vegetable oils such as sunflower and palm oil (Draaisma et al., 2013), and could serve as a source of nutraceuticals, for example DHA and EPA, providing a vegetarian alternative to fish oils (Scott et al., 2007). Finally, as algal derived oils are closely related to petrochemicals, they can be easily transformed into other commodity chemicals, besides fuels (Hatti-Kaul et al., 2007).

A significant reduction in production cost is needed to make microalgal lipids compete with lipids derived from oleaginous crops or fossil oil (Wijffels and Barbosa, 2010). An important target for improving process economics is the optimisation of algal lipid production. This requires proper understanding of the physiology and regulation of lipid metabolism in microalgae. Although the insight in the biology of microalgal lipid metabolism is steadily increasing, important knowledge gaps still exist.

In this chapter, an overview of the current understanding of microalgal lipid metabolism is given and the most important existing knowledge gaps are identified. Based on current developments in the field and the research presented in this thesis, three hypotheses on the cause and function of lipid accumulation under adverse growth conditions are proposed. With these hypotheses in mind, several considerations for improving lipid productivity and optimising commercial outdoor production are presented, both via improving photobioreactor operational strategies, as well as via strain improvement.

6.2 Biology of lipid synthesis in microalgae

Microalgae produce a large variety of lipid like compounds, such as waxes, sterols, hydrocarbons, and glycerolipids. Current research on microalgal lipids is mainly focussed on the latter type because of their many applications, as mentioned earlier. Therefore,

this discussion will be limited to glycerolipids and any further reference to 'lipids' will regard glycerolipids in particular.

6.2.1 Lipid types

Glycerolipids are characterised by a glycerol backbone with one, two or three fatty acyl groups attached and can be divided into two large subclasses based on their specific function, being membrane lipids and storage lipids (Harwood, 2004). Membrane lipids contain two fatty acyl groups and generally have a polar side group at the sn-3 position of their glycerol backbone. These lipids are the essential building blocks for cell and organelle membranes. Two major classes can be distinguished being the plastid and thylakoid membranes, which are unique to green organisms, and the extraplastidic membranes, which can also be found in eukaryotes and bacteria. In microalgae, the plastid and thylakoid membranes mainly consist of the non-phosphorous galactolipids monogalactosyldiacylglycerol (MGDG, 40-55%) and digalactosyldiacylglycerol (DGDG, 15-35%) and the sulfolipid sulfoquinovosyldiacylglycerol (SQDG, 10-20%). The extraplastidic membranes in microalgae contain phospholipids and the betaine lipid DGTS (diacylglyceryl-*N,N,N*-trimethylhomoserine). As the plastid and thylakoid membrane are predominant, their composition largely determines the average membrane lipid composition of microalgae. (Harris, 2009; Harwood, 2004).

Storage lipids have a third fatty acyl group, attached at the sn-3 position, and are also known as triacylglycerides (TAG). TAGs are typically produced in algae under adverse growth conditions and are accumulated in specialized organelles, the lipid bodies (LBs). After prolonged exposure to adverse growth conditions, such as nitrogen deprivation, the TAG fraction of microalgae ranges from 20-60% (w/dw) (Griffiths and Harrison, 2009). TAG is of particular interest for the production of biofuels and petrochemicals, since it gives a clean product without contamination of phosphorous or sulphur, which is detrimental for fuel quality (Mittelbach, 1996). Also, the fatty acyl groups in TAG are generally more saturated than those present in membranes, providing higher oxidation stability (Durrett et al., 2008). Moreover, the fatty acyl groups of the algal TAG can consist for as much as 50% of oleic acid (C18:1) (Breuer et al., 2012), which is the preferred fatty acyl group for biodiesel production. The single double bond in oleic acid provides its methyl ester with good cold flow and viscosity properties without compromising on oxidative stability (Knothe, 2005).

6.2.2 Lipid metabolism

Until recently our knowledge of lipid biosynthesis in algae was largely based on the as-

sumption that plant and algal lipid biosynthesis pathways are similar. However, as more microalgal genome sequences became available, the differences with plant lipid biosynthesis became apparent. Examples of this are distinct fatty acyl groups and differences in the overall subcellular organization of glycerolipid metabolism (Liu and Benning, 2013).

Figure 6.1 shows a schematic representation of lipid biosynthesis in algae, which starts with the synthesis of the fatty acids. *De novo* fatty acid synthesis in eukaryotic green organisms takes place in the chloroplast and is initiated by the conversion of acetyl-CoA to malonyl-CoA by the enzyme Acetyl-CoA carboxylase (ACCase) (Riekhof and Benning, 2009). In both plants and algae, ACCase activity is controlled at various levels and as such is regarded as the central enzyme in regulating the initiation of fatty acid biosynthesis (Ohlrogge and Jaworski, 1997). After malonyl-CoA synthesis, the malonyl group is transferred to an acyl carrier protein (ACP) by malonyl-CoA:ACP transacylase (MCT) and undergoes a series of condensation, reduction, and dehydration reactions in which the acyl chain is extended by two carbon atoms in each reaction cycle. This series of reactions is catalysed by the fatty acid synthase (FAS) complex, which consists of MCT, 3-ketoacyl ACP synthase (KAS), 3-ketoacyl ACP reductase (KAR), hydroxyacyl ACP dehydratase (HAD) and enoyl ACP reductase (EAR).

When the fatty acyl chain reaches its full length, usually C16:0-ACP or C18:0-ACP, it is removed from the ACP group and is either directly transferred to glycerol-3-phosphate by glycerol-3-phosphate acyltransferase (GPAT) to produce lysophosphatidic acid (Lyso-PA), or hydrolysed by acyl-ACP esterase (AAE) to produce free fatty acids. The fatty acyl group of acyl-ACP can also be transferred to Lyso-PA by Lyso-PA acyltransferase (LPAT), yielding phosphatidic acid (PA), the common precursor of all algal glycerolipids.

For the production of major membrane constituents MGDG, DGDG and SQDG for plastid membranes and DGTS for the other membranes, as well as for the production of TAG, PA is dephosphorylated by PA phosphatase (PAP), forming diacylglyceride (DAG). Subsequently, a side group is added to the vacant position on the DAG molecule, being a (di)galactosyl group in the case of MDGD and DGDG, a sulfoquinovosyl group in the case of SQDG, trimethylhomoserine for the production of DGTS and addition of a third fatty acyl group for TAG

The final fatty acyl group added to DAG in the production of TAG can come from two sources. The first possible source is acyl-ACP, from which the fatty acyl group is transferred by diacylglycerol acyltransferase (DGAT). This route is the final step of what is known as the Kennedy Pathway, which entails the three sequential acylation steps of glycerol 3 phosphate. The other potential fatty acyl donors for production of TAG are

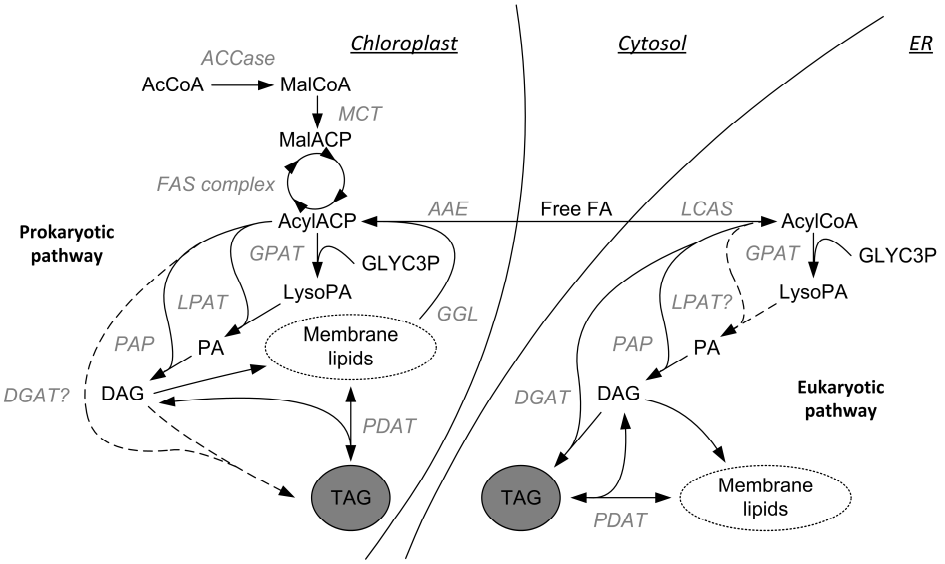

Figure 6.1 *Schematic representation of lipid biosynthesis in microalgae. All enzymes are indicated in grey and their substrates in black. Dotted lines and the use of '?' indicate uncertainty about the existence of these enzymes.*

membrane lipids, from which a fatty acyl group can be transferred to DAG by phospholipid:diacylglycerol transferase (PDAT). In *C. reinhardtii*, the substrate of PDAT is not limited to phospholipids as in fungi and plants, but also includes MGDG and even DAG (Yoon et al., 2012). This use of membrane lipids as fatty acyl donors for TAG formation is also known as the acyl-CoA independent pathway. Alternative to functioning as a direct donor, plastid membrane lipid MGDG can indirectly provide a fatty acyl group to TAG by the action of galactoglycerolipid lipases (GGL), which produces free fatty acids. Next, the formed free fatty acid is converted to AcylACP or AcylCoA and subsequently the fatty acyl group can serve as a substrate for any acyltransferase, as described by (Li et al., 2012) for *C. reinhardtii.*

Two possible locations can be distinguished for lipid biosynthesis from glycerol-3-phosphate and fatty acids (Figure 6.1) being the plastid (Prokaryotic Pathway) and the ER (Eukaryotic Pathway). To feed the latter pathway, free fatty acids are transported over the plastid membrane and subsequently attached to acyl-CoA by Long-chain Acetyl-CoA synthase (LCAS). From there, the eukaryotic pathway follows the same sequence of reactions as its plastidic counterpart for the production of glycerolipids, while using acyl-CoA as a substrate instead of acyl-ACP. In plants, the location of synthesis of a glycerolipid can be determined based on the fatty acyl group occupying the sn-2 posi-

tion, as plastidic and cytosolic LPAT show a strict but distinct substrate specificity. A 16 carbon acyl group at the sn-2 position is indicative of plastid origin, while an 18 carbon acyl group at this position only occurs in ER derived lipids (Roughan and Slack, 1982). Whether this specific signature is also maintained in algae cannot be confirmed, as up to now, extraplastidic LPAT has not been discovered in all but one microalga being *Micromonas sp*, an ancestral green alga which is thought to possess the same characteristics as the last common ancestor of green algae and land plants (Worden et al., 2009). Perhaps, later emerging green algae species such as *C. reinhardtii* lost the extraplastidic form of LPAT. (Merchant et al., 2012) suggests that the eukaryotic pathway in these strains can only be functional with a divergent protein, or broader substrate specificity of GPAT, which might also mean a distinct signature for plastid and cytosol derived lipids in microalgae.

Assuming that the signature for plastid derived lipids is the same in algae as it is in plants, (Giroud et al., 1988) found that MGDG, DGDG and SQDG in *C. reinhardtii* are exclusively of chloroplast origin, while DGTS and phospholipids are solely synthesized in the cytoplasm. This would suggest that microalgae maintain a strict compartmentalisation of membrane lipid synthesis, whereas in plants each individual pathway (Prokaryotic and Eukaryotic) provides lipids for both the plastidic, as well as in the extraplastidic membranes (Ohlrogge and Browse, 1995). TAG biosynthesis in plants occurs exclusively outside the plastid (Lung and Weselake, 2006). In microalgae, this view was initially adopted and confirmed for *C. reinhardtii* as the six DGAT encoding genes identified lack a plastid targeting sequence (Liu and Benning, 2013). In contrast to this assumption, (Goodson et al., 2011) and (Li et al., 2013) found LBs to be often physically connected or even merged with the plastid membrane, which suggests the plastid as an alternative location for TAG synthesis. Also, (Fan et al., 2011) found that approximately 90% of the TAG produced in *C. reinhardtii* carried the signature of plastid derived DAG. Again, if the signature for plastid derived lipids is the same in algae as it is in plants and this signature remains unchanged in TAG synthesis, the finding of (Fan et al., 2011) argues for the existence of a chloroplast pathway for TAG synthesis in microalgae.

The available knowledge on glycerolipid metabolism in microalgae is largely based on the accepted reference for microalgal metabolism, *Chlamydomonas reinhardtii*, as knowledge on this alga is ample, its genome sequence is available (Merchant et al., 2007), and it can be genetically transformed (Kindle, 1990). However, this alga is possibly not the best reference for oleaginous algae, because *C. reinhardtii* predominantly accumulates starch as storage metabolite and has a rather stable lipid content (James et al., 2011). Starchless mutants that do accumulate TAG, provided an opportunity to

study storage lipid biosynthesis in this species (Li et al., 2010b; Merchant et al., 2012). However, whether this artificial induction of TAG accumulation in *C. reinhardtii* is fully representative of TAG production in algae that are oleaginous by nature remains a question.

6.2.3 TAG accumulation

An important focal point for improving the process economics of algal lipid production is increasing the lipid content and/or productivity of lipids in microalgae. The most applied strategy to increase the production of lipids in microalgae is to subject the culture to nutrient, and in particular nitrogen, limitation (Hu et al., 2008). Under these conditions, cell division is hampered, and oleaginous algae accumulate TAG in specialised organelles, the lipid bodies (LBs). Although the regulating mechanism responsible for TAG accumulation is unknown, several hypotheses exist as to what the function of TAG storage in specialised LBs could be.

TAG as a carbon and/or energy reserve

The most well-known function of TAG accumulation in many organisms is storage of carbon and energy. Also in algae TAG storage is thought to allow for continuous capturing of energy and carbon when a lack in nitrogen limits functional biomass production. The carbon and energy stored in TAG can be mobilised again when favourable growth conditions are restored.

An approach in determining whether TAG functions as a carbon or energy storage, or both, is to study its fate after growth has been restored. Labelling studies are particularly interesting for studying the fate of molecules in metabolism. These type of studies already revealed TAG derived fatty acids are being used in the production of chloroplast lipids after nitrogen replenishment (Khozin-Goldberg et al., 2000; Khozin-Goldberg et al., 2005). It is not known whether TAG is also metabolised and respired when growth is restored, and therefore it would be interesting to determine if labelled carbon in TAG is released as CO_2.

Co-accumulation and labelling of starch in oleaginous algae could lead to problems in labelling approaches, as it will not be possible to determine whether labelled CO_2 and membrane lipids stem from TAG or starch. Using a starch mutant is not an option, because lipid respiration after nitrogen recovery could be artificially increased in these mutants in absence of starch as a carbon and energy reservoir. Possibly, using labelling during different phases of nitrogen starvation would allow for differential labelling of starch and TAG, as starch is often accumulated at the beginning of the stress phase, while TAG

is typically synthesized in a later stage (Siaut et al., 2011).

TAG functions as electron scavenger under adverse growth conditions

Under nitrogen replete conditions, more than one third of the NADPH generated in algal photosystems is used for nitrogen assimilation and protein synthesis (Chapter 5). When exposed to nitrogen shortage, cells are thus confronted with a tremendous surplus of NADPH. As a result of this, a dangerous overreduction of the photosynthetic electron transport chain can occur. If this excess reducing potential is not safely channelled away it can be transferred to oxygen, creating reactive oxygen species (ROS), which could damage vital cell components (Ledford and Niyogi, 2005). The accumulation of highly reduced compounds such as TAG, is thought to provide an alternative sink for excess reducing potential under adverse growth conditions (Hu et al., 2008; Li et al., 2013).

Several observations support the close interaction of TAG accumulation with chloroplast redox metabolism. For example, the sensitivity of lipid and in particular *de novo* TAG synthesis to the redox state of the plastid is illustrated by the reductive activation of ACCase (Kozaki et al., 2001). ACCase is the first committed enzyme in fatty acid synthesis and thus brings the lipid biosynthetic pathway under redox regulatory control. Furthermore, (Li et al., 2012) demonstrated that *C. reinhardtii* TAG-deficient mutants (pgd1) were less viable under nitrogen depleted conditions and showed a much higher extent of ROS formation compared to the wild type. Based on their observations, (Li et al., 2012) concluded that microalgae employ TAG synthesis to lower the reductive state of the photosynthetic electron transport chain.

To quantify to which extent TAG synthesis contributes to lowering the reductive state, we evaluated the electron distributions in nitrogen limited *Neochloris oleoabundans.* We found that indeed the amount of electrons channelled to TAG linearly increased with the nitrogen shortage experienced by the cells (Chapter 3), supporting previous observations that TAG synthesis is a response to redox imbalances experienced by the cell. However, only a mere 8.6% of the potential excess electrons that could be generated under nitrogen limitation was ending up in TAG. The largest fraction of the excess light was either not converted to electrons at all and directly dissipated or converted to electrons that were used for catabolic processes. Thus, TAG synthesis in *N. oleoabundans* is triggered by the imbalance between photosynthesis and anabolism, and scavenges some of the generated electrons. However, a decrease in LET seems to be the primary mechanism of this alga to deal with an excess in reduction potential (Chapter 5).

TAG filled LBs as temporary plastid component storage deposit

Another possible explanation for TAG accumulation would be that LBs serve as a reservoir for chloroplast derived membrane lipids. Chloroplast size and structure is severely reduced under adverse growth conditions. Chlorosis (loss of pigmentation) and photosynthetic membrane degradation are observed in cells exposed to high light intensities as well as to nutrient deprived conditions (Falkowski and LaRoche, 1991; Rhiel et al., 1985; Turpin, 1991). Possibly, TAG accumulation by means of the acyl-CoA independent pathway and subsequent LB synthesis serves as an efficient route to temporarily store redundant plastid membranes and photosystem building blocks. As the reduction of plastid size and structure will lower the absorptive cross section and thus the photosynthetic energy intake of a cell, such a function of TAG synthesis also directly contributes in reducing the excess of reducing potential.

Several observations support this hypothesis. First of all, the plastid membrane galactoglycerolipid pool was identified as an important donor of fatty acids for TAG synthesis using labelling studies in TAG-deficient mutants and wild type *C. reinhardtii* (Li et al., 2012). Also, the ROS formation in these mutants, which is explained by the authors as being caused by the absence of TAG as an electron sink, could similarly be caused by the sheer size of the plastid. Possibly, the mutation reduces the transfer of redundant plastid membrane into LBs, which prevents the reduction of the cell's absorptive cross section and thereby mitigates ROS formation. Furthermore, previously mentioned observations that localize TAG synthesis in proximity of the plastid, such as LBs merged with the plastid membrane, make it likely that TAG accumulation could serve as a means to quickly degrade plastid membranes and transport their components to LBs.

As mentioned in Chapter 2, it is possible that LBs serve as a temporary storage, not only for redundant plastid membranes, but also for photosynthetic pigments and proteins. Such a plastid storage reservoir would allow the rapid rebuilding of a functional plastid after growth promoting environmental conditions have been restored, and as such could provide an evolutionary advantage. This view is supported by an observation of (Davis et al., 2012), who found unbound chlorophyll in the LBs of nitrogen starved *N. oleoabundans*. Co-accumulation of secondary pigments in LBs is generally accepted in pigment overproducing algae such as *Dunaliella salina* (Rabbani et al., 1998) and *Chlorella zofingiensis* (Bar et al., 1995), but primary pigments had not been observed before to appear in LBs. In absence of published data on primary pigments in LBs, further exploration of LBs pigment composition will show if transient storage of photosynthetic pigments in LBs is a general response to energy imbalances. In addition, the discovery of 'refugee proteins' with no obvious connection to LB function (i.e. lipid metabolism and

trafficking) in the LBs of several eukaryote cells suggests that LB might even function as a dynamic protein storage site (Farese Jr and Walther, 2009; Hodges and Wu, 2010). The few published proteome studies of algal LB have revealed proteins involved in LB function (Peled et al., 2011) and lipid metabolism (Nguyen et al., 2011). However, the latter study also revealed some stromal or thylakoid associated proteins in the isolated LB fraction. It is possible that the latter mentioned proteins are originating from contaminating plastid components, but it could also be explained by the hypothesis that algal LBs function as reservoir for all types of plastid constituents.

6.2.4 The extent and function of TAG accumulation are species specific

Not all microalgae exhibit the same capacity to accumulate TAG under adverse growth conditions. Differences in TAG production rates can be caused by co-accumulation of other compounds competing for carbon and energy. A typical example of this is starch in *C. reinhardtii*, an alga that only accumulates large amounts of TAG when the pathway for starch synthesis is blocked (Li et al., 2010a). Another cause can be found in the extent to which a species is capable of maintaining photosynthetic rates under the adverse growth conditions that stimulate TAG accumulation, which can be very different for various species (Breuer et al., 2012).

The plastidic turnover ratio of ATP/NADPH is severely affected under sudden nitrogen starvation (Simionato et al., 2013) and the absolute turnover rates of these energy carriers are reduced when growth is limited by nitrogen (Chapter 5). Therefore, it is not surprising that there is an intricate link between nitrogen metabolism and photosynthesis. The principle of 'photosynthetic control', as described by (Foyer et al., 1990), postulates that algae constantly adapt photosynthesis to meet metabolic demands, and when these metabolic demands fall short under nitrogen depletion, excess absorbed photons can be dissipated as heat or fluorescence (Müller et al., 2001). Also, algae severely reduce their photosynthetic capacity by a reduction in pigmentation (chlorosis), photosynthetic membrane, photosynthetic proteins and active PS reaction centres (Chapter 2; Falkowski et al., 1989; Herrig and Falkowski, 1989; Kolber et al., 1988; Rhiel et al., 1985), but the extent to which this happens is species specific.

Differences in photosynthetic capacity and TAG accumulation rates under nutrient stress between algal species, might point towards a difference into the extent that TAG accumulation serves as a carbon or energy reserve, a sink for excess reducing potential, and as temporary storage of redundant plastid components. For example, *N. oleoabundans* primarily dissipates energy under nitrogen limited conditions and disintegrates its plastid in order to reduce its energy intake (This thesis; Breuer et al., 2012), while storing

redundant plastid components in its LBs (Davis et al., 2012). On the other hand, a species such as *Nannochloropsis gaditana* also decreases its plastid membrane, but retains chloroplast structure and photosynthetic activity, which results in almost similar biomass production rates for both nitrogen sufficient and nitrogen starved conditions (Simionato et al., 2013). Combined with the observation that most of the TAG in this species is produced *de novo*, TAG synthesis in this species seems to be predominantly employed to scavenge electrons and efficiently store carbon and energy.
Perhaps, the apparent different function of TAG accumulation in these particular species, can be explained by their very distinct original habitats. *Nannochloropsis sp*, isolated from sheltered rock pools and marine coastal water (Hibberd, 1981), possibly benefits from its ability to maintain photosynthetic capacity under adverse growth conditions, in order to outcompete competitors for the available light. On the other hand, an arid soil species such as *N. oleoabundans*, isolated from a sand dune in the Rub al Kali desert in Saudi Arabia (Chantanachat and Bold, 1962), might have an evolutionary advantage by quickly degrading and rebuilding its plastid. Under such intense radiation, converting all available solar energy into lipids and starch could quickly have posed such a physical burden on these cells that they were unable to divide. Insight into the possible correlations between the natural growth environment and photosynthetic capacity under adverse growth conditions, as was demonstrated by (Hanelt et al., 1997), and to what extent this capacity influences TAG accumulation rates, might help in localising the preferred habitat of the most efficient TAG producing species.

In conclusion, important gaps still exist in our knowledge on algal glycerolipid metabolism in general and TAG metabolism in particular. Although it seems likely that the redox/energy imbalance is important for triggering both TAG accumulation as well as a decrease in photosynthetic capacity, the exact mechanisms and signalling pathways involved remain unknown. With some important Kennedy pathway enzymes still unidentified in microalgae, the pathway and exact location (chloroplast or ER) of TAG synthesis remains a question. Although TAG always is a carbon sink as its synthesis requires the consumption of carbon, the extent to which it functions as a sink for excess electrons under adverse growth conditions may vary between algae and consequently TAG may have additional functions in some species, like storage of plastid building blocks. With non-oleaginous microalgae *C. reinhardtii* as a model species, additional research into lipid synthesis in truly oleaginous microalgae, such as that presented in this thesis, is highly necessary to answer the many questions on microalgal lipid production that exist today.

6.3 Considerations for improving the TAG production process

To produce microalgal TAG for the biodiesel market, and to compete with fossil feedstock, the current cost of production should be decreased by a factor 10 (Wijffels and Barbosa, 2010). This could be partly realised by increasing TAG productivity and yield, which currently amount up to about one third of what is possible in theory (Chapter 5). Several considerations for taking TAG production to the next level by improving photobioreactor operation strategies and strain improvement are presented in the following section.

6.3.1 Photobioreactor operational strategies for TAG production

Many strategies can be applied that result in an imbalance between energy produced in photosynthesis and energy used on growth, and as such stimulate the synthesis of TAG (Hu et al., 2008). Of these strategies nitrogen shortage is the most effective approach, as it quickly creates a large imbalance in available and consumed NADPH. Nitrogen assimilation alone takes up about 14% of plastidic NADPH, while for example sulphur assimilation uses only 0.3% (Chapter 5). This could be an explanation for the fact that in general nitrogen shortage is more effective than sulphur shortage in obtaining TAG accumulation in microalgae.

Two conditions with respect to nitrogen shortage can be distinguished, being nitrogen limitation and nitrogen starvation (Rodolfi et al., 2009). It is important to stress the difference between these two strategies, as they are often confused in scientific literature.

- **Nitrogen starvation** can be considered the classic approach to TAG production. The vast majority of scientific publications on TAG accumulation in microalgae uses this technique. The process is characterised by a biomass production phase followed by a starvation phase in which nitrogen is absent from, and not supplied to, the medium. In this latter stage the production of functional biomass (i.e. biomass that is able to reproduce itself) is stopped and TAG is accumulated. After prolonged exposure to nitrogen starved conditions cells will stop to accumulate TAG, start degrading it and eventually they will die. Therefore, nitrogen starvation is a finite, batch process.
- **Nitrogen limitation** is the situation where nitrogen is supplied to the culture in such a way, that the production rate of functional biomass is limited by the rate at which nitrogen can be consumed. An energy imbalance

is thus created and TAG will be accumulated while cell proliferation and division are continued. Therefore, nitrogen limitation can be applied in a continuous process, as described in Chapter 2.

Both batch and continuous cultivation conditions have their advantages and disadvantages when considering commercial TAG production (Figure 6.2), of which the most important will be discussed below.

Revenue

The TAG productivity of a nitrogen limited system is stable and continuous, while TAG production rates during nitrogen starvation typically show an increase after a few hours to days, followed by a decline towards the end of the process (Breuer et al., 2012; Siaut et al., 2011). Despite the loss of TAG productivity at the end of a batch phase, the time averaged productivities and yields that can be obtained over a longer stress period are currently considerably higher than those obtained in a typical limitation experiment. For example, to reach a maximum lipid content of over 40% w/dw, a time averaged TAG productivity of 216 mg L^{-1} d^{-1} was measured for *N. oleoabundans* under nitrogen starvation by (Breuer et al., 2012). This is almost fourfold higher than the predicted maximum TAG productivity of 55 mg L^{-1} d^{-1} using the same alga in a nitrogen limited turbidostat where 90% of the available light is absorbed (Chapter 3). Moreover, the overall TAG content of the biomass produced in the latter example (20% w/dw) is considerably lower, which is a consequence of the simultaneous production of functional biomass.

Besides the coincident production of TAG and functional biomass, another explanation for the lower productivities (and TAG yields on light) during continuous operation can be found in the energy losses through dissipation. It was demonstrated in Chapter 2 that algae are physiologically adapted to reduce their photosynthetic energy intake during continuous cultivation, and as a result the bulk of excess energy is dissipated instead of used for TAG synthesis (Chapter 3 and 5). Similarly, (Pan et al., 2011) found that the decrease in TAG productivity during a batch coincided with a steady loss of photosynthetic capacity. Due to its transient nature with initially a low energy dissipation rate that gradually increases during the starvation phase, the average dissipation rates may well be lower in a batch process than in a continuous process and as a result there is more energy available for TAG synthesis. Also the experienced energy imbalance, which is considered the main trigger for TAG formation (Li et al., 2013), will be larger in case of nitrogen starvation due to the complete stop of nitrogen assimilation. Using an algal species that is less adaptive and maintains a considerable photosynthetic rate under nitrogen short-

age, such as *Nannochloropsis sp*, (Simionato et al., 2013), would be beneficial for increasing TAG productivity and yield in both processes, but especially in nitrogen limited cultures.
Furthermore, it should be realised that a batch is a finite process that requires system preparation and the cultivation of sufficient biomass between each consecutive batch. Thus in order to translate reported average volumetric TAG production rates that only refer to the nitrogen starvation phase to large scale production, down time and the biomass production phase should be included. These factors could easily reduce the yearly volumetric TAG productivity of a batch system by one third.

Suitability for large scale operation

In general, applying nitrogen starvation is more straight forward and robust than operating a continuous system under nitrogen limited conditions, as starvation requires less monitoring and control. However, to produce microalgal TAG for the biodiesel market, production should take place outdoor and is thus subjected to varying irradiances and a day night cycle. The light availability to a microalgal culture during nitrogen starvation is of great influence on the volumetric TAG production rates (Breuer et al., 2013). Light availability under outdoor conditions is first of all dependent on the natural available irradiance, but also on culture density, reactor design and reactor orientation. In a batch process these cannot be influenced throughout the day and therefore the TAG accumulation rates during starvation cannot be controlled. In contrast, in a continuous process a variable dilution rate allows for the adaptation of nitrogen supply rate and culture density in response to the available radiation, in order to meet the optimal conditions for TAG accumulation. A flexible set point of the outgoing light intensity (Cuaresma et al., 2011) and a nitrogen supply separate from the diluting medium (Chapter 2) would allow for even more control. Moreover, the use of a feedback loop that monitors culture's photosynthetic capacity using a PAM fluorometer (Grobbelaar, 2000), and actively adjusts outgoing light settings and/or nitrogen supply rates accordingly, could be beneficial in maximising the fraction of solar energy used in TAG synthesis throughout the day.
Most studies on TAG metabolism are performed under laboratory conditions with constant light and consequently knowledge on the effect of light/dark cycles on TAG accumulation is limited. It is known that the synthesis of the various biomass components is regulated by the circadian clock, which helps to orchestrate cellular processes so that they are happening at the most suitable moment (Lacour et al., 2012a; Mittag and Kwang, 2001; de Winter et al., In press). For example storage components such as starch are respired at night in order to sustain cell division and maintenance (Cohen and Par-

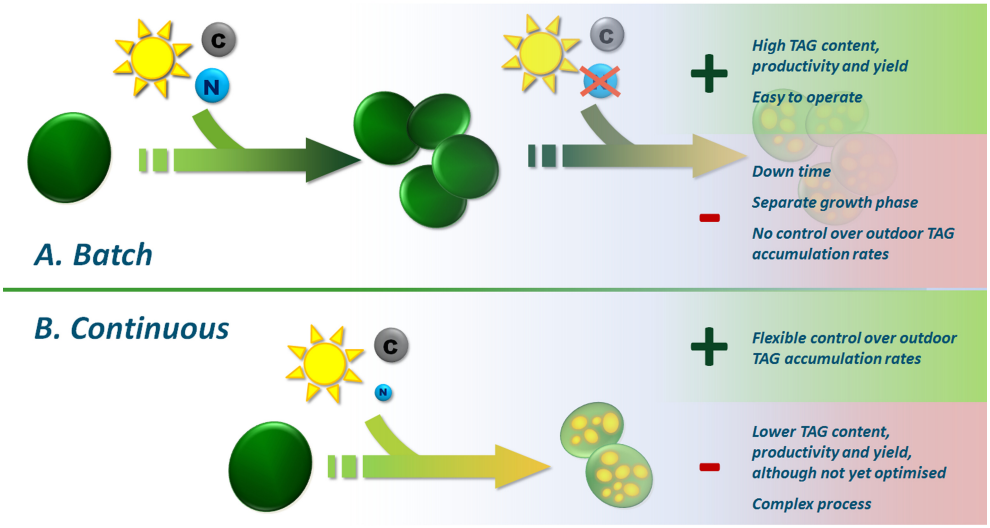

Figure 6.2 *Batch and continuous cultivation conditions have their advantages and disadvantages for commercial TAG production.*

nas, 1976; Turpin, 1991). Respirational carbon losses can be as high as 20-25% of the pervious 12h carbon uptake (Marra and Barber, 2004). Only two studies have confirmed that TAG can also be used for nocturnal respiration (Iwamoto and Suzuki, 1958; Lacour et al., 2012a), which could decrease the overall TAG productivity of an outdoor system. Especially in starch mutants, that are often mentioned for their high potential as TAG producing organisms, nocturnal respiration of TAG will be considerable, as no alternative energy source is available. Another possible cause for respirational TAG losses might arise from nocturnal nitrogen assimilation (Cuhel et al., 1984), which could become a problem when using continuous systems. As it is not known to what extent nocturnal respiration and other circadian processes influence TAG production, it is not possible to compare nitrogen starvation and limitation processes on this aspect and further research into the effect of day/night cycles on TAG accumulation is necessary.

Hybrid systems; combining the best of both worlds

The higher contents and productivities that can be obtained in systems under nitrogen starvation, are countered by a lack of control over the TAG accumulation rate and time losses in between consecutive batches. On the contrary, simultaneous growth and TAG accumulation seems to result in low production rates and yields due to cell adaptation. A way to combine the advantages of continuous production and the necessity for two separate phases to prevent adaptation would be to use a hybrid system in which two photo-

bioreactors are connected in series. The first reactor would continuously produce viable biomass at a high efficiency and is operated in such a way that the residual nitrogen concentration in the outgoing stream is zero. Subsequently, this outgoing stream is fed into the next photobioreactor, where the cells are subjected to nitrogen starvation. A hybrid system allows changes in the dilution rate to the second system, and as such, TAG content and accumulation rate can be controlled in response to the varying outdoor irradiation. Recent work of (Lucas-Salas et al., 2013) shows that a hybrid system can be operated in steady state on lab scale, although the small increases in lipid contents suggests that some further optimisation should be done.

Summarizing, nitrogen starvation in a batch cultivation process currently delivers the highest TAG content, productivity and yield. However, continuous TAG accumulation under nitrogen limited conditions is in its infancy and the added benefit of less down time and control over TAG synthesis rates under outdoor conditions, reduces the apparent advantage of batch over continuous cultivation. Further exploration of continuous cultivation for outdoor cultivation besides the classic batch approach is therefore desirable.

6.3.2 Strain improvement for optimising TAG production

Besides adapting photobioreactor designs and operation strategies to create the optimal conditions for TAG accumulation, it also is possible to modify the algae. It was already mentioned that choosing an algal species with desirable photosynthetic properties, such as a species that retains a high photosynthetic capacity under nitrogen stress, will be beneficial for TAG productivity. As most of the algae species available in nature remain unexplored today, additional screening for interesting production strains would be an interesting option.

A more targeted approach would be to enhance the currently available production species in such a way that more energy and carbon is directed towards TAG synthesis. Genetic engineering approaches have been effectively applied in several plant species, increasing seed oil contents or inducing oil synthesis in tissue that normally does not produce oil (Yu et al., 2011). Genetic engineering of microalgae is currently in its infancy as reliable nuclear transformation systems, like those used in plants, are only limitedly available. Nuclear transformation has proven successful in only a few species, including the model green alga *C. reinhardtii* (Kindle, 1990), the oleaginous diatom *Phaeodactylum tricornutum* (Apt et al., 1996), and more recently, the robust TAG producer *Nannochloropsis sp*. (Kilian et al., 2011). The molecular toolboxes necessary for transformation of

each of these species are very distinct and therefore it is expected that despite the fact that the number of successful transformation techniques is growing (Radakovits et al., 2010), it will take considerable additional research to develop the proper techniques for transforming other interesting candidates.

Increasing the flux trough lipid biosynthesis pathways

As the techniques for altering metabolic pathways in microalgae are limited, only one example of a targeted overexpression of an enzyme involved in lipid biosynthesis is currently known, being the overexpression of native cytosolic ACCase in *Cyclotella cryptica*. However, a 2 to 3 fold increase in ACCase activity did not affect TAG levels (Sheehan et al., 1998), which might be explained by the fact that ACCase is a heavily regulated enzyme. Feedback inhibition throughout the lipid biosynthetic pathway might compensate an increased activity of this enzyme.

In plants, increasing the oil content and/or accumulation rate of lipids by targeting the enzymes responsible for lipid formation have shown mixed results, as extensively reviewed by (Radakovits et al., 2010) and (Yu et al., 2011). In general, overexpression of more upstream enzymes, such as ACCase and those associated with the FAS complex, resulted in a marginal 5-10% increases of seed oil content (Dehesh et al., 2001; Roesler et al., 1997), while targeting of some of the enzymes of the Kennedy pathway led to a more substantial 10-20% increase in seed oil in *A. thaliana* and rape seed (*Brassica napus)* (Jain et al., 2000; Jako et al., 2001; Weselake et al., 2007; Zou et al., 1997). The most dramatic increase was obtained in rape seed by overexpression of a yeast glycerol-3-phosphate-dehydrogenase (Vigeolas et al., 2007), which catalyses the conversion of dihydroxyacetone phosphate into glycerol-3-phosphate. An increase of 40% in seed oil content indicated that in this species TAG formation during seed development is highly limited by provision of the glycerol backbone for TAG.

Algal and plant lipid biosynthesis pathways exhibit some significant differences, and moreover, the regulation of TAG synthesis in committed oil accumulating organs may be profoundly different from that in single cell microalgae. Therefore, it is to be expected that the results obtained in plants cannot be directly translated to microalgae. More insight into how algae regulate fluxes throughout the lipid biosynthetic pathway can be provided by detailed pathway analysis using metabolic flux models such as presented in Chapters 4 and 5, preferably combined with gene expression analysis and proteomics techniques. The thus obtained insight in genetic and posttranslational regulation will play an important role when developing the future engineering targets for increasing TAG production rates in microalgae.

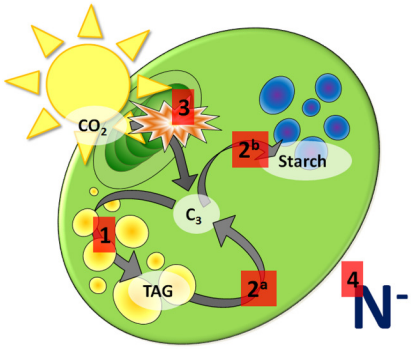

Figure 6.3 *Targets for strain improvement for increased oil production.*

1. *Increase the flux through lipid biosynthetic pathways*
2. *Disable TAG catabolism (a) and competing pathways (b).*
3. *Increase photosynthetic efficiency under nitrogen deprivation*
4. *Decouple TAG accumulation and nitrogen deprivation*

Disabling of competing pathways

A very successful approach in directing more carbon towards TAG biosynthesis, proved to be the knocking down of competing pathways. The most well-known example are the starch mutants that have been developed for *C. reinhardtii* (Li et al., 2010a), for which under nitrogen limitation the TAG levels reached were 10 fold higher than in the wild type. Although this approach seems very effective in increasing lipid output under controlled indoor conditions with continuous light supply, it still remains a question how these mutants will perform under the outdoor light dark cycles of industrial production. As starch is a very important energy source for nocturnal respiration, replete growth of these mutants under day/night cycles may be severely reduced. Also, nocturnal TAG losses are expected to be higher, which again highlights the importance of further research into the effect of day/night cycles on stress metabolism.

Another competing pathway that is possibly worthwhile to knock down is lipid catabolism. This approach proved successful in *A. thaliana*, where inhibition of fatty acid catabolism resulted in the increase of TAG levels in leaf tissue (Slocombe et al., 2009). Besides possibly boosting TAG levels in microalgae, such a knock down could also decrease nocturnal TAG losses due to respiration.

Increasing photosynthetic efficiency under nitrogen stress

The loss in photosynthetic capacity under nitrogen limitation generally goes hand in hand with a loss in TAG productivity. As the reducing equivalent imbalance is alleviated by a decrease in linear electron transport (LET, chapter 5), the need for TAG accumulation slowly subsides. Preventing this reduction in LET, might prove an efficient strategy in increasing TAG levels, assuming that TAG will function as an alternative electron sink.

For example, *C. reinhardtii* mutants unable to form violaxanthin from zeaxanthin, which normally plays an important role in thermal dissipation of excess energy in the wild type, showed less PSII inactivation and therefore higher LET rates, under high light conditions (Jahns et al., 2000). Such a mutation may also provide increased LET rates under nitrogen starvation and possibly, higher TAG accumulation rates.
On the other hand, as TAG synthesis may also function as a shuttle for redundant plastid membrane storage under adverse growth conditions, creating an alga that simply contains more plastid membranes might also prove beneficial for TAG accumulation under adverse growth conditions. Photosystem mutants have shown various deformations of plastid ultrastructure, amongst which hyper-stacking of thylakoid membranes (Goodenough and Levine, 1969). A mutant with more plastid membrane should get rid of more membrane lipids in order to reduce its absorptive cross section under nitrogen starvation, and potentially exhibit increased TAG accumulation rates.

Triggering TAG accumulation without applying an energy imbalance
As described TAG accumulation is induced by nitrogen starvation and is accompanied by a decrease in the photosynthetic rate. Although it seems likely that the redox/energy imbalance is important for triggering these processes, the exact mechanisms and signalling pathways involved remain unknown. Insight in these signalling routes may make it possible to uncouple TAG synthesis from adverse growth conditions and the accompanying decrease in photosynthetic rate. This will allow for TAG formation under nitrogen replete conditions at high photosynthetic efficiencies, where more energy can be channelled towards the product of interest.

6.4 Conclusion

Increasing TAG accumulation rates in microalgae is an important target for cost reduction of microalgal lipid production. Under optimised laboratory conditions the highest obtained TAG yields are only one third of what is possible in theory. Further optimisation requires proper understanding of the physiology and regulation of lipid metabolism in oleaginous microalgae. Important knowledge gaps are the compartmentalisation of TAG synthesis, variations in TAG production rates throughout the day/night cycle, TAG accumulation regulation and its relation to photosynthesis. Filling these knowledge gaps is necessary to indicate potential bottlenecks in TAG production and targets for metabolic engineering.
Besides the accepted functions of TAG synthesis as energy storage and redox scavenging another function may be the temporary storage of plastid components. The domi-

nant function of TAG synthesis appears to be species specific and therefore the optimal metabolic engineering approach as well as the optimal cultivation strategy for maximized TAG production will be different for each species. Currently, the classic nitrogen starvation approach shows TAG production rates up to a factor 4 higher than continuous TAG accumulation under nitrogen limited conditions. However, the continuous operation strategy is in its infancy and higher rates are likely after further optimisation. Moreover, the added benefit of less down time and control over TAG synthesis rates under outdoor conditions, reduces the apparent advantage of batch over continuous cultivation.

TAG accumulation is a multifaceted process that shows different characteristics in each algal species and each type of culture system. Therefore, process and strain optimisation should not be seen as alternative but rather as complementary strategies. Hence, multidisciplinary research in which intelligent growth strategies are combined with the latest of molecular tools and discoveries is indispensable when aiming at commercial microalgal lipid production at fossil fuel prices.

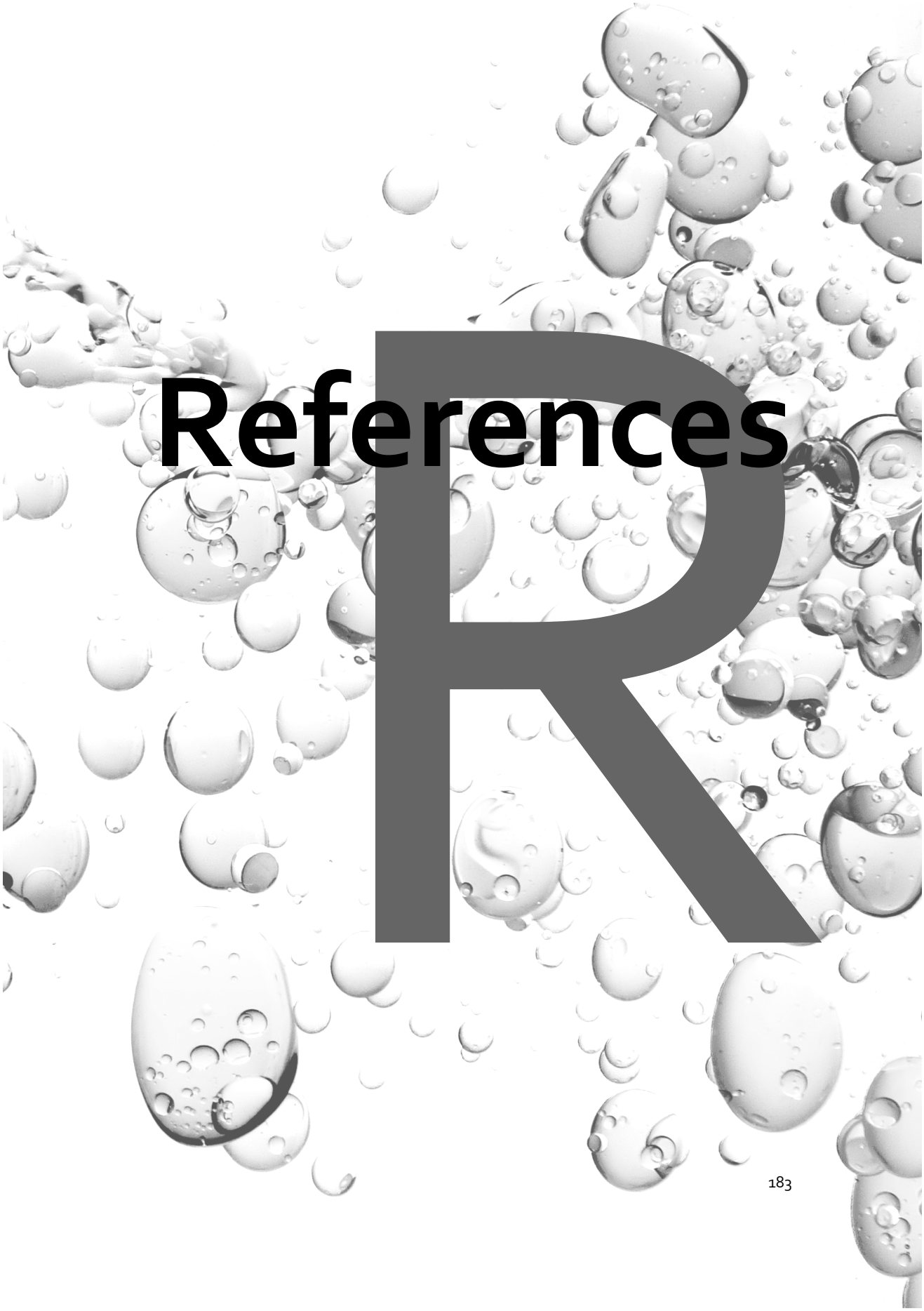

References

A

Allen, J.F. 2003. Cyclic, pseudocyclic and noncyclic photophosphorylation: new links in the chain. Trends in Plant Science. 8, 15-19.

Altschul, S.F., Gish, W., Miller, W., Myers, E.W., Lipman, D.J. 1990. Basic local alignment search tool. Journal of Molecular Biology. 215, 403-410.

Apt, K.E., Grossman, A.R., Kroth-Pancic, P.G. 1996. Stable nuclear transformation of the diatom *Phaeodactylum tricornutum*. 252, 572-579.

B

Baart, G.J.E., Willemsen, M., Khatami, E., Haan, A., Zomer, B., Beuvery, E.C., Tramper, J., Martens, D.E. 2008. Modeling *Neisseria meningitidis* B metabolism at different specific growth rates. Biotechnology and Bioengineering. 101, 1022-1035.

Baker, N.R., Harbinson, J., Kramer, D.M. 2007. Determining the limitations and regulation of photosynthetic energy transduction in leaves. Plant, Cell & Environment. 30, 1107-1125.

Ball, S.G., Dirick, L., Decq, A., Martiat, J.-C., Matagne, R. 1990. Physiology of starch storage in the monocellular alga *Chlamydomonas reinhardtii*. Plant Science. 66, 1-9.

Bar, E., Rise, M., Vishkautsan, M., Arad, S. 1995. Pigment and structural changes in *Chlorella zofingiensis* upon light and nitrogen stress. Journal of Plant Physiology. 146, 527-534.

Becker, E.W. 2007. Micro-algae as a source of protein. Biotechnology Advances. 25, 207-210.

Ben-Amotz, A., Katz, A., Avron, M. 1982. Accumulation of β-carotene in halotolerant algae: purification and characterization of β-carotene-rich globules from *Dunaliella bardawil* (*Chlorophyceae*). Journal of Phycology. 18, 529-537.

Bennoun, P. 2004. Chlororespiration, sixteen years later. in: *The Molecular Biology of Chloroplasts and Mitochondria in Chlamydomonas*, (Eds.) J.D. Rochaix, M. Goldschmidt-Clermont, S. Merchant, Vol. 7, Springer Netherlands. Dordrecht, pp. 675-683.

Berg, J.M., Tymoczko, J.L., Stryer, L. 2003. *Biochemistry*. *5th edition ed*. Freeman, New York.

Bjorkman, O., Demmig, B. 1987. Photon yield of O_2 evolution and chlorophyll fluorescence characteristics at 77 K among vascular plants of diverse origins. Planta. 170, 489-504.

Bligh, E.G., Dyer, W.J. 1959. A rapid method of total lipid extraction and purification. Canadian Journal of Biochemistry and Physiology. 37, 911-917.

Borodina, I., Krabben, P., Nielsen, J. 2005. Genome-scale analysis of *Streptomyces coelicolor* A3(2) metabolism. Genome Research. 15, 820-829.

Bosma, R., Miazek, K., Willemsen, S.M., Vermuë, M.H., Wijffels, R.H. 2008. Growth inhibition of *Monodus subterraneus* by free fatty acids. Biotechnology and Bioengineering. 101, 1108 - 1114.

Boyd, C. 1968. Fresh-water plants: a potential source of protein. Economic Botany. 22, 359-368.

Boyle, N.R., Morgan, J.A. 2009. Flux balance analysis of primary metabolism in *Chlamydomonas reinhardtii*. BMC Systems Biology. 3.

Bräutigam, A., Weber, A.P.M. 2011. Do metabolite transport processes limit photosynthesis? Plant Physiology. 155, 43-48.

Breuer, G., Lamers, P.P., Martens, D.E., Draaisma, R.B., Wijffels, R.H. 2013. Effect of light intensity, pH, and temperature on nitrogen starvation induced triacylglycerol (TAG) accumulation in *Scenedesmus obliquus*. Bioresource Technology. 143, 1-9.

Breuer, G., Lamers, P.P., Martens, D.E., Draaisma, R.B., Wijffels, R.H. 2012. The impact of nitrogen starvation on the dynamics of triacylglycerol accumulation in nine microalgae strains. Bioresource Technology. 124, 217-226.

Britton, G. 1995. UV/visible spectroscopy. in: *Carotenoids*, (Eds.) G. Britton, S. Liaaen-Jensen, H. Pfander, Vol. 1B, Birkhäuser. Basel, pp. 13-62.

Burgard, A.P., Vaidyaraman, S., Maranas, C.D. 2001. Minimal reaction sets for *Escherichia coli metabolism* under different growth requirements and uptake environments. Biotechnology Progress. 17, 791-797.

Carlson, R., Srienc, F. 2004. Fundamental *Escherichia coli* biochemical pathways for biomass and energy production: Creation of overall flux states. Biotechnology and Bioengineering. 86, 149-162.

Chang, R.L., Ghamsari, L., Manichaikul, A., Hom, E.F.Y., Balaji, S., Fu, W., Shen, Y., Hao, T., Palsson, B.O., Salehi-Ashtiani, K., Papin, J.A. 2011. Metabolic network reconstruction of Chlamydomonas offers insight into light-driven algal metabolism. Molecular Systems Biology. 7, 1-13.

Chantanachat, S., Bold, H.C. 1962. Phycological studies. II. Some algae from arid soils. University of Texas Publications. 6218, 1-74.

Childers, D.L., Gosselink, J.G. 1990. Assessment of cumulative impacts to water quality in a forested wetland landscape. J. Environ. Qual. 19, 455-464.

Chisti, Y. 2007. Biodiesel from microalgae. Biotechnology Advances. 25, 294-306.

Cogne, G., Gros, J.B., Dussap, C.G. 2003. Identification of a metabolic network structure representative of *Arthrospira* (Spirulina) *platensis* metabolism. Biotechnology and Bioengineering. 84 667 - 676

Cohen, D., Parnas, H. 1976. An optimal policy for the metabolism of storage materials in unicellular algae. Journal of Theoretical Biology. 56, 1-18.

Cooper, M.S., Hardin, W.R., Petersen, T.W., Cattolico, R.A. 2010. Visualizing "green oil" in live algal cells. Journal of Bioscience and Bioengineering. 109, 198-201.

Cuaresma, M., Janssen, M., van den End, E.J., Vílchez, C., Wijffels, R.H. 2011. Luminostat operation: A tool to maximize microalgae photosynthetic efficiency in photobioreactors during the daily light cycle? Bioresource Technology. 102, 7871-7878.

Cuaresma, M., Janssen, M., Vílchez, C., Wijffels, R.H. 2009. Productivity of *Chlorella sorokiniana* in a short light-path (SLP) panel photobioreactor under high irradiance. Biotechnology and Bioengineering. 104, 352-359.

Cuhel, R.L., Ortner, P.B., Lean, D.R. 1984. Night synthesis of protein by algae. American Society of Limnology and Oceanography. 29, 731-744.

D

Davis, R.W., Volponi, J.V., Jones, H.D.T., Carvalho, B.J., Wu, H., Singh, S. 2012. Multiplex fluorometric assessment of nutrient limitation as a strategy for enhanced lipid enrichment and harvesting of *Neochloris oleoabundans*. Biotechnology and Bioengineering. 109, 2503-2512.

de Gucht, L.P.E., van der Plas, L.H.W. 1995. Growth kinetics of glucose-limited *Petunia hybrida* cells in chemostat cultures: Determination of experimental values for growth and maintenance parameters. Biotechnology and Bioengineering. 47, 42-52.

de Winter, L., Klok, A.J., Cuaresma, M., Barbosa, M.J., Wijffels, R.H. In press. The synchronized cell cycle of *Neochloris oleoabundans* and its influence on biomass composition under constant light conditions. Algal Research.

Dehesh, K., Tai, H., Edwards, P., Byrne, J., Jaworski, J.G. 2001. Overexpression of 3-ketoacyl-acyl-carrier protein synthase IIIs in plants reduces the rate of lipid synthesis. Plant Physiology. 125, 1103-1114.

Delrue, B., Fontaine, T., Routier, F., Decq, A., Wieruszeski, J.M., Van Den Koornhuyse, N., Maddelein, M.L., Fournet, B., Ball, S. 1992. Waxy *Chlamydomonas reinhardtii*: monocellular algal mutants defective in amylose biosynthesis and granule-bound starch synthase activity accumulate a structurally modified amylopectin. Journal of Bacteriology. 174, 3612-3620.

Dortch, Q., Roberts, T.L., Clayton Jr., J.R., Ahmed, S.I. 1983. RNA/DNA ratios and DNA concentrations as indicators of growth rate and biomass in planktonic marine organisms. Marine Ecology Progress Series. 13, 61-71.

Draaisma, R.B., Wijffels, R.H., Slegers, P.M., Brentner, L.B., Roy, A., Barbosa, M.J. 2013. Food commodities from microalgae. Current Opinion in Biotechnology. 24, 169-177.

Dubinsky, Z., Falkowski, P.G., Wyman, K. 1986. Light harvesting and utilization by phytoplankton. Plant and Cell Physiology. 27, 1335-1349.

Dubinsky, Z., Stambler, N. 2009. Photoacclimation processes in phytoplankton: mechanisms, consequences, and applications. Aquatic Microbial Ecology. 56, 163-176.

Dubois, M., Gilles, K.A., Hamilton, J.K., Rebers, P.A., Smith, F. 1956. Colorimetric method for determination of sugars and related substances. Analytical Chemistry. 28, 350 - 356.

Durrett, T.P., Benning, C., Ohlrogge, J. 2008. Plant triacylglycerols as feedstocks for the production of biofuels. The Plant Journal. 54, 593-607.

E

Emerson, R., Lewis, C.M. 1943. The dependence of the quantum yield of *Chlorella* on wavelength of light. American Journal of Botany. 30, 165-178.

Endo, T., Asada, K. 2006. Photosystem I and photoprotection: cyclic electron flow and water-water cycle. in: *Photoprotection, Photoinhibition, Gene Regulation, and Environment*, (Eds.) B. Demmig-Adams, W.W. Adams, A.K. Mattoo, Vol. 21, Springer Netherlands. Dordrecht, pp. 205-221.

Escoubas, J.M., Lomas, M., LaRoche, J., Falkowski, P.G. 1995. Light intensity regulation of cab gene transcription is signaled by the redox state of the plastoquinone pool. Proceedings of the National Academy of Sciences. 92, 10237-10241.

Evans, J.R. 1987. The dependence of quantum yield on wavelength and growth irradiance. Australian Journal of Plant Physiology. 14, 69-79.

F

Falkowski, P.G., LaRoche, J. 1991. Acclimation to spectral irradiance in algae. Journal of Phycology. 27, 8-14.

Falkowski, P.G., Sukenik, A., Herzig, R. 1989. Nitrogen limitation in *Isochrysis Galbana* (Haptophyceae). II. relative abundance of chloroplast proteins. Journal of Phycology. 25, 471-478.

Fan, J., Andre, C., Xu, C. 2011. A chloroplast pathway for the de novo biosynthesis of triacylglycerol in *Chlamydomonas reinhardtii*. FEBS Letters. 585, 1985-1991.

Farese Jr, R.V., Walther, T.C. 2009. Lipid Droplets Finally Get a Little R-E-S-P-E-C-T.

Cell. 139, 855-860.

Forster, J., Famili, I., Fu, P., Palsson, B.O., Nielsen, J. 2003. Genome-scale reconstruction of the *Saccharomyces cerevisiae* metabolic network. Genome Research. 13, 244-253.

Foyer, C., Furbank, R., Harbinson, J., Horton, P. 1990. The mechanisms contributing to photosynthetic control of electron transport by carbon assimilation in leaves. 25, 83-100.

Frada, M.J., Burrows, E.H., Wyman, K.D., Falkowski, P.G. 2013. Quantum requirements for growth and fatty acid biosynthesis in the marine diatom *Phaeodactylum tricornutum* (*Bacillariophyceae*) in nitrogen replete and limited conditions. Journal of Phycology. 49, 381-388.

Geider, R.J., Macintyre, H.L., Kana, T.M. 1997. Dynamic model of phytoplankton growth and acclimation: responses of the balanced growth rate and the chlorophyll a: carbon ratio to light, nutrient-limitation and temperature. Marine Ecology Progress Series. 148, 187-200.

Gfeller, R.P., Gibbs, M. 1984. Fermentative metabolism of *Chlamydomonas reinhardtii:* I. Analysis of fermentative products from starch in dark and light. Plant physiology / American Society of Plant Physiologists. 75, 212-218.

Ghirardi, M.L., Zhang, L., Lee, J.W., Flynn, T., Seibert, M., Greenbaum, E., Melis, A. 2000. Microalgae: a green source of renewable H_2. Trends in Biotechnology. 18, 506-511.

Giroud, C., Gerber, A., Eichenberger, W. 1988. Lipids of Chlamydomonas reinhardtii. Analysis of Molecular Species and Intracellular Site(s) of Biosynthesis. Plant and Cell Physiology. 29, 587-595.

Goldman, J.C. 1979. Outdoor algal mass cultures - II. Photosynthetic yield limitations. Water Research. 13, 119-136.

Goodenough, U.W., Levine, R.P. 1969. Chloroplast ultrastructure in mutant strains of *Chlamydomonas reinhardi* lacking components of the photosynthetic apparatus. Plant Physiology. 44, 990-1000.

Goodson, C., Roth, R., Wang, Z.T., Goodenough, U. 2011. Structural correlates of cytoplasmic and chloroplast lipid body synthesis in *Chlamydomonas reinhardtii* and stimulation of lipid body production with acetate boost. Eukaryotic Cell. 10, 1592-1606.

Gouveia, L., Marques, A.E., da Silva, T.L., Reis, A. 2009. *Neochloris oleabundans* UTEX #1185: a suitable renewable lipid source for biofuel production. Journal of Indus-

trial Microbiology and Biotechnology1-6.

Grabherr, M.G., Haas, B.J., Yassour, M., Levin, J.Z., Thompson, D.A., Amit, I., Adiconis, X., Fan, L., Raychowdhury, R., Zeng, Q., Chen, Z., Mauceli, E., Hacohen, N., Gnirke, A., Rhind, N., di Palma, F., Birren, B.W., Nusbaum, C., Lindblad-Toh, K., Friedman, N., Regev, A. 2011. Full-length transcriptome assembly from RNA-Seq data without a reference genome. Nature Biotechnology. 29, 644-652.

Griffiths, M.J., Harrison, S.T.L. 2009. Lipid productivity as a key characteristic for choosing algal species for biodiesel production. Journal of Applied Phycology. 21, 493-507.

Griffiths, M.J., van Hille, R.P., Harrison, S.T.L. 2011. Lipid productivity, settling potential and fatty acid profile of 11 microalgal species grown under nitrogen replete and limited conditions. Journal of Applied Phycology1-13.

Grobbelaar, J. 2000. Physiological and technological considerations for optimising mass algal cultures. 12, 201-206.

Guschina, I.A., Harwood, J.L. 2009. Algal lipids and effect of the environment on their biochemistry. in: *Lipids in Aquatic Ecosystems*, (Eds.) M. Kainz, M.T. Brett, M.T. Arts, Springer. New York, pp. 1-24.

Haik, Y., Selim, M.Y.E., Abdulrehman, T. 2011. Combustion of algae oil methyl ester in an indirect injection diesel engine. Energy. 36, 1827-1835.

Hanelt, D., Melchersmann, B., Wiencke, C., Nultsch, W. 1997. Effects of high light stress on photosynthesis of polar macroalgae in relation to depth distribution. Marine Ecology Progress Series. 149, 255-266.

Harris, E.H. 2009. *The Chlamydomonas sourcebook: a comprehensive guide to biology and laboratory use*. *Second edition ed*. Academic Press, San Diego.

Harrison, P.J., Thompson, P.A., Calderwood, G.S. 1990. Effects of nutrient and light limitation on the biochemical composition of phytoplankton. Journal of Applied Phycology. 2, 45-56.

Harrison, S.T.L., Richardson, C., Griffiths, M.J. 2013. Analysis of microalgal biorefineries for bioenergy from an environmental and economic perspective focus on algal biodiesel. in: *Biotechnological Applications of Microalgae: Biodiesel and Value Added Products*, (Ed.) F. Bux, CRC Press. Boca Raton, pp. 113-136.

Harwood, J.L. 2004. Membrane Lipids in Algae. in: *Lipids in Photosynthesis: Structure, Function and Genetics*, (Eds.) S. Paul-André, M. Norio, Vol. 6, Springer Netherlands, pp. 53-64.

Hatti-Kaul, R., Törnvall, U., Gustafsson, L., Börjesson, P. 2007. Industrial biotechnology

for the production of bio-based chemicals – a cradle-to-grave perspective. Trends in Biotechnology. 25, 119-124.

Heber, U. 1974. Metabolite exchange between chloroplasts and cytoplasm. Annual Review of Plant Physiology. 25, 393-421.

Heifetz, P.B., F"rster, B., Osmond, C.B., Giles, L.J., Boynton, E. 2000. Effects of acetate on facultative autotrophy in *Chlamydomonas reinhardtii* assessed by photosynthetic measurements and stable isotope analyses. Plant.Physiol. 122, 1439.

Heijnen, J.J., Kleerebezem, R., Flickinger, M.C. 2009. Bioenergetics of Microbial Growth. in: *Encyclopedia of Industrial Biotechnology*, John Wiley & Sons, Inc.

Heldt, H.W. 1969. Adenine nucleotide translocation in spinach chloroplasts. FEBS Letters. 5, 11-14.

Herbert, D., Phipps, P.J., Strange, R.E., Norris, J.R., Ribbons, D.W. 1971. Chemical analysis of microbial cells. in: *Methods in Microbiology.*, Academic Press. London and New York, pp. 209-344.

Herrig, R., Falkowski, P.G. 1989. Nitrogen limitation in *Isochrysis galbana* (haptophyceae): I. Photosynthetic enegry conversion and growth efficiencies. Journal of Phycology. 25, 462-471.

Hibberd, D.J. 1981. Notes on the taxonomy and nomenclature of the algal classes Eustigmatophyceae and Tribophyceae (synonym Xanthophyceae). Botanical Journal of the Linnean Society. 82, 93-119.

Hodges, B.D.M., Wu, C.C. 2010. Proteomic insights into an expanded cellular role for cytoplasmic lipid droplets. Journal of Lipid Research. 51, 262-273.

Hoefnagel, M.H.N., Atkin, O.K., Wiskich, J.T. 1998. Interdependence between chloroplasts and mitochondria in the light and the dark. Biochimica et Biophysica Acta. 1366, 235-255.

Hoffmann, M., Marxen, K., Schulz, R., Vanselow, K.H. 2010. TFA and EPA productivities of *Nannochloropsis salina* influenced by temperature and nitrate stimuli in turbidostatic controlled experiments. Marine Drugs. 8, 2526-2545.

Hu, Q., Sommerfeld, M., Jarvis, E., Ghirardi, M., Posewitz, M., Seibert, M., Darzins, A. 2008. Microalgal triacylglycerols as feedstocks for biofuel production: perspectives and advances. Plant Journal. 54, 621-639.

Huppe, H.C., Turpin, D.H. 1994. Integration of carbon and nitrogen metabolism in plant and algal cells. Annual Review of Plant Physiology and Plant Molecular Biology. 45, 577-607.

Hutner, S.H., Provasoli, L., Schatz, A., Haskins, C.P. 1950. Some approaches to the study of the role of metals in the metabolism of microorganisms. Proceedings of

the American Philosophical Society. 94, 152-170.

I

Iwamoto, H., Suzuki, A. 1958. Fat synthesis in unicellular algae. Part IV. Nocturnal affect on fat accumulation in Chlorella. Bulletin of the Agricultural Chemical Society of Japan. 22, 420-425.

J

Jahns, P., Depka, B., Trebst, A. 2000. Xanthophyll cycle mutants from *Chlamydomonas reinhardtii* indicate a role for zeaxanthin in the D1 protein turnover. Plant Physiology and Biochemistry. 38, 371-376.

Jain, R.K., Coffey, M., Lai, K., Kumar, A., MacKenzie, S.L. 2000. Enhancement of seed oil content by expression of glycerol-3-phosphate acyltransferase genes. Biochemical Society Transactions. 28, 959-960.

Jako, C., Kumar, A., Wei, Y., Zou, J., Barton, D.L., Giblin, E.M., Covello, P.S., Taylor, D.C. 2001. Seed-specific over-expression of an *Arabidopsis* cDNA encoding a diacylglycerol acyltransferase enhances seed oil content and seed weight. Plant Physiology. 126, 861-874.

Jakob, T., Wagner, H., Stehfest, K., Wilhelm, C. 2007. A complete energy balance from photons to new biomass reveals a light- and nutrient-dependent variability in the metabolic costs of carbon assimilation. Journal of Experimental Botany. 58, 2101-2112.

James, G.O., Hocart, C.H., Hillier, W., Chen, H., Kordbacheh, F., Price, G.D., Djordjevic, M.A. 2011. Fatty acid profiling of *Chlamydomonas reinhardtii* under nitrogen deprivation. Bioresource Technology. 102.

Janssen, M., de Winter, M., Tramper, J., Mur, L.R., Snel, J.F.H., Wijffels, R.H. 2000. Efficiency of light utilization of *Chlamydomonas reinhardtii* under medium-duration light/dark cycles. Journal of Biotechnology. 78, 123-137.

Johnson, X., Alric, J. 2013. Central carbon metabolism and electron transport in *Chlamydomonas reinhardtii*: metabolic constraints for carbon partitioning between oil and starch. Eukaryotic Cell. 12, 776-793.

K

Kanehisa, M., Goto, S. 2000. KEGG: Kyoto Encyclopedia of Genes and Genomes. Nucl. Acids Res. 28, 27-30.

Kayser, A., Weber, J., Hecht, V., Rinas, U. 2005. Metabolic flux analysis of *Escherichia coli* in glucose-limited continuous culture: I. Growth-rate dependent metabolic efficiency at steady state. Microbiology-Sgm. 151, 693-706.

Khozin-Goldberg, I., Shrestha, P., Cohen, Z. 2005. Mobilization of arachidonyl moieties

from triacylglycerols into chloroplastic lipids following recovery from nitrogen starvation of the microalga Parietochloris incisa. Biochimica et Biophysica Acta (BBA) - Molecular and Cell Biology of Lipids. 1738, 63-71.

Khozin-Goldberg, I., Yu, H., Adlerstein, D., Didi-Cohen, S., Heimer, Y., Cohen, Z. 2000. Triacylglycerols of the red microalga *Porphyridium cruentum* can contribute to the biosynthesis of eukaryotic galactolipids. 35, 881-889.

Kieldsen, K.R., Nielsen, J. 2009. In silico genome-scale reconstruction and validation of the *Corynebacterium glutamicum* metabolic network. Biotechnology and Bioengineering. 102, 583-597.

Kilian, O., Benemann, C.S.E., Niyogi, K.K., Vick, B. 2011. High-efficiency homologous recombination in the oil-producing alga Nannochloropsis sp. Proceedings of the National Academy of Sciences. 108, 21265-21269.

Kindle, K.L. 1990. High-frequency nuclear transformation of Chlamydomonas reinhardtii. Proceedings of the National Academy of Sciences. 87, 1228-1232.

Kleinegris, D., Janssen, M., Brandenburg, W.A., Wijffels, R.H. 2010. The Selectivity of Milking of *Dunaliella salina*. Marine Biotechnology. 12, 14-23.

Kliphuis, A.J., Janssen, M., End, E., Martens, D., Wijffels, R. 2011. Light respiration in *Chlorella sorokiniana*. Journal of Applied Phycology. 23, 935-947.

Kliphuis, A.M.J., de Winter, L., Vejrazka, C., Martens, D.E., Janssen, M., Wijffels, R.H. 2010. Photosynthetic efficiency of *Chlorella sorokiniana* in a turbulently mixed short light-path photobioreactor. Biotechnology Progress. 26, 687-696.

Kliphuis, A.M.J., Klok, A.J., Martens, D.E., Lamers, P.P., Janssen, M., Wijffels, R.H. 2012. Metabolic modeling of *Chlamydomonas reinhardtii*: energy requirements for photoautotrophic growth and maintenance. Journal of Applied Phycology. 24, 253-266.

Klöck, G., Kreuzberg, K. 1989. Kinetic properties of asn-glycerol-3-phosphate dehydrogenase purified from the unicellular alga Chlamydomonas reinhardtii. Biochimica et Biophysica Acta (BBA) - General Subjects. 991, 347-352.

Klok, A.J., Martens, D.E., Wijffels, R.H., Lamers, P.P. 2013a. Simultaneous growth and neutral lipid accumulation in microalgae. Bioresource Technology. 134, 233-243.

Klok, A.J., Verbaanderd, J.A., Lamers, P.P., Martens, D.E., Rinzema, A., Wijffels, R.H. 2013b. A model for customising biomass composition in continuous microalgae production. Bioresource Technology. 146, 89-100.

Knothe, G. 2005. Dependence of biodiesel fuel properties on the structure of fatty acid alkyl esters. Fuel Processing Technology. 86, 1059-1070.

Kok, B. 1955. On the inhibition of photosynthesis by intense light. Biochimica et Bio-

physica Acta. 21, 234-244.

Kolber, Z., Zehr, J., Falkowski, P. 1988. Effects of Growth Irradiance and Nitrogen Limitation on Photosynthetic Energy Conversion in Photosystem II. Plant Physiology. 88, 923-929.

Kozaki, A., Mayumi, K., Sasaki, Y. 2001. Thiol-disulfide exchange between nuclear-encoded and chloroplast-encoded subunits of Pea acetyl-CoA carboxylase. Journal of Biological Chemistry. 276, 39919-39925.

Krause, G.H., Weis, E. 1991. Chlorophyll fluorescence and photosynthesis: The Basics. Annu.Rev.Plant Physiol.Plant Mol.Biol. 42, 313-349.

Lacour, T., Sciandra, A., Talec, A., Mayzaud, P., Bernard, O. 2012a. Diel variations of carbohydrates and neutral lipids in nitrogen-sufficient and nitrogen-starved cyclostat cultures of *Isochrysos sp. 1*. Journal of Phycology. 48, 966-975.

Lacour, T., Sciandra, A., Talec, A., Mayzaud, P., Bernard, O. 2012b. Neutral lipid and carbohydrate productivities as a response to nitorgen status in *Isochrysis sp* (T-iso; haptophyceae): starvation versus limitation. Journal of Phycology. 48, 647-656.

Lamers, P.P., Janssen, M., De Vos, R.C.H., Bino, R.J., Wijffels, R.H. 2012. Carotenoid and fatty acid metabolism in nitrogen-starved *Dunaliella salina*, a unicellular green microalga. Journal of Biotechnology. 162, 21-27.

Lamers, P.P., Janssen, M., De Vos, R.C.H., Bino, R.J., Wijffels, R.H. 2008. Exploring and exploiting carotenoid accumulation in *Dunaliella salina* for cell-factory applications. Trends in Biotechnology. 26, 631-638.

Lamers, P.P., van de Laak, C.C.W., Kaasenbrood, P.S., Lorier, J., Janssen, M., de Vos, R.C.H., Bino, R.J., Wijffels, R.H. 2010. Carotenoid and fatty acid metabolism in light-stressed *Dunaliella salina*. Biotechnology and Bioengineering. 106, 638-648.

Ledford, H.K., Niyogi, K.K. 2005. Singlet oxygen and photo-oxidative stress management in plants and algae. Plant, Cell & Environment. 28, 1037-1045.

Ley, A.C., Mauzerall, D. 1982. Absolute absorption cross-sections for photosystem II and the minimum quantum requirement for photosynthesis in *Chlorella vulgaris*. Biochimica et Biophysica Acta. 680, 95-106.

Li, X., Moellering, E.R., Liu, B., Johnny, C., Fedewa, M., Sears, B.B., Kuo, M.-H., Benning, C. 2012. A galactoglycerolipid lipase is required for triacylglycerol accumulation and survival following nitrogen deprivation in *Chlamydomonas reinhardtii*. The Plant Cell Online. 24, 4670-4686.

Li, Y., Han, D., Hu, G., Dauvillee, D., Sommerfeld, M., Ball, S., Hu, Q. 2010a. *Chlamydo-*

monas starchless mutant defective in ADP-glucose pyrophosphorylase hyper-accumulates triacylglycerol. Metabolic Engineering.

Li, Y., Han, D., Hu, G., Sommerfeld, M., Hu, Q. 2010b. Inhibition of starch synthesis results in overproduction of lipids in *Chlamydomonas reinhardtii*. Biotechnology and Bioengineering. 107, 258-268.

Li, Y., Han, D., Sommerfeld, M., Hu, Q. 2011. Photosynthetic carbon partitioning and lipid production in the oleaginous microalga *Pseudochlorococcum sp.* (*Chlorophyceae*) under nitrogen-limited conditions. Bioresource Technology. 102, 123-129.

Li, Y., Han, D., Yoon, K., Zhu, S., Sommerfeld, M., Hu, Q. 2013. Molecular and cellular mechanisms for lipid synthesis and accumulation in microalgae: biotechnological implications. 2 ed. in: *Handbook of microalgal culture: biotechnology and applied phycology*, (Eds.) A. Richmond, Q. Hu, Wiley-Blackwell. Chichester.

Linka, M., Weber, A.P.M. 2005. Shuffling ammonia between mitochondria and plastids during photorespiration. Trends in Plant Science. 10, 461-465.

Liu, B., Benning, C. 2013. Lipid metabolism in microalgae distinguishes itself. Current Opinion in Biotechnology. 24, 300-309.

Lourenço, S.O., Barbarino, E., Marquez, U.M.L., Aidar, E. 1998. Distribution of intracellular nitrogen in marine microalgae: basis for the calculation of specific nitrogen-to-protein conversionfactors. Journal of Phycology. 34, 798-811.

Lucas-Salas, L.M., Castrillo, M., Martínez, D. 2013. Effects of dilution rate and water reuse on biomass and lipid production of *Scenedesmus obliquus* in a two-stage novel photobioreactor. Bioresource Technology. 143, 344-352.

Lung, S.-C., Weselake, R. 2006. Diacylglycerol acyltransferase: A key mediator of plant triacylglycerol synthesis. 41, 1073-1088.

Mairet, F., Bernard, O., Masci, P., Lacour, T., Sciandra, A. 2011. Modelling neutral lipid production by the microalga *Isochrysis aff. galbana* under nitrogen limitation. Bioresource Technology. 102, 142-149.

Malkin, S., Fork, D.C. 1996. Bill Arnold and calorimetric measurements of the quantum requirement of photosynthesis - once again ahead of his time. Photosynthesis Research. 48, 41-46.

Manichaikul, A., Ghamsari, L., Hom, E., Lin, C., Murray, R., Chang, R., Balaji, S., Hao, T., Shen, Y., Chavali, A., Thiele, I., Yang, X., Fan, C., Mello, E., Hill, D., Vidal, M., Salehi-Ashtiani, K., Papin, J. 2009. Metabolic network analysis integrated with transcript verification for sequenced genomes. Nature Methods. 6, 589-592.

Marra, J., Barber, R.T. 2004. Phytoplankton and heterotrophic respiration in the surface layer of the ocean. Geophysical Research Letters. 31, L09314.

Mata, T.M., Martins, A.A., Caetano, N.S. 2010. Microalgae for biodiesel production and other applications: A review. Renewable and Sustainable Energy Reviews. 14, 217 -232.

Meeuwse, P., Tramper, J., Rinzema, A. 2011. Modeling lipid accumulation in oleaginous fungi in chemostat cultures: I. Development and validation of a chemostat model for *Umbelopsis isabellina*. Bioprocess and Biosystems Engineering. 34, 939-949.

Melis, A. 1999. Photosystem-II damage and repair cycle in chloroplasts: what modulates the rate of photodamage in vivo? Trends in Plant Science. 4, 130-135.

Melis, A., Zhang, L., Forestier, M., Ghirardi, M.L., Seibert, M. 2000. Sustained photobiological hydrogen gas production upon reversible inactivation of oxygen evolution in the green alga *Chlamydomonas reinhardtii*. Plant Physiology. 122, 127-135.

Merchant, S.S., Kropat, J., Liu, B., Shaw, J., Warakanont, J. 2012. TAG, You're it! *Chlamydomonas* as a reference organism for understanding algal triacylglycerol accumulation. Current Opinion in Biotechnology. 23, 352-363.

Merchant, S.S., Prochnik, S., Vallon, O., Harris, E.H., Karpowicz, S.J., Witman, G.B., Terry, A., Salamov, A., Fritz-Laylin, L.K., Sanderfoot, A.A., Spalding, M.H., Kapitonov, V.V., Ren, Q., Ferris, P., Lindquist, E., Shapiro, H., Lucas, S., Grimwood, J., Schmutz, J., Grigoriev, I.V., Rokhsar, D.S., Grossman, A.R. 2007. The *Chlamydomonas* Genome Reveals the Evolution of Key Animal and Plant Functions. Science. 318.

Mittag, M., Kwang, W.J. 2001. Circadian rhythms in microalgae. in: *International Review of Cytology*, Vol. Volume 206, Academic Press, pp. 213-247.

Mittelbach, M. 1996. Diesel fuel derived from vegetable oils, VI: Specifications and quality control of biodiesel. Bioresource Technology. 56, 7-11.

Müller, P., Li, X.-P., Niyogi, K.K. 2001. Non-photochemical quenching. A response to excess light energy. Plant Physiology. 125, 1558-1566.

N

Nguyen, H.M., Baudet, M., Cuiné, S., Adriano, J.-M., Barthe, D., Billon, E., Bruley, C., Beisson, F., Peltier, G., Ferro, M., Li-Beisson, Y. 2011. Proteomic profiling of oil bodies isolated from the unicellular green microalga *Chlamydomonas reinhardtii*: With focus on proteins involved in lipid metabolism. PROTEOMICS. 11, 4266-4273.

Noctor, G., Foyer, C.H. 1998. A re-evaluation of the ATP:NADPH budget during C3 photosynthesis: a contribution from nitrate assimilation and its associated respirato-

ry activity? Journal of Experimental Botany. 49, 1895-1908.

Ohlrogge, J., Browse, J. 1995. Lipid biosynthesis. The Plant Cell Online. 7, 957-70.

Ohlrogge, J.B., Jaworski, J.G. 1997. Regulation of fatty acid synthesis. Annual Review of Plant Physiology and Plant Molecular Biology. 48, 109-136.

Packer, A., Li, Y., Andersen, T., Hu, Q., Kuang, Y., Sommerfeld, M. 2011. Growth and neutral lipid synthesis in green microalgae: A mathematical model. Bioresource Technology. 102, 111-117.

Pan, Y.-Y., Wang, S.-T., Chuang, L.-T., Chang, Y.-W., Chen, C.-N.N. 2011. Isolation of thermo-tolerant and high lipid content green microalgae: Oil accumulation is predominantly controlled by photosystem efficiency during stress treatments in Desmodesmus. Bioresource Technology. 102, 10510-10517.

Peled, E., Leu, S., Zarka, A., Weiss, M., Pick, U., Khozin-Goldberg, I., Boussiba, S. 2011. Isolation of a novel oil globule protein from the green alga *Haematococcus pluvialis* (*Chlorophyceae*). 46, 851-861.

Pirt, S.J. 1965. The maintenance energy of bacteria in growing cultures Proceedings of the Royal Society of London, Series B: Biological Sciences. 163.

Platt, T., Jassby, A.D. 1976. The relationship between photosynthesis and light for natural assemblages of coastal marine phytoplankton. Journal of Phycology. 12, 421-430.

Porra, R. 2002. The chequered history of the development and use of simultaneous equations for the accurate determination of chlorophylls a and b. Photosynthesis Research. 73, 149-156.

Pottier, L., Pruvost, J., Deremetz, J., Cornet, J.F., Legrand, J., Dussap, C.G. 2005. A fully predictive model for one-dimensional light attenuation by *Chlamydomonas reinhardtii* in a torus photobioreactor. Biotechnology and Bioengineering. 91, 569-582.

Pramanik, J., Keasling, J.D. 1998. Effect of *Escherichia coli* biomass composition on central metabolic fluxes predicted by a stoichiometric model. Biotechnology and Bioengineering. 60, 230-238.

Pruvost, J., Van Vooren, G., Cogne, G., Legrand, J. 2009. Investigation of biomass and lipids production with *Neochloris oleoabundans* in photobioreactor. Bioresource Technology. 100, 5988-5995.

Pulz, O., Gross, W. 2004. Valuable products from biotechnology of microalgae. 65, 635-648.

Quinn, J., de Winter, L., Bradley, T. 2011. Microalgae bulk growth model with application to industrial scale systems. Bioresource Technology. 102, 5083-5092.

Rabbani, S., Beyer, P., Lintig, J.v., Hugueney, P., Kleinig, H. 1998. Induced β-carotene synthesis driven by triacylglycerol deposition in the unicellular alga *Dunaliella bardawil*. Plant Physiology. 116, 1239-1248.

Radakovits, R., Jinkerson, R.E., Darzins, A., Posewitz, M.C. 2010. Genetic engineering of algae for enhanced biofuel production. Eukaryotic Cell. 9, 486-501.

Rhiel, E., Mörschel, E., Wehrmeyer, W. 1985. Correlation of pigment deprivation and ultrastructural organization of thylakoid membranes *Cryptomonas maculata* following nutrient deficiency. Protoplasma. 129, 62-73.

Richardson, B., Orcutt, D.M., Schwertner, H.A., Martinez, C.L., Wickline, H.E. 1969. Effects of nitrogen limitation on the growth and composition of unicellular algae in continuous culture. Applied Microbiology. 18, 245-250.

Richmond, A. 2004. Principles for attaining maximal microalgal productivity in photobioreactors: an overview. in: *Asian Pacific Phycology in the 21st Century: Prospects and Challenges*, (Ed.) P.O. Ang Jr., Vol. 173, Springer Netherlands. Dordrecht, pp. 33-37.

Riekhof, W.R., Benning, C. 2009. Glycerolipid biosynthesis. 2 ed. in: *The Chlamydomonas sourcebook: organellar and metabolic processes.*, (Ed.) D. Stern, Vol. 2, Elsevier. Amsterdam.

Rismani-Yazdi, H., Haznedaroglu, B., Hsin, C., Peccia, J. 2012. Transcriptomic analysis of the oleaginous microalga *Neochloris oleoabundans* reveals metabolic insights into triacylglyceride accumulation. Biotechnology for Biofuels. 5, 1-16.

Rodolfi, L., Chini Zittelli, G., Bassi, N., Padovani, G., Biondi, N., Bonini, G., Tredici, M.R. 2009. Microalgae for oil: Strain selection, induction of lipid synthesis and outdoor mass cultivation in a low-cost photobioreactor. Biotechnology and Bioengineering. 102, 100-112.

Roels, J.A. 1983. Relaxation times and their relevance to the construction of kinetic models. in: *Energetics and kinetics in Biotechnology*, Elsevier Biomedical Press, pp. 205-221.

Roesler, K., Shintani, D., Savage, L., Boddupalli, S., Ohlrogge, J. 1997. Targeting of the *Arabidopsis* homomeric acetyl-Coenzyme A carboxylase to plastids of rapeseeds. Plant Physiology. 113, 75-81.

Roughan, P.G., Slack, C.R. 1982. Cellular organization of glycerolipid metabolism. An-

nual Review of Plant Physiology. 33, 97-132.

Roy, S., Llewellyn, C., Egeland, E., Johnson, G. 2011. *Phytoplankton pigments: characterization, chemotaxonomy and applications in oceanography*. Cambridge University Press, New York.

Santos, A.M., Janssen, M., Lamers, P.P., Evers, W.A.C., Wijffels, R.H. 2012. Growth of oil accumulating microalga *Neochloris oleoabundans* under alkaline-saline conditions. Bioresource Technology. 104, 593-599.

Schmidt, B.J., Lin-Schmidt, X., Chamberlin, A., Salehi-Ashtiani, K., Papin, J.A. 2010. Metabolic systems analysis to advance algal biotechnology. Biotechnology Journal. 5, 660-670.

Scott, D.D., Srirama, K., Carani, B.S. 2007. Omega-3 fatty acids for nutrition and medicine: Considering microalgae oil as a vegetarian source of EPA and DHA. Current Diabetes Reviews. 3, 198-203.

Sheehan, J., Dunahay, T., Benemann, J.R., Roessler, P. 1998. A look back at the U.S. Department of Energy's Aquatic Species program: Biodiesel from algae. N R E L / T P -580-24190.

Siaut, M., Cuine, S., Cagnon, C., Fessler, B., Nguyen, M., Carrier, P., Beyly, A., Beisson, F., Triantaphylides, C., Li-Beisson, Y., Peltier, G. 2011. Oil accumulation in the model green alga *Chlamydomonas reinhardtii*: characterization, variability between common laboratory strains and relationship with starch reserves. BMC Biotechnology. 11, 7.

Simionato, D., Block, M.A., La Rocca, N., Jouhet, J., Maréchal, E., Finazzi, G., Morosinotto, T. 2013. The response of *Nannochloropsis gaditana* to nitrogen starvation includes *de novo* biosynthesis of triacylglycerols, a decrease of chloroplast galactolipids, and reorganization of the photosynthetic apparatus. Eukaryotic Cell. 12, 665-676.

Slocombe, S.P., Cornah, J., Pinfield-Wells, H., Soady, K., Zhang, Q., Gilday, A., Dyer, J.M., Graham, I.A. 2009. Oil accumulation in leaves directed by modification of fatty acid breakdown and lipid synthesis pathways. Plant Biotechnology Journal. 7, 694-703.

Sousa, C., de Winter, L., Janssen, M., Vermuë, M.H., Wijffels, R.H. 2012. Growth of the microalgae *Neochloris oleoabundans* at high partial oxygen pressures and subsaturating light intensity. Bioresource Technology. 104, 565-570.

Spolaore, P., Joannis-Cassan, C., Duran, E., Isambert, A. 2006. Commercial applications of microalgae. Journal of Bioscience and Bioengineering. 101, 87-96.

Stephanopoulos, G.N., Aristidou, A., Nielsen, J. 1998. *Metabolic Engineering, principles and methodologies*. Academic Press, San Diego.

Sueoka, N., Chiang, K.S., Kates, J.R. 1967. Deoxyribonucleic acid replication in meiosis of *Chlamydomonas reinhardi:* I. Isotopic transfer experiments with a strain producing eight zoospores. Journal of Molecular Biology. 25, 47-66.

Sukenik, A., Wahnon, R. 1991. Biochemical quality of marine unicellular algae with special emphasis on lipid composition. I. Isochrysis galbana. Aquaculture. 97, 61-72.

Takache, H., Christophe, G., Cornet, J.-F., Pruvost, J. 2010. Experimental and theoretical assessment of maximum productivities for the microalgae *Chlamydomonas reinhardtii* in two different geometries of photobioreactors. Biotechnology Progress. 26, 431-440.

Tanada, T. 1951. The photosynthetic efficiency of carotenoid pigments in *Navicula minima*. American Journal of Botany. 38, 276-283.

Taymaz-Nikerel, H., Borujeni, A.E., Verheijen, P.J.T., Heijnen, J.J., van Gulik, W.M. 2010. Genome-derived minimal metabolic models for *Escherichia coli* MG1655 with estimated in vivo respiratory ATP stoichiometry. Biotechnology and Bioengineering. 107, 369-381.

Turpin, D.H. 1991. Effects of inorganic N availability on algal photosynthesis and carbon metabolism. Journal of Phycology. 27, 14-20.

Valle, O., Lien, T., Knutsen, G. 1981. Fluorometric determination of DNA and RNA in *Chlamydomonas* using ethidium bromide. Journal of Biochemical and Biophysical Methods. 4, 271-277.

van der Heijden, R.T.J.M., Heijnen, J.J., Hellinga, C., Romein, B., Luyben, K.C.A.M. 1994. Linear constraint relations in biochemical reaction systems: I. Classification of the calculability and the balanceability of conversion rates. Biotechnology and Bioengineering. 43, 3-10.

van der Tol, C., Verhoef, W., Rosema, A. 2009. A model for chlorophyll fluorescence and photosynthesis at leaf scale. Agricultural and Forest Meteorology. 149, 96-105.

Vejrazka, C., Janssen, M., Streefland, M., Wijffels, R.H. 2011. Photosynthetic efficiency of *Chlamydomonas reinhardtii* in flashing light. Biotechnology and Bioengineering. 108, 2905-2913.

Vigeolas, H., Waldeck, P., Zank, T., Geigenberger, P. 2007. Increasing seed oil content in oil-seed rape (*Brassica napus L.*) by over-expression of a yeast glycerol-3-

phosphate dehydrogenase under the control of a seed-specific promoter. Plant Biotechnology Journal. 5, 431-441.

W

Weber, A., Flügge, U.I. 2002. Interaction of cytosolic and plastidic nitrogen metabolism in plants. Journal of Experimental Botany. 53, 865-874.

Weesepoel, Y., Vincken, J.-P., Pop, R.M., Liu, K., Gruppen, H. 2013. Sodiation as a tool for enhancing the diagnostic value of MALDI-TOF/TOF-MS spectra of complex astaxanthin ester mixtures from *Haematococcus pluvialis*. Journal of Mass Spectrometry. 48, 862-874.

Weselake, R., Shah, S., Taylor, D.C., Zou, J., Laroche, A., Moloney, M.M., Rakow, G., Raney, J.P., Harwood, J. 2007. Transformation of *Brassica napus* with diacylglycerol acyltransferase-1 results in increased seed oil content. in: *Current Advances in the Biochemistry and Cell Biology of Plant Lipids*, (Eds.) C. Benning, J. Ohlrogge, Aardvark Global Publishing Company. Salt Lake City, Idaho, pp. 232-234.

Wijffels, R.H., Barbosa, M.J. 2010. An outlook on microalgal biofuels. Science. 329, 796-799.

Wijffels, R.H., Barbosa, M.J., Eppink, M.H.M. 2010. Microalgae for the production of bulk chemicals and biofuels. Biofuels, Bioproducts and Biorefining. 4, 287-295.

Wijffels, R.H., Kruse, O., Hellingwerf, K.J. 2013. Potential of industrial biotechnology with cyanobacteria and eukaryotic microalgae. Current Opinion in Biotechnology. 24, 405-413.

Worden, A.Z., Lee, J.-H., Mock, T., Rouzé, P., Simmons, M.P., Aerts, A.L., Allen, A.E., Cuvelier, M.L., Derelle, E., Everett, M.V., Foulon, E., Grimwood, J., Gundlach, H., Henrissat, B., Napoli, C., McDonald, S.M., Parker, M.S., Rombauts, S., Salamov, A., Von Dassow, P., Badger, J.H., Coutinho, P.M., Demir, E., Dubchak, I., Gentemann, C., Eikrem, W., Gready, J.E., John, U., Lanier, W., Lindquist, E.A., Lucas, S., Mayer, K.F.X., Moreau, H., Not, F., Otillar, R., Panaud, O., Pangilinan, J., Paulsen, I., Piegu, B., Poliakov, A., Robbens, S., Schmutz, J., Toulza, E., Wyss, T., Zelensky, A., Zhou, K., Armbrust, E.V., Bhattacharya, D., Goodenough, U.W., Van de Peer, Y., Grigoriev, I.V. 2009. Green evolution and dynamic adaptations revealed by genomes of the marine Picoeukaryotes *Micromonas*. Science. 324, 268-272.

Y

Yang, C., Hua, Q., Shimizu, K. 2000. Energetics and carbon metabolism during growth of microalgal cells under photoautotrophic, mixotrophic and cyclic light-autotrophic/dark-heterotrophic conditions. Biochemical Engineering Journal. 6,

87-102.

Yoon, K., Han, D., Li, Y., Sommerfeld, M., Hu, Q. 2012. Phospholipid:diacylglycerol acyltransferase is a multifunctional enzyme involved in membrane lipid turnover and degradation while synthesizing triacylglycerol in the unicellular green microalga *Chlamydomonas reinhardtii*. The Plant Cell Online. 24, 3708-3724.

Yu, J., Woo, K.C. 1988. Glutamine Transport and the Role of the Glutamine Translocator in Chloroplasts. Plant Physiology. 88, 1048-1054.

Yu, W.-L., Ansari, W., Schoepp, N., Hannon, M., Mayfield, S., Burkart, M. 2011. Modifications of the metabolic pathways of lipid and triacylglycerol production in microalgae. 10, 1-11.

Yun, Y.S., Park, J.M. 2001. Attenuation of monochromatic and polychromatic lights in *Chlorella vulgaris* suspensions. Applied Microbiology and Biotechnology. 55, 765-770.

Z

Zhao, Y., Tang, H., Ye, Y. 2011. RAPSearch2: a fast and memory-efficient protein similarity search tool for next generation sequencing data. Bioinformatics. 28, 125-126.

Zijffers, J.W., Schippers, K.J., Zheng, K., Janssen, M., Tramper, J., Wijffels, R.H. 2010. Maximum photosynthetic yield of green microalgae in photobioreactors. Marine Biotechnology. 12, 708-718.

Zou, J., Katavic, V., Giblin, E.M., Barton, D.L., MacKenzie, S.L., Keller, W.A., Hu, X., Taylor, D.C. 1997. Modification of seed oil content and acyl composition in the *Brassicaceae* by expression of a yeast sn-2 acyltransferase gene. The Plant Cell Online. 9, 909-23.

Summary

Microalgae are a promising platform for the production of many sustainable resources, such as pigments, proteins, carbohydrates and lipids. They can be grown year round on non-arable land, using only sunlight, sea or waste water and a few added nutrients. The projected productivities that can be obtained with microalgae grown in controlled photobioreactors are much higher than those obtained with traditional agricultural crops. But currently, the production costs of algae only allow commercial production of high value products such as β-carotene, astaxanthin and ω-3 fatty acids. For the economical production of bulk products, additional developments are necessary that decrease photobioreactor operation costs, increase photosynthetic capacity, increase the productivity of biomass and/or product, and that facilitate the harvesting and further processing of biomass.

A good example of a microalgal bulk product is triacylglycerol (TAG), a lipid consisting out of a glycerol molecule with 3 fatty acyl chains attached. The composition of microalgal TAG is comparable to that of commonly used vegetable oils, making TAG suitable for the production of many food products, as well as a raw material for an effective biofuel. To increase productivity, insight into the mechanism that causes the accumulation of TAG is indispensable. Therefore the aim of this thesis was to obtain more insight in the mechanism of TAG accumulation in microalgae that are exposed to adverse growth conditions, and to translate the obtained knowledge to optimal culture conditions for efficient TAG production. Although the exact mechanism of TAG accumulation is unknown, it is often hypothesised that TAG accumulation serves as a sink for excess energy when algae are exposed to adverse growth conditions, such as nitrogen limitation. Under these conditions, light energy is continuously harvested while lower metabolism is hampered, causing an overreduction of the photosystems that could result in the formation of dangerous reactive oxygen species (ROS). The accumulation of products that do not contain nitrogen, such as TAG, is thought to serve as an emergency route for the efficient capturing of excess reducing potential.

In **Chapter 2** it was tested whether TAG accumulation indeed serves as an energy sink when microalgae are exposed to an energy imbalance caused by nutrient limitation. A novel continuous growth system was presented, which combined turbidostat control with a separate continuous nitrogen supply. This growth system allowed for the combination of excess light absorption and growth-limiting nitrogen supply rates, which resulted in accumulation of TAG (from 1.5 to 12.4% w/w) in visible lipid bodies in *Neochloris oleoabundans*, while cell replication was sustained. The fourfold increase in TAG productivity that was obtained by reducing the nitrogen supply to the system while

maintaining equal light absorption rates, showed that TAG accumulation was probably caused by an imbalance between energy supply and demand. TAG indeed served as an energy sink under these conditions, but the simultaneous decrease in biomass yields showed that a large part of the energy absorbed by the system under nitrogen limitation was not ending up in biomass. This energy was dissipated instead, which probably occurred in the photosystems. The energy dissipation increased with progressive levels of nitrogen limitation, and the extent of energy dissipation under nitrogen limited conditions is likely to be species specific. Therefore, it was suggested to screen for strains that have a higher photosynthetic capacity under nitrogen shortages, as these species might channel more of the available energy towards TAG and thus exhibit higher TAG production rates.

The kinetics of TAG accumulation and energy use under nitrogen limitation were further explored in **Chapter 3.** A kinetic model was developed based on the measured electron distributions in *N. oleoabundans* grown in the nitrogen limited turbidostat. These electron distributions revealed that starch was used as primary energy and carbon sink, and that its synthesis rate declined when the specific growth rate declined due to progressive nitrogen starvation. Also, it was found that only 8.6% of the excess electrons caused by nitrogen limitation ended up in TAG. The bulk of electrons was used in catabolism to generate the ATP necessary for maintenance and biomass synthesis, or lost in dissipative processes in the plastid.
Model simulations were used to further explore the potential of the nitrogen limited turbidostat for the production of algal biomass. It was shown that by manipulating the cultivation conditions in this system, the algal biomass composition, and the volumetric productivities and yields on light of each of the major biomass constituents (protein, starch and TAG) can be controlled on demand. This is a very important feature, considering the fact that the full potential of algal biomass must be exploited to be able to produce TAG at a competitive price. The optimum for TAG yield on light coincides with the optimum for TAG content, which makes low light supply rates and severe nitrogen limitation favourable cultivation conditions for TAG production in a nitrogen limited turbidostat.

To obtain more insight into the microalgal metabolism under various cultivation conditions, metabolic models were used. In **Chapter 4**, a genome based model was presented that describes the primary metabolism of model green microalga *Chlamydomonas reinhardtii* in more than 300 enzymatic steps. By lumping linear pathways, a more practical

network that contained 160 reactions and 164 compounds was obtained.
Data obtained in seven chemostat experiments operated under low irradiances at several dilution rates were used as input for the metabolic model, allowing for determination of the energy requirements for growth and maintenance *in vivo*. The ATP requirement for biomass formation from biopolymers was determined to be 109 mmol g^{-1} (18.9 mol mol^{-1}) and the maintenance requirement was determined to be 2.85 mmol g^{-1} h^{-1}.
Further model simulations confirmed that cultivating microalgae at low growth rates is unfavourable because of the high maintenance requirements relative to the energy use on biomass production. As a result, biomass yields will be low. On the other hand, biomass yields will decrease under high light supply rates, due to light saturation effects. Thus, to optimize biomass yield on light energy in photobioreactors, an optimum between low and high light supply rates should be found. With these simulations it was illustrated how metabolic flux analysis can be used as a tool to gain insight into the metabolism of algae and ultimately can be used for the maximization of algal biomass and product yield.

In **Chapter 5**, the metabolic model for *C. reinhardtii* was extended to accurately describe the primary metabolism of oleaginous algae. The resulting model consisted of 373 reactions divided over two cellular compartments (the chloroplast and the cytosol). The presence of the 226 unique enzymes responsible for these reactions was validated using a *de novo* constructed transcriptome of *N. oleoabundans*. Subsequently, the model was used to study the interaction between nitrogen assimilation, photosynthesis and TAG accumulation.
It was found that under nitrogen replete conditions, over one third of the plastidic NADPH is used in nitrogen fixation and protein synthesis, indicating that nitrogen shortage will result in a considerable surplus of NADPH. Under steady state nitrogen limitation however, *N. oleoabundans* was able to balance its metabolic energy demands with the photosynthetic energy supply by redirecting carbon and energy towards TAG synthesis and reducing linear electron transport. Also, the ATP/NADPH turnover ratio was not affected by nitrogen limitation which shows that nitrogen limitation is distinctly different from nitrogen starvation, where ATP/NADPH turnover ratio are known to be affected by the sudden lack of protein synthesis.
In several optimisation scenarios the capacity of algal metabolism to produce TAG was evaluated. It was revealed that optimising photosynthetic capacity under nitrogen limitation provides a larger potential in improving TAG yields on light, than redirecting carbon away from competing metabolites, such as starch. Finally, the model was used to

evaluate the maximum capacity of *N. oleoabundans* to produce TAG. The maximum theoretical yield of TAG on light is 0.81-1.07 g (mol photons)$^{-1}$, depending on the maximum capacity of the GAP/3PG shuttle. This is more than 3 times higher than what is currently obtained under optimal conditions, and the optimal yield presented here can serve as a point of reference for future optimisation of TAG yield on light.

Increasing TAG accumulation rates in microalgae is an important target for cost reduction of microalgal lipid production. This requires proper understanding of the physiology and regulation of lipid metabolism in oleaginous microalgae. Important knowledge gaps were indicated in **Chapter 6**, such as the compartmentalisation of TAG synthesis, variations in TAG production rates throughout the day/night cycle, and TAG accumulation regulation and its relation to photosynthesis. Solving these knowledge gaps is necessary to identify potential bottlenecks in TAG production and targets for metabolic engineering.

Based on current developments in the field and the research presented in this thesis, three hypotheses on the cause and function of TAG accumulation were proposed. Although TAG always is an electron and a carbon sink since its synthesis requires the consumption of NADPH and carbon, the extent to which it functions as a sink for excess electrons under adverse growth conditions may vary between species. Consequently TAG may have additional functions in some algae, such as storage of plastid building blocks. Therefore, the optimal cultivation strategy and metabolic engineering approach for optimising TAG production might be different for each species.

Several points for optimising the productivity of TAG for bulk applications were addressed. Besides the classic approach of two stage TAG production, where biomass production is followed by a nitrogen starvation phase, continuous systems in which growth and TAG production are occurring simultaneously should be further investigated. In such a continuous system considerable time and production costs could be saved, because the production phase for biomass and the system preparations between consecutive batches are omitted. Although the small scale productivities currently are a factor 4 lower than in the classic two-stage approach, continuous TAG production is in its infancy and further optimisation could further increase the output of this system. Moreover, continuous production has the added benefit that it allows for control of TAG accumulation rates under the varying irradiances and day/night cycles that are experienced outdoors.

Finally, it was suggested how metabolic engineering could be applied for increasing the TAG content and productivity in the current production strains. Besides increasing the

fluxes through the lipid biosynthetic pathways by enzyme overexpression and knocking down competing pathways for carbon and energy, preventing the photosynthetic losses associated with nitrogen limitation should be the most important target for metabolic engineering strategies. Moreover, further investigation into the signalling mechanisms that control TAG accumulation and photosynthetic adaptation under nitrogen shortage is necessary. Ultimately this may unlock options for the uncoupling of TAG synthesis from adverse growth conditions and the accompanying decrease in photosynthetic rate. Detailed pathway analysis by metabolic flux models combined with gene expression analysis and proteomics techniques will play an important role in identifying promising engineering targets for maximized TAG production rates in microalgae.

The results presented in this thesis signify a step ahead towards cost efficient production of microalgal lipids for bulk applications. In addition, this work provides an outlook on the future efforts that are necessary to make sure that the promise of microalgae can become a reality.

Samenvatting

Microalgen zijn een veelbelovende bron voor een groot aantal duurzaam vervaardigde producten, zoals pigmenten, eiwitten, koolhydraten en vetten. Deze eencellige planten kunnen het hele jaar door gekweekt worden zonder gebruik te maken van vruchtbare landbouwgrond, met behulp van voldoende zonlicht, zee- of afval water en enkele nutriënten. De verwachte biomassaproductiviteit van microalgen, gekweekt in gecontroleerde fotobioreactoren, is vele malen hoger dan die van traditionele gewassen. Echter de kosten van het productieproces zijn op dit moment dusdanig hoog dat alleen producten met een hoge marktwaarde, zoals β-caroteen, astaxantine en ω-3 vetzuren, commercieel geproduceerd kunnen worden. Voor een rendabele commercialisatie van bulkproducten zijn er ontwikkelingen nodig die de kosten van het productieproces verlagen. Hierbij kan gedacht worden aan het reduceren van de kosten voor het gebruik van fotobioreactoren, verhoging van de fotosynthetische capaciteit, de productiviteit van biomassa en/of product, en het eenvoudiger maken van de oogst en verdere verwerking van biomassa.
Een goed voorbeeld van een bulkproduct dat gewonnen kan worden uit microalgen is triacylglycerol (TAG), een vet dat bestaat uit een glycerol molecuul met daaraan 3 vetzuurketens. De compositie van TAG uit microalgen is vergelijkbaar met die van gangbare plantaardige oliën, wat maakt dat TAG geschikt is voor menselijke consumptie, maar ook als grondstof voor hoogwaardige biodiesel. Om de productie van TAG te kunnen verhogen is begrip van het biologische mechanisme dat TAG vorming veroorzaakt onontbeerlijk. Het doel van dit onderzoek was dan ook om meer inzicht te krijgen in het mechanisme van TAG accumulatie in microalgen die blootgesteld zijn aan nadelige groeicondities, en om de verkregen kennis te vertalen naar optimale kweekcondities voor TAG productie. Alhoewel het precieze mechanisme van TAG accumulatie onbekend is, wordt vaak gesuggereerd dat TAG vorming dient als een manier om overtollige energie weg te sluizen wanneer microalgen worden blootgesteld aan nadelige groeicondities, zoals bij stikstof limitatie. Onder deze condities wordt er voortdurend licht energie opgevangen, terwijl door de afwezigheid van stikstof het metabolisme wordt afgeremd. Dit veroorzaakt overbelasting van de fotosystemen, wat vervolgens de vorming van verschillende zuurstofradicalen teweeg kan brengen. Het vormen van TAG, waar geen stikstof voor nodig is, zou dienen als noodvoorziening waarmee de overtollige energie wordt weggevangen.

In **Hoofdstuk 2** werd onderzocht of TAG accumulatie inderdaad dienst doet als noodopslag van overtollige energie wanneer microalgen worden blootgesteld aan een energie onbalans, veroorzaakt door nutriëntlimitatie. Een nieuw continu productiesysteem werd

gepresenteerd, waarin een turbidostaat regeling werd gecombineerd met een aparte stikstof toevoer. Deze kweekmethode maakte het mogelijk om een overschot van licht te combineren met een tekort aan stikstof, waardoor TAG zich ophoopte (van 1.5 tot 12.4% van de droge biomassa) in zichtbare vetbolletjes in *Neochloris oleoabundans*, terwijl celreplicatie bleef aanhouden. Een viervoudige toename in TAG productiviteit werd verkregen door de stikstof toevoer te reduceren, terwijl de lichtabsorptie gelijk werd gehouden. Hierdoor werd aangetoond dat TAG accumulatie veroorzaakt werd door een onbalans tussen energieopname en consumptie. Onder deze condities diende TAG accumulatie inderdaad als manier om energie weg te sluizen, maar een gelijktijdig verlies in biomassaopbrengst liet zien dat een groot deel van de geabsorbeerde lichtenergie niet werd gebruikt in de synthese van biomassa. Deze energie ging verloren en werd waarschijnlijk weggesluisd via de fotosystemen. Het energieverlies nam toe wanneer de stikstoftoevoer werd verlaagd, en het is zeer waarschijnlijk dat de mate van energieverlies onder stikstoflimitatie soortafhankelijk is. Om die reden kan zou het rendabel kunnen zijn om te zoeken naar microalgen met een hoge fotosynthetische capaciteit bij stikstofgebrek, omdat deze mogelijk meer van de beschikbare energie voor TAG synthese aanwenden en dus een hogere TAG productiviteit laten zien.

De kinetiek van TAG accumulatie en energie gebruik onder stikstof limitatie werden verder onderzocht in **Hoofdstuk 3**. Een kinetisch model werd ontwikkeld gebaseerd op gemeten elektronenverdelingen in *N. oleoabundans*, gekweekt in een stikstof gelimiteerde turbidostaat. Deze elektronenverdelingen lieten zien dat zetmeel voornamelijk werd aangewend voor primaire energie- en koolstofopslag, en dat de synthesesnelheid van zetmeel lager werd zodra de groeisnelheid afnam door toenemende stikstoflimitatie. Ook werd gevonden dat maar 8.6% van het overschot aan elektronen veroorzaakt door stikstoflimitatie, eindigde in TAG. De meerderheid van elektronen ging verloren in de plastide, of werd gebruikt in katabolisme om de ATP te genereren die verbruikt wordt in celonderhoud en bij de aanmaak van biomassa.
Het kinetisch model werd gebruikt om de mogelijkheden van de stikstof gelimiteerde turbidostaat te onderzoeken. De modelsimulaties lieten zien dat door het aanpassen van de kweekcondities, de volumetrische productiviteit en opbrengst van de belangrijke biomassa componenten (eiwit, zetmeel en TAG) op lichtenergie naar wens gecontroleerd kunnen worden. Ook de cel compositie kan op deze manier voorspeld worden, wat een belangrijk pluspunt is van dit kweeksysteem, gezien het feit dat de volledige biomassa moet worden benut om TAG concurrerend te kunnen produceren. De optimale kweekcondities voor TAG productie liggen bij lage lichttoevoer en extreme stikstof

limitatie, omdat bij deze instellingen het optimum voor TAG opbrengst op lichtenergie samen valt met dat voor TAG gehalte.

Om meer inzicht te krijgen in het effect van verschillende kweekcondities op het metabolisme van microalgen zijn metabole modellen ontwikkeld. In **Hoofdstuk 4** werd een genoom schaal model gepresenteerd dat het primaire metabolisme van de groene 'model' alg *Chlamydomonas reinhardtii* beschrijft in meer dan 300 enzymatische reacties. Door lineaire routes samen te voegen is een handzamer model verkregen, met 160 reacties en 164 metabolieten.
C. reinhardtii werd gekweekt onder lage licht toevoer en verschillende verdunningssnelheden. De data van zeven chemostaat experimenten konden gebruikt worden als invoer voor het metabole model en hiermee kon het energieverbruik voor groei en celonderhoud *in vivo* uitgerekend worden. Het ATP verbruik voor biomassa synthese vanuit de verschillende macromoleculen was 109 mmol g^{-1} (18.9 mol mol^{-1}) en dat voor celonderhoud was 2.85 mmol g^{-1} h^{-1}.
Verdere simulaties bevestigden dat het kweken van microalgen bij lage groeisnelheden nadelig is, omdat dan de energiekosten voor celonderhoud relatief hoog zijn ten opzichte van het energieverbruik voor biomassa productie. Hierdoor valt de biomassa opbrengst op basis van lichtenergie laag uit onder lage licht toevoer. Aan de andere kant vermindert de biomassa opbrengst ook onder te hoge toevoer van licht door het optreden van lichtverzadigingseffecten. Daarom moet voor het maximaliseren van de opbrengst van biomassa op lichtenergie in fotobioreactoren worden gezocht naar een optimum tussen lage en hoge lichttoevoer.
De gepresenteerde modelsimulaties illustreren hoe metabole flux analyse aangewend kan worden om het inzicht in het metabolisme van microalgen te vergroten, en uiteindelijk ook gebruikt kan worden om de opbrengst van biomassa of een specifiek product te verhogen.

In **Hoofdstuk 5**, werd het metabole model voor *C. reinhardtii* uitgebreid om het metabolisme van olie ophopende algen te kunnen beschrijven. Het resulterende model bestaat uit 373 reacties verdeeld over 2 cel compartimenten (de chloroplast en het cytosol). De aanwezigheid van de 226 verschillende enzymen die deze reacties katalyseren, werd aangetoond met behulp van het *de novo* geassembleerde transcriptoom van *N. oleoabundans*. Vervolgens werd dit nieuwe model gebruikt om de interacties te bestuderen tussen stikstofassimilatie, fotosynthese en TAG accumulatie.
Aangetoond werd dat onder groeicondities met voldoende stikstof, meer dan een derde

van de NADPH die gegenereerd wordt in de plastide, gebruikt wordt in stikstofassimilatie en eiwitsynthese Dit geeft aan dat een stikstofgebrek zal resulteren in een enorm overschot van NADPH. Echter, onder stabiele stikstoflimitatie kon *N. oleoabundans* de metabole energie vraag balanceren met de toevoer van licht energie in fotosynthese, door meer energie en koolstof te gebruiken in TAG synthese en lineair elektronen transport te verminderen. Ook werd aangetoond dat de ATP/NADPH omzet ratio niet aangetast werd door stikstoflimitatie, wat aangeeft dat limitatie duidelijk een ander effect heeft dan volledige stikstofdepletie, waarvan bekend is dat het de ATP/NADPH omzet ratio verschuift door het plotseling wegvallen van eiwitsynthese.
Verschillende scenario's werden doorgerekend om de capaciteit van het algen metabolisme om TAG te produceren te evalueren. Er kwam naar voren dat om de TAG opbrengst op lichtenergie te verhogen, het effectiever is om de fotosynthetische capaciteit onder stikstoflimitatie te verhogen dan de koolstoffluxen van concurrerende metabolieten af te wenden. Ook werd de maximale capaciteit van het metabolisme van *N. oleoabundans* voor TAG productie uitgerekend. De maximale theoretische opbrengst van TAG op lichtenergie is 0.81-1.07 g (mol photonen)$^{-1}$, waarin het verschil bepaald werd door de maximale capaciteit van de GAP/3PG shuttle. De optimale opbrengst die hier berekend is, is meer dan 3 keer hoger dan wat momenteel gehaald wordt onder optimale omstandigheden, en kan gebruikt worden als referentie voor toekomstige optimalisatie van de TAG opbrengst op licht.

Het verhogen van TAG accumulatie snelheden is een belangrijk aspect in het verlagen van de kosten van olieproductie met behulp van microalgen. Begrip van de fysiologie en de regulatiemechanismen in het lipidenmetabolisme zijn hierbij onmisbaar. De meest belangrijke onduidelijkheden omtrent het lipidenmetabolisme zijn op een rijtje gezet in **Hoofdstuk 6**, zoals de cellulaire locatie van TAG synthese, het effect van een dag/nacht ritme op TAG productie snelheden, en de regulatie van TAG ophoping en de relatie hiervan tot fotosynthese. Het invullen van deze onduidelijkheden is noodzakelijk om de mogelijke beperkingen in het TAG metabolisme aan te wijzen en daarmee de doelen te identificeren waar ingegrepen kan worden met moleculair biologische technieken.
Gebaseerd op de laatste ontwikkelingen in het veld en het onderzoek dat beschreven is in dit proefschrift, werden drie hypothesen voorgesteld die de oorzaak en functie van TAG accumulatie kunnen verklaren. Allereerst zal TAG altijd functioneren als energie- en koolstofopslag, omdat deze nodig zijn voor de biosynthese. Daarnaast is de mate waarin TAG biosynthese functioneert als noodroute voor een teveel aan gegenereerde elektronen onder ongunstige kweekomstandigheden verschillend voor elke algensoort.

Als laatste lijken vetbolletjes met TAG in sommige algen ook te dienen als tijdelijke opslagplek voor overbodig geworden onderdelen van de plastide.
Verschillende punten werden genoemd waarmee de productiviteit van TAG voor bulk toepassingen verhoogd kan worden. Naast de klassieke aanpak van tweetraps TAG productie, waarbij een fase van biomassa productie gevolgd wordt door een fase waarin stikstof ontbreekt, zal continue kweek onder stikstoflimitatie, waarin groei en TAG accumulatie tegelijk plaats vinden, verder onderzocht moeten worden. Met een dergelijke kweekmethode kunnen zouden productietijd en –kosten aanzienlijk kunnen worden teruggebracht, omdat de productiefase van biomassa wegvalt en het daardoor minder vaak nodig is de productie stil te leggen voor het herstarten van een kweek. Hoewel in het lab de productiviteit van continue TAG productie een factor 4 lager is dan bij het klassieke systeem, staat continue kweek nog in de kinderschoenen. Verdere optimalisatie kan de opbrengst van dit systeem verder verhogen. Bovendien heeft continue productie het voordeel dat het controle mogelijk maakt over variaties in TAG accumulatiesnelheden onder de veranderende beschikbaarheid van licht gedurende de dag, die bij buitenkweek het systeem zal beïnvloeden.
Als laatste is uitgelegd hoe moleculair biologische technieken kunnen worden toegepast in microalgen om het TAG gehalte en de productiviteit van de huidige productiestammen te verhogen. Behalve het verhogen van de capaciteit van de metabole routes voor lipidensynthese door overexpressie van de verantwoordelijke enzymen of het uitschakelen van concurrerende routes, zou het voorkomen van het fotosynthetisch energieverlies dat samengaat met stikstofgebrek het belangrijkste doel moeten zijn. Daarnaast is verder onderzoek naar de regulatie van TAG ophoping en de aanpassing van het fotosysteem in microalgen met stikstofgebrek noodzakelijk. Inzicht in deze regulatie biedt de mogelijkheid hierin in te grijpen, en zo TAG synthese helemaal los te koppelen van nadelige groeicondities en de daarbij horende terugloop van fotosynthese. Gedetailleerd onderzoek van het metabolisme met behulp van metabole modellen, gecombineerd met de analyse van genexpressie en veranderende enzymconcentraties, zal een belangrijke rol spelen in het identificeren van nieuwe strategieën voor het verhogen van TAG productiesnelheden in microalgen.

Het onderzoek dat beschreven wordt in dit proefschrift is een stap vooruit in de commercialisatie van algenolie voor grootschalige toepassingen. Daarnaast verschaft dit werk een aantal handvaten die in de toekomst gebruikt kunnen worden om de belofte die 'microalgen' heet, waar te maken.

Dankwoord

Eindelijk, het is af! Nouja, bijna dan, want nu komt het allerbelangrijkste en meest gelezen deel van het proefschrift, het dankwoord! En terecht, want dit proefschrift was er niet geweest zonder de steun en inspiratie van heel veel mensen. Ik zal proberen de meest belangrijke te benoemen, maar het wordt proppen, ik heb nog maar 3 pagina's...

Allereerst, mijn begeleiders. Altijd waren jullie stand-by voor commentaar, peptalks en brainstorm sessies. Dankjewel dat ik altijd heb mogen zeggen wat ik dacht. **Packo**, bedankt voor het lenen van je hoofd af en toe, die extra processor heeft me vaak geholpen de boel op een rijtje te krijgen. Ik kon je soms schieten als ik mijn revisies terugkreeg, maar je inspiratie en alziend oog voor detail hebben onze papers echt goed gemaakt. En dan **Dirk**, bedankt voor je geduld, scherpe opmerkingen en altijd aanwezige overzicht. Je bent de beste crisismanager die ik ken. **René**, wat vond ik het spannend om bij de eerste werkoverleggen mijn werk aan 'de professor' voor de leggen. Ik vind het echt heel tof om te kunnen concluderen dat we, aan het eind van mijn promotietraject, vrienden zijn geworden. Bedankt voor de kansen die je me hebt gegeven en nog steeds geeft!

Hoofdstuk 3 was er niet geweest zonder **Arjen**. Je was mijn begeleider tijdens m'n eerste afstudeervak en toen heb je me geleerd dat modeleren helemaal niet 'eng' is, en dat 'het eigenlijk net zoiets is als rekenen, en dat kun je best'. Ik hoop dat ik jou heb bij kunnen brengen dat algen minstens net zo leuk zijn als schimmels! Then, Chapter 5 and transcriptomics. Too bad the 'cherry to the pie' did not make this thesis, systems biology turns out to be quite a challenge. Thanks to **Peter** and **Benoit** it starts to make a bit more sense to me; surely we will publish our work soon.

De studenten die ik heb mogen begeleiden hebben allemaal iets bijgedragen aan mijn onderzoek, ook al is niet alles direct in dit proefschrift terug te vinden. **Tim**, jij was mijn eerste student en we waren bijna even oud (gek hé?), maar volgens mij hebben we het alle twee voorbeeldig gedaan. **Ilse**, jammer dat er geen tijd was die labeling-proeven in het echt te doen, maar wie weet komt het in mijn vervolgprojecten nog te pas. Vind het in ieder geval heel tof dat we weer samenwerken! **Joep**, Mr. 'ik ben niet zo handig in het lab, maar draai wel in m'n uppie 3 steady states als m'n begeleider weg is', succes met het vinden van een baan! **Jannik**, the two-step hybrid growth system we tested when I co-supervised you with **Guido** is one of the most exciting things we tried during my project: it is a good alternative for continuous production and I'll be keeping it in mind for my next projects.

Dan zijn er een aantal algenmeisjes die genoemd moeten worden. **Annette,** mijn algenmama, je hebt me geïntroduceerd in de wondere wereld van de algen. En met succes, ik ben verslaafd geraakt volgens mij. Na een thesis bij jou werden we collega's en vriendinnen, en schreven we samen het mooiste eerste paper wat ik me maar kon wensen. Dank voor alles wat je me geleerd hebt en we hebben al die begeleiders van ons toch maar goed gemanaged! **Lenneke,** mijn liefste PhD zusje, kamergenootje en paranimf, we zijn samen begonnen en wat hebben we veel meegemaakt. Ik ben blij dat ik met jou in de achtbaan die 'promoveren' heet zat! Nouja, misschien is 'het leven' hier meer toepasselijk, we komen er nog wel eens achter hoe het in elkaar zit, als we in de 80 zijn en al menig kat overleeft hebben. **Marjon,** op oudejaarsavond 2008 kwamen we erachter we allebei in januari een afstudeervak zouden beginnen. We vergaten elkaar alleen te vertellen waar, en 5 dagen later kwam ik je weer tegen bij de nieuwjaarsborrel van BPE: 'huh, jij hier?'. En toen werden we roomies, vriendinnen en daarna weer collega's, ik gok zo dat we voorlopig nog niet van elkaar af zijn. **Maria Barbosa,** jij bent de meest recente toevoeging aan mijn rijtje algen-vriendinnetjes, ook al zit je al langer in het veld dan elk van ons allen. Echt heel gaaf dat je mijn baas wordt bij AlgaePARC, bedankt voor de kans en hoop dat ik nog een heleboel van je kan leren.

Wat zou een PhD moeten zonder technicians? **Fred,** jij staat nog te programmeren aan mijn reactor terwijl je eigen jubileumfeestje 10 minuten later begint. Fijn dat jij in de buurt was als Murphy weer eens toesloeg. **Sebas,** een soort van wervelwind op pootjes en ik snap nooit hoe jij al je werk voor elkaar krijgt in de tijd die je hebt en op de een of andere manier kan je ook altijd nog even komen kletsen over mijn bestelling, en, en… **Wendy,** met bewondering heb ik gekeken hoe je je binnen no time opwerkte van groentje naar volwaardig technician. Jouw record voor snelste vetzuuranalyse staat nog steeds en ik denk dat jij eigenlijk de enige bent die het kan breken.

Wat promoveren op algen leuk maakt is niet alleen het onderwerp, maar ook de mensen die je tegenkomt onderweg. First of all I would like to thank my roomies: the desk-hours were a lot more fun thanks to **Lenneke, Packo, Petra, Nicholas, Ana** en **Abdulaziz**. Dan zijn er nog de Young Algaeneers, **Guido, Kim, Lenneke, Lenny, Marjon,** en **Tim,** we hebben met z'n allen het leukste en origineelste algen-symposium ooit neergezet en ik ben heel trots dat in 2014 de 2^{e} editie op de agenda staat. My Wetsus-buddies: **Ana, Anja, Claudia, Ellen, Lenneke, Sina** and **Zlatica,** although Leeuwarden felt a bit far away sometimes, meeting you guys there made the trip worth the travel. **Sina, Klaske** en **Dorinde,** bedankt voor alle tips in het kader van 'promoveren voor dummies'. **Ward,**

je ontzettende relaxedheid is bewonderingswaardig: een keer sampelen op een dag is inderdaad meer dan genoeg. Bedankt voor de 'later-als-groot-ben' adviezen, **Mathieu**! **Pieter,** jouw opmerkingen tijdens de koffiepauze waren vaak zonder meer ongepast en kregen menig collega op de kast, maar jij kan het maken en dat maakt je des te leuker. **Miranda,** gelukkig hebben we op BPE secretaresses die gewoon op zaterdag (om 9 uur 's ochtends) even een promotiedatum willen regelen, dankjewel! And finally, thanks to all the other **PhD and staff of BPE and FPE** for the 'gezelligheid' during the coffee-breaks, lunches, many borrels, lab-uitjes, christmasdinners, etc.

Dan zijn er een aantal mensen die ik wil bedanken voor al hun hulp en steun tijdens de moeilijkste periode in mijn leven, die toevallig ook nog eens tijdens mijn promotietraject viel. Zonder jullie was dit boekje er ook niet geweest. **Jan** en **Suus**: bedankt voor al die keren dat jullie voor ons klaarstonden, met draaiboeken, maaltijden, schouders om op uit te huilen, lieve woorden en alleen al de wetenschap dat jullie in de buurt waren. **Karin,** het lot heeft ons op een nogal vreemde manier bij elkaar gebracht maar toch is het goed. Bedankt voor je coaching en je steun. Je bent een heel bijzonder en lief persoon. **Elsbeth,** we kennen elkaar maar kort en er is een kans dat we elkaar over een tijdje niet meer zien, maar in die korte tijd heb je heel veel voor me betekend. Je was in staat door alleen al te luisteren de chaos in mijn hoofd te temmen, en je rake opmerkingen aan het eind van mijn monologen werden al snel levenslessen. Bedankt voor je luisterend oor.

Mijn lieve familie, ze zitten erop, 4 jaar promoveren. Er is in die 4 jaar veel meer gebeurd dan me lief is, en ik hoop dat er wat rustigere tijden aankomen nu. **Papa** en **Mama,** ik ben er trots op dat jullie mijn ouders zijn. Ik heb ontzettend veel respect voor hoe jullie je de afgelopen 5 jaar staande hebben gehouden in alles. Ik hoop dat jullie zien hoe goed jullie het gedaan hebben met ons alle drie. **Machteld,** lief zusje, ook al ben je niet meer hier, over m'n schouder kijk je mee en haal je het beste in me naar boven. **Bas,** mijn kleine grote broertje, wat fijn dat jij naast me zit als paranimf (para-wattes?). Weet dat ik ook heel trots ben op jou, meneer de 'veurzitter'!

Lenny, lief, ik kan niet in woorden vatten hoe belangrijk je bent voor mij. Je bent mijn alles en samen zijn we sterker. Ik gok dat er niks meer is wat we níet met z'n tweeën aankunnen. Kom maar op!

Anne

Curriculum Vitae

Anne José Klok was born in Den Helder, The Netherlands, on January 13 1986. She attended Gymnasium Celeanum in Zwolle, where she obtained her diploma in 2004, with majors in *Natuur en Gezondheid* and *Natuur en Techniek.*

In the same year, she started her study Biotechnology at Wageningen University. In her minor thesis project at the Bioprocess Engineering group of Wageningen University, she worked on the design of a kinetic model that described the growth and lipid production of the fungus *Umbelopsis isabellina* on a solid substrate. During her internship at the R&D division of PepsiCo Nederland, she worked on the reformulation of savoury snack Nibb'it. Anne completed her major thesis at the Bioprocess Engineering group of Wageningen University, working on the design and validation of a metabolic model of microalgae *Chlamydomonas reinhardtii.* She graduated *Cum laude* in 2008 (BSc) and 2009 (MSc).

After completing her studies, she continued working as a PhD at the Bioprocess Engineering group of Wageningen University, on the project *Optimisation of lipid production in microalgae*. During her PhD, she co-founded and organised the first International Young Algaeneers Symposium, a symposium that aims to connect and inspire young scientist working in the field of microalgal biotechnology.

Anne continued her research in the field of microalgal biotechnology, and is currently working as a Postdoc at AlgaePARC and the Bioprocess Engineering group of Wageningen University. She is involved in the NWO project AG-Switch, which aims to unravel the metabolic switch between starch and lipid accumulation in microalgae, and the FP7 project Feul4Me, which aims to establish a sustainable chain for biofuel production using microalgae as a production platform.

List of Publications

Kliphuis, A.M.J., **Klok, A.J.**, Martens, D.E., Lamers, P.P., Janssen, M., Wijffels, R.H. 2012. Metabolic modeling of *Chlamydomonas reinhardtii*: energy requirements for photoautotrophic growth and maintenance. Journal of Applied Phycology. 24, 253-266.

Meeuwse, P., **Klok, A.J.**, Haemers, S., Tramper, J., Rinzema, A., 2012. Growth and lipid production of *Umbelopsis isabellina* on a solid substrate - Mechanistic modeling and validation. Process Biochemistry 47, 1228-1242 .

Klok, A.J., Martens, D.E., Wijffels, R.H., Lamers, P.P. 2013. Simultaneous growth and neutral lipid accumulation in microalgae. Bioresource Technology. 134, 233-243.

Klok, A.J., Verbaanderd, J.A., Lamers, P.P., Martens, D.E., Rinzema, A., Wijffels, R.H. 2013. A model for customising biomass composition in continuous microalgae production. Bioresource Technology. 146, 89-100.

de Winter, L, **Klok A.J.**, Cuaresma Franco, M., Barbosa, M.J., Wijffels, R.H. 2013. The synchronized cell cycle of *Neochloris oleoabundans* and its influence on biomass composition under constant light conditions. Algal Research 2 (4), 313-320

Klok, A.J., Lamers, P.P., Martens, D.E., Draaisma, R.B., Wijffels, R.H. Edible oils from microalgae: insights in TAG accumulation. Submitted for Publication

Overview of completed training activities

Discipline specific activities

Courses

SolarH2 Photobioreactor School (Nantes, France, 2009)
Advanced Course on Microbial Physiology and Fermentation Technology (Delft, 2010)
Advanced Course on Metabolomics for Microbial Systems Biology (Delft, 2010)
International Course on Biodiesel Production from Microalgae (Almeria, Spain, 2011)

Symposia

Netherlands Biotechnology Congress (Ede, 2009, 2012[1])
ABO Summit (Phoenix, USA, 2010) [1]
KIVI NIRIA Jaarcongres (Delft, 2011) [2]
Wetsus Internal Congress (Leeuwarden, 2011) [2]
9th European Workshop on Biotechnology of Microalgae (Nuthetal, Germany, 2012) [2]
1st International Young Algaeneers Symposium (Wageningen, 2012) [2,3]

General courses

PhD Competence Assessment (Wageningen, 2009)
Advanced Course Guide to Scientific Artwork (Wageningen, 2010)
Project and Time Management (Wageningen, 2010)
VLAG PhD Week (Baarlo, 2010)
Teaching and Supervising Thesis Students (Wageningen, 2010)
Basic Statistics (Wageningen, 2011)
PhD Scientific Writing (Wageningen, 2012)

Optionals

Wetsus Team Meetings and Symposia (Leeuwarden, 2009-2013) [1,2]
Bioprocess Engineering Brainstorm Days (2009, 2010 and 2012) [2]
Bioprocess Engineering PhD excursion USA (2010) [1,2]
Bioprocess Engineering PhD excursion Spain (2012) [1,2,3]

[1] Poster
[2] Presentation
[3] Organisation

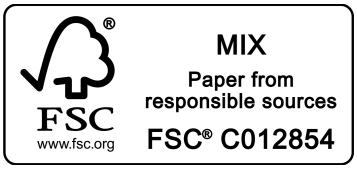

Printed by : Gildeprint Drukkerijen - Enschede
Coverphoto: Nexus7 via Dreamstime

This study was carried out at the Bioprocess Engineering Group of Wageningen University, Wageningen, The Netherlands, within the cooperation framework of Wetsus, centre of excellence for sustainable water technology (www.wetsus.nl). Wetsus is co-funded by the Dutch Ministry of Economic Affairs and Ministry of Infrastructure and Environment, the European Union Regional Development Fund, the Province of Fryslân and the Northern Netherlands Provinces. The author would like to thank the participants of the research theme "Algae" for the discussions and their financial support.